Transmutation of Nuclear Waste in Accelerator-Driven Systems

Adonai Herrera-Martínez

Darwin College

Hinc lucem et pocula sacra

Department of Engineering

University of Cambridge

A dissertation submitted to the

University of Cambridge for the degree of

Doctor of Philosophy

September 2004

A mis abuelos, en especial a María y José por su constante cariño y atención.

A mi padre, por los buenos recuerdos que perduran en mi memoria.

Con todos ellos me hubiera gustado compartir este día.

Abstract

Today more than ever energy is not only a cornerstone of human development, but also a key to the environmental sustainability of economic activity. In this context, the role of nuclear power may be emphasized in the years to come. Nevertheless, the problems of nuclear waste, safety and proliferation still remain to be solved.

It is believed that the use of accelerator-driven systems (ADSs) for nuclear waste transmutation and energy production would address these problems in a simple, clean and economically viable, and therefore sustainable, manner.

This thesis covers the major nuclear physics aspects of ADSs, in particular the spallation process and the core neutronics specific to this type of systems. The need for accurate nuclear data is described, together with a detailed analysis of the specific isotopes and energy ranges in which this data needs to be improved and the impact of their uncertainty. Preliminary experimental results for some of these isotopes, produced by the Neutron Time-of-Flight (n_TOF) experiment at CERN, are also presented.

The detailed design analysis of the TRIGA Accelerator-Driven Experiment (TRADE), the first ADS experiment at real power, is presented together with the time evolution of the system and some investigations which validate the concept of transmutation in ADSs.

A further design of the Energy Amplifier Demonstrator Facility (EADF), an 80 MW_{th} lead-bismuth cooled subcritical device, is presented, where the intrinsic advantages of the use of fast neutrons and the safety features of the device are demonstrated, using a state-of-the-art Monte Carlo burn-up code (EA-MC).

Finally, Several high-level waste transmutation strategies are assessed. These include thorium-based systems to transmute waste transuranics and long-lived fission fragments, as well as the double strata approach, where plutonium is eliminated through the use of mixed oxide fuel (MOX) and the accumulated minor actinides (MAs) are eliminated in dedicated MA burners.

The conclusion of this research recapitulates the key features found in the design of both ADS experimental facilities and indicates their impact on nuclear waste transmutation. The safety features of the proposed ADS are summarised, together with design limitations due to the lack of accurate nuclear data. Finally, a possible nuclear waste transmutation scenario is proposed with an intermediate step, which includes the development of MA burners, progressively shifting nuclear power towards the more acceptable thorium fuel cycle.

Acknowledgements

First and foremost, I wish to convey my sincere gratitude to my supervisors Yacine Kadi, at CERN, and Geoffrey Parks, at the University of Cambridge, for their invaluable help and support in carrying out the research included in this dissertation. I would also like to thank Prof. Carlo Rubbia for his guidance and expertise in a wide range of fields, from transmutation of nuclear waste to photon detection and Monte Carlo codes.

I had the great pleasure of working with the Emerging Energy Technologies group at CERN. The kindness of every single member of this group, both past and present, made my stay at CERN a very enjoyable one. Special thanks go to Paolo Cennini for his steadfast sympathy during these years, Enrico Chiaveri for his support in finishing this thesis, Alberto Mengoni for his patience and expertise in nuclear data and my colleague and friend Vasilis Vlachoudis, from whom I have learnt about innumerable subjects and who, together with his wife Vivian Synteta, I hold dear.

I am especially grateful to numerous former and present students of the University of Cambridge and Darwin College for making my stay there unforgettable, and in particular, to my good friends Fady El-Nahal, Elizabeth Son and the Frank Young House – Valencia group, among many others. I am greatly indebted to Roselle Dalzine, whose love and caring have brought joy to my life from the day I met her, and whose support has been essential to the successful completion of this dissertation.

Last and most importantly, I must express my deep gratitude to my family, especially my mother, Natividad Martínez Sanchez, my second mother and aunt, Amparo Martínez Sanchez and my stepfather, Ramón Nemesio Ruiz for their love and unfaltering support in spite of the physical distance.

Adonai Herrera Martínez

Cambridge, September 2004

As required by the University regulations, I hereby state that this dissertation is my own work and contains nothing which is the outcome of work done in collaboration with others, except as specified and referenced in the text and Acknowledgements.

This dissertation contains no more than 68,000 words and 150 figures, including bibliography, footnotes, tables and equations.

Adonai Herrera Martínez

Adonai@cantab.net

Contents

List of Figures

List of Tables

Glossary

ADS	Accelerator-Driven System
AISI	American Iron and Steel Institute
ALI	Annual Limits of Intake
ANL	Argonne National Laboratory (US)
ARC	Adiabatic Resonance Crossing
ATW	Accelerator Transmutation of Waste
BOC	Beginning-Of-Cycle
BOL	Beginning-Of-Life
BTL	Beam Transfer Line
BWR	Boiling Water Reactor
CANDU	CANadian Deuterium-Urarium reactor
CEA	Commissariat à l'Energie Atomique (France)
CERN	Conseil Européen pour la Recherche Nucléaire
CIEMAT	Centro de Investigaciones Energéticas, Medioambientales y Tecnológicas (ES)
DOE	Department Of Energy (US)
EA	Energy Amplifier
EA-MC	Energy Amplifier Monte Carlo
EADF	Energy Amplifier Demonstration Facility
EET	Emerging Energy Technologies group at CERN

ENDF	Evaluated Nuclear Data File
ENEA	Ente per le Nuove Tecnologie, l'Energia el'Ambiente (Italy)
EOC	End-Of-Cycle
EOL	End-Of-Life
EURATOM	European Atomic Energy Community
EXFOR	EXchange FORmat experimental nuclear data files
FBR	Fast Breeder/Burner Reactor
FC	Fuel Configuration
FEAT	First Energy Amplifier Test
FERFICON	Fertile-to-Fissile Conversion Program
FF	Fission Fragment
FIC	Fission Ionisation Chamber
FLUKA	FLUktuierende Kaskade (Fluctuating Cascades) code
HLW	High-Level Waste
IAEA	International Atomic Energy Agency
INL	Idaho National Laboratory (US)
IPHI	Injecteur de Protons Haute Intensité project
IPPE	Institute of Physics and Power Engineering (Russia)
JAERI	Japan Atomic Energy Research Institute (Japan)
JEFF	Joint Evaluated Fission and Fusion file
JENDL	Japanese Evaluated Nuclear Data Library
JINR	Joint Institute for Nuclear Research (Russia)
LBE	Lead-Bismuth Eutectic
LEU	Low-Enriched Uranium
LINAC	LINear ACcelerator
LLFF	Long-Lived Fission Fragment

LOCA	Loss-Of-Coolant Accident
LWR	Light Water Reactor
MA	Minor Actinide
MAG	Ministers' Advisors Group
MASURCA	MAquette de SURgénérateur à CAdarache facility
MC	Monte Carlo
MEGAPIE	MEGAwatt Pilot Experiment
MOX	Mixed OXide Fuel
MTA	Materials Testing Accelerator
MUSE	MUltiplication Source Externe experiment
N_TOF	Neutron Time-of-Flight experiment
ND	Nuclear Data
NEA	Nuclear Energy Agency
OECD	Organisation for Economic Co-operation and Development
OMEGA	Options Making Extra Gains for Actinides and Fission Fragments
OPEC	Organisation of Petroleum Exporting Countries
ORNL	Oak Ridge National Laboratory (US)
P&T	Partitioning and Transmutation
PDF	Probability Distribution Function
PS	Proton Synchrotron particle accelerator at CERN
PSI	Paul Scherrer Institute (Switzerland)
PTB	Physikalisch-Technische Bundesanstalt (Germany)
PWR	Pressurized Water Reactor
R&D	Research and Development
TAC	Total Absorption Calorimeter
TARC	Transmutation by Adiabatic Resonance Crossing

TRADE TRIGA Accelerator-Driven Experiment

TRASCO TRAsmutazione SCOrie project

TRIGA Training, Research, Isotopes, General Atomics reactor

TRU Transuranic element

TWG Technical Working Group on ADSs

UNFCCC United Nations Framework Convention on Climate Change

UOX Uranium OXide fuel

UZrH Uranium-Zirconium-Hydride

XADS eXperimental Accelerator-Driven System

XADT eXperimental Accelerator-Driven Transmutation

Chapter 1

Introduction

The production of energy, in its many different forms, has always been a major concern for humanity and has become one of the cornerstones of social development. In fact, a major reason for the exponential technological development that occurred during the 20th century is the development in the use of petroleum, discovering a major energy source with large specific energy.

Nevertheless, this technological evolution has not come without cost: the pressure on the resources of the planet and the effect of major economic growth have bestowed upon the environment a large burden in the form of particle and gaseous emissions, and climate change.

The production of energy through the use of nuclear interactions (i.e. nuclear fusion and fission) could play a major role in overcoming these problems. Unlike fusion, the technology associated with the splitting of the nucleus (fission) is well proven. Nevertheless, present nuclear energy programs meet strong opposition in large parts of the globe for several reasons:

- Public concern about plant safety and the consequences of accidents, magnified by the accidents of Chernobyl (1986, a prompt-supercritical reactivity excursion) and Three-Mile Island (1979, a loss-of-coolant accident resulting in a core meltdown).
- Increasing international awareness about the possible diversion of this technology towards military purposes, and in particular towards terrorism.
- The problem of waste, implicit in any human activity, which represents in this case a major drawback due to the long-lived radiotoxicity of some of the by-products.

In this context, the transmutation of nuclear waste through the use of a subcritical assembly based on the thorium cycle [1] potentially answers both the environmental need, as well as the growing social demands, for a safe carbon dioxide-free energy source. The use of a proton accelerator to generate additional neutrons through the spallation reaction, necessary to maintain reactor operation, ensures the control of the subcritical system, avoids criticality accidents and allows a flexibility in the composition of the fuel unachievable in critical reactors. Moreover, the choice of thorium, an element abundant in the earth's crust, as the breeding matrix for the fuel reduces by several orders of magnitude the quantity of transuranic elements (TRUs) produced by neutron capture in some of the isotopes present in the fuel.

1.1 Energy Generation Problems

The level of development of any country is directly related to its energy consumption and depends to a great extent on its capability to produce this energy. In order to maintain the economic situation in the Western World and to allow the rest of the world to achieve similar levels of welfare, without jeopardising the biosphere, alternative sources of energy, as well as more reasonable and efficient consumption methods, should be developed.

These goals are not only a matter of interest to the developed world, but also a moral obligation towards the rest, and majority, of the world and towards our future generations. Hence, the minimisation of the global warming, particle emission and pollution effects should be a major goal while defining future international energy policies.

Figure 1.1 presents some indicators of the human influence on the atmosphere, such as CO_2, SO_2, N_2O and CH_4. The exponential increase in the concentration of these elements, coinciding with the industrial revolution, presents a serious threat to the environmental sustainability of, not only specific ecosystems (confirmed by, for instance, the systematic deforestation caused by the acid rain in some parts of Europe), but if the trends continue, of the planet as a whole.

In this sense, nuclear energy should be part of the R&D necessary to develop these alternative sources, since the use of nuclear power releases neither green house gases nor other chemical pollutants, such as NO_x (a critical component of photochemical smog), SO_x (the main source of acid rain) or dust particles and aerosols. Therefore, a fundamental requirement may be to transform nuclear power in such a way as to be accepted by the general public, by dealing with its main drawbacks.

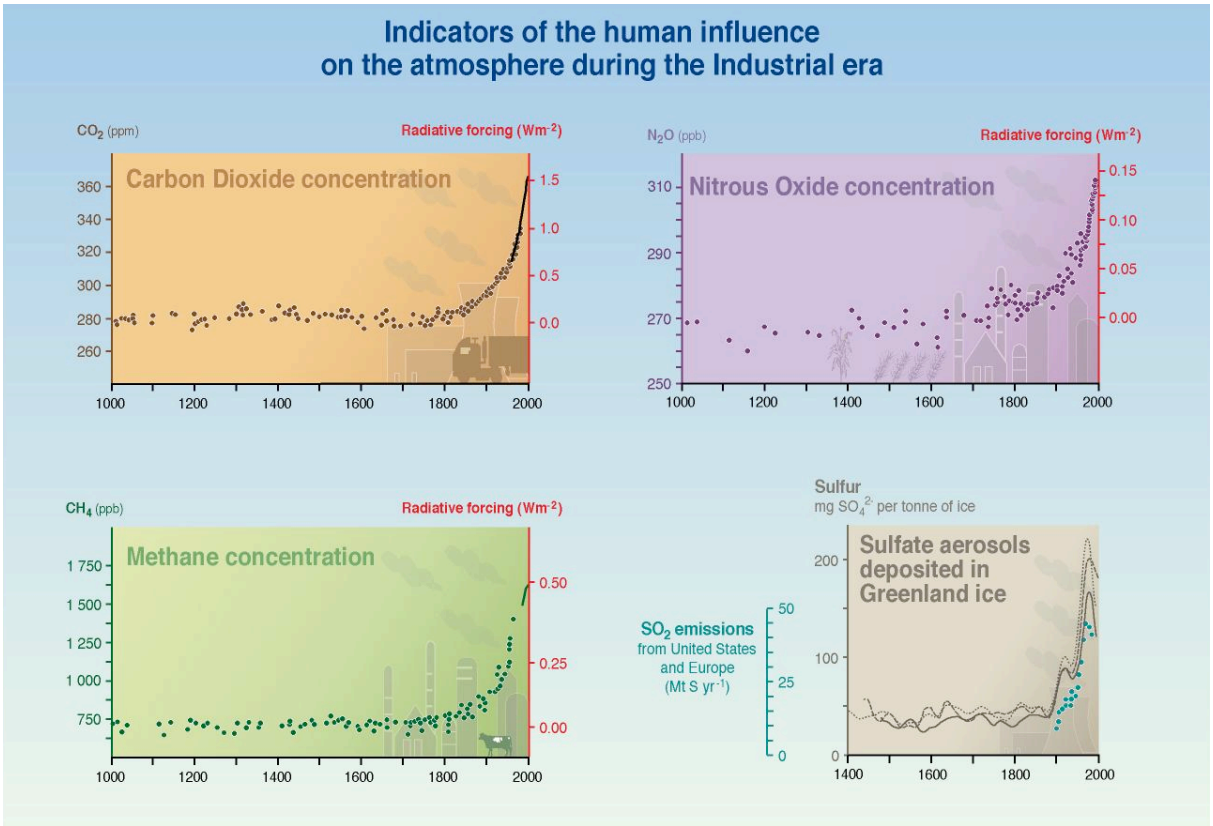

Figure 1.1. Atmospheric concentrations during the last millennium for some pollutants produced by human activity [2].

1.1.1 Global Warming

The energy sector, from primary energy extraction to end-use, is one of the main sources of greenhouse gas emissions, in particular CO_2, that raise concerns because of their consequences for global warming and climate change. Figure 1.2 shows two possible scenarios predicting the impact of increasing CO_2 levels on the average global temperature, included in [2], a study carried out by the World Meteorological Organisation and the United Nations Environment Programme. Even the most optimistic scenario (the blue curve), reducing CO_2 emissions in order to maintain the concentration in the atmosphere to about 550 ppm, would imply a global temperature rise of more than 2 °C in this century. Climate change is a major global issue on the agenda of policy-makers, and, hence, a key objective will be the implementation of measures aiming towards reducing greenhouse gas emissions from the energy sector in the medium and long term, since the greenhouse gas emissions related to energy use are estimated to represent some 75 to 90 percent of total anthropogenic emissions [3].

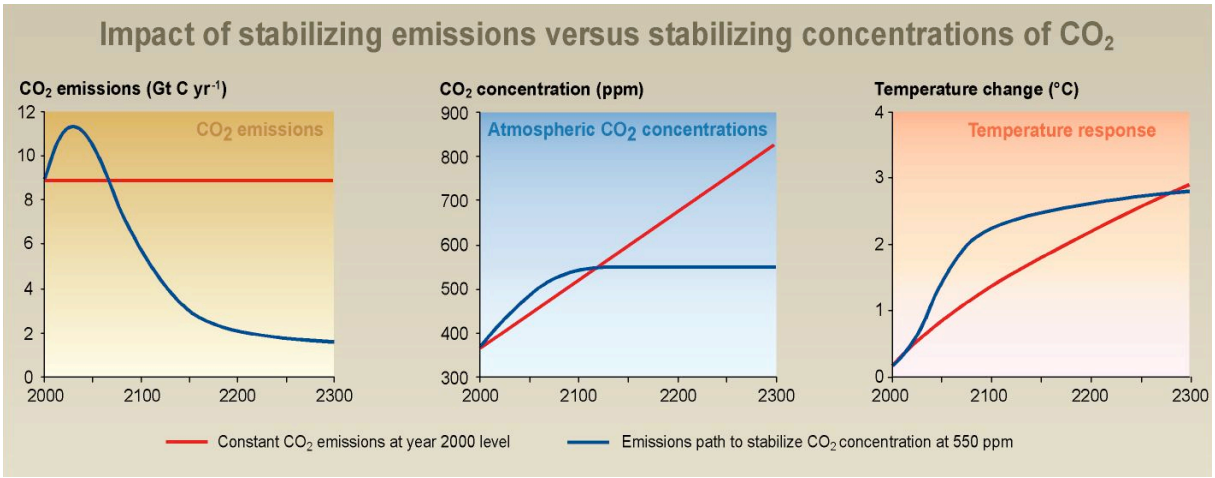

Figure 1.2. Effect of CO_2 emissions on the average temperature of the planet for two different scenarios [2].

Although these emissions are currently dominated by the industrialised countries, they will increase substantially once developing countries (in particular the rapidly growing economies of China and India) reach the status of developed countries. Table 1.1 presents energy consumption and CO_2 emission levels at different times for different regions of the world. The predictions show a massive increase in CO_2 emissions over the next quarter of the century if present energy policies continue, implying a worse case scenario than the constant production case (the red curve) presented in Figure 1.2.

Table 1.1. Energy consumption and CO_2 emissions for different regions and time [4].

Region	Energy consumption ($\times 10^{18}$ J)				CO_2 emissions (10^6 metric tonnes carbon equivalent)			
	1990	2001	2010	2025	1990	2001	2010	2025
Industrialised countries	192.9	223.1	253.3	304.2	2844	3179	3572	4346
Former Soviet Union	80.5	56.2	69.5	86.8	1337	856	1038	1267
Developing countries	94.2	146.9	184.3	284.4	1691	2487	3075	4749
Asia	55.4	89.7	116.2	184.2	1089	1640	2075	3263
Middle East	13.8	21.9	26.6	38.0	231	354	420	601
Africa	9.8	13.1	15.2	21.1	179	230	261	361
Latin America	15.2	22.0	26.6	41.1	192	263	319	523
Total World	367.6	426.1	507.0	675.3	5872	6522	7685	10361

Following the 1992 Rio de Janeiro conference on sustainable development, 159 countries met in Kyoto from 2nd to 11th December 1997 to adopt a common policy in the fight against global warming. In the latter, known as the Kyoto Protocol, agreed upon by the Parties to the United Nations Framework Convention on Climate Change (UNFCCC), countries committed to reduce their greenhouse gas emissions. Also, the Protocol states that the developed countries (listed in annex 1 [5]) "shall undertake promotion, research, development and increased use of new and renewable forms of energy, of CO_2 sequestration technologies and of advanced and

innovative environmentally sound technologies". One important option that could be covered by the last phrase, and is not specifically mentioned, is nuclear energy, which is essentially carbon-free. This option is rather unexploited, as revealed in Table 1.2, where the relative world energy consumption in the year 2002 from the main primary energy sources is presented (commercial renewable energies are estimated to represent less than 2.5% of the total [6]).

Table 1.2. Relative energy consumption from the main primary sources for different regions in 2002 [6].

Relative energy consumption	Oil	Natural gas	Coal	Nuclear	Hydro electric
North America	39.2%	26.2%	21.8%	7.5%	5.2%
Latin America	47.9%	19.7%	4.0%	1.0%	27.4%
Europe & Eurasia	32.7%	33.2%	17.9%	9.9%	6.3%
Middle East	51.5%	45.9%	2.1%	0.0%	0.5%
Asia Pacific	36.5%	10.9%	43.5%	4.3%	4.7%
Africa	40.8%	20.9%	31.1%	1.0%	6.4%
Total World	37.5%	24.3%	25.5%	6.5%	6.3%
Of which: European Union	43.2%	23.6%	14.8%	13.7%	4.7%

There are a number of technical options that could help in reducing, or at least slowing the increase of, greenhouse gas emissions from the energy sector. The list of options includes: improving the efficiency of energy conversion and end-use processes; shifting to less carbon intensive energy sources (such as shifting from coal and oil to natural gas); developing carbon-free or low-carbon energy sources; and carbon sequestration (e.g. planting forests or capturing and storing carbon dioxide). However, when the technological readiness and costs of the various options are taken into account, there are only a few options that could be implemented in the short and medium term at an acceptable cost. Moreover, while a shift towards the use of natural gas may reduce the problem of CO_2 and particle emission to a certain extent, its generalised use would not solve the problem since the energy extraction depends on burning (oxidising) the fuel, thus producing carbon oxides.

Nuclear power is one of the few options that are: currently available in the market; competitive in a number of countries, especially if global costs to society of alternative options are considered; practically free of emissions of CO_2 and other greenhouse gases; and sustainable at large-scale deployment (i.e. large energy supply can be supported by natural resources which are plentiful and have no other use). Moreover, non-electrical applications of nuclear energy, such as heat, potable water and hydrogen production, can be developed, and these applications could enlarge significantly nuclear power's contribution to greenhouse gas emission reduction.

1.1.2 Availability and Reliability of Resources

The reliability of the different energy sources is a matter of concern, particularly in view of the economic and political repercussions (e.g. surges in unemployment and inflation rates) of the 1973 (the nationalisation of oil fields by the OPEC states and the Arab countries' oil embargo as a punishment for western support to Israel during the Yom Kippur war) and 1979 (the drastic reduction in crude exports by Iran after the Revolution) oil crises. These events, in addition to the effects of the miners' strikes in 1972, 1974 and 1984 in the United Kingdom, showed the industrialised countries the risks of dependence on few energy sources and external (and in many cases unpredictable) suppliers, and compelled countries such as France and the UK to revise their energy policies diversifying their energy sources and consequently reducing their external energy dependency. In the case of France, these policies have resulted in the use of nuclear energy as their major source of electricity (76.4% of the total in the year 2000 [7]).

However, a larger, although more predictable, matter of concern is the depletion of primary energy sources, in particular crude oil. It is well know that the oil reserves in the world are limited and at the present rate of consumption (thus, assuming the optimistic scenario of no increase in demand) will be extinguished within this century. In fact, the BP Statistical Review of World Energy 2003 [6] predicts the exhaustion of the world's oil reserves in 40 years.

A similar scenario is expected for natural gas, since the proven reserves are predicted to last for 60 years at the present rate of production [6]. This energy source, although less polluting when compared to petroleum, presents no major alternative to the latter in terms of source lifetime, given that the reserves of both will be predictably depleted in half a century.

In the case of coal, the reserves are estimated to last around 200 years at the present rate of consumption. This could extend the use of fossil fuels over a century, at the expense of a larger environmental impact due to the higher emission of pollutants arising through the use of this fuel. Even though desulphurisation and particle-filtering techniques are well established, coal is arguably the most polluting of the fossil fuels, a source of large quantities of carbon, sulphur and nitrogen oxides, soot and other aerosols.

As mentioned earlier, there are few available alternatives that could take over on a large scale. The use of renewable energies is a major goal since they are practically non-polluting and the resources are inextinguishable. Nevertheless, the impact on world energy production of these sources is rather small (estimated to be about 2.5% [6]) due to the low efficiency and the low specific energy of most of them (for instance, in order to produce 1 GW_e using photovoltaic panels, thousands of square kilometres would have to be covered). There is an obvious need

of investing in these types of technologies, but there is also a need to look for alternatives since these sources cannot fulfil global needs in the short or medium terms.

In addition, the hydropower may also contribute to reduce the weight of the fossil fuels in the energy schemes. It is likely that micro-hydro-schemes will continue to expand this form of electricity generation worldwide since large hydroelectric dams attract a lot of scepticism and criticism due to their large ecological impact in the region where they are constructed [8]. Nonetheless, the total amount of energy available from these sources is limited by economical and environmental factors, which imply that in several developed countries the production capabilities are being reached.

1.1.3 The Role of Nuclear Power

As indicated in the previous section, no fossil fuel is neither non-polluting nor a reliable energy source on which international energy policies could rely for sustainable development. The short lifespan of these sources and particularly their intrinsic polluting by-products make them unsuitable for balancing the world's increasing energy demands with a sustainable means of production, minimising their impact on the environment.

On the other hand, renewable energies do not yet represent a full-scale alternative, capable of substituting for fossil fuels in a medium timescale, nor is hydropower. The production of energy through nuclear fusion is not yet technically available and probably will not be industrially available for more than half a century.

In the current situation, nuclear power will inevitably play a major role in the future, not only in industrialised countries but also in developing countries where energy demand is surging. However, to make nuclear energy socially acceptable, the aforementioned concerns should be properly addressed. Of these concerns the back-end of the fuel cycle is arguably the most technically complex and politically controversial.

1.2 Problematic Aspects of Nuclear Waste

The problem of radioactive waste is a major drawback of the production of energy through nuclear power. The long half-lives of some isotopes, reaching millions of years, make this problem a crucial one to solve. The fate of these radionuclides has given rise, for several decades already, to questions regarding the long-term safety of radioactive waste disposal. Many proposals have been made: geological disposal in deep underground facilities specifically designed for this purpose, launching them into outer space, and burning them into dedicated nuclear facilities.

The generation of spent fuel and highly active waste materials amounts to quantities far in excess of the capabilities of any outer space disposal programme, and such a practice would create contamination risks for both the atmosphere and the biosphere [9]. Thus, there is a general consensus among countries holding nuclear installations that geological disposal is an adequate solution for short and medium-lived wastes. Conversely, public opposition to disposal sites for high-level wastes (HLWs) have caused delays in the development of these facilities.

Partitioning and Transmutation (P&T) of radioactive and long-lived elements from the highly radioactive waste streams in order to reduce or possibly to eliminate their radiotoxicity is the third option under consideration. During the last decade, interest in P&T has grown, due mainly to the uncertainties about the safety of long-term repositories for HLW, their effect on proliferation and the possibility of obtaining extra-gain (producing energy) from the otherwise long lasting highly radiotoxic waste.

1.2.1 Nature of Nuclear Waste

The definition of nuclear waste is a controversial one, since what may be considered waste in some countries may be considered valuable fuel in others. The most obvious example is the plutonium in the spent fuel, considered waste in, for example, Spain and the US and then used as part of the mixed oxide fuel (MOX) in others, as it is the case in the France and Japan. This ambivalence is extensive to a large part of the spent fuel, which could be used as fuel in fast systems.

Nonetheless, considering the large number of elements present in the spent fuel, only the unused uranium and some isotopes of plutonium can be recycled into fresh fuel for thermal systems. Therefore, the rest of the elements forming the spent fuel are generally considered waste products and their existence raises the issue of the closing of the fuel cycle.

These waste elements are predominantly formed by fission fragments (FFs, originated mostly by the fission of ^{235}U) of which the most hazardous are the long-lived fission fragments (LLFFs) and TRUs produced by neutron capture in the fuel and the subsequent decay chains. By separating the plutonium from the TRUs it is possible to obtain the minor actinides (MAs), elements such as neptunium, americium and curium, which, in general, present low thermal fission cross-section.

At present most nuclear waste is kept under surveillance in shallow depth-storage facilities (e.g. cooling ponds in nuclear power plants). However, concerns about leaks to the biosphere and the proliferation risks imply that this can only be a standby solution to be followed either by permanent storage in deep geological repositories and/or transmutation into less radioactive nuclear species.

1.2.2 Storage in Deep Geological Repositories

One of the few viable options to deal with the most hazardous elements of the nuclear waste is the storage of these in an underground repository, where they would lie for centuries until their radiotoxicity was reduced to reasonable levels. The surveillance of these sites would be a requirement, although the control of the state of the containment elements is not always considered.

Several possibilities appear in this scenario, such as vitrification of the waste or the use of different containment methods. The access to the waste after some time is also an issue since, for example, countries like Sweden have decided to perpetually seal the repositories once filled up.

This approach has several important drawbacks, since the basic idea of this approach is hiding the waste and not the elimination of the hazardous elements. In particular, the great difficulties in assessing the seclusion of the containment during the hundreds of thousands of years make this option unreliable to the eyes of a large part of the scientific community and public opinion.

1.2.3 Safety Issues

The intrinsic radiotoxicity of some of the elements present in the spent fuel justifies the great concern of the safety authorities in the control of these substances. The possible leakage of some of these elements into the biosphere could have unpredictable consequences for public health and for the environment in general.

The penetration of water into the repository could also set the conditions for a recriticalisation of the waste [10], due to the reflection and thermalisation of the radiation, which would otherwise escape from the waste canisters. A recriticalisation of the waste elements could have fatal consequences no only for the containing units but also for the whole repository.

Moreover, the persistence of these elements makes possible that the geological conditions of their storage may change thus facilitating the escape of radiotoxic waste centuries after the closure of the repository.

1.2.4 Proliferation Aspects

Nuclear power is burdened by the fact that it was first developed to build an explosive device used for destructive purposes. The nuclear weapons era was launched abruptly upon the world with the first explosion of a nuclear weapon at Alamogordo, New Mexico (US), on July 16, 1945. This was followed by two detonations in the war against Japan. By the early 1960s there were five nuclear weapons countries [11].

Since then, fear of the diversion of civil nuclear elements towards military use has been present in all civil nuclear programs. These fears were confirmed by the "horizontal" spread of nuclear weapons during the 1960s and 1970s when more countries joined the "nuclear club". The risks of open proliferation of sensitive nuclear materials led US Presidents H.S. Truman and J. Carter to ban reprocessing and plutonium recycling.

The risk of diversion (through theft or development by a "rogue" state) of some of these materials towards terrorist purposes is currently a major concern in public opinion. Technically, the relatively large abundance of weapons-grade plutonium in conventional nuclear waste could be a source of future nuclear weapons proliferation. Moreover, some of the minor actinides, such as ^{243}Am ($\tau_{1/2}$ = 7370 yr, α-decay into ^{239}Np followed by β^--decay, $\tau_{1/2}$ = 2.35 d), could contribute in a few thousand years to the generation of weapons-grade ^{239}Pu, which could be a hazard for future generations.

On the other hand, the elimination of a large part of the existing nuclear arsenal was generally accepted with the end of the Cold War and the start of nuclear weapons elimination programs. Nevertheless, due to the age of some of these weapons, the presence of some daughter isotopes, e.g. ^{241}Am ($\tau_{1/2}$ = 432.2 yr from the β^--decay of ^{241}Pu, $\tau_{1/2}$ = 14.29 yr) prevent these materials from being disposed of as fuel in conventional reactors.

1.2.5 Transmutation of Nuclear Waste

The remaining technically viable option would be to eliminate in dedicated systems the hazardous elements originated in the conventional nuclear reactors. Fortunately, 99.995% of the long lasting (> 500 years) radiotoxicity is found in a few elements and about 1% of the spent fuel (~300 kg/GW$_e$/yr) [9].

The spent fuel contains several elements which are resistant to further elimination in thermal reactors. Therefore, conventional fission and transmutation cannot be done in ordinary light water reactors (LWRs). In order to eliminate these resilient nuclei (TRUs and LLFFs) in an efficient way, fast neutrons are necessary. However, TRUs can only be eliminated by fission, while LLFFs can be primarily transmuted by neutron capture; hence, different methods will have to be used to get rid of them.

Very fast neutrons are produced by spallation by protons accelerated to a medium energy (~1 GeV) by a dedicated, compact, high-current accelerator. This device called an Accelerator-Driven System (ADS) is:

- Non-critical, since the reaction rate is fully controlled by the current of the accelerator.
- Preferable to a fast breeder reactor, as it offers higher safety, flexibility and efficiency.

The transmutation goals are to eliminate 99.9% of the TRUs and up to 95% of the LLFFs (^{99}Tc and ^{129}I). These goals are technically feasible and economically viable [12], and present a realistic and safer alternative to the geological repositories in order to eliminate the HLW. Moreover, the use of thorium as a fuel matrix presents several advantages due to the abundance of this element and the lower TRU production compared to uranium.

1.3 Thesis Overview

This thesis gives an overview of the subjects related to the transmutation of nuclear waste in accelerator-driven systems and summarises the major reasons for the development of this technology, highlighting its advantages. The main objective of the research is to assess the best methods of transmutation of nuclear waste through the use of ADSs, and to contribute to the design and development of some of the most relevant ongoing experiments in the field.

A detailed study of the nature and origin of nuclear waste is presented in Chapter 2. The global dimension of this consequence of human activity is quantified together with an assessment of the hazards of these materials. The alternatives for waste disposal are also analysed.

Chapter 3 serves as an introduction to the required background for studying ADSs, illustrating the historical evolution of this type of systems. The physics related to these systems is also detailed, through discussion of the spallation process, taking place in the target and the reactor core, where the transmutation process takes place, together with an overview of the computational methods used in reactor analysis.

The limitations in the design of these devices are addressed in Chapter 4. The need for reliable nuclear data is discussed and an extensive sensitivity analysis of different systems to this factor is presented. Moreover, preliminary experimental neutron cross-section data, which is being obtained by the neutron Time-Of-Flight facility (n_TOF) developed at the European Organisation for Nuclear Research (CERN), is presented.

The first ADS experiment at real power, which foresees the coupling of a General Atomic TRIGA reactor with a proton accelerator, is currently in the design phase. Chapter 5 deals with the neutronic design of this experiment, as well as with an analysis of the transmutation capabilities of this device. The need to use fast neutrons in order to effectively transmute some the components of the nuclear wastes is evidenced.

Chapter 6 presents a detailed analysis of the Energy Amplifier Demonstration Facility (EADF), an 80 MW_{th} ADS cooled by lead-bismuth eutectic, dedicated to the demonstration of

the transmutation concept in this type of devices. The neutronic characteristics together with the fuel burn-up evolution and transmutation efficiency of this fast system are explained. To conclude this chapter, two different transmutation strategies, i.e. the use of thorium-based ADS and the double strata approach, are analysed.

Finally, Chapter 7 presents the final conclusions of the thesis, describing the most relevant technical aspects of the systems analysed and indicating their effect on the transmutation schemes. A clear distinction between the requirements for TRUs and LLFFs elimination is made, together with a precise evaluation of different transmutation schemes. The optimal approaches to effectively reduce the stockpile of these elements are summarised and final recommendations for future work are given.

Chapter 2

Nuclear Waste

Nuclear power constantly produces spent fuel containing a wide range of elements with different physical characteristics. The composition of these by-products depends on several factors, such as the composition of the fresh fuel, the level of burn-up or the reactor type. However, all the constituents of the spent fuel can be classified as fission products or as actinides.

Apart from the short-lived fission products, the spent fuel contains significant quantities of actinides and fission products with very long half-lives, which constitute a long-term (over 10,000 years) radiotoxic hazard. The effects of a possible leakage of some of these elements into the biosphere can hardly be predicted due to the diversity of these elements, the large number of pollution channels, and the stochastic nature of their effects, as well as the long time span of the analysis.

Therefore, several alternatives for dealing with this nuclear waste have been considered, from shipping it into space to burying it under the seabed or dumping it into ocean trenches. However, there are only a few alternatives which are technically and economically viable and which give some degree of control over the fate of the nuclear waste. These options fall into two categories: the creation of deep geological repositories, or the elimination of the most hazardous elements in dedicated systems (transmutation). The latter option is the only one implying the total elimination of the most radiotoxic elements, which would prevent the aforementioned long-term leakage or proliferation problems.

2.1 Origin and Constituents of the Nuclear Waste

Waste can arise at a number of different points in the nuclear fuel cycle, starting with the mining of uranium ore, during its enrichment, in the nuclear reactor and as a result of the reprocessing of the spent fuel. The many types of waste involved may be classified according to different factors, such as their origin, physical state or level of radiotoxicity. The International Atomic Energy Agency (IAEA) produced a five-level classification of radioactive waste based on radioactivity and heat output [13]. This is a particularly useful method of labelling nuclear waste as it highlights its two main hazards, namely heat and radioactivity, and gives an immediate assessment of the degree of radiotoxicity of the element, containment required and the time span involved [14].

In particular, elements included in categories I (high-level of radioactivity, long-lived) and II (intermediate-level, long-lived) are considered the most hazardous materials and grouped as HLW. Since dealing with these elements is quite problematic, their storage or elimination involves a great amount of R&D, as well as continuous political discussion (e.g. the creation of a HLW repository in Yucca Mountain has been appealed in court several times by the state of Nevada, US).

Chemically, the two main components of the HLW are TRUs and LLFFs, representing respectively 1.1% and 4% of the conventional spent nuclear fuel from a LWR. Table 2.1 summarises the waste composition originating from a LWR for UOX and MOX, and different average thermal burn-ups. The isotope and element masses in the waste are given for UOX with an enrichment of 4.2%, an average thermal burn-up of ~50 gigawatts-day per tonne of heavy metal (GWd/tHM) and after 5 years of cooling time. Since the relative isotopic composition changes with the type of fuel and the level of burn-up, three cases are presented, highlighting 33 GWd/tHM (~0.1 tonnes of fuel per day) as the most common level of LWR burn-up.

As mentioned in 1.2.1, the TRUs are produced through consecutive neutron captures and decays in uranium in the fuel. These elements are responsible for most of the long-term radiotoxicity, both due to their profusion in the waste and their long half-lives combined with complicated decay chains. Clearly, fission is the most effective process to eliminate this type of waste, avoiding the production of further actinides.

Fission fragments are the by-products of the fission reaction and, due to their nuclear instability (excess of neutrons compared to the number of protons), most of them decay promptly into more stable species. Nevertheless, some of them, such as ^{99}Tc or ^{129}I, are quite abundant in the waste (both are close to the peaks of the fission product yields for thermal fission) and have lengthy half-lives and chemical properties that would enhance their

diffusion into the biosphere (high mobility). Therefore, although the transmutation of these particular LLFFs presents several technological and radiological difficulties, their elimination represents a goal of the same level of importance as the MAs.

Table 2.1. Composition of the nuclear waste (LWR) for different types of fuel and levels of burn-up [9] & [15].

Nuclide	Isotope ($kg/GW_e/yr$) 50 GWd/tHM	Element ($kg/GW_e/yr$) 50 GWd/tHM	Half-life (yr)	Isotopic composition with burn-up (%)		
				UOX		MOX
Actinides				33 GWd/tHM 3.5% ^{235}U	50 GWd/tHM 4.2% ^{235}U	43 GWd/tHM 8.2 % Pu
^{234}U	5.2	20765.0 (U)	2.5×10^{5}	0.03%		
^{235}U	173.0		7.0×10^{8}	0.8%		
^{236}U	136.0		2.3×10^{7}	0.7%		
^{238}U	20424.0		4.5×10^{9}	98.5%		
^{237}Np	16.0	16.0 (Np)	2.1×10^{6}	100.0 %		
^{238}Pu	8.6	255.2 (Pu)	87.7	1.7%	3.4%	4.4%
^{239}Pu	125.3		2.4×10^{4}	58.8%	49.1%	37.4%
^{240}Pu	71.2		6.6×10^{3}	22.8%	27.9%	31.1%
^{241}Pu	30.3		14.3	11.7%	11.9%	14.5%
^{242}Pu	19.8		3.7×10^{5}	5.0%	7.8%	12.6%
^{241}Am	11.6	16.4 (Am)	432.7	72.6%	66.4%	61.2%
^{243}Am	4.8		7.4×10^{3}	27.2%	33.6%	38.8%
^{243}Cm	0.01	1.7 (Cm)	29.1	1.3%	0.6%	1.5%
^{244}Cm	1.5		18.1	92.9%	91.5%	86.8%
^{245}Cm	0.1		8.5×10^{3}	4.9%	6.2%	10.9%
^{246}Cm	0.03		4.7×10^{3}	0.8%	1.7%	0.7%

FFs	Isotope ($kg/GW_e/yr$)	Element ($kg/GW_e/yr$)	Half-life (yr)	Activity (Bq/GWe-yr)	Decay Q-value (MeV)[1]
^{79}Se	0.2	1.4 (Se)	1.1×10^{6}	2.4×10^{10}	0.15 (β^-)
^{90}Sr	15.0	26.0 (Sr)	28.79	8.1×10^{16}	0.55 (β^-)
^{93}Zr	23.1	117.8 (Zr)	2.1×10^{5}	2.4×10^{12}	0.03 (β^-)
^{99}Tc	26.6	26.6 (Tc)	1.5×10^{6}	1.6×10^{13}	0.29 (β^-)
^{107}Pd	7.5	14.6 (Pd)	6.5×10^{6}	1.4×10^{11}	0.03 (β^-)
^{126}Sn	0.7	2.4 (Sn)	1.0×10^{5}	7.4×10^{11}	0.38 (β^-)
^{129}I	5.8	7.1 (I)	1.6×10^{7}	3.9×10^{10}	0.19 (β^-)
^{135}Cs	12.5	85.7 (Cs)	2.3×10^{6}	4.6×10^{11}	0.27 (β^-)
^{137}Cs	35.8		30.1	1.2×10^{17}	1.18 (β^-)

As indicated in the previous table, the production rate of plutonium is about 255 $kg/GW_e/yr$, whereas the quantity of MAs produced is 34 $kg/GW_e/yr$. Concerning the FFs, the total amount present in the waste is approximately 800 $kg/GW_e/yr$ of which 130 $kg/GW_e/yr$ are LLFFs. Since the average energy production of a LWR is 1 GW_e these can be taken as the average values per reactor (LWR), loaded with ~26 tonnes of fuel.

Consequently, the quantity of nuclear waste produced worldwide by the 437 operating conventional nuclear power plants (producing 362.9 GW_e) during 2004 [16] totals ~7,930

1 The decay Q-value accounts for the energy of the parent isotope in the excited state minus the energy of the daughter isotope in the ground state, determining the maximum possible energy of the emitted β^-. Hence, the decay will take place through the emission of a β^- and its subsequent anti-υ_e carrying part of the energy of the excited nucleus, and possibly some characteristic γ's, which will take the daughter isotope to the ground state.

tonnes of which 7,535 comes from uranium. The remaining 395 tonnes are divided into 290 tonnes of FFs (of which 47 tonnes are LLFFs), 93 tonnes of plutonium and 12 tonnes of MAs. Extending these quantities to 40 years of average lifetime for a conventional nuclear reactor, the global stockpile of HLW rises to approximately 6,000 tonnes, assuming no further commissioning of new facilities (although there are 30 of these under construction and 32 planned and 72 proposed, in 2004).

These figures illustrate the great problem health and safety authorities in various countries are presently facing in order to manage these large amounts of HLW, with which something will eventually have to be done. Furthermore, the problem of military waste should also be considered, since the decay of the plutonium in the nuclear warheads, as well as the non-proliferation policies, may add a significant amount of radiotoxic material to the already large HLW stockpile.

The use of plutonium to enrich the uranium fuel (MOX) slows the increase of the plutonium stockpile to a certain extent (there is a limit on the quantity of the plutonium isotopes that can be added to the fuel due to their low delayed neutron fraction (β), as further explained in 2.3.2). This practice increases the production of MAs and plutonium isotopes resistant to thermal fission, thereby shifting the problem towards the accumulation of these species, also hindering the fuel reprocessing due to the high radiotoxicity of some of these isotopes. The use of MOX can be beneficial (as contemplated in the multi-tier strategies for closing the fuel cycle [9]) as long as the large amounts of TRUs produced are dealt with in an acceptable manner, since the accumulation of these species entails serious containment problems due to the diversity in the chemical nature of these elements (e.g. americium is a volatile element compared to plutonium).

2.2 Radiotoxicity and its Effects

The potential radiotoxicity is defined as the activity of a certain quantity of radionuclides weighted by the intake dose factors, thus indicating the dose received by all those who might have ingested or inhaled these substances. The calculation of this value obviously depends on the physical properties of the radionuclides, but also, and above all, on their post-incorporation biokinetics.

Actinides (mainly α and γ-decay) and LLFFs (β^- and γ-decay) present in the waste may therefore be ranked on the basis of their intrinsic hazard (effective dose coefficients, Sv/Bq) coupled with their radioactive concentrations in the spent fuel or HLW (Bq/tHM). In these terms, the following ranking can be made [17] for spent fuel seven years after discharge from

the reactor: $^{238, 239, 240, 241, 242}Pu > ^{241, 243}Am > ^{242, 243, 244, 245, 246}Cm >> ^{237}Np$. In spite of this classification, the short-term radiotoxicity of some FFs is comparable to that of actinides for approximately one century. Beyond 300 years only LLFFs remain significantly radioactive and, thus, their radiotoxicity represents 0.1% that of the actinides [9].

The radiotoxic inventory can also be related to the Annual Limits of Intake (ALI, [18]), thus defining the potential hazard index of the radionuclide as the ratio of the amount of the nuclide to its ALI value. Figure 2.1 shows the potential hazard over 10 million years of the HLW present in one tonne of spent fuel from a PWR (33 GWd/tHM and, uranium and 99.5% of the plutonium, recycled) and the level of radiological hazard of the 5 tonnes of natural uranium needed to produced this amount of fresh fuel.

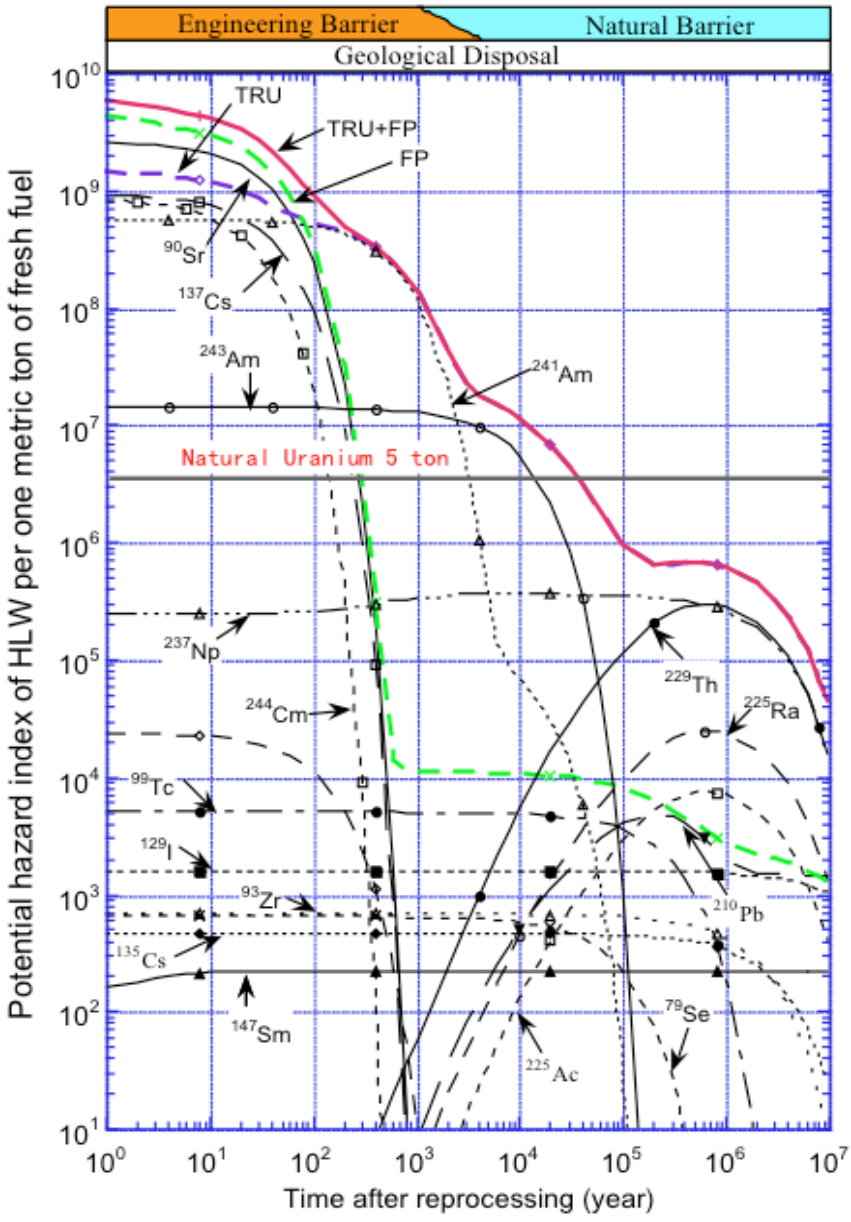

Figure 2.1. Potential hazard index of the HLW from PWR spent fuel [19].

The previous graph shows the influence on the radiotoxic inventory of the major isotopes present in the nuclear waste. For the first hundred years, the activity in dominated by the short and medium-lived FFs, principally ^{90}Sr and ^{137}Cs (assuming plutonium is mostly removed from the waste). Between one hundred and ten thousand years, the activity is primarily generated by the americium isotopes, to be later dominated by ^{237}Np due to its longer half-life and its production from the decay of ^{241}Am. The potential hazard of the LLFFs is orders of magnitude smaller than that of the MAs, but, since the confinement of all these species can only be guaranteed for a short period (compared to the duration of their activity), the high mobility of the LLFFs (and ^{237}Np) in the biosphere increases their potential danger.

2.3 Alternatives for Waste Disposal

Several alternatives for the final disposal of the HLW have been considered in order to close the fuel cycle. As mentioned earlier, sending the most hazardous materials into space, burying them in the shallow layer of the seabed or in the ice caps, and dumping them into the ocean trenches were discarded due to economic non-viability and the unpredictable consequences of an accident or a possible change in the environmental conditions.

Hence, the two favoured alternatives for nuclear waste disposal are storage in deep geological repositories, and the transmutation of the most hazardous elements in dedicated systems and the subsequent mid-term storage of the waste.

2.3.1 Storage in Deep Geological Repositories

The accumulation of the nuclear waste in underground facilities, vitrified or in any other solid or liquid form, has been favoured for a long time by the nuclear community due to the, allegedly, technical simplicity and low costs. Nevertheless, this solution presents serious conceptual problems related to the isolation of the radioactive species (some of them being water soluble) and the extended period of the required containment.

The basic requirement for any geological formation is its ability to contain and isolate the radioactive wastes from the human environment until the activity of the waste has decayed to non-hazardous levels. In order to reduce the probability of failure of confinement, most concepts rely on a system of independent, and often redundant, barriers such as leach-resistant waste compounds, corrosion-resistant containers or the nature of the geological formation. It is proposed to store permanently LWR waste directly from the reactor in bentonite (US) or after reprocessing and vitrification (Europe).

2.3.1.1 Decay heat production

Before the final disposal of HLW, some period of interim storage, either on site or at a centralised location, is needed due, in particular, to the high α activity of some isotopes, e.g. 1 cm^3 of ^{244}Cm (13.5 g/cm^3, $\tau_{1/2}$ = 18.1 yr and 5.9 MeV α-emission as the decay channel) generates 38 W of decay heat, which would raise the temperature of the same volume of water at a rate of 9 °C/s. During this time, the temperature and radioactivity of the HLW decrease systematically, making possible the later handling and transportation of the remaining waste.

Therefore, a cool-down period is necessary independent of the waste disposal method. Nonetheless, in the case of a final geological repository, a continuous amount of heat will have to be removed from the canisters, not only degrading the properties of the container materials but also resulting in a large decay heat release inside the storage cave, leading to high working temperatures for all the components involved in the storage, thus threatening the confinement of the waste. Furthermore, the risk of recriticality of the confined waste due to a change in the surrounding conditions, i.e. water infiltration, would amplify the degradation of the confinement [10]. In this aspect, a clear example of recriticality can be found today in Oklo (Gabon), where several natural reactors occurred about 2,000 million years ago.

2.3.1.2 Radioactive waste leakage into the biosphere

There are serious concerns about possible leaks to the biosphere of, principally, ^{135}Cs, ^{129}I, ^{99}Tc, ^{93}Zr and ^{237}Np after a long period of time. The filtration of these isotopes into underground water streams is a potential risk due to their high solubility. This would result in the release of a certain quantity of these species into the biosphere. The contamination of the water streams could have fatal consequences to the environment and the people living close to the repository.

Moreover, the permanent closure of the repository once filled up would make it impossible to repair the source of the leakage, transforming this problem into a permanent one with no easy solution.

2.3.1.3 Proliferation Aspects

On the other hand, the possibility of intrusions into the repository after its closure cannot be ignored. As mentioned in 1.2.4, since the use of nuclear power was first developed for military purposes, fear of the diversion of nuclear material towards the construction of weapons is obviously justified.

Currently, the use of nuclear material by a terrorist group to produce weapons is also a major concern. Since the waste contains a great amount of weapons-grade plutonium, nuclear waste repositories would be seen as major sources of these elements for a long period of time.

Moreover, the decay of some of the elements constituting the waste, such as ^{243}Am, could also generate a large amount of fissile material, literally producing plutonium mines in a few thousands years. Indeed, in 25,000 years the decay of 90% of this isotope would produce an almost pure ^{239}Pu mine.

2.3.1.4 Costs of the repositories

In addition to the previous drawbacks, it should be noted that storage of HLW in deep geological repositories is technically possible but not easy, and may turn out to be very expensive (~1000 US$/kg of spent fuel). The estimated costs of geological storage are shown in Figure 1.2, where the actual packaging and disposal, preparation and R&D costs are indicated. Reprocessing is added, whenever appropriate (700 US$/kg) [20].

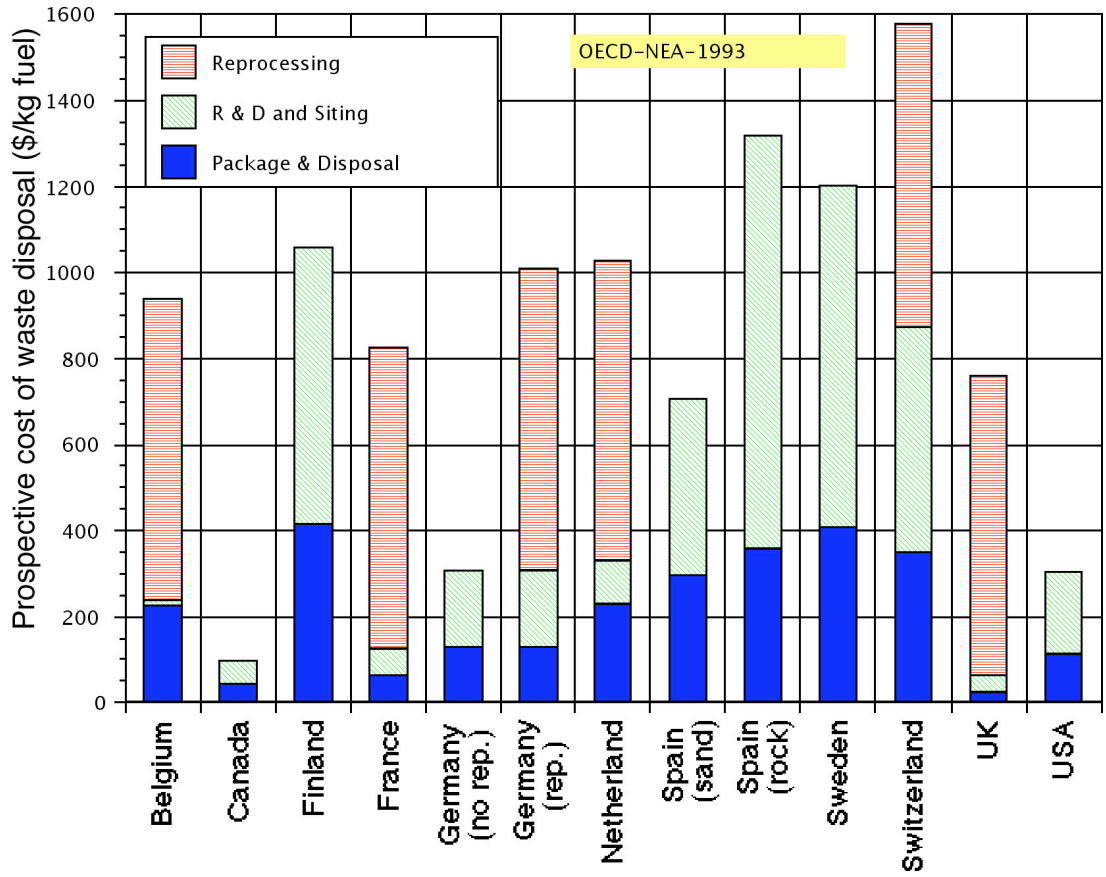

Figure 2.2. Estimated costs of geological waste disposal for unit fuel mass [20].

Underground storage may be performed either with or without reprocessing. Reprocessing is presumed to offer added security to containment, since it allows vitrification and optimal packing according to the nature of each element, but at extra cost. Note the large amount of R&D and siting costs before the actual packaging and disposal costs and the added costs due to reprocessing. These figures may well be underestimates, since, for instance, a full

benchmark study of all the consequences of deep storage of subcritical mixtures has not been performed and the additional costs of public opposition are still hard to assess.

The actual cost of a geological repository is therefore rather uncertain, as evidenced by the spread figures given in Figure 1.2. At the estimated cost of 700 US$/kg for Spain (for the sand solution and no reprocessing) this would represent a projected cost of about 7.7 billion US$ to store the waste produced by that country's 11 power generating nuclear reactors during their lifetimes [21].

2.3.1.5 Conclusion on storage in deep repositories

This strategy of disposal cannot be relied upon in the long term to provide the necessary permanent isolation of the HLW from the human environment, and future generations should not bear the risk of coexisting with the hazardous species left behind by their ancestors. The risk of intrusion into the repositories by a hostile group would present a threat not only to current international security but also into the future. Finally, it should be borne in mind that the cost of development of these repositories may well be beyond any of the present estimations, since the public opposition to the few ongoing projects has substantially increased the already high price of these facilities (e.g. the cost of the Yucca Mountain repository is ~60 Billion US$).

2.3.2 Transmutation of the Radioactive Waste

The elimination of radioactive species from nuclear waste has motivated the research of numerous scientists since the development of nuclear power for civil purposes. But public opinion and environmental concerns now make the full development of this kind of technology a priority. Since most of the long-term raditoxicity (99.99%) is due to a few isotopes (less than 1% of the waste, ~300 kg/GW_e/yr), the technical difficulties related to the handling of the different elements are greatly reduced. Moreover, the elimination of actinides clearly implies use of the fission process. As the technology to separate them chemically from the rest of the waste already exists, the option of producing transmutation fuel directly from these elements (after a cooling down period) may seem the most appropriate to simplify the process.

Figure 1.3 predicts the evolution of the radiotoxicity of the waste for different scenarios of HLW elimination. This plot shows the radiotoxicity of the MAs and LLFFs reaching the level of the radiotoxic inventory of 5 tonnes of natural uranium (needed to produce one tonne of fresh fuel) in about 40,000 years. If 90%, 99.5% and 99.9% of MAs and LLFFs were eliminated from the waste, the radiotoxicity would reach the indicated level in 2,500 years, 400 years and 300 years respectively. This large reduction in the potential hazard from the

waste would result in a qualitative change in dealing with the HLW, since engineering barriers could ensure the safe storage of the remaining waste. It should be noted that, even if transmutation were chosen as a method to eliminate HLW, some kind of disposal strategy would also be needed, although the requirements for this type of storage would be less stringent.

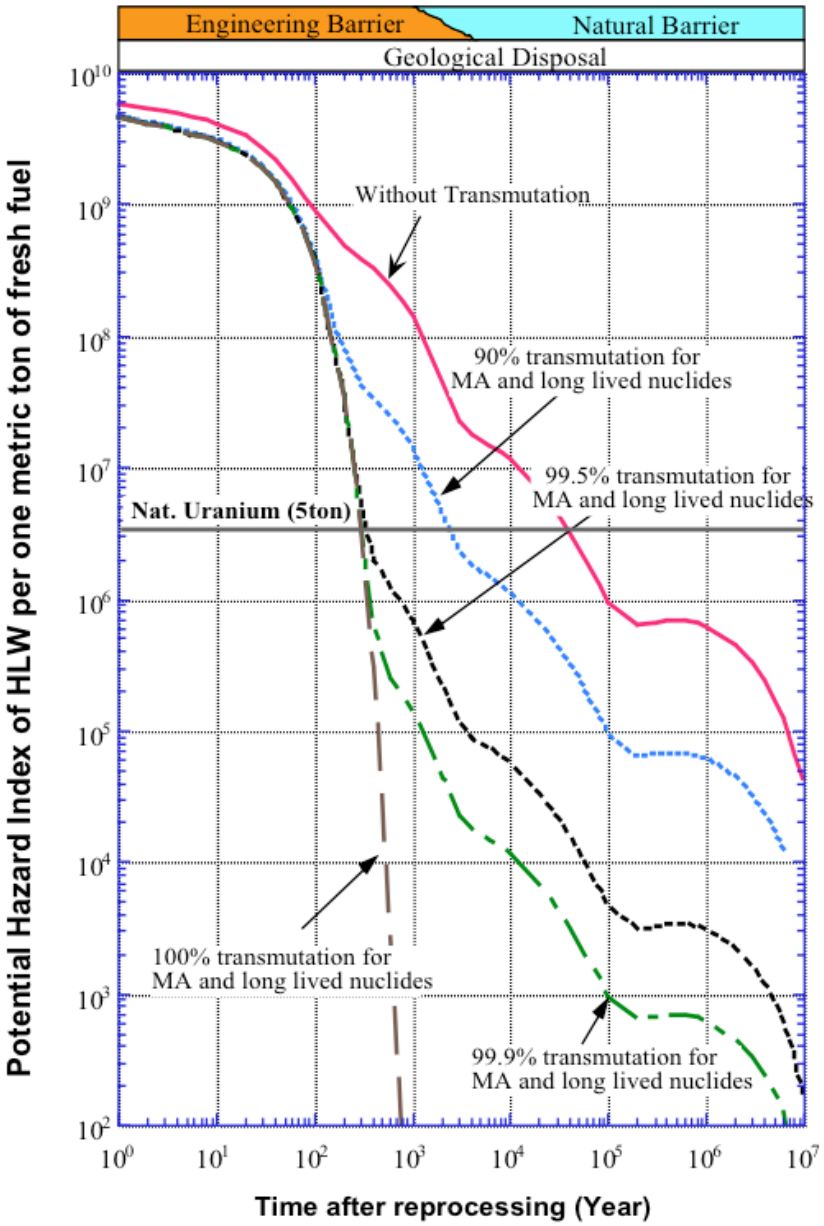

Figure 2.3. Evolution of the potential hazard index before and after transmutation of the HLW [19].

At first glance, the elimination of the HLW could be carried out by adding small fractions of these elements to the LWR fuel or configuring dedicated pins in order to transmute these isotopes. This approach has major drawbacks due to the fact that MAs generally present small fission cross-sections at thermal energies. Figure 1.4 shows the fission and the capture cross-

section for ^{240}Pu and the ratio between both as a function of the energy of the absorbed neutron. This ratio increases dramatically for neutron energies above 100 keV for all actinides (even for the fissile ones), as exemplified by the cases of ^{240}Pu and ^{241}Am. The low values of the fission-to-capture ratio for thermal energies would degrade the neutron economy in the reactor, thus forcing an increase in enrichment, and, for some isotopes, the TRU production rate would be greater than the removal rate [22].

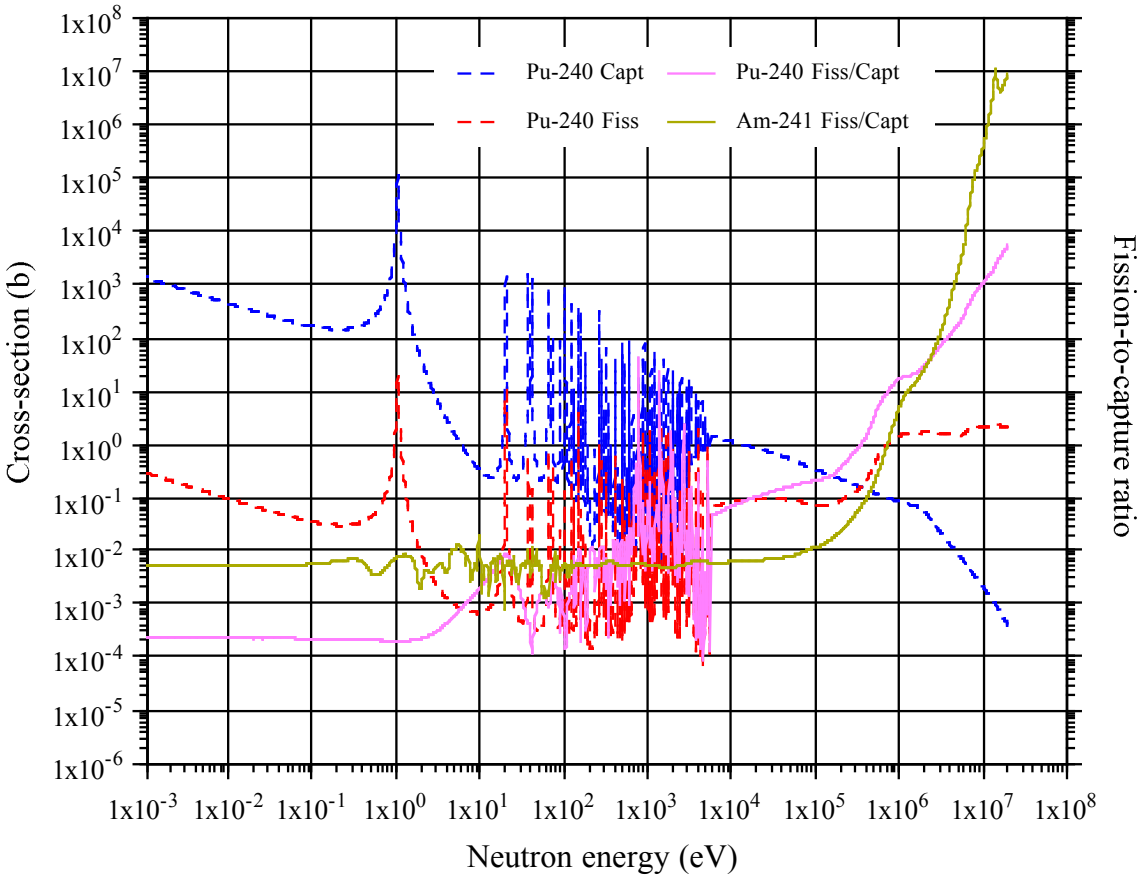

Figure 2.4. Comparison between fission and capture cross-sections vs. neutron energy for ^{240}Pu and ^{241}Am.

The transmutation of LLFFs at thermal energies would theoretically be possible, but, since the capture cross-section at this energy range is generally small for most LLFFs, high neutron fluxes (considerably larger than the usual LWR flux of ~10^{14} n/cm^2/s) would be needed in order to produce significant transmutation rates.

Therefore, a transmutation strategy for HLW based on a conventional LWR would not really be feasible and would be technically inefficient. In such a case, the use of fast neutrons would increase the transmutation of MAs through a two-fold effect: First, increasing the probability of fission, and thus, destruction of the MAs, and, second, reducing their production by capture. For the LLFFs, a fast system could benefit from a high neutron flux (~10^{15} n/cm^2/s), in particular at the epithermal energy range, where the capture resonances, and thus the high

capture probabilities, lie. This method is known as Transmutation by Adiabatic Resonance Crossing (TARC) [23], and is explained in more detail in 3.2.1.2.

Nevertheless, the transmutation of TRUs in critical systems, especially in fast systems where the prompt neutron lifetime tends to be shorter, presents serious safety problems. As shown in Table 2.2, the fraction of delayed neutrons emitted per fission for TRUs is several times smaller than that of ^{235}U and ^{238}U. This fact has enormous implications for the control of the reactor by reducing the already short reactor period of a fast system (typically 0.1 μs for a fast-breeder/burner reactor, FBR [24]). Therefore, the insertion of a significant amount of HLW would degrade the kinetic properties of a critical reactor hindering the control of the system.

Table 2.2. Values of ν and β for relevant actinides at 500 keV extracted from ENDF/B-VI nuclear data library.

Isotope	Neutrons per fission (ν)	Delayed neutrons per fission	Delayed neutron fraction (β)
^{232}Th	3.21	0.053	1.66%
^{233}Th	2.08	0.074	3.57%
^{233}Pa	2.20	0.023	1.03%
^{233}U	2.50	0.007	0.27%
^{234}U	2.43	0.010	0.43%
^{235}U	2.49	0.016	0.65%
^{236}U	2.44	0.022	0.92%
^{238}U	2.52	0.048	1.91%
^{237}Np	2.61	0.012	0.47%
^{238}Pu	2.97	0.005	0.16%
^{239}Pu	2.94	0.006	0.21%
^{240}Pu	2.86	0.009	0.32%
^{241}Pu	3.01	0.016	0.53%
^{242}Pu	2.95	0.018	0.62%
^{241}Am	3.30	0.005	0.14%
^{242}Am	3.36	0.007	0.19%
^{243}Am	3.29	0.010	0.29%
^{244}Cm	3.34	0.004	0.13%
^{245}Cm	3.60	0.006	0.17%

Moreover, TRUs present in general little or no negative reactivity feedbacks due to Doppler broadening in the capture resonances; thus, the use of dedicated fuels for transmutation, lacking isotopes with large capture resonances such as ^{238}U, would degrade the temperature safety parameters of a reactor loaded with this fuel [25]. For a critical system, this process could have undesirable consequences in the overall safety parameters of the reactor, whereas for a device continuously operating below criticality it may be acceptable.

Another possible alternative would be the direct use of high-energy neutrons (e.g spallation neutrons) to transmute this waste. In this case, roughly 30% of the energy produced in a

fission reaction (~60 MeV out of 200 MeV/fission) would be needed just to transmute the LLFFs [26]. This option seems economically unviable, since the process is highly inefficient and it would imply spending a very large amount of the energy produced in the nuclear power plants to eliminate just part of the radioactive waste.

Hence, the transmutation of HLW in a subcritical fast system seems the most technically feasible and economically viable alternative. In order to maintain operation in such a system, an external neutron source would be needed. Generally, a proton accelerator is proposed to make up the deficit of neutrons to maintain criticality through the spallation reaction. Such a device, commonly called an Accelerator-Driven System (ADS) would have the advantage of a flexible fuel configuration (including the use of large amounts of TRUs and LLFFs) since it could operate at different subcriticality levels. In fact, as estimated in [25], the minimum level of subcriticality (multiplication coefficient, k_{eff}) in which such a device could operate in order to be self-sufficient is $k_{eff} \sim 0.7$, although generally an ADS would be designed to operate in the range $0.90 < k_{eff} < 0.99$. Chapter 3 thoroughly describes these systems, with special attention to their physics underlying their design.

Chapter 3

ADS Background and Physics

As explained in the previous chapters, accelerator-driven subcritical reactors represent a realistic and viable technology for the elimination of high-level nuclear waste. The potential elimination of the entire HLW stockpile by using a diverse range of fuels represents a major advantage of these systems.

Although classical neutron diffusion theory can be applied to the analysis of an ADS, analogously to conventional nuclear reactors, there are certain aspects of their operation that require detailed analyses due to, for example, the presence of an external neutron source. These individualities have produced new research perspectives in the mature field of reactor physics, recently inducing experiments in order to validate innovative concepts specifically developed for the field of ADS, such as the neutron source importance.

The analysis methods also require revision given that these systems involve interactions of high-energy charged particles (hundreds of MeV) and heterogeneous fuel compositions. Theses peculiarities make Monte Carlo (MC) methods particularly suitable for the simulation of these systems, facilitating the design of the systems and analysis of their evolution in time.

3.1 ADS Description

The term accelerator-driven subcritical system, or ADS, refers to a device formed by the coupling of a subcritical nuclear reactor core with a charged-particle accelerator, generally a proton cyclotron or a proton linear accelerator (LINAC), as illustrated by Figure 3.1. In such a system, the energy is produced as the result of the multiplying nuclear cascades initiated by

the accelerated protons (or charge particles) interacting with the spallation target, rather than of a self-sustained chain reaction as in conventional nuclear reactors.

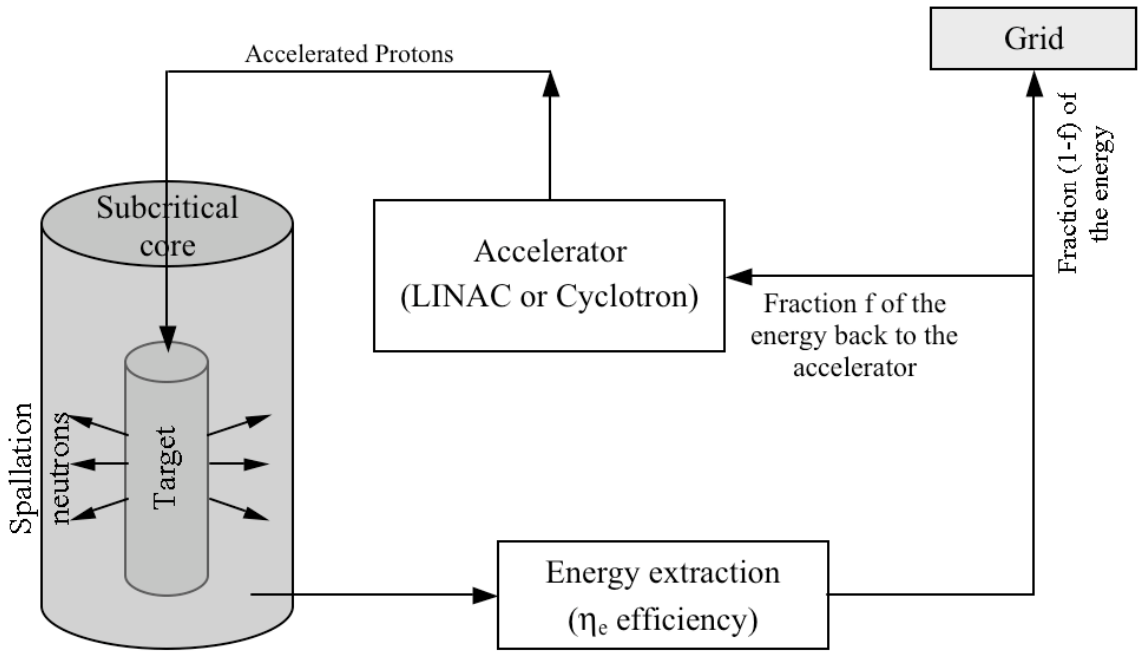

Figure 3.1. Schematic view of the main components of an accelerator-driven system (ADS).

The term subcritical refers to the fact that an ADS operates in a non-self-sustained chain reaction mode (the usual values of the neutron multiplication coefficient are $0.95 \leq k \leq 0.98$), thus minimising the possibility of criticality. The subcritical configuration depends on the fission-to-capture ratio (and hence on the fuel composition, core geometry, proton energy etc.) but it is independent of the proton current.

A subcritical blanket surrounds the spallation target, multiplying the spallation neutrons through fission; therefore, all nuclear processes in the core are subordinated to the operation of the accelerator, and the power produced is directly proportional to the intensity of the injected beam, thus providing a mechanism for controlling the operation of the core and the output power, reducing the number of mechanical elements to control the reactor. Figure 3.2 shows a comparison between the nuclear processes taking place in a conventional nuclear critical reactor and in an Energy Amplifier (EA) [1], a lead-cooled ADS originally designed at the European Organisation for Nuclear Research (CERN). Figure 3.3 shows the general layout of the Energy Amplifier Demonstration Facility (EADF [27]), a prototype designed to validate the concept of the EA, highlighting the main components of the reactor core.

As a consequence of the subcritical operation and the decoupling of the neutron source (producing spallation neutrons) from the fissile fuel (generating fission neutrons), the range of

possible fuels broadens, allowing the incorporation in the fuel of elements such as MAs, high plutonium contents and LLFFs, which degrade the neutronic characteristics of the nuclear core to unacceptable levels in critical reactors.

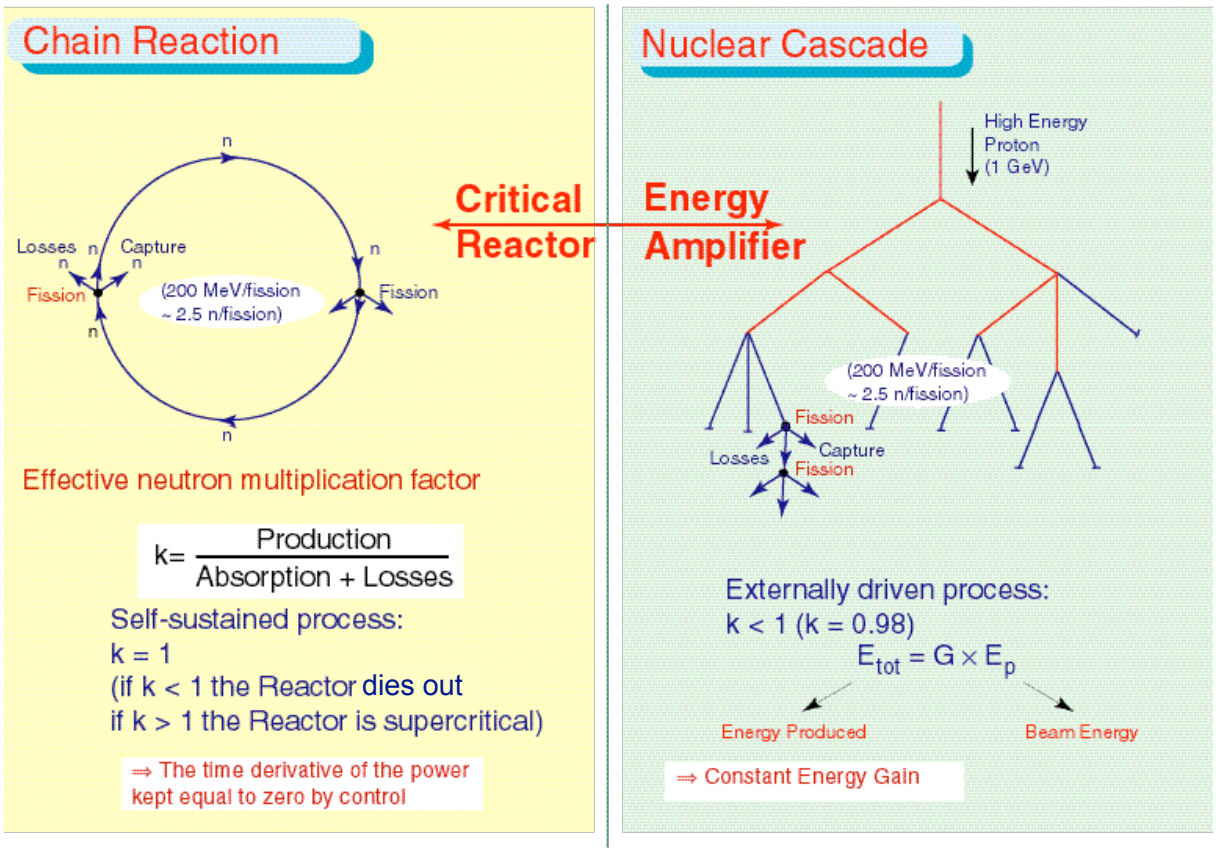

Figure 3.2. Comparison of the nuclear processes involved in the operation of a critical reactor and an ADS [26].

The energy gain, G, is defined as the energy produced in the ADS relative to the energy dissipated by the high-energy proton beam, and it is given by Equation 3.1:

$$G = \frac{G_0}{1-k} = \frac{G_0}{1-\eta\cdot(1-L)} \qquad \text{(Eq. 3.1)}$$

where G_0 is the gain proportionality constant, typically 2.4-2.5 for a properly designed ADS [1] (validated through the FEAT experiment [28]); k is the fission-driven multiplication coefficient $k = \eta\cdot(1–L)$; L is the sum of fractional losses of neutrons (lost through several processes, such as captures in structure and coolant, in fission-product poisons, leakage from the vessel etc.); η is the spectrum-averaged number of fission neutrons produced by a neutron absorbed in the fissile isotope.

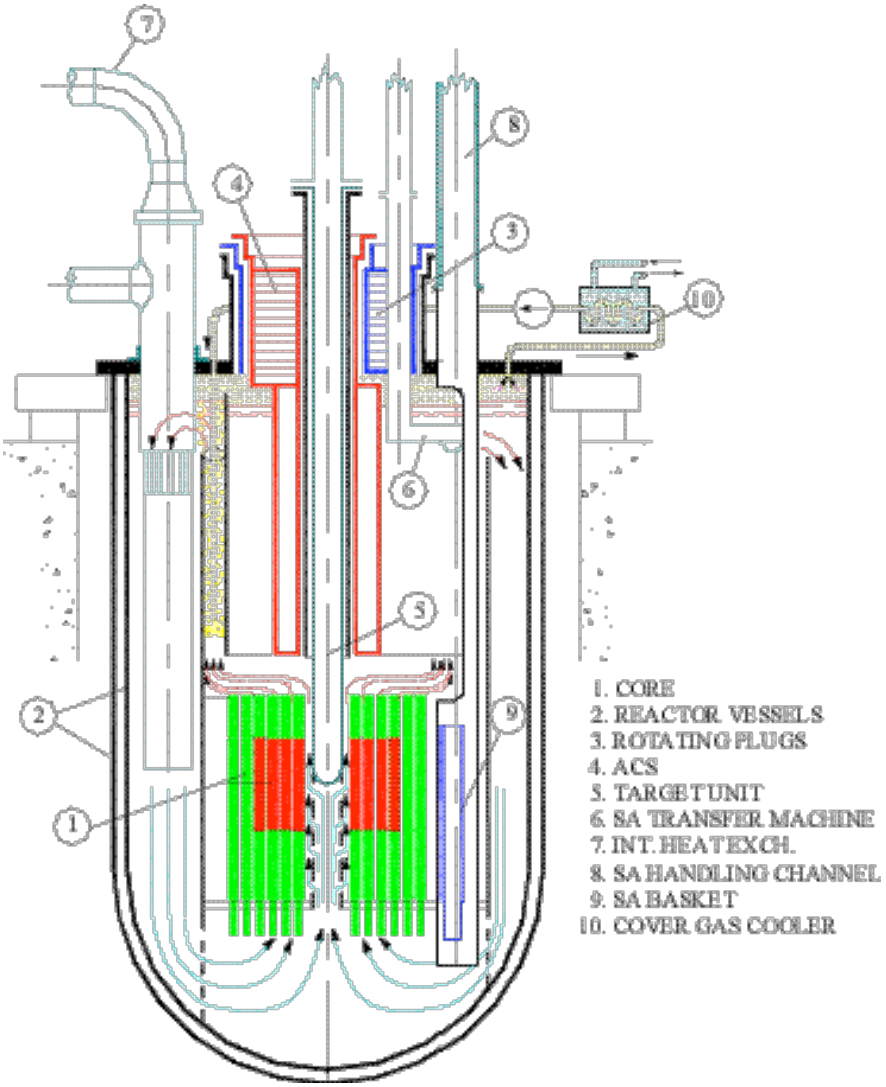

Figure 3.3. Schematic layout of the EADF reactor core and auxiliary systems [27].

3.2 History of the Accelerator-Driven Systems

Even though it is only in the last few years that ADSs have become widely known to the public, the history of these systems goes as far back as the military nuclear program itself. The use of an accelerator in nuclear physics for different purposes (e.g. to produce exotic isotopes or to drive a subcritical core) has been extensively explored on several occasions in the last fifty years, but it is only now that technological developments, both in accelerator science and in reactor technology, permit the construction of a full power accelerator-driven subcritical device.

3.2.1 Early History

In 1941, G. Seaborg produced the first man-made plutonium using an accelerator. However, the first practical attempts to promote accelerators to generate potential neutron sources were made in the late 1940's by E.O. Lawrence in the United States, and W.N. Semenov in the former Soviet Union. During the period 1950-54, the MTA (Materials Testing Accelerator) programme [29] at Lawrence Livermore (at that time the Livermore Research Laboratory) investigated in detail the use of accelerators to produce fissionable material. This project was soon abandoned when high-grade uranium ores were discovered in the United States.

Almost concurrently in Canada, W.B. Lewis realised the value of accelerator breeding in the power programme and initiated spallation neutron yield measurements with the McGill cyclotron [30]. The Canadian team at Chalk River has always been a strong proponent of such a producer of fissile material, which could be used in conjunction with a conversion-efficient CANDU reactor.

A materials production accelerator – the Electronuclear Reactor – was patented in 1960 by Lawrence et al. [31] to provide adequate quantities of material that could only be produced artificially. The targets considered were natural uranium and thorium and the artificially produced materials were ^{239}Pu and ^{233}U respectively. This concept of accelerator breeding was also studied by Russian scientists who, under the guidance of V.I. Goldanski and R.G. Vassylkov, made a neutron yield experiment in depleted uranium blocks using the accelerator in Dubna. Later studies (1975-88) in the Fertile-to-Fissile Conversion (FERFICON) Programme [32] – a collaborative effort between various laboratories – investigated the energy dependence, up to 800 MeV, of the fertile-to-fissile conversion efficiency using standardised target materials and geometries.

A rather realistic ADS concept in the present sense, where safety issues and transmutation of waste play an important role, was developed in the late 1980's by a research group at Brookhaven National Laboratory led by H. Takahashi and G. Van Tuyle and is now being researched in Japan as part of the OMEGA programme [33].

The first detailed design of a transmutation facility using thermal neutrons was published by C. Bowman's Los Alamos group in 1991 introducing a common name: The Accelerator Transmutation of Waste (ATW) [34 & 35].

In 1993 a group of CERN scientists led by C. Rubbia presented the basic concepts of a so-called "Energy Amplifier" [1], a subcritical nuclear system based on the thorium cycle, fed by a high intensity proton accelerator, intended to generate energy with small amounts of MAs and LLFFs production. Later on, the scientific feasibility and verification of the principle of

energy amplification by a high-energy cascade were established in experiments such as FEAT [28] (autumn 1994) and TARC [23] (1997-1998).

3.2.1.1 First Energy Amplifier Test (FEAT)

The concept of the EA was originally developed on the basis of a computer simulation of the rather complex interplay between the production of neutrons by spallation and their subsequent fission-based multiplication in a subcritical assembly. Even though there existed indirect evidence that these simulations were valid, there was an obvious need to test this concept in a small experiment.

The main idea, which gave the EA its name, was the production of a great amount of energy from an initial energy source, supplied by the accelerator in the form of kinetic energy to the protons. The concept of G is therefore immediate; this gain was predicted to be 30-60 [1]. The main purpose of FEAT was therefore to ascertain that there was such a gain and that its magnitude was in agreement with the value predicted by the FLUKA / EA-MC [36, 37 & 38] simulations. The experiment was carried out at CERN with the participation of research groups from France, Greece, Italy, Spain and Switzerland.

The overall power produced in the experiment was 1 W, and the energy of the incoming protons could be varied; therefore the relation between the gain and the proton energy could be measured. The validation of the MC simulations that came from the agreement with the experiment was another basic goal achieved through FEAT. Once the energy released was calculated for different incoming proton energies, the results showed that the relationship was like that of a first-order system, with constant gain above 1 GeV, and decreasing significantly below 800 MeV, as shown in Figure 3.4.

The neutron distribution in the experiment was calibrated with an Am-Be neutron source inserted in the centre of the device. The results confirmed the expected exponential behaviour as a function of the distance from the source. The multiplication factor for a point-like centred source was found to be $k = 0.915 \pm 0.010$. This was in good agreement with the MC simulations which gave $k = 0.920 \pm 0.005$ [38].

The results demonstrated that using the critical reactor formulation to describe a subcritical system was inaccurate, since all the higher harmonics from the solution of the diffusion equation with an external neutron source needed to be evaluated, not just the fundamental one. They also validated the precision of the FLUKA / EA-MC code results applied to these source systems.

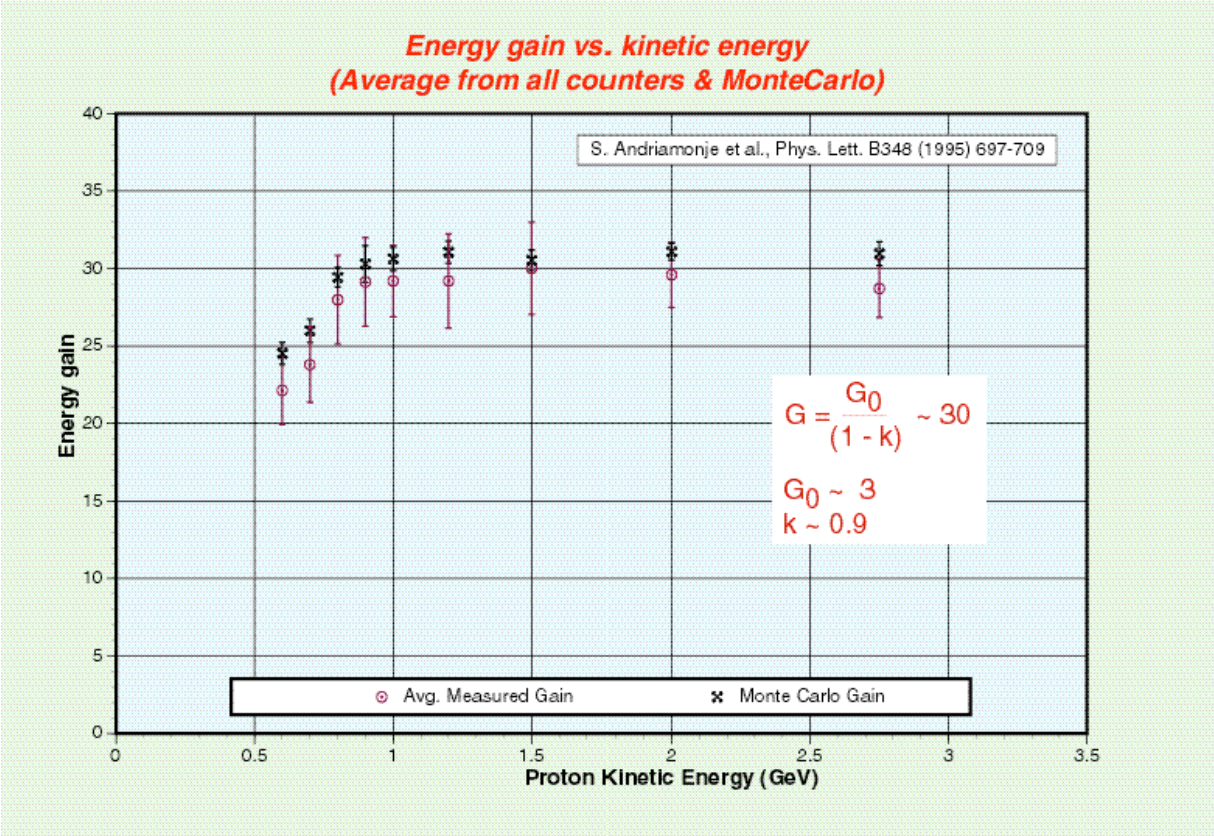

Figure 3.4. Average energy gain as a function of the proton beam kinetic energy in the FEAT experiment [28].

3.2.1.2 Transmutation by Adiabatic Resonance Crossing (TARC)

This experiment was part of a wider research program to test some of the physics concepts in the field of radioactive waste elimination. In an ADS dedicated to nuclear waste transmutation, where the TRUs are destroyed by fission, the long-term radiotoxicity would be dominated by LLFFs, whose elimination generally involves neutron capture followed by nuclear decay. The main goal of this experiment was to test the idea of adiabatic resonance crossing (ARC), based on the properties of spallation neutrons diffusing in lead, to efficiently transmute LLFFs. The object was also to perform a systematic study of the phenomenology of spallation neutrons in pure lead.

Neutrons were produced by spallation at relatively high energy (some MeV), and, after having been promptly moderated through (n, xn) and inelastic scattering (n, ni) reactions down to energies of a few hundred keV, they were slowed down quasi-adiabatically, with their energy decreasing by small steps and reaching the capture resonance energy of an element to be transmuted, where neutrons have a high probability of being captured. This is the case for ^{99}Tc, which has a strong neutron capture resonance at 5.6 eV (4000 barns), covering four average lethargy steps in lead. The ^{99}Tc resonance integral is 310 barns, while the cross-section at thermal neutron energies is only of the order of 20 barns. Neutron capture in ^{99}Tc

($\tau_{1/2}$ = 211,100 yr) produces ^{100}Tc ($\tau_{1/2}$ = 15.8 s), which then decays to ^{100}Ru, a stable element. Thus, the radiotoxicity could be eliminated in a single neutron capture, and, since ^{100}Ru has a small neutron capture cross-section and both ^{101}Ru and ^{102}Ru are stable, essentially, no new radioactive elements were produced. Figure 3.5 shows a schematic view of the TARC experiment, numbering the different positions where samples were placed inside the lead block, were and describes the underlying physical principles. The source (spallation) neutrons are produced at high energies and are diffused inside the lead bloc to produce an isolethargic spectrum. The resonance capture probability is therefore maximised due to the small energy steps in the neutron moderation.

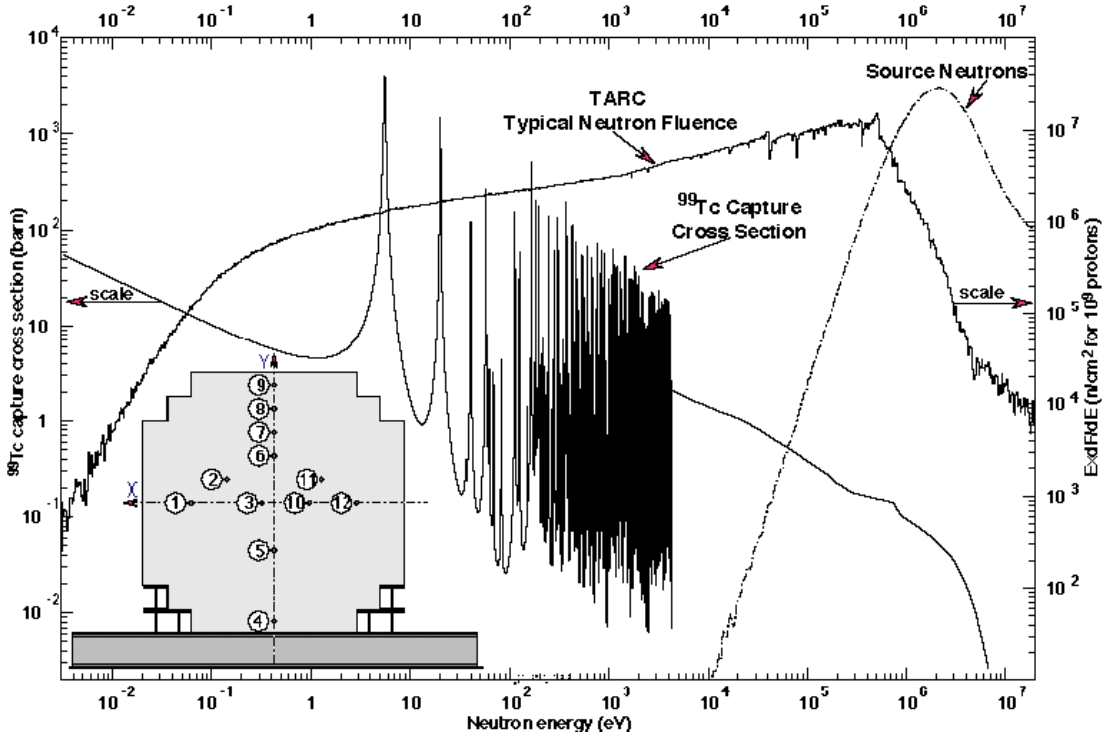

Figure 3.5. Principles and layout of the TARC experiment [23].

The experiment was designed in such a way that several basic processes involved in accelerator-driven systems could be studied in detail. The neutron production by GeV protons hitting a large lead volume and neutron transport properties were analysed, and the efficiency of transmutation of LLFFs in the neutron flux produced by spallation neutrons was assessed. The entire program was fulfilled by performing neutron flux measurements over an energy range from thermal up to a few MeV, and neutron capture rate measurements on ^{99}Tc and on ^{127}I and ^{129}I. A comparison of the experimental results with the MC simulations was also performed, further validating these computational tools for transmutation purposes.

3.2.1.3 MUltiplication Source Externe (MUSE)

MUSE (1-4) is a series of experiments hosted by the French Commissariat à l'Énergie Atomique (CEA) in the MAquete SURgénératrice de CAdarache (MASURCA) facility in CEA-Cadarache. The general purpose of these experiments was to study the physics of subcritical systems coupled with an accelerator, to understand the physical phenomena involved in their modelling and validate experimentally the main principles of these systems. These studies were conducted in a low power mock-up (< 5 kW) of a subcritical assembly, where temperature effects are negligible. The mock-up was coupled to a well-calibrated external neutron source, in terms of intensity and neutron energy, allowing the separation of the experimental validation of the multiplying medium behaviour from the experimental validation of the source characteristics.

This program started in 1995 with the short, exploratory MUSE-1 experiment [39], providing some insight into the physical behaviour of the neutron population in subcritical systems. and the MUSE-2 experiment [40], in 1996, devoted to the experimental study of diffusing materials (sodium and stainless steel) placed around the external source.

The MUSE-3 experiment was performed [41] over three months in 1998. An external neutron source (~10^8 n/s) based on the (d, t) reaction was used. This neutron generator operating in both continuous and pulsed modes allowed the completion of the study of diffusing materials (sodium and pure lead) and the exploration of the dynamic behaviour of the multiplying medium for different subcriticality levels, and the observation of the dependence of the core responses as a function of the subcriticality levels.

From 2000 to 2003, the MUSE-4 [42] experiments were performed within the framework of a large international collaboration including research and technology institutes from Belgium, Germany, UK, Italy, The Netherlands, Spain and Sweden, via the EURATOM 5th Framework Program of the European Commission (EC). The MUSE-4 program was based on a parametric approach (1 critical + 3 subcritical sodium-cooled configurations, 1 configuration with a lead-cooled zone, 2 kinds of target, and variation of the neutron generator frequency) and on the use of several experimental techniques and analysis methods. These methods were aiming to study, first, the decreasing neutron population after the modification of the source level by the pulsed neutron source method and frequency variation method), and, second, the neutronic fluctuations in the fission chains (noise measurements). The determination of the reactivity level was of prime importance among the other neutronic parameters, since this assessment is decisive for the acceptability of an ADS. The validation of the simulation techniques and nuclear data (ND) to properly predict ADS behaviour was also a major objective of these tests.

3.2.2 Recent developments in Europe

In 1998 the Research Ministers of France, Italy and Spain, recognising the potential of ADSs for the transmutation of HLW, decided to set up a group of advisors (Ministers' Advisors Group – MAG) to define a common R&D European platform for ADS.

A Technical Working Group (TWG) under the chairmanship of C. Rubbia was also established with the task of identifying the critical technical issues in which R&D in such a demonstration programme is needed. In October 1998, the TWG issued an interim report [43], which, in particular, highlighted the need for a demonstration programme, the basic components and the different options for the proposed facility, and the R&D directly relevant to the realisation of such a facility.

In September 1999, the European TWG – composed of representatives of Austria, Belgium, Finland, France, Germany, Italy and Spain – issued a new technical report [44] aimed at providing an overview of the different ongoing ADS activities in various European countries.

In 2000, the ETWG (further enlarged to include representatives of the EU-Joint Research Centres, Portugal and Sweden), recognising that the ADS R&D programme had reached a turning point with regard to programme co-ordination and resource deployment in Europe, and also taking into account the substantial recent progress on the subject in the United States and in Japan, issued a so-called "four-page document" [45] on a strategy for the implementation of an ADS programme in Europe. In particular, the document called for the urgent definition of a consensual European "Roadmap" towards the demonstration of feasibility of a European waste transmutation facility.

In the European Roadmap towards the experimental demonstration of ADS [46], several experiments are indicated which should allow the validation of the separate components of an ADS. This is the case for the accelerator (IPHI [47], TRASCO [48]), the spallation target (e.g. the MEGAPIE experiments [49]) and the subcritical core (FEAT, TARC and MUSE). The coupling of the components will be performed in a new system, with all innovative features included, with the exception of the subcritical core fuel, for which further research should be carried out. However, the case for the licensing of such a system will present some difficulty, in the absence of a preliminary coupling experiment at power. A way forward is simply to set up an experiment where an "existing" low power reactor, with well-known safety features, is made subcritical and coupled with an accelerator, which should provide the needed protons to induce spallation reactions on a target hosted inside the core.

As regards coupling, such an experiment would not need a high neutron yield from spallation. In fact, it could run with a neutron per proton production rate as low as one, since an optimisation in terms of efficiency or transmutation will not be a requirement.

The domain of interest of such an experiment would be to demonstrate reliable system operation, from start-up to nominal power level, up to shutdown, in the presence of thermal reactor feedback effects. The presence of control rods in the system would allow the verification of different modes of operation during fuel irradiation and the determination and monitoring of reactivity levels with ad hoc techniques. The joint cooling of the target and of the subcritical core would be demonstrated, together with the solution of some practical engineering problems of generic interest for an ADS, such as the configuration of the beam access to the core.

The possibility of running the experiment at different levels of subcriticality (e.g. achieved by appropriate fuel loading patterns), would allow experimental exploration of the transition from an "external" source-dominated regime, to a core thermal-feedback-dominated regime. This transition is relevant, in particular, to understand the dynamic behaviour of an ADS, which, in the future full-scale demonstrations of transmutation, could have both a very low β and very low Doppler reactivity feedbacks.

The proposed location for this pilot experiment, which would be the first example of ADS component coupling at "real size", is the TRIGA reactor at the ENEA-Casaccia Centre (Italy), an existing pool reactor of 1 MW thermal power, cooled by natural convection of water in the reactor pool. The TRADE project [50] is based on the coupling of an upgraded commercial proton cyclotron with a tantalum solid target, surrounded by the TRIGA reactor in a subcritical configuration, as further explained in Chapter 5.

3.3 ADS Physics

As previously mentioned, ADS are nuclear multiplicative assemblies that operate in a subcritical configuration with the help of an external neutron source. This provides specific characteristics to these systems, such as operational flexibility and safety, and the ability to use a wide range of fuels. Hence, the basic physics that governs these systems is different to that of conventional critical reactors. In addition, the operation and behaviour in accident conditions require specific technological considerations, new to reactor engineering.

This section reviews the basic physics principles involved in the operation of such a device and the processes driving the major components of an ADS, i.e. the external neutron source and subcritical assembly. The sections on neutron multiplication in a subcritical system and diffusion in the coolant examine general nuclear reactor concepts from the specific point of view of a subcritical assembly subject to a non-thermal neutron spectrum.

3.3.1 The Spallation Process

The concept of spallation covers the interaction of high-energy (from a few tens of MeV to a few GeV) hadrons or light nuclei with nuclear targets. In other words, it corresponds to the reaction mechanism by which a high-energy hadronic projectile knocks out of the nuclear target some nucleons and/or light particles, leaving a residual nucleus (spallation product). Depending upon the conditions, the number of emitted light particles, and especially neutrons, may be quite large. This is, of course, a feature of utmost importance for an ADS. Figure 3.6 describes the spallation reaction produced by a 1 GeV proton in a group of heavy nuclei.

At such a high projectile energy – high compared to the most probable energy of thermal neutrons (the peak in the Maxwell distribution of energies [51]) of 0.0253 eV – it is no longer correct to think of the nuclear reaction as proceeding through the formation of a compound nucleus. As shown in Figure 3.6, high-energy protons produce a wide range of reactions through the interactions with the nuclei. At first, the fast direct process induced is an Intra-Nuclear Cascade (nucleon-nucleon collisions inside the nucleus); this reaction depends on the geometrical cross-section of the different elements rather than the common reaction cross-sections used at lower energies. Pre-Compound Stage (including pre-equilibrium, multi-fragmentation, Fermi break-up) and Compound Nuclei (evaporation of neutrons mostly and high-energy fissions) are subsequent models of interactions between the secondary particles and the nuclei of the spallation source. Finally, Low-Energy Inelastic Reactions – (n, xn), (n, α), (n, γ), etc. – are produced once the energy of the secondary particles has decreased below a certain threshold (assumed to be around 20 MeV for neutrons).

The relevant aspects of the spallation process are mainly characterised by:

- *Spallation Neutron Yield* (i.e. multiplicity of emitted neutrons), which determines the requirement in terms of the accelerator power (current and energy of incident proton beam).
- *Spallation Neutron Spectrum* (i.e. energy distribution of emitted neutrons), which determines the damage to and activation of the structural materials (design of the beam window and spallation target) and the kind of materials to be transmuted by the source. The spectrum of spallation neutrons evaporated from an excited heavy nucleus bombarded by high-energy particles is similar to the fission neutron spectrum slightly shifting to higher energies. The average neutron energy $\langle E_n \rangle \approx$ 3-4 MeV, higher than the ~2 MeV of the fission neutrons due to the contribution of direct knockout neutrons. This higher average energy makes these source neutrons more suitable transmuting elements with different resonance spectra, although the damage to the structural materials is also more intense.

- *Spallation Product Distribution,* determining the radiotoxicity of the residues (radioprotection requirements).
- *Energy Deposition*, which determines the thermal-hydraulic requirements (cooling capabilities and nature of the spallation target).

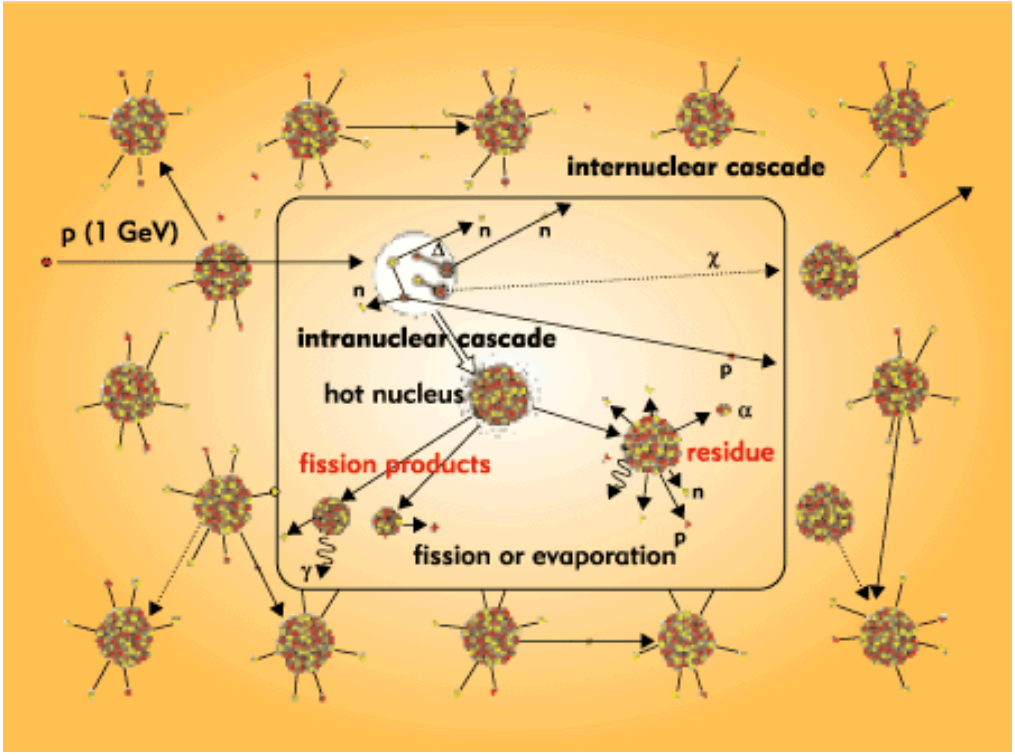

Figure 3.6. Representation of the spallation process caused by a proton interacting with heavy nuclei [52].

Several nuclear reactions are capable of producing neutrons, as presented in Table 3.1, which summarises the most common accelerator-based neutron sources. However the use of protons minimises the energetic cost of the neutrons produced, especially because of the high neutron yield and the simplicity of their production.

Table 3.1. Neutron sources based on fusion, photonuclear, fission and spallation reactions [26 & 53].

Nuclear reactions	Incident particle & typical energies	Beam current (part/s)	Neutron yield (n/inc.part.)	Target power (MW)	Energy deposited per neutron (MeV)	Neutrons emitted (n/s)
(e^-, γ) & (γ, n)	e^- (60 MeV)	5×10^{15}	0.04	0.045	1500	2×10^{14}
^3H (d, n) He^4	^2H (0.3 MeV)	6×10^{19}	$10^{-5} - 10^{-4}$	0.3	10^4	10^{15}
Fission			~1	57	200	2×10^{18}
Spallation (non-fissile target)	p (1 GeV)	10^{15}	14	0.09	37	2×10^{16}
Spallation (fissile target)			30	0.4	55	4×10^{16}

Deuteron and triton projectiles produce more neutrons by spallation than protons in the energy range below 1-2 GeV, but they also produce a higher contamination of the accelerator (activation of the cyclotron).

The number of emitted neutrons varies as a function of the target nucleus and the energy of the incident particle; for protons as projectiles, it saturates around 2 GeV. Figures 3.7(a) and 3.6(b), produced by the author using the FLUKA Monte Carlo code, show this fact, as well as the neutron yield for different elements. Clearly, heavier elements, such as natural uranium (actinides in general), produce a higher number of neutrons by spallation; the main drawback is that they may also fission and the products of both reactions are highly radioactive. On the other hand, the most efficient energies to produce spallation neutrons are given by the ratio between the neutron yield and the proton energy, shown in Figure 3.7(b). In the case of lead, the maximum yield is obtained at ~1.2 GeV whereas for a lighter nuclei such as aluminium the optimal energy is ~0.6 GeV. For elements presenting higher yields than lead (e.g. tungsten and uranium), the optimal energy to maximise the spallation cascade seems to be ~1.8 GeV.

In the case of tungsten ($^{184}_{74}W$), although this element is lighter than lead ($^{208}_{82}Pb$, double magic number), the density of the former is higher (ρ_W = 19.3 g/cm^3, ρ_{Pb} = 11.4 g/cm^3) and therefore the interaction rate in this element is greater. The choice of lead as the spallation target for the majority of full-scale ADS designs is partly due to the advantages of a liquid target over a solid one (the melting temperature for lead is low, T_M = 327 °C, whereas for tungsten T_M = 3422 °C), since a liquid target presents less mechanical constraints and offers better thermal properties, and partly due to the fact that lead reaction products are noticeably less active than the ones of any other acceptable spallation source.

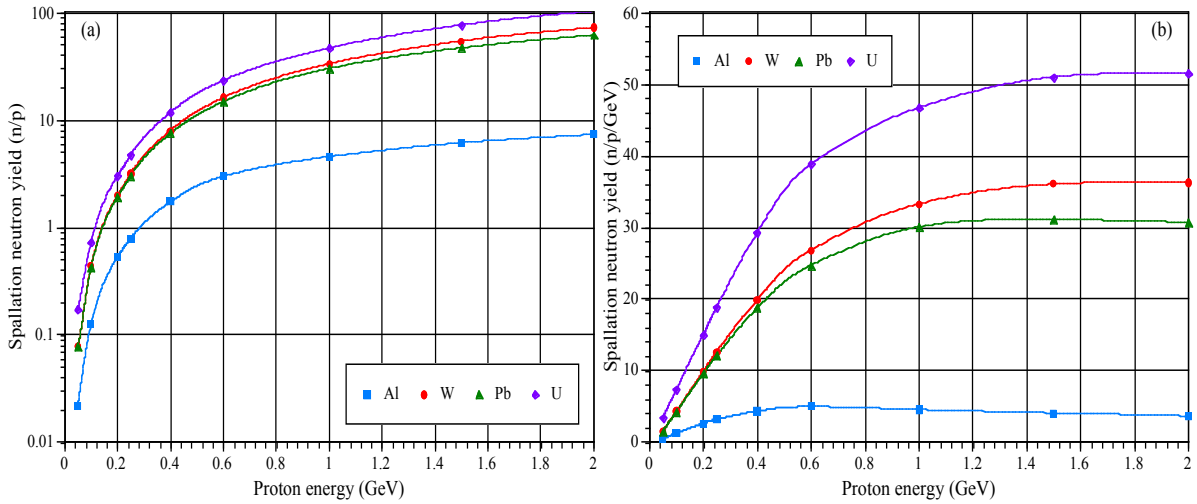

Figure 3.7. Spallation neutron yield for different materials and neutron energies calculated with FLUKA.

The spallation product distribution varies as a function of the target material and incident proton energy. It has a very characteristic shape: at high masses it is characterised by the presence of two peaks corresponding to (i) the initial target nuclei and (ii) those obtained after evaporation, three very narrow peaks corresponding to the evaporation of light nuclei, and an intermediate zone corresponding to nuclei produced by high-energy fissions. Both peaks of product composition can clearly be observed in Figure 3.8, produced by the author using

FLUKA, which shows the spallation product distribution by mass number (blue curve, A), and by atomic number (dashed red curve, Z) generated by 1 GeV protons on a lead target.

As explained before, the highest peak shown in Figure 3.8 is centred on the mass of the target isotopes (in this case, A ~207 amu). The isotopes above this mass are produced by activation, i.e. neutron capture in the target material. For an atomic mass 160 < A < 200, the isotopes are produced through evaporation, therefore originating from the same initial nuclei as the low mass peak (1 < A < 10). The peaked distribution in this energy region is mainly due to the production of α-particles, ^{3}He, deuterons and tritons. The central region contains the distribution of the isotopes produced through high-energy fission.

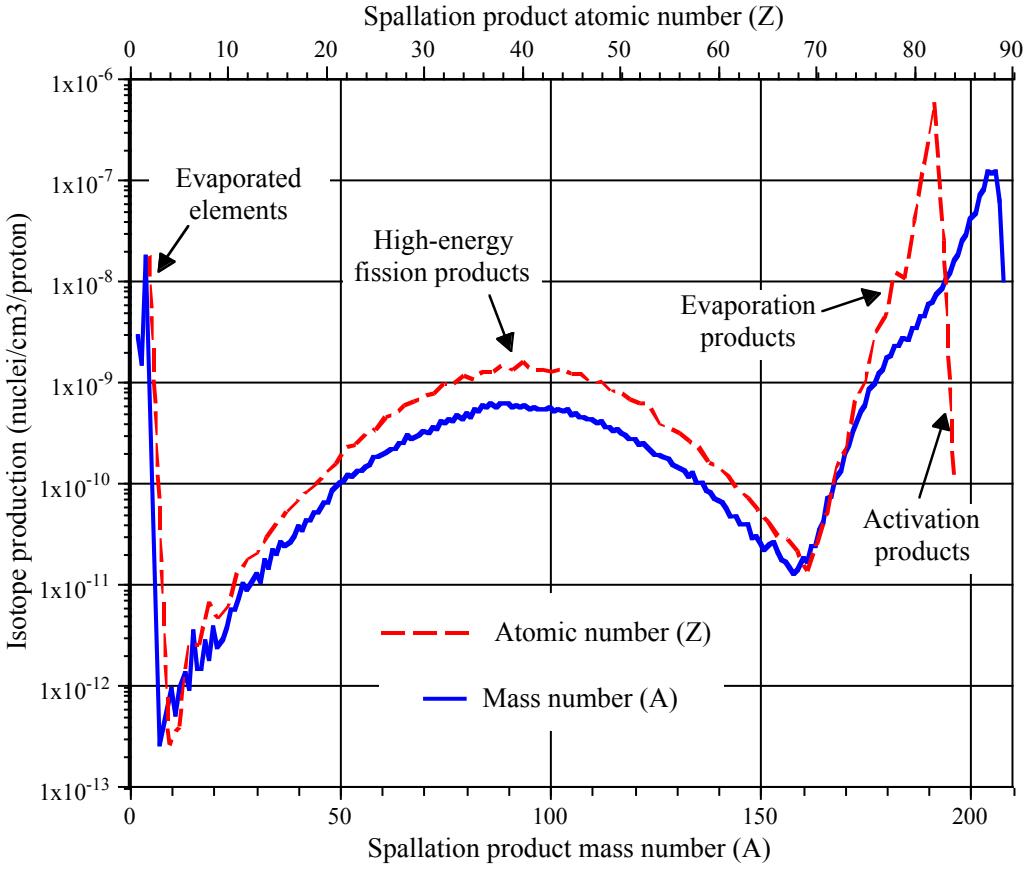

Figure 3.8. Spallation product distribution on lead for 1 GeV protons.

In fact, at high neutron energies, fission accounts for the majority of the nuclear interactions occurring in actinides. Similarly, high-energy fissions are also relevant in lead, as illustrated in Figure 3.8 by the symmetric fission fragment distribution. This distribution covers a large number of elements, between 30 < A < 160, and is centred in A ~90 (Z ~40), thus yielding a more uniform fragment distribution than the two-humped fragment distribution produced by thermal fission in fissile actinides (i.e. $^{233,\ 235}$U and ^{239}Pu). These FFs are also lighter on average than those produced through thermal fission, since the initial mass of lead is ~12 % smaller than that of uranium.

The radiotoxicity of these spallation products is therefore a key issue to address in order to evaluate the ADS potential to eliminate nuclear waste, given that the main objective of these systems is to reduce the radiotoxicity of the waste. Figure 3.9, produced by the author using the EA-MC code package, shows the origin of the radiotoxicity of the different spallation products in the lead target and its time evolution. At first, the doses are dominated by the evaporation products until their exponential decay ~4,000 years after irradiation. From that moment, mainly the activation products endure until their almost complete decay after ~400,0000 years. The contribution of the high-energy fission fragments to the radiotoxicity is important for ~100 years, strongly decreasing afterwards.

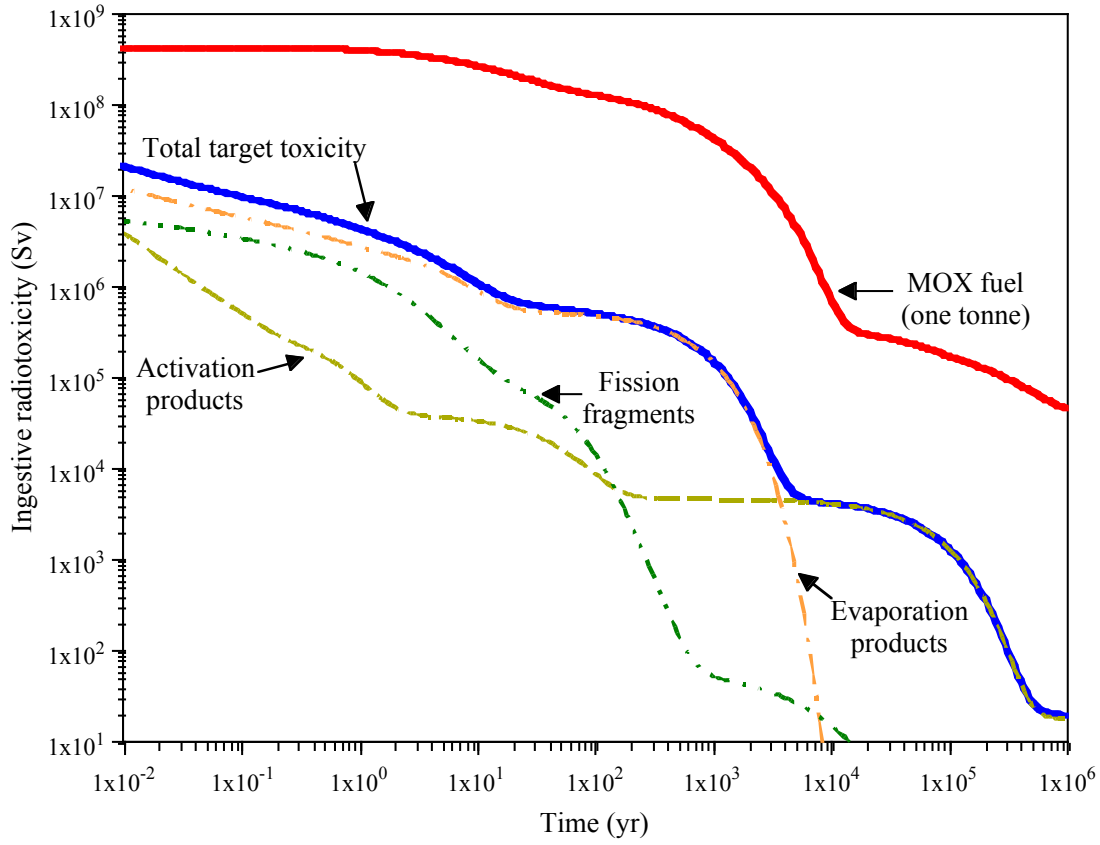

Figure 3.9. Comparison between the evolution of the radiotoxicity of the spallation products of a 1 GeV proton target and 1 tonne of fresh MOX fuel.

Figure 3.9 also shows the time evolution of the radiotoxicity of 1 tonne of MOX fuel (initially 20 % plutonium) compared with that of the spallation products of a 1 GeV, 10 mA lead spallation target after an extended period of ~7 years of irradiation.

Initially, fresh MOX (which itself is much less radiotoxic than spent fuel, as will be seen in Chapter 6) is ~20 times more hazardous than the spallation products. In addition, MOX goes from ~125 times higher radiotoxicity 2 years after irradiation to ~250 times higher after 10 years. For longer periods of time, the difference between radiotoxic levels of MOX and the

spallation products continue to increase, in particular once the evaporation products in lead have decayed. After 400,000 years, the toxicity of the target has dropped to ~40 Sv, while that of the fresh MOX fuel is still $\sim 8 \times 10^4$ Sv.

The previous comparison shows large differences between the radiotoxicity of a spallation target subject to an intense and extended irradiation and MOX fuel before irradiation. If these results are compared with Figure 2.1, the differences are even larger, demonstrating that the radiation hazard of the spallation target is orders of magnitude smaller than that of spent fuel it would help to eliminate.

3.3.2 Neutron Multiplication in a Subcritical System

In a critical system the loss of neutrons by absorption is exactly compensated by their production due to fission, therefore maintaining a constant population of neutrons in the system. This is not the case in a subcritical system, where the number of neutrons produced by fission is insufficient to compensate for their absorption, making the neutron population exponentially decay with time. Evidently, the closer the system is to the critical state the more neutron generations will be produced (continuing the multiplication longer in time) and the larger the spread will be due to the diffusion of the neutrons in the medium. A thorough comparison of the dynamic behaviour of neutrons (both fission and spallation) in thermal and fast systems is presented in Chapters 5 and 6.

Therefore, in order to maintain continuous operation, an external source must supply the neutron deficit, and its intensity will increase as the system becomes more subcritical. This fact has some important implications transforming the essence of neutron multiplication in the system. In a critical system, the start-up phase and normal operation are decoupled, in the sense that the steady state is completely independent of the details of the source (i.e. position, intensity and energy spectrum) used to start the chain reaction, since these elements only affect the start-up phase. Consequently, it is sufficient to evaluate the fundamental mode (eigenfunction) of a critical system when its stationary operation is studied.

In a subcritical device, since an external neutron source is necessary to compensate for the lack of reactivity, the system operates in the so-called source dominated regime, analogous to the start-up condition. This implies that several modes (not just the fundamental one) will be continuously excited, subordinating the reactor operation to the source characteristics (e.g. the power produced by the core will be proportional to the intensity of the source).

3.3.3 Neutron Source Multiplication: k_{src}

These facts suggest a reconsideration of the definition of parameters such as the multiplication coefficient (k). If N_j is the number of neutrons in j^{th} generation, and k the ratio of the number of neutrons between one neutron generation and the previous one, then:

$$N_j < N_{j-1} < N_0 \qquad k_j = \frac{N_j}{N_{j-1}} \qquad \text{with } k_j < 1 \text{ for } \forall j \geq 1 \qquad \text{(Eq. 3.2)}$$

Thus, the total number of neutrons, N_T, produced by fission multiplication (plus the original source, N_0) in the system during m generations, is expressed by Equation 3.3:

$$N_T = N_0 + N_1 + ... + N_m = N_0 \cdot \left(1 + k_1 + k_1 \cdot k_2 + ... + \prod_{j=1}^{m} k_j \right) \qquad \text{(Eq. 3.3)}$$

In this sense, the present definition of the multiplication coefficient is essentially different, although related, to the definition of k_{eff}, taking into account the effect of the source in the multiplication process. From Equation 3.3, the total net multiplication of the system, M_n, representing the source amplification, can be defined:

$$M_n = \frac{N_T}{N_0} \qquad \text{(Eq. 3.4)}$$

In addition to this, if the system is close enough to criticality and the neutron population is dominated by the fissions, $k_j \cong k_k \cong k$. In such a situation, the geometric series converges if $|k| < 1$, as presented in Equation 3.5:

$$N_T = N_0 \cdot \sum_{j=0}^{m} k^j = N_0 \cdot \frac{1-k^m}{1-k} \xrightarrow{\lim_{m\to\infty}} \frac{N_0}{1-k} \qquad \text{(Eq. 3.5)}$$

These results permit the definition of k_{src} as:

$$N_T \equiv \frac{N_0}{1-k_{src}}, \text{ thus, } k_{src} = 1 - \frac{1}{M_n} \qquad \text{(Eq. 3.6)}$$

Therefore, generally $k_{eff} \neq k_{src}$, even though, under normal operation (i.e. system close to criticality) both parameters tend to have similar values. Conceptually, k_{eff} is a parameter intrinsic to the system (i.e. independent of the source), which indicates how close the system is to the critical state. In the case of subcritical systems, this parameter is useful to characterise the response of the system to variations of its configuration. In contrast, k_{src} relates the neutron population to the source intensity and the other characteristics of the source; hence k_{src} depends on the system geometry, materials and on the source characteristics.

3.3.4 Neutron Source Importance: φ^*

By definition constant power operation requires ν/k_{eff} neutrons per fission, which means that an external source has to provide a number of neutrons per fission, which, in the case of being distributed exactly as the eigenfunction of the stationary problem, is given by Equation 3.7:

$$\mu_{eff} = \nu \cdot \left(\frac{1}{k_{eff}} - 1 \right) = \frac{\nu}{M_{eff} - 1} \qquad \text{(Eq. 3.7)}$$

In the case of an arbitrary external source, this equation becomes:

$$\mu_{src} = \nu \cdot \left(\frac{1}{k_{src}} - 1 \right) = \frac{\nu}{M_{src} - 1} \qquad \text{(Eq. 3.8)}$$

The ratio is known as the importance of source neutrons, as presented in Equation 3.9:

$$\frac{\mu_{eff}}{\mu_{src}} = \frac{\left(1 - k_{eff}\right) / \left(k_{eff} / \nu\right)}{\left(1 - k_{src}\right) / \left(k_{src} / \nu'\right)} = \varphi^* \qquad \text{(Eq. 3.9)}$$

This ratio evaluates the relative importance of the source neutrons with respect to the fission neutrons generated in the subcritical assembly.

The operational safety margin on k_∞ for an ADS with multiplication M (Figure 3.10(a)) can be written as:

$$\Delta k_\infty^{crit}(M) = k_\infty(M) \cdot \frac{\varphi^*}{M - 1} \qquad \text{(Eq. 3.10)}$$

Figure 3.10(a) shows the neutron amplification M versus k_{eff}. The dashed line is the amplification that one would compute using k_{eff} instead of k_{src}. The vertical and horizontal arrows indicate, respectively, the difference in the amplification at given k_{eff} and the difference in k_{src} (and hence the safety margin) at given amplification due to the distinction between the two criticality factors, k_{src} and k_{eff}. For example, for a k_{src} ~0.98, the net multiplication of the system M = 50. If the spallation source is removed, e.g. the proton beam is stopped, M would drop to ~30, and consequently the multiplication coefficient of the system, would decrease to the value of k_{eff} ~0.967.

This effect has important implications on the safety of an ADS, since this system will always have a higher k_{src} than k_{eff}, which is not modified by the spallation source. This fact guarantees that the system will become more subcritical after the spallation neutrons are removed, conferring another intrinsic safety factor to the device.

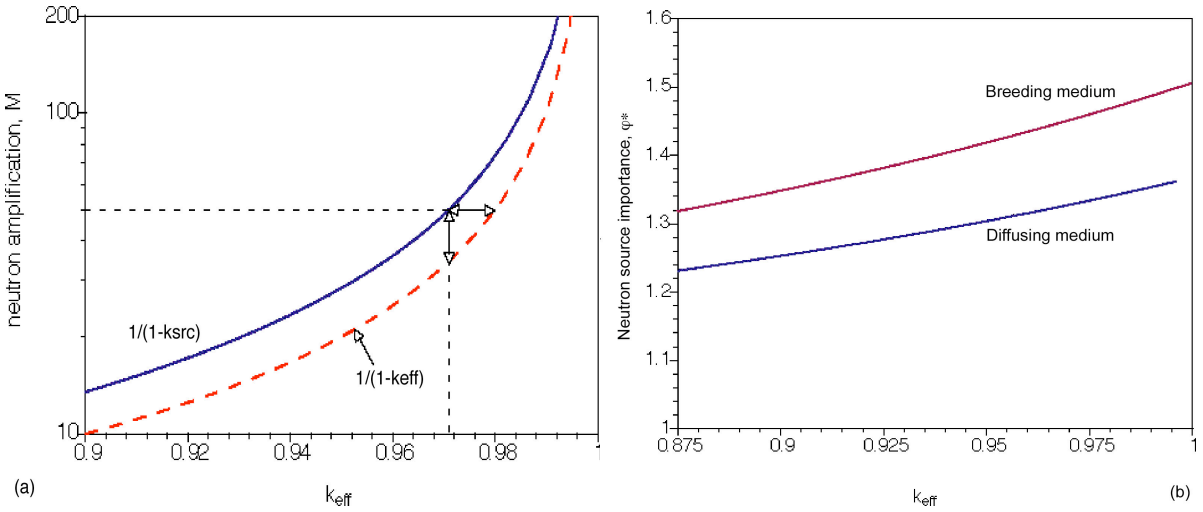

Figure 3.10. Comparison of the relation between M and the two of neutron multiplications (k_{eff} and k_{src}) [26].

Figure 3.10(b) represents function φ^*, the ratio of the actual safety margin to ($1–k_{src}$) vs k_{eff}, as computed by a simple diffusive model for two cases with geometry schematising that of a typical ADS: (i) the fissile core is surrounded by a breeder (such as ^{238}U blanket); (ii) the core is surrounded by a diffuser (such as lead). In both cases, φ^* is well above unity and grows with k_{eff}.

In general, it is found that φ^* grows with k (Figure 3.10(b)). At a given k, φ^* increases with:

- the "containment" of the neutron source;
- the ratio of the neutron diffusion length to the size of fissile core;
- the presence of an absorbing medium "enclosing" the fissionable core, which in a sense limits the "widening" of the neutron flux distribution as k is increased.

This parameter basically summarises how efficiently the source neutrons are used with respect to the fission neutrons since in a ADS the energy distribution and behaviour of both types of neutrons (and type of reactions they induce, survival probability etc.) differs noticeably. Chapters 5 and 6 analyse these differences in the context of a thermal (TRADE) and a fast (EADF) ADS, respectively.

Moreover, [26] shows that the relation between the proton beam current i_p, the power in the core and its subcriticality is given by:

$$i_p(A) = \frac{\nu \cdot \left(\frac{1}{k_{eff}} - 1\right)}{\varphi^* \cdot Z} \cdot \frac{W}{\varepsilon_f} \qquad \text{(Eq. 3.11)}$$

where W is the power produced in the core, ε_f is the energy per fission and Z is the number of neutrons per incident proton (neutron yield). Thus, φ^* plays an important role in ADS

performance assessment, where a higher value can sensibly reduce the proton beam requirement, for a given subcriticality level.

3.4 Neutron Diffusion Theory for ADS

The neutron flux distribution ($\phi_{x,y,z,t}$) is a basic parameter in the design of a nuclear reactor, particularly since the fuel consumption and the power distribution are generally proportional to this parameter. In conventional nuclear reactors the flux distribution is mainly determined by the boundary conditions due to the fact that they are designed to reach criticality and therefore sustain a chain reaction. As explained in this section, for an ADS a precise definition of the geometry and the energy distribution of the initial high-energy cascade is necessary in order to obtain an accurate solution of the diffusion equation.

3.4.1 Solution to the Diffusion Equation

To illustrate some basic ideas, a simple uniform rectangular model will be considered, diffusing mono-energetic neutrons and operated away from criticality. The flux distribution in space and time is represented by the one-group diffusion equation:

$$\frac{\partial n}{\partial t} = s + P - A + R \qquad \text{(Eq. 3.12)}$$

where s is the neutron source term; P represents the net rate at which neutrons are produced per unit volume by fission: $P = (\nu - 1) \cdot \Sigma_f \cdot \phi$, where ν is the average number of neutrons released per fission and Σ_f is the macroscopic cross-section for fission; A is the neutron capture rate: $A = \Sigma_c \cdot \phi$. One-group diffusion theory describes the neutron leakage R in a given uniform material through Fick's law, $J = -D \cdot \nabla\phi$, where D is the diffusion coefficient, ϕ is the neutron flux and J is the neutron current, which represents the net vector flow of neutrons through a surface. Fick's law of diffusion shows that J is proportional to the gradient of the neutron flux, but oppositely directed; in other words, neutrons diffuse (or flow increases) with decreasing neutron flux.

The neutron leakage in a unit volume is the difference between the incoming and outgoing neutron current:

$$\frac{\partial}{\partial t} n(x,y,z,t) \cdot \Delta x \Delta y \Delta z = \left[J(x,t) - J(x+\Delta x,t)\right] + \left[J(y,t) - J(y+\Delta y,t)\right] + \left[J(z,t) - J(z+\Delta z,t)\right]$$

(Eq. 3.13)

The above equation is the differential form of the principle of conservation of mass, assuming that the spatial neutron distribution in every coordinate is linearly independent. A Taylor series expansion of Equation 3.13 gives the diffusion equation in a non-absorbing non-multiplying medium:

$$\frac{\partial n}{\partial t} = -\nabla J = D\nabla^2\phi \qquad \text{(Eq. 3.14)}$$

Hence, in the general diffusion equation, the neutron leakage corresponds to $R = \mathrm{D}\cdot\nabla^2\phi$. The concept of material buckling B_m^2 can be defined as:

$$B_\mathrm{m}^2 = \frac{\nu\cdot\Sigma_f - \Sigma_a}{D} \qquad \text{(Eq. 3.15)}$$

Assuming the system is in steady state, the one-group diffusion equation takes the following form:

$$\nabla^2\phi + B_\mathrm{m}^2\phi + \frac{s}{D} = 0 \qquad \text{(Eq. 3.16)}$$

where $D \approx \lambda_\mathrm{tr}/3$ is the diffusion coefficient, λ_tr is the neutron transport mean free path, given by $\lambda_\mathrm{tr} = \left(\Sigma_t - \bar{\mu}\cdot\Sigma_s\right)^{-1}$, where Σ_t, Σ_s and Σ_a are respectively the macroscopic total, scattering and absorption cross-sections and $\bar{\mu}$ is the average value of the cosine of the scattering angle. For the specific case of neutrons diffusing in a high-Z material, such as lead, $\lambda_\mathrm{tr} \cong \left(\Sigma_a + \Sigma_s\right)^{-1}$ is a valid approximation [54].

The neutron flux is the solution of the Equation 3.16, where s is the contribution of the external source (neutrons per unit volume and unit time); B_m^2 can also be defined as:

$$B_\mathrm{m}^2 = \frac{k_\infty - 1}{L^2} \qquad \text{(Eq. 3.17)}$$

where k_∞ and L are, respectively, the infinite multiplication factor and the diffusion length, as defined by Equation 3.18 and Equation 3.19:

$$k_\infty = \frac{\nu\cdot\Sigma_f}{\Sigma_a} \qquad L = \sqrt{\frac{D}{\Sigma_\mathrm{a}}} \qquad \text{(Eq. 3.18 \& Eq. 3.19)}$$

In particular, when the reactor is an isotropic volume of fissile material and the neutrons are mono-energetic, k_∞ and η are equivalent.

Considering a finite system, the boundary conditions of Equation 3.16 are vanishing flux and source at the boundaries. This problem can be solved using the method of the eigenfunctions

[55], whose central idea is that it is possible to obtain a solution to the diffusion equation in terms of solutions to another differential equation. Thus, consider the wave equation:

$$\nabla^2\psi + H^2\psi = 0 \qquad \text{(Eq. 3.20)}$$

where H is a constant and the function ψ is required to satisfy the same boundary conditions as the flux. Given that Equation 3.20 is an eigenfunction equation, its solutions form a complete orthonormal basis, each eigenfunction ψ_n corresponding to an eigenvalue H_n.

Moreover, the general solution to Equation 3.20 is:

$$\psi(x) = F\,sin(Hx) + K\,cos(Hx) \qquad \text{(Eq. 3.21)}$$

Since ϕ is an even function due to symmetry in space, only the even solutions (cosine functions) of the general one should be considered. The boundary condition at $x = a/2$ (or at $x = -a/2$) gives:

$$\psi\left(\frac{a}{2}\right) = K\,cos\left(\frac{H\cdot a}{2}\right) = 0 \qquad \text{(Eq. 3.21)}$$

which leads to an infinite series of values for H, since Equation 3.21 will be satisfied by $K = 0$ (the trivial solution) and $H_n = n\cdot\pi/a$.

To form an orthonormal basis, the eigenfunctions in the solution must comply with $\int|\psi_n|^2 dx = 1$, which implies that $K = \sqrt{2/a}$.

The orthogonality condition can be expressed as:

$$\int_{-a/2}^{a/2}\psi_n(x)\cdot\psi_m(x)\cdot dx = \frac{2}{a}\cdot\int_{-a/2}^{a/2}cos\left(\frac{m\pi x}{a}\right)\cdot cos\left(\frac{n\pi x}{a}\right)\cdot dx = \delta_{nm} \equiv \begin{cases}1 \leftarrow m = n\\ 0 \leftarrow m \neq n\end{cases} \qquad \text{(Eq. 3.22)}$$

By analogy to problems in acoustics, the eigenfunction corresponding to the lowest value of n ($n = 1$) is called the fundamental eigenfunction or first harmonic; all the other eigenfunctions are referred to as higher harmonics.

Since the solution basis is a complete one, any function in the domain of the solutions of Equation 3.20 (and, therefore, of Equation 3.16, since the differential operator and the boundary conditions are the same) can be expressed as a linear combination of the eigenfunctions:

$$f(x) = \sum_{n=1}^{\infty} C_n\psi_n(x) \qquad \text{(Eq. 3.23)}$$

Any linear coefficient C_m is found by projecting $f(x)$ on ψ_m (using the orthogonality condition) as shown in Equation 3.24:

$$C_m = \int_{-a/2}^{a/2} f(x) \cdot \psi_m \cdot dx \qquad \text{(Eq. 3.24)}$$

Hence, the unknown neutron flux and the source can be expressed in the same way:

$$\phi(x) = \sum_{n=1}^{\infty} Q_n \psi_n(x) \qquad s(x) = \sum_{n=1}^{\infty} S_n \psi_n(x) \qquad \text{(Eq. 3.25 \& Eq. 3.26)}$$

Inserting Equations 3.25 and 3.26 into 3.16 yields:

$$\sum_{n(odd)} Q_n \left[\frac{d^2 \psi_n}{dx^2} + B_m^2 \psi_n \right] = -\frac{1}{D} \sum_{n(odd)} S_n \psi_n \qquad \text{(Eq. 3.27)}$$

Given that ψ_n satisfies Equation 3.20, Equation 3.27 becomes:

$$\sum_{n(odd)} Q_n \left[\left(-H_n^2 + B_m^2 \right) \psi_n \right] = -\frac{1}{D} \sum_{n(odd)} S_n \psi_n \qquad \text{(Eq. 3.28)}$$

Due to the orthogonality of the eigenfunctions, Equation 3.28 can be decoupled into an infinite series of equations of the following type:

$$Q_n \left(B_m^2 - H_n^2 \right) \psi_n = -\frac{S_n}{D} \psi_n \qquad \text{(Eq. 3.29)}$$

Rearranging Equation 3.29, substituting Q_n into Equation 3.25 and substituting for B_m and D:

$$\phi(x) = \sum_{n(odd)} \frac{1}{\Sigma_a} \cdot \frac{S_n}{1 - \left(k_\infty - H_n^2 \cdot L^2 \right)} \psi_n = \sum_{n(odd)} \frac{S_n}{\Sigma_a \left(1 + H_n^2 \cdot L^2 \right)} \cdot \frac{1}{1 - k_n} \psi_n \qquad \text{(Eq. 3.30)}$$

where k_n is defined by:

$$k_n = \frac{k_\infty}{1 + H_n^2 \cdot L^2} \qquad \text{(Eq. 3.31)}$$

It follows that if all k_n's are smaller than unity, then the flux is given by a linear superposition of eigenmodes; as soon as $k_1 = 1$ the system becomes critical; the source is no longer needed to sustain the system, and the only surviving mode is the fundamental one.

If $B_m^2 > 0$, the system is supercritical, and therefore the source term is cancelled, resulting in:

$$\phi(x, y, z) = \sum_{n(odd)} \psi_{lmq} = \sum_{n(odd)} \sqrt{\frac{8}{abc}} \cos \pi \frac{lx}{a} \cdot \cos \pi \frac{my}{b} \cdot \cos \pi \frac{qz}{c} \qquad \text{(Eq. 3.32)}$$

On the other hand, if $B_m^2 < 0$, the system is subcritical, and the solutions are of exponential form:

$$\begin{bmatrix} \psi(x) = A_1 \cdot e^{-\gamma \cdot x} + B_1 \cdot e^{\gamma \cdot x} \\ \psi(y) = A_2 \cdot e^{-\gamma \cdot y} + B_2 \cdot e^{\gamma \cdot y} \\ \psi(z) = A_3 \cdot e^{-\gamma \cdot z} + B_3 \cdot e^{\gamma \cdot z} \end{bmatrix} \quad \text{when} \quad -\gamma^2 = \frac{k_\infty - 1}{L^2} \qquad \text{(Eq. 3.33)}$$

As shown in Figure 3.11, the neutron spatial distributions in an ADS and a conventional reactor are rather different. Compared to the well-known cosine solution for the neutron flux in the diffusion equation in critical reactors, ADS have both exponential and sinusoidal components in the solution. If the subcritical system is far from criticality, the neutron flux distribution falls exponentially from the target region, decreasing rapidly and therefore depleting the fuel around the target and imposing a highly non-uniform composition on the core.

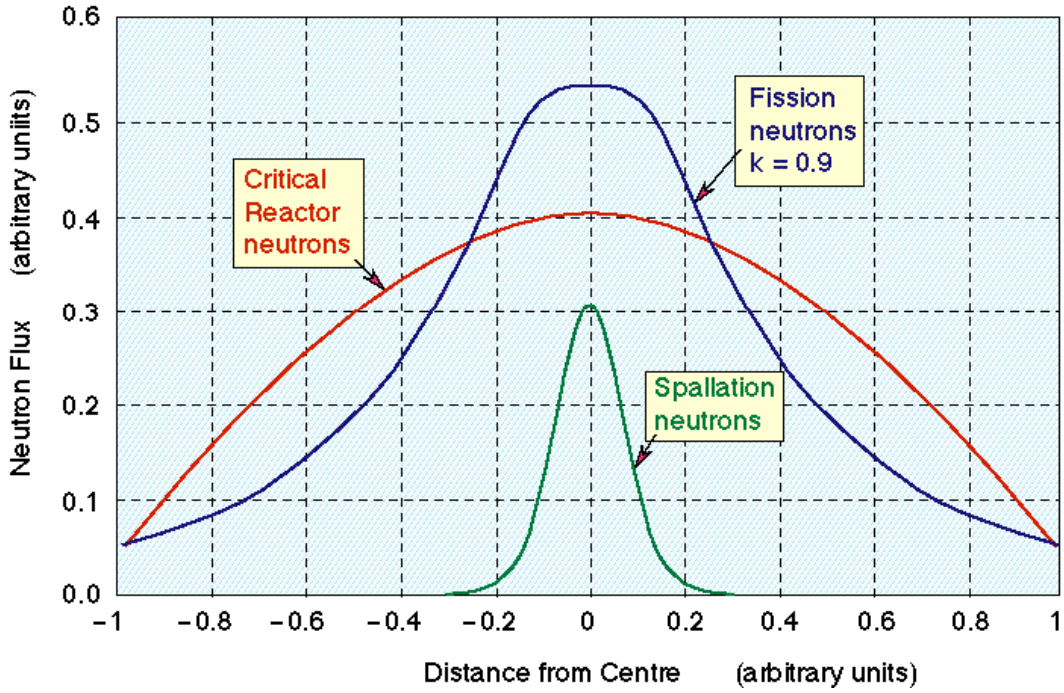

Figure 3.11. Neutron flux distribution for spallation, subcritical (k = 0.9) and critical systems [26].

3.4.2 Diffusion in a High-Z Material

The diffusion of neutrons in the core includes a whole range of rather complicated nuclear interactions, such as elastic (n, ne) and inelastic (n, ni) scattering, radioactive capture (n, γ), (n, 2n) and (n, 3n) – usually referred to as (n, xn) – fission, spallation (described in 3.3.1), etc. Of all these reactions, elastic scattering is arguably the most common one, having a decisive influence on the neutron energy spectrum, and, thus, on the reactor behaviour. Therefore, the

basic principles underlying this type of nuclear interaction, as well as the differences due to the nature of the target nuclei are important to the development of ADS for nuclear waste transmutation.

This basic process takes place when a neutron is elastically scattered from a nucleus at rest. The nucleus recoils from the site of the collision; thus the kinetic energy of the scattered neutron is lower than its initial energy. Let p_n and E_n be, respectively, the momentum and kinetic energy of the neutron before the collision, $p_n^{'}$ and $E_n^{'}$ the momentum and kinetic energy of the neutron after being scattered, and P_M and E_M the momentum and kinetic energy of the nucleus after the collision (Figure 3.12). The energy loss in elastic scattering can be found from the laws of conservation of energy ($E_n = E_n^{'} + E_M$) and momentum. ($\vec{p}_n = \vec{p}_n^{'} + \vec{P}_M$).

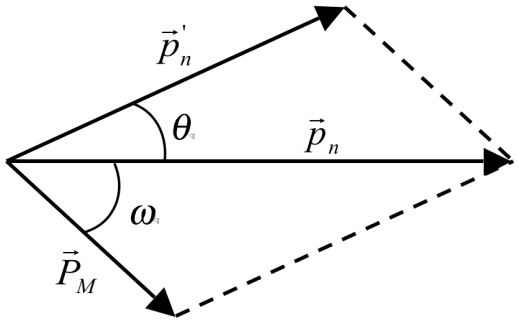

Figure 3.12. Vector diagram for the conservation of momentum during an elastic collision.

Applying the law of cosines to the momentum conservation:

$$P_M^2 = p_n^2 + (p_n^{'})^2 - 2 \cdot p_n \cdot p_n^{'} \cdot cos\theta \qquad \text{(Eq. 3.34)}$$

Given that $p^2 = 2ME$, combining momentum conservation with Equation 3.34, and since M (the mass of the target nucleus) over m (the neutron mass) is approximately A (the atomic number of the target nucleus),

$$A \cdot E_M = E_n + E_n^{'} - 2\sqrt{E_n \cdot E_n^{'}} \cdot cos\theta \qquad \text{(Eq. 3.35)}$$

Using conservation of energy to substitute for E_M in Equation 3.35:

$$(A+1) \cdot E_n^{'} - 2 \cdot \sqrt{E_n} \cdot cos\theta \cdot \sqrt{E_n^{'}} - (A-1) \cdot E_n = 0 \qquad \text{(Eq. 3.36)}$$

This quadratic equation in $\sqrt{E_n^{'}}$ has the solution:

$$E_n^{'} = \frac{E}{(A+1)^2} \cdot \left(cos\theta + \sqrt{A^2 - sin^2\theta}\right)^2 \qquad \text{(Eq. 3.37)}$$

since the other solution for the equation is non-physical.

Thus, for a minor collision $\theta \approx 0$, the energy of the neutron after the elastic interaction is $E_n \approx E_n^{'}$. From Equation 3.37, it follows that the maximum energy loss $(E_n^{'})_{min}$ occurs when $\theta = \pi$, when the neutron is scattered backwards. In this case Equation 3.37 yields:

$$\left(E_n^{'}\right)_{min} = \left(\frac{A-1}{A+1}\right)^2 \cdot E_n = \alpha \cdot E_n \qquad \text{(Eq. 3.38)}$$

where $\alpha = \left(\frac{A-1}{A+1}\right)^2$ is the so-called collision parameter.

Hence, α ranges from 0 for ^{1}H to 0.716 for ^{12}C, 0.931 for ^{56}Fe and 0.981 for ^{208}Pb. This fact has important implications in the physics of transmutation, since it conditions the neutron energy spectrum of the system. As mentioned in Chapter 2, the LLFFs have generally small cross-sections except for very specific and narrow resonances. The neutron flux in these resonances could have a large impact on the transmutation rate of these isotopes [23], and this neutron flux depends only on ξ – the average change in lethargy[2] – which in turn depends on only the atomic mass of the target (and not the neutron energy). Thus, heavy nuclei produce small ξ, which may increase the neutron flux inside the resonances and, therefore, gives higher transmutation rates. In the case of the actinides, the fission-to-capture ratio is orders of magnitude larger in the high-energy range (above 1 MeV) for most of them. Therefore, only a neutron energy spectrum presenting large values in the resonance (epithermal) and fast regions, together with a large absolute value, may suit the purpose of transmuting these nuclear species.

In this sense, the use of lead as a coolant seems favourable, since the maximum energy loss of a neutron undergoing an elastic interaction (a head-to-head collision) is less than a 2% of the neutron energy, with an average mean free path $\lambda_{elas} \approx 3.4$ cm independent of the neutron energy (σ_{elas} is constant between 10^{-3} and 10^{5} eV, except for small resonances, as observed in Figure 3.13, produced by the author from the JENDL-3.2 data library).

Lead also presents a very low capture cross-section (the main isotope in natural lead, ^{208}Pb, is double magic [56], and thus exceptionally stable), improving the neutron economy. Moreover, the large mass number, the largest A of the stable isotopes together with ^{209}Bi, qualifies lead as a exceptional coolant for transmutation purposes, given the small energy loss in every collision and the large λ, providing a high neutron flux with a hard energy spectrum.

[2] In treating the neutron slowing down process the energy variable may be replaced with the neutron *lethargy*, defined as $u = ln(E_0/E)$, where E_0 is the maximum energy of a neutron in the system. Since $du = -dE/E$, the changes in lethargy are independent of the neutron energy. The average change in lethargy, ξ, is generally approximated as $\xi \approx 2/(A+0.667)$, where A is the mass number of the target.

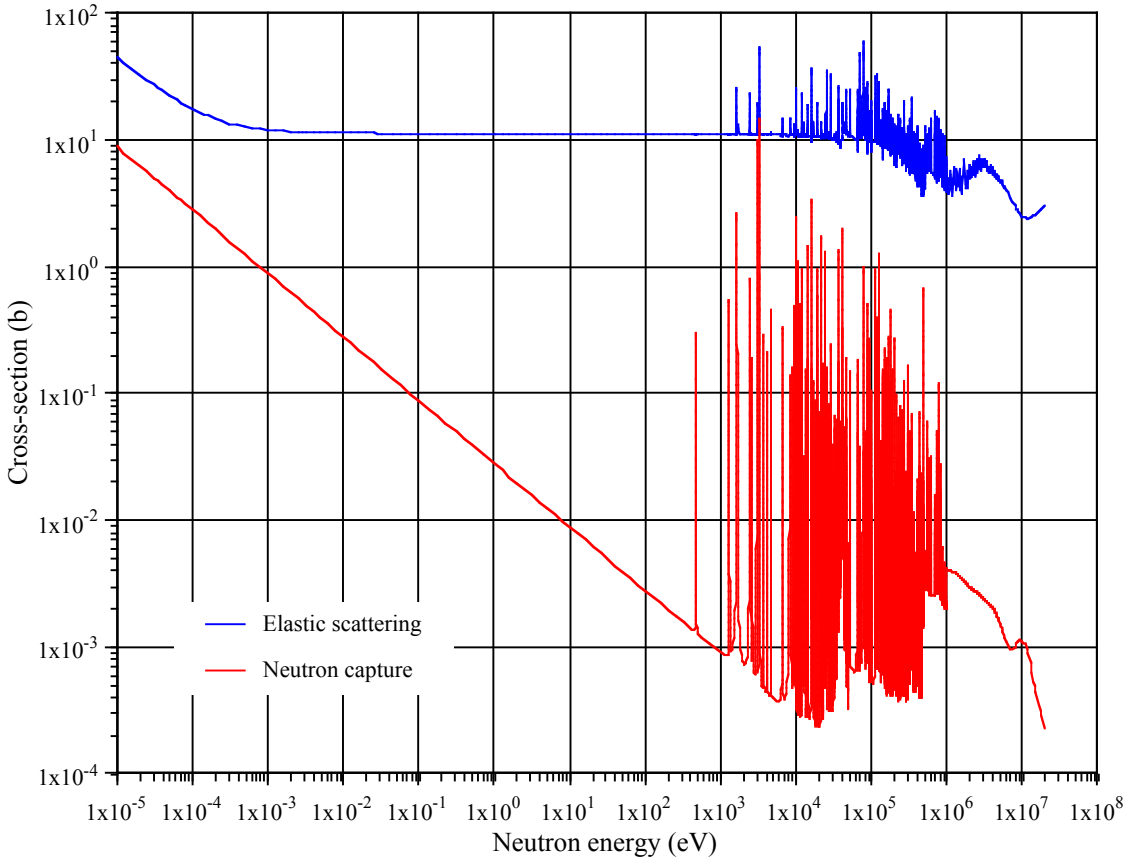

Figure 3.13. Comparison between the elastic scattering and capture cross-sections for natural lead.

3.5 Fuels for ADS: Thorium Fuel Cycle

At a first stage, fuel-breeding systems were designed to operate using the ^{239}Pu breeding cycle from ^{238}U. This plutonium breeding cycle presents a number of problems common to both the use of MOX fuel and the operation of plutonium fast breeders. These problems include the production of very large quantities of TRUs, which, as explained in Chapter 2, are highly radiotoxic and difficult to eliminate.

Although fast critical systems may alleviate the plutonium stockpile, the spent fuel from these systems would contain large amounts of MAs. These elements present very unfavourable safety parameters, such as a very small delayed neutron fraction (0.21 % for ^{239}Pu, 0.14 % for ^{241}Am or 0.13 % for ^{244}Cm compared to 0.65 % for ^{235}U and 1.91 for ^{238}U, as shown in Table 2.2) and very low temperature feedback. The effect of Doppler broadening is less patent since the fast systems operate above the resonance region of many elements and MAs do not generally present distinctive capture resonances decoupled from the fission resonances, as is the case of ^{238}U.

Additionally, the already small negative void coefficient in these systems may even become positive in the case of an increase in the coolant void due to a temperature rise or a Loss-Of-Coolant-Accident (LOCA). In fact, the void coefficient of a sodium cooled fast reactor is not distinctly negative for some temperatures. Moreover, the MOX fuel in these systems presents a temperature coefficient of $\sim -2\times10^{-5}$ per K (−2 pcm/K), which decreases with burn-up.

The thorium fuel cycle raised the interest of the nuclear industry since the 1950's. Nowadays, these interest has increased even further as a means of eliminating TRUs. On the other hand, the fissile element in this cycle, namely ^{233}U, presents a small delayed neutron fraction, thus hindering the control of a critical system, and specifically a fast critical system loaded with a large amount of higher actinides. Moreover, the production of ^{233}Pa (intermediary in the breeding process) and a larger fraction of ^{135}Xe (1.4 % direct yield from ^{233}U, compared to the 0.3 % for ^{235}U) and other samarium precursors (e.g. ^{147}Nd and ^{149}Pm) depletes the neutron population due to the large thermal capture cross-section of these elements. This fact would require a higher level of fuel enrichment and would limit the length of the burn-up period.

Therefore, since an ADS may operate with a wide range of fuel mixtures and burn-up schemes, several designs of ADS have chosen the thorium cycle as a way of reducing the stockpile of plutonium waste from conventional reactors and nuclear warheads. Equation 3.39 shows the breeding process taking place in the thorium cycle (as opposed to the ^{239}Pu breeding process from ^{238}U commonly used in sodium-cooled fast reactors):

$$^{232}\mathrm{Th}(n,\gamma)^{233}\mathrm{Th}\xrightarrow{\beta^-,\tau_{1/2}=22\,min}{}^{233}\mathrm{Pa}\xrightarrow{\beta^-,\tau_{1/2}=27\,days}{}^{233}\mathrm{U}(\tau_{1/2}=1.6\times10^5\,yr) \quad \text{(Eq. 3.39)}$$

During operation, the TRUs load would be fissioned, while ^{233}U would progressively be produced. The freshly bred ^{233}U could compensate for the loss of reactivity due to the elimination of fissile plutonium and the poisoning produced by the FFs. Therefore, operation over long burn-ups (120-150 GWd/tHM [1]) could be possible.

As mentioned earlier, the thorium fuel cycle has several advantages over the uranium fuel cycle. The radiotoxicity accumulated is much smaller, since the production of TRUs during an operating cycle is drastically reduced compared with the use of ^{238}U as the matrix of the fuel. This fact is highlighted by Figure 3.14, where the differences between the paths to be followed by ^{232}Th and ^{238}U to produce MAs by neutron capture can be appreciated. In the ^{232}Th chain there are two isotopes, namely ^{233}U and ^{235}U, for which the fission cross-section is orders of magnitude larger than the capture cross-section, therefore greatly reducing the production of TRUs. This issue is of great relevance given that a major part of the HLW is composed of these elements, which generally have a small total cross-section, and hence are difficult to eliminate.

Availability is another strong point in favour of this fuel cycle. Thorium is an abundant element in the earth's crust, about 12 g/tonne, three times the value for uranium [57], ranking 35th by abundance, just after lead, and it is spread over the surface of the planet. In fact, [58] claims that there may be more energy available for use from thorium in the minerals of the earth's crust than from all combined uranium and fossil fuel sources.

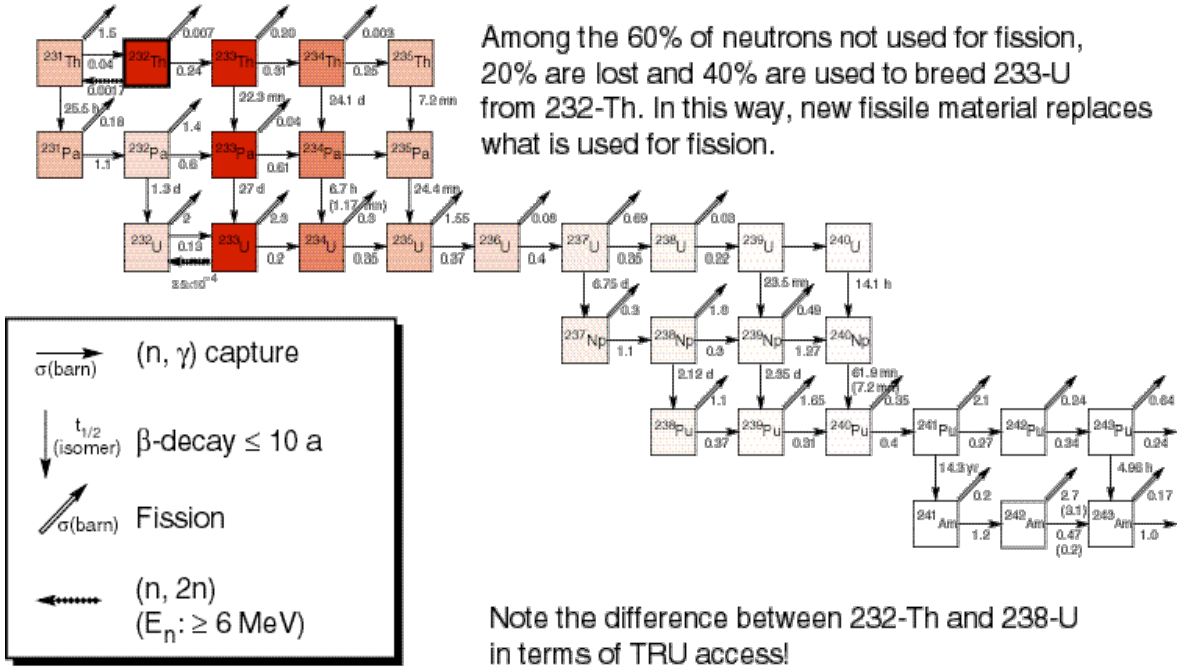

Figure 3.14. Decay chains of different actinides in the thorium fuel cycle [26].

The estimates of thorium abundance presume around 6×10^6 tonnes in the whole world, which could produce ~15,000 TW·yr of energy if used in EAs [1], about a factor of 100 larger than the known reserves of oil or gas and a factor 10 larger than coal, corresponding to 12.5 centuries at the present world's total rate of power consumption (10 TW) [57].

3.6 ADS Simulation using Monte Carlo Methods

The sequence of phenomena occurring in an ADS, from the high-energy proton induced cascades within the target producing neutrons that are subsequently absorbed, to the multiplication of these source neutrons in the fuel, is a coupled physical problem requiring innovative computational methods to be accurately solved. Therefore, for a correct simulation of an ADS, it is essential to understand the details of the physics related to all these phenomena. In this context, an innovative simulation code was developed at CERN [37 & 38] using Monte Carlo (MC) techniques, and validated through several experiments, such as FEAT and TARC.

The analysis of an ADS requires powerful simulation tools for:

- The modelling of the high-energy cascade and of the neutron production;
- The transport of the low energy ($E \leq 20$MeV) neutrons;
- The description of the fuel evolution as a result of neutron interactions and nuclear decays;
- The nuclear transmutation and activation of the structural materials and coolant due to the presence of a neutron fluence and of the proton beam induced high-energy cascade.

These requirements imply that the tools commonly used to simulate conventional critical reactors cannot be applied to ADS, since the neutron flux strongly depends on the high-energy cascade.

3.6.1 Monte Carlo Methods

MC methods are statistical methods (as opposed to deterministic methods, which solve the transport equation), which sample a given problem with random numbers in order to solve it. Hence, the accuracy of the results depends strongly on the number of trials given to the problem.

In the case of nuclear reactor engineering, these simulation methods take into account the probabilities of different reactions occurring (i.e. cross-sections), while random numbers are generated and depending on the probability distribution function (PDF) for every case, different reactions occur which may drive other reactions (also depending on their PDFs and the new random numbers generated).

There are several advantages in the use of MC methods to simulate an ADS. The large amount of information provided by the point-like cross-sections, the continuous spatial resolution, accurate geometrical definition, full treatment of resonances and full 3D calculation of activation and spectrum-dependent transmutation effects are hardly achievable by deterministic methods.

Deterministic codes are based on the solution of the neutron transport equations, and in order to make the problem solvable by the computer, a discretisation is introduced both in space and in energy. These codes operate on a spatial grid and on a fixed number of energy groups. While this approach is viable in many applications, and widely used to simulate critical reactors, it has certain drawbacks when applied to the simulation of an ADS. Deterministic codes calculate k_{eff} via an eigenvalue search of the multi-group equation system [59]. These may ignore in their scattering matrix non-fission multiplicative processes such as (n, xn), which are of great importance for lead-cooled fast reactors and the thorium fuel cycle due to the large (n, 2n) cross-sections for thorium and lead.

The interplay between resonances in a material of time-varying composition would be a complicated problem to solve using a multi-group analytical code; the self-consistent fluence field would have to be computed and then used to condense the cross-sections at every burn-up step, with the supplementary condition of all fluences converging simultaneously, since the fluence in each region affects any other region. This fact, added to the space-dependent time evolution of the fuel, would make difficult the computation of such a problem by an analytical code.

On the other hand, MC methods have several limitations which can affect the accuracy of their results. These limitations could be summarised as:

(a) the need for correct ND, in particular, cross-section information. Clearly, the accuracy of the cross-section data for a broad neutron energy range (10^{-5}-2×10^{7} eV) may affect the final results of the reactor neutronic calculations, especially those for transmutation in ADS, since the isotopes involved and the energy range are rare in conventional reactor physics. Nevertheless, this effect is common to all transport codes and the ND is being continuously improved by ongoing experiments, e.g. n_TOF [60], as elaborated in Chapter 4;

(b) the physical model used to define high-energy reactions (especially neutron production at the source); for low energy neutron transport this is mainly expressed by the data (partial reaction cross-sections, double differential cross-sections, etc.).

Another drawback of MC methods is the slow statistical convergence due to the random nature of the events generated, correlated with the number of trial events N. This statistical error convergence is unfortunately proportional to $\sqrt{N}$ (rather than N) making it rather slow. Moreover, this rate of convergence is guaranteed only provided the variance of the distribution is finite. For example, this is not the case for the energy losses due to the ionisation cascade of a charged particle in an ordinary medium, where the Landau distribution has a variance which is infinite: its width (due to fluctuations) slowly decreases with the number of collisions $\log(\sqrt{N})$. On the other hand, for a fission driven sub-critical multiplying medium, the variance of the distribution is large but finite [61], although the mean multiplication factor M and related fluctuations are dominated by a few cascades with large fission multiplication. Therefore, accurate results for complex, time-dependent, 3D-geometry ADS problems are currently achievable, in an acceptable time frame, by the use of fast parallel computers which can generate many events simultaneously.

3.6.2 The FLUKA / EA-MC Code Package

FLUKA / EA-MC is a three-dimensional point-energy MC code which stochastically calculates the distribution of neutrons in space as a function of energy and time. The neutron

data are derived from the latest ND libraries, such as ENDF/B-VI (US), JENDL-3 (Japan), JEFF-3 (Europe) etc. Figure 3.15 shows the general architecture of the code package and the information flow.

The FLUKA / EA-MC simulation package integrates neutron transport and evolution of the material composition in the same code. To take into account the time evolution a burn-up step is defined (e.g. 1 day), and, depending on the statistical requirements of the system, i.e. the number of neutrons (or equivalent protons) to reach convergence, the results are scaled up to the accelerator current in order to obtain the operational values of the device.

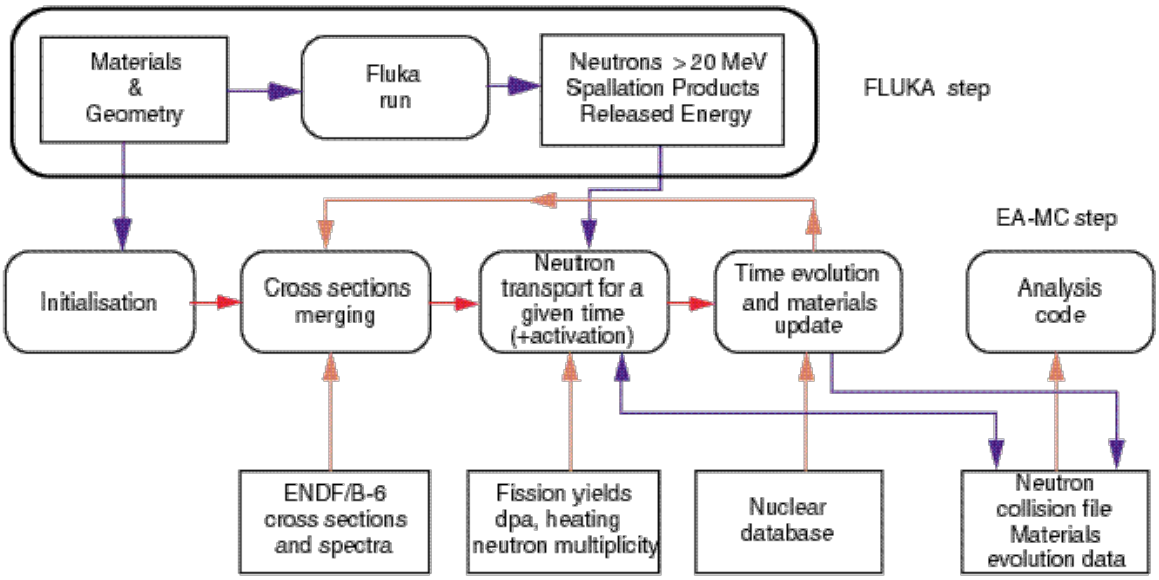

Figure 3.15. General architecture of the EA-MC simulation of neutron transport and element evolution [38].

The spallation neutron source distribution is generated by FLUKA, transporting the neutrons down to an energy of 19.6 MeV, and then writing to a history file. 19.6 MeV is selected for neutrons as being just below the upper limit (20 MeV) of neutron cross-section data sets. FLUKA performs the de-excitation of the nuclei in several steps:

- Interaction point selection and projectile tracking through the nucleus, according to Fermi motion (movement of nucleons inside the nucleus [62]), averaged hadron-nucleon cross-sections and nuclear mean field, including the Coulomb field;
- Secondary tracking into the nucleus, until interaction, escape, or energy cut-off.
- Pre-equilibrium stage: whenever all excited nucleons are below a given energy threshold (typically a few tens of MeV).
- Evaporation stage: whenever the pre-equilibrium stage is finished, or all particles are below a given threshold (usually of the order of the binding energy), and the system can be assumed to be in equilibrium.

- Final de-excitation stage: when the excitation energy is below the threshold for particle emission and it is dissipated through photon emission.

The EA-MC code follows all neutrons generated in the cascade initiated by the spallation source produced by FLUKA. The neutron transport is modelled in time steps which vary adaptively according to the burn-up phase, since by reaching equilibrium the system changes composition slower. The material evolution is performed between transport steps, and the material composition is updated according to the neutron interactions simulated in every material zone. High-energy spallation products coming from FLUKA are added to the material composition on a proton-by-proton basis. The contribution of all fission, spallation, decay and activation products is considered explicitly during neutron transport.

The cross-sections are used directly from the pre-processing codes, without approximations; in some cases the cross-section for a single reaction channel can contain more than 60,000 points – such is the case for thorium.

Every material can have a different temperature, inherited by the nuclear species produced there. New temperatures can be generated during the simulation either by Doppler broadening or by linear interpolation of existing evaluations. The fuel material in the core can contain several hundred elements with cross-sections and up to 2000 different nuclear species. Due to this fact, the code was optimised to reduce the time to transport the particles, which for a neutron is approximately 8 μs/processor on a Convex SPP2000 machine [38].

The solution of the Bateman equations, involving thousands of elements, is computed in order to avoid approximations in the concentration evolution. Finally, a combination of storage techniques, such as the sorting of the cross-sections of the commonly produced elements and the most used energy ranges, together with decay chain algorithms, allows the evolution of all materials. The use of smoothing techniques in the case of very short-lived elements or strong concentration gradients is also necessary in order to correctly compute concentrations between burn-up steps.

As mentioned before, the neutron data is derived from the latest ND libraries: ENDF/B-VI release 8 (US), JENDL-3.3 (Japan), JEFF-3.0 (Europe), EAF-4.2 (Europe), CENDL-2.1 (China), EFF-2.4 (Europe) and BROND-2 (Russia). The user has the option to utilise individual libraries or the CERN compilation of ND, JAR-95. For each nuclide in JAR-95, one evaluation out of those available has been selected on the basis of a systematic comparison [63]. The selection was done isotope per isotope according to the evaluation of the resonances and the number of reaction cross sections. When both the resonance region and the number of cross sections evaluated were similar, the most recently evaluated cross section was selected.

This Monte Carlo code package is used to perform the analyses presented in Chapters 5 and 6, from the transport of the high-energy particles (including the electromagnetic shower) to the neutronic simulation of the ADSs and their burn-up evolution. In fact, the wide range of problems where this code may be applied and the accuracy of the results, especially concerning the isotopic evolution, are some of the benefits of using FLUKA / EA-MC.

Chapter 4

Nuclear Data

Accurate neutron cross-section data is fundamental to the reliable design of any transmutation device, and, in particular, of an ADS. Calculations of the behaviour of the core depend strongly on the cross-section data: parameters such as the multiplication coefficient, power densities or reactivity may vary significantly depending on the Nuclear Data (ND) library used, since there is not yet a single universal data file with recommended best neutron cross-section values.

Moreover, the prediction of the nature of the waste generated in the nuclear fuel cycle and its radiotoxicity is closely related to the accuracy of the ND. Given that the ultimate goal in the field of transmutation is to reduce the radiotoxicity of the nuclear waste, the assessment of the production and destruction rates for the most hazardous isotopes requires precise knowledge of the related ND.

The possible discrepancies between different ND libraries justify the need to improve the present data for several isotopes and reaction channels, for a wide range of neutron energies from thermal to high-energy.

In this context, the n_TOF-ND-ADS project of the EURATOM 5^{th} Framework Program was conceived with the purpose of improving the ND related to transmutation in ADS. This project involves the measurement of cross-section data for a wide range of isotopes and reaction channels in a neutron time-of-flight facility based at CERN. In particular, the measurement of capture and fission cross-sections between 1 eV and 250 MeV of several isotopes involved in ADS nuclear waste transmutation (e.g. MAs, lead or ^{209}Bi), thorium fuel cycle (e.g. ^{232}Th, $^{231, 233}$Pa or $^{232, 233, 234, 236}$U) and stellar nucleosynthesis (such as ^{151}Sm or zirconium) are of especial relevance in this project.

An analysis of the effects of different cross-section data was required in order to set a priority list for the isotopes to be measured. Parameters such as source multiplication coefficient k_{src}, neutron spectra, neutron balance and one-group cross-sections for different isotopes using different ND evaluations had to be compared, highlighting the relative importance of different isotopes and assessing the required accuracy for the given reaction cross-sections, thus establishing the required precision of the measurements to be performed in the n_TOF experiment.

4.1 The Importance of Nuclear Data

The experimental determination of neutron cross-sections for all the isotopes in the Mendeleiev table has always been of primary importance in nuclear physics. Many of the outstanding features of nuclear levels can be determined from the resonant structure of such cross-sections and their decay schemes. These cross-sections have many different channels and exhibit a complex phenomenology with numerous resonances over a very wide energy spectrum, extending from a fraction of eV to hundreds of keV of neutron kinetic energy.

In addition to such primary interest, current developments in fields such as nuclear engineering, radioisotope production for medical applications [64], humanitarian demining [65] and even propulsion for deep-space travel [66] have raised the practical need for better known cross-sections. In the case of modern nuclear reactor physics, the development of accelerator-driven devices to safely eliminate nuclear waste and produce energy in a clean, reliable way demands levels of accuracy in the knowledge of ND previously unnecessary. The wide neutron energy range in which these devices operate and the diversity of elements involved in their design justify an exhaustive research program to improve the present knowledge of ND.

The design analysis of an ADS commonly makes use of MC techniques in order to predict their behaviour in a variety of possible configurations and operating conditions. In contrast with the conventional multi-group methods used in reactor studies, the subcritical nature of the device, in which all fundamental modes are excited following a high-energy cascade, as presented in Chapter 3, can only be properly studied with MC simulations of the complex nuclear phenomena. Thus, the extensive use of these techniques increases the importance of the accuracy of the libraries of cross-sections for neutron-induced reactions. The relatively high energies involved require that not only neutron capture and fission, but also a larger variety of channels, such as, for instance, (n, 2n), (n, 3n), (n, np), etc., should be taken into consideration. The presence of a high-energy cascade necessitates the extension of the exploration to energies up to several hundreds of MeV's.

Consequently, the availability of reliable cross-section data for several channels and appropriate energies is a fundamental prerequisite for any computational method. Unfortunately, the available compilation databases present many uncertainties and substantial differences between them, due to the different fitting procedures and their reliance on different theoretical models. Thus, these nuclear databases may not be completely accurate either to design in detail an ADS prototype with a given precision (~50 pcm in k_{src}) nor to simulate in detail the behaviour of such a machine with a variety of different fuels, as required for transmutation of HLW. Indeed, while some uranium related cross-sections are relatively well known for some specific energies in the low-energy range, there are sometimes large differences between databases when it comes to neptunium, americium (Figure 4.1) and curium, or more generally to TRUs (even some plutonium isotopes such as ^{238}Pu or ^{242}Pu).

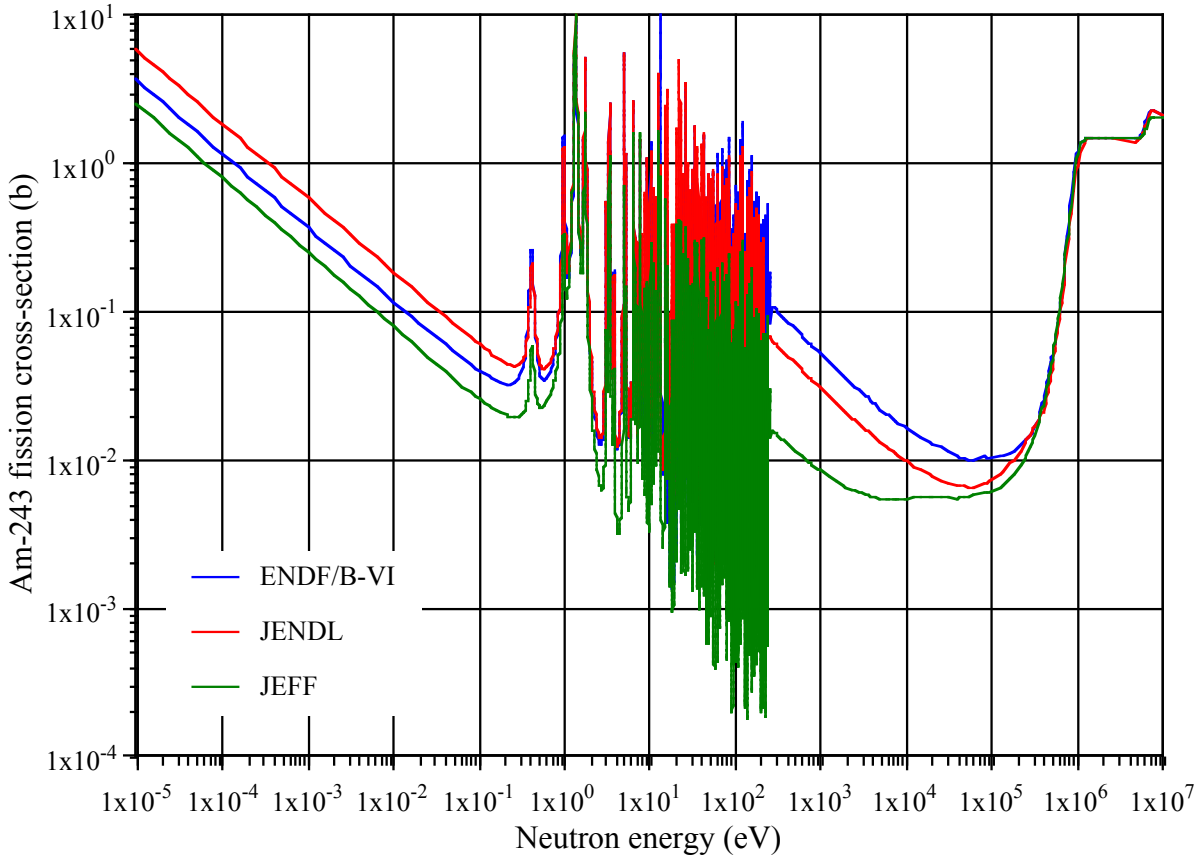

Figure 4.1. ^{243}Am fission cross-section for ENDF/B-VI.8, JENDL-3.3 and JEFF-3.0.

Furthermore, the comprehensive elimination of HLW implies consideration of the transmutation of several LLFFs into stable species. For such elements, the information is even more scarce and in many important cases, such as, for instance, ^{137}Cs (Figure 4.2) or ^{90}Sr, there are orders of magnitude discrepancies in the experimental data, which is mostly confined to the region of thermal or epithermal neutrons. In addition, the TARC method [23] requires precise information on the resonances and specifically their widths.

4.2 Status of Nuclear Data Cross-Sections

A brief description of the present situation of the ND concerning the most relevant nuclei for nuclear waste transmutation is necessary. In particular, this description concentrates on the major discrepancies in fission and capture cross-sections of actinides, since these not only affect their transmutation rates but also the safety parameters of the system by, for example, increasing the uncertainties related to the value of k_{eff}, Doppler or void reactivity coefficients. The cross-section data in this section are those presently available in the internationally recognised ENDF/B-VI evaluated data format [67] and the Exchange Format (EXFOR) experimental data files [68] containing descriptive information on neutron, charged-particle and photon induced reactions on different target nuclei. The data from two different libraries, ENDF/B-VI.8 [69] and JENDL-3.3 [70], are compared, given that JEFF-3.0 [71] is for many isotopes a carry-over from ENDF/B data.

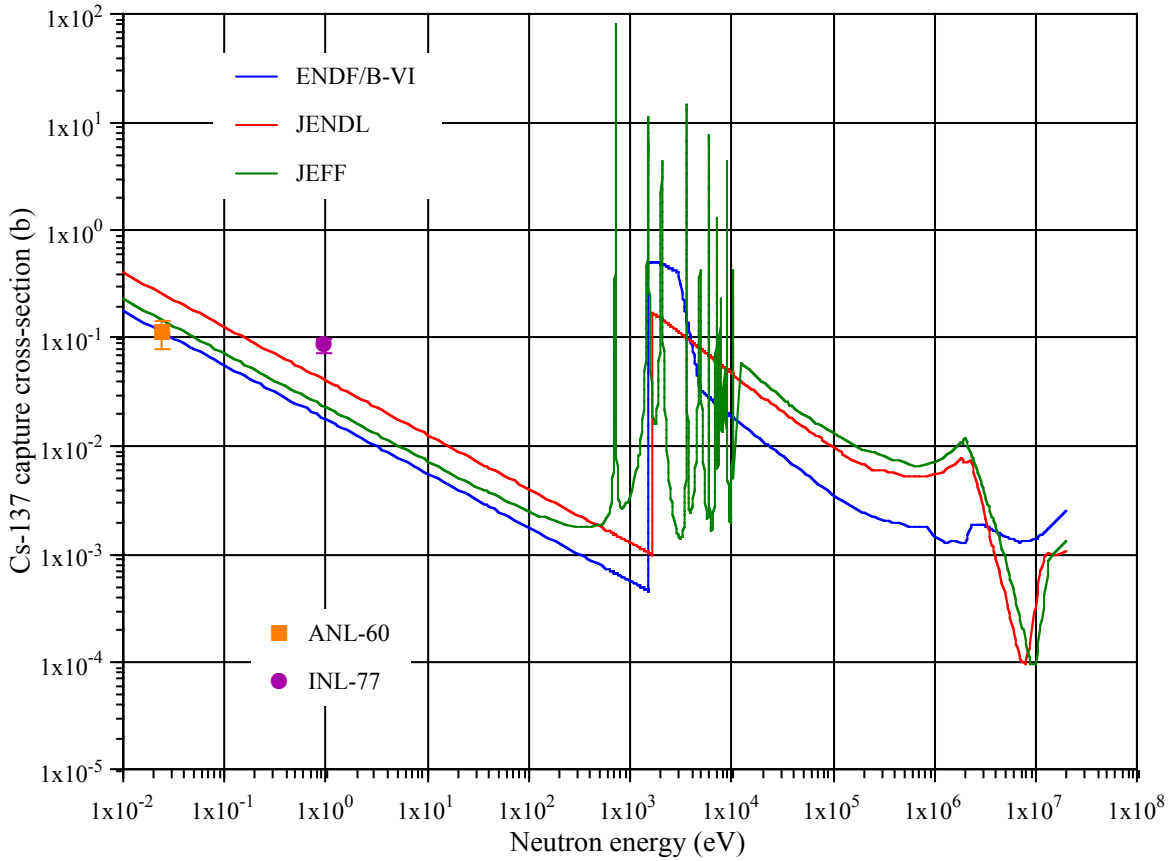

Figure 4.2. ^{137}Cs experimental and evaluated capture data for ENDF/B-VI.8, JENDL-3.3 and JEFF-3.0.

The difference between experimental and evaluated data is sometimes enormous, such as in the case of ^{137}Cs (Figure 4.2), where the EXFOR files present few experimental points, and only at 0.025 eV (ten entries) and 1 eV (one entry), such as the measurements in Argonne National Laboratory (ANL) in 1960, and the one in Idaho National Laboratory (INL) in 1977.

In this case, ND libraries predict rather different nuclear structures, depending on which theoretical model was applied to evaluate the cross-section.

This case is typical of the major part of the LLFFs ND, since few measurements have been performed due to the high activity and radiotoxicity of these elements (and the need for a high flux, high repetition-rate facility). For example, the EXFOR data present four measurements of the capture cross-section of ^{135}Cs at 0.025 eV (8 b), twelve measurements for ^{129}I and ten measurements at 0.025 eV and 0.5 eV for ^{90}Sr.

4.2.1 Thorium Cycle Isotopes

The experimental data for the isotopes involved in this cycle is rather incomplete and mostly based upon theoretical models and nuclear systematics [72]. In particular, isotopes, such as ^{234}U or ^{233}Pa, present no experimental cross-sections for (n, xn) reactions, and for ^{232}Th and ^{233}U the information is fairly limited. A similar situation appears when inelastic scattering is analysed. Few direct measurements of capture cross-section of ^{233}U in the fast energy region have been performed and information on the fission cross-sections above 6 MeV for ^{232}Th and $^{233, 234}$U is also scarce.

It should be noted that a large part of the experimental data present in the ND files was generated several decades ago. Moreover, the ND for MAs and thorium cycle isotopes is much more scarce than for the uranium-plutonium cycle.

The man-made isotope ^{233}U is mainly obtained through breeding in ^{232}Th, as shown in Equation 3.39, and therefore plays a major role in the thorium cycle, as the main fissile isotope. Ideally, the fission cross-section should be known in the energy region of interest to a very high accuracy, namely 1%. Generally, the fission cross-sections of ^{235}U and ^{239}Pu have been measured in precise experiments with a claimed accuracy of 2-3%.

Figure 4.3 presents the data for capture in ^{233}U in the EXFOR files and the evaluated data in ENDF/B-VI.8 and JENDL-3.3, showing large gaps of unmeasured energies which are filled by the values calculated theoretically. Conversely, measured values are sometimes replaced by calculated averages; such is the case of the unresolved resonance region, where the space between resonances is so narrow that these are hardly distinguishable. For example, in Figures 4.3 and 4.5 these regions correspond to an energy range between 200-2000 eV and 2-200 keV respectively.

Special attention should be given to the data in the high-energy resonance region, which is available but not properly fitted to any model, and thus averaged for both libraries. There is also an important gap in the experimental data between 20 keV and 300 keV that may be essential for a thorium-fuelled fast reactor. The absolute value of the relative difference in the

cross-sections (green curve) seems to be about 10% in the energy range 1-10 eV and increases several orders of magnitude at the end of the resonance region, reaching 2000% at 100 eV. This increase is due to the fact that the unresolved resonance region for ENDF/B-VI.8 starts at 60 eV whereas for JENDL-3.3 it starts at 150 eV.

The main differences in the ^{233}U fission cross-section occur in the energy range 10-1000 eV. As in the case of capture in ^{233}U, the discrepancies in the fission cross-section for this energy range stay around 10%, peaking at 90 eV where they reach ~600%. Obviously, if the cross-sections are grouped (in order to reduce computing time) the differences are reduced due to within-group cancellation; therefore, the fewer the groups the smaller the discrepancies, but this also implies a lower accuracy in the calculations, since less details, i.e. resonances, are present in the ND. The experimental data seems reasonably good except for a gap between 10-70 keV and above 3 MeV. Hence an accurate evaluation of the data, together with new differential measurements to fill in the gaps and to confirm previous measurements upon which these evaluations were based, seems necessary.

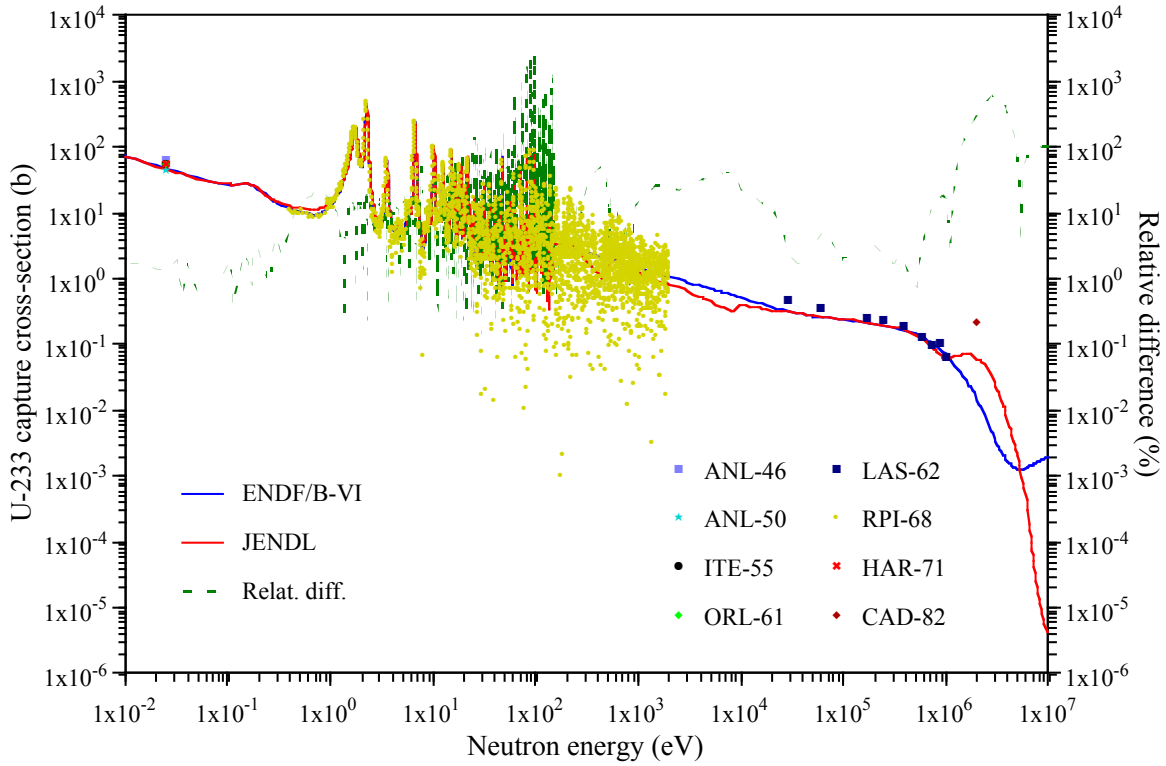

Figure 4.3. Main discrepancies in the capture cross-section for ^{233}U between ENDF/B-VI.8 and JENDL-3.3.

The main fertile isotope of the thorium cycle is ^{232}Th, which has an extensive experimental database of cross-sections. However, the evaluated data shows major discrepancies between libraries and between these and the experimental data, far from the accuracy for ^{238}U, the equivalent fertile isotope in the uranium-plutonium cycle. The capture process in ^{232}Th

directly dictates the breeding of ^{233}U fuel, thus having a direct impact on power densities, k_{eff} and fuel burn-up.

Moreover, the cross-section resonances need to be well known to predict the Doppler reactivity effect. Figure 4.4 shows that the low energy resonance region presents a capture cross-section value over 10% larger for ENDF/B-VI.8. For the higher energy resonances, both libraries seem slightly shifted in energy, although JENDL-3.3 presents a larger number of resonances. Another interesting discrepancy is the fact that the resonance region ends at 3.5 keV in JENDL-3.3 but goes up to 4 keV for ENDF/B-VI.8.

There is scarce experimental data for (n, 2n) on ^{232}Th, which after the β^- decay of ^{231}Th, leads to the production of ^{231}Pa, one of the major contributors to the long-lived radiotoxicity of the spent fuel in the thorium cycle, as explained in Chapter 6. Therefore, new precise measurements related to this threshold reaction (starting from ~50 keV) needs to be performed.

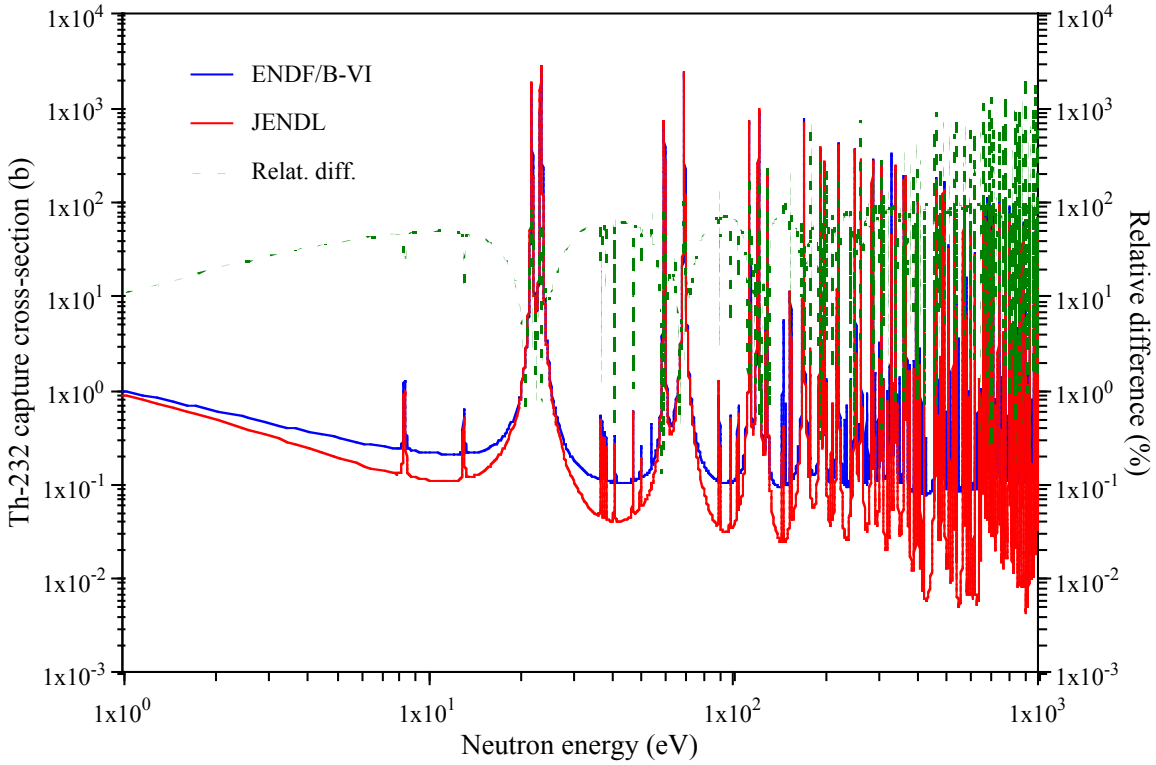

Figure 4.4. Main discrepancies in the capture cross-section for ^{232}Th between ENDF/B-VI.8 and JENDL-3.3.

Present in both fuel cycles, ^{234}U gains importance in the thorium cycle because it is generated by capture in ^{233}U, as well as by capture in ^{233}Pa and the β^--decay of ^{234}Pa. Its abundance and behaviour are similar to ^{240}Pu in the uranium-plutonium cycle. An interesting feature of the discrepancies between ENDF/B-VI.8 and JENDL-3.3 for fission is the two orders of magnitude lower thermal cross-section in the latter, as shown by Figure 4.5. The EXFOR data shows a lack of measurements for low-energies and sizable discrepancies between evaluated

and experimental data in the region 7-20 eV and for the resonance and the unresolved resonance regions, which seem to show a constant 30% discrepancy. For the capture cross-section, both libraries seem to agree better, except for some small discrepancies in the resonance and high-energy regions.

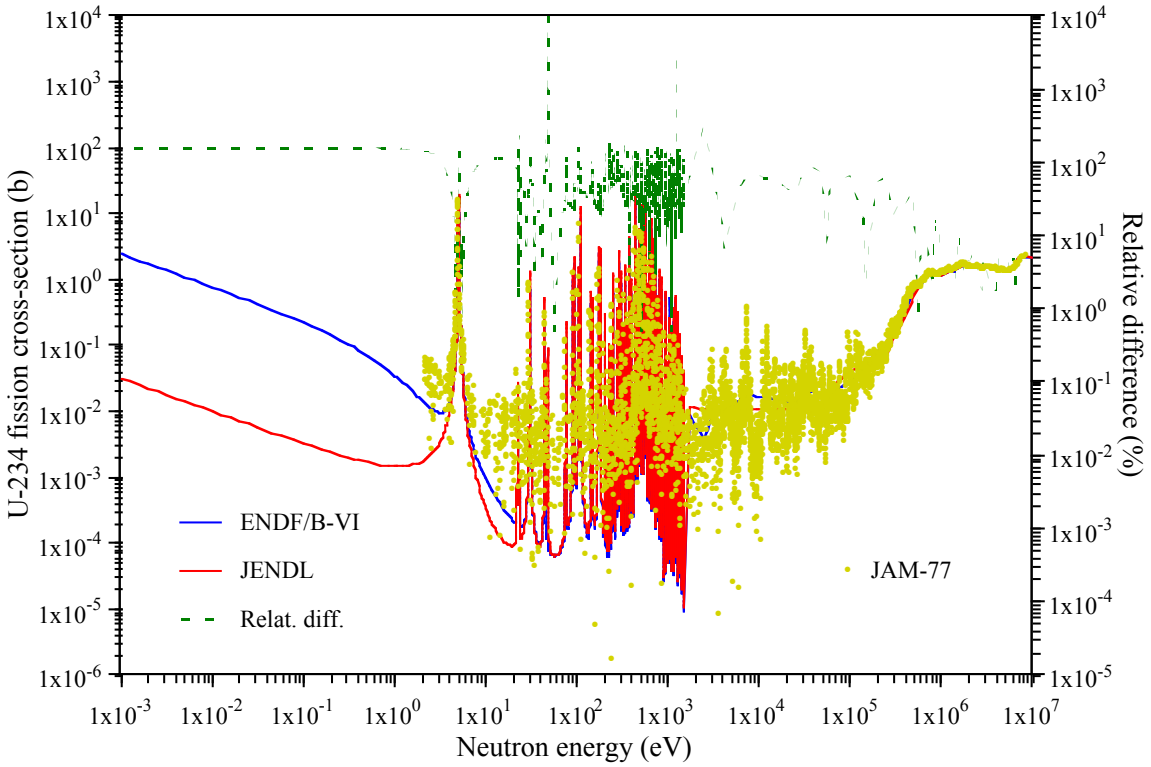

Figure 4.5. Discrepancies in the fission cross-section for ^{234}U between libraries and experimental data.

The discrepancies in the ND for ^{236}U and ^{232}U, in particular for the resonance and high-energy regions, are rather relevant. The first takes part in both the uranium and the thorium cycles, contributing to the radiotoxicity of the waste ($\tau_{1/2}$ ~2.34×10^{7} yr), as well as being the precursor of the production of ^{237}Np. The second, generated through (n, 2n) reactions in ^{233}U, is a relevant isotope in thorium-based fast systems due to the importance of (n, xn) reactions at high-energies. Its half-life ($\tau_{1/2}$ ~90 yr) and strong α-decay (~5.3 MeV) are partially responsible of the medium term (below 100 yr) radiotoxicity of the thorium-based spent. In fact, this role of this isotope in the thorium cycle is similar to the role of ^{238}Pu in the uranium cycle.

Finally, in the case of protactinium, and in particular to ^{231}Pa and ^{233}Pa, the evaluated data also shows important differences. For ^{231}Pa, as previously mentioned, major contributor to the long-term radiotoxicity in the thorium cycle spent fuel, presents important differences for the capture cross-section in the unresolved resonance region (starting at ~20 eV for JENDL-3.0 and at ~100 eV for ENDF/B-VI.8 and JEFF-3.0) and higher energies. The fission cross-sections are poorly known, showing significant discrepancies among the ND libraries for all

the energy range, from thermal to high-energy energies. The case of ^{233}Pa is quite similar, showing differences in the range of the capture resonances and in the value of the capture cross-section above 10 keV. Concerning the ^{233}Pa threshold fission, the EXFOR files show only two experimental data sets, the first measurement performed at 1.5 MeV (1966) and the second one carried out in Geel (Belgium) in 2002, where 11 points were obtained between 1 – 8.5 MeV.

4.2.2 Plutonium Isotopes

For the plutonium fissile isotopes, ^{239}Pu and ^{241}Pu, fission and capture cross-sections are rather well known at thermal energies. Nevertheless, the resonance region and, in particular, the high-energy resonances (1-50 keV) present slight differences in the case of ^{239}Pu.

Arguably, the least known isotopes are ^{238}Pu and ^{242}Pu, which represent a small amount of conventional spent fuel, but would increase their presence in the case of multiple plutonium recycling and in the case of TRUs transmutation ((n, 2n) in ^{239}Pu and capture followed by β^--decay in ^{237}Np and ^{241}Am respectively). The fission and, to some extent capture, cross-section for ^{238}Pu presents noticeable discrepancies from 1 eV upwards, as described by Figure 4.6.

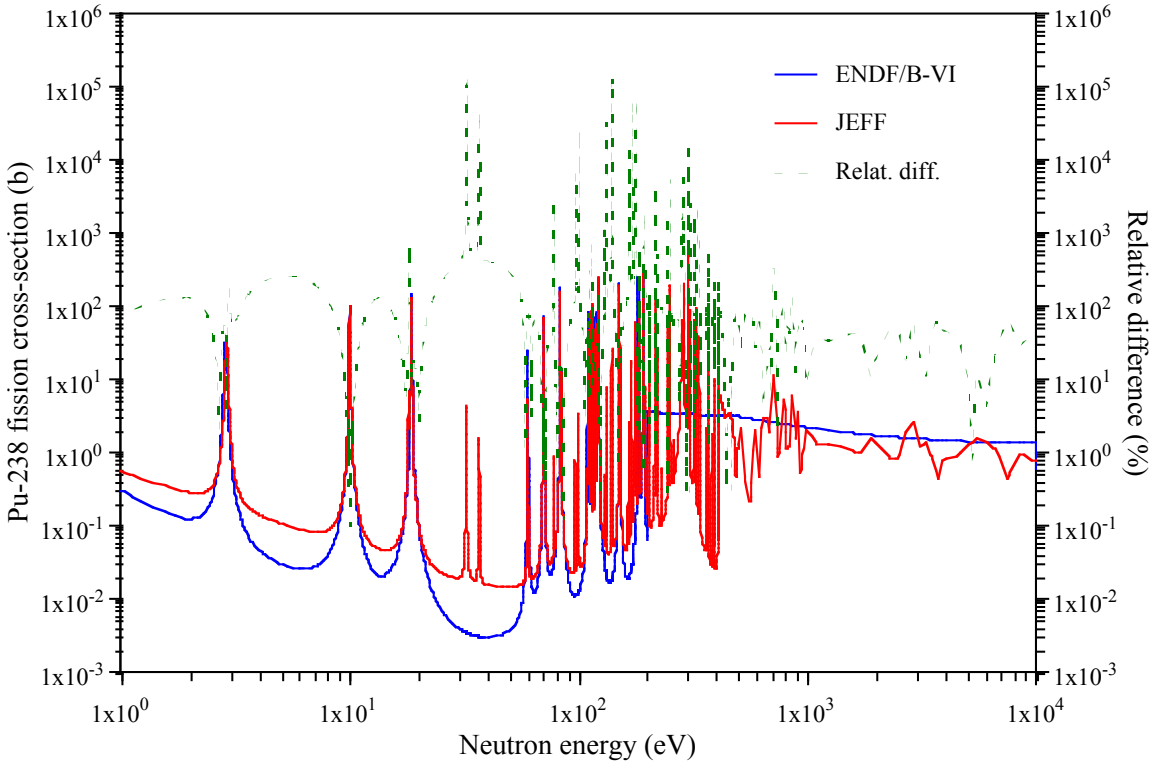

Figure 4.6. Main discrepancies in the fission cross-section for ^{238}Pu between ENDF/B-VI.8 and JEFF-3.0.

The high-energy resonances, together with the unresolved resonance region, seem to be a common point of discrepancy for most of the isotopes studied, and happen to be of extreme importance in fast systems, since the neutron flux peaks around those energies, and ^{238}Pu ($\tau_{1/2}$

~90 yr, 5.5 MeV α-decay) contributes significantly to the medium-term radiotoxicity of the MOX spent fuel.

For ^{242}Pu, the fission cross-section differs one order of magnitude even for thermal energies between JEFF-3.0 and ENDF/B-VI.8, this last library lacking a major resonance at ~2 eV. In fact, the libraries only seem to agree for high-energy fission. Data for fission and capture for ^{240}Pu seem to agree with the exception of the high-energy resonance and unresolved resonance regions, where different evaluations assign different amplitudes to these resonances for all three libraries.

4.2.3 Minor Actinides

The experimental cross-section data for MA's are quite limited, especially for some transmutation schemes which foresee high concentrations of these elements in the fuel for dedicated transmutation systems.

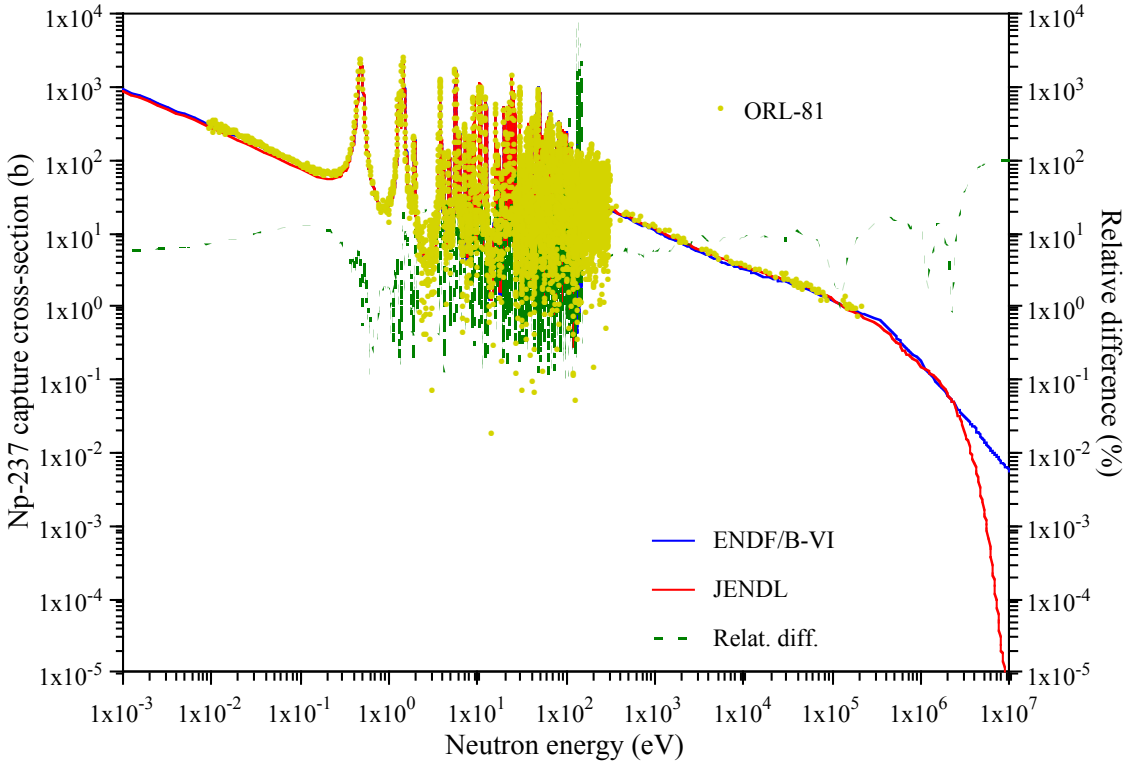

Figure 4.7. Discrepancies in the capture cross-section for ^{237}Np between libraries and experimental data.

Several measurements of the fission cross-section of ^{237}Np have already been made, below and above fission threshold (Figure 4.7). However, the quality of the data is not always acceptable, in accuracy, as well as in terms of the energy range covered. In particular, in the sub-threshold resonance energy region, ^{237}Np has a small fission cross-section which is important for transmutation studies in fast systems, where the epithermal neutron flux is not negligible in the periphery of the fuel core, and where some proposals to perform

heterogeneous transmutation of minor actinides have been made. The capture data, although more complete, also presents important discrepancies in the resonance region, in particular unresolved resonances above 150 eV, and no experimental data beyond 200 keV, as may be observed in Figure 4.7.

Measurements of the cross-sections of ^{241}Am are difficult to perform because of its high activity ($\tau_{1/2}$ = 433 yr). In addition to this difficulty, the fission cross-section of ^{241}Am is lower than 0.5 b over the range 1-300 keV. Several measurements exist in the threshold region, but the most recent ones differ between each other by more than 14%, below that point. The capture cross-section presents deviations of more than 10% in the unresolved resonance region. This reaction leads to the production of ^{242}Cm ($\tau_{1/2}$ ~163 d, α-decay), which in turn generates the hazardous ^{238}Pu.

Figure 4.1 shows the evident lack of ND for fission in ^{243}Am across the energy range. Libraries largely differ in the thermal region and the discrepancies rise as far as 700% in the unresolved resonance region. Capture is better known for this isotope, although it presents some discrepancies in the amplitude of some resonances.

Curium isotopes present large uncertainties in the cross-sections for every reaction across the energy range, especially ^{244}Cm due to its high α activity, making its measurement extremely hard to perform. JEFF-3.0 and JENDL-3.3 seem to agree for capture at low energies presenting a capture cross-section 50% higher than ENDF/B-VI.8, but disagree about its value, again, in the unresolved resonance region. Discrepancies in the fission cross-section for this isotope follow the same tendency except for larger discrepancies, of around 80%, for low energies.

The differences between libraries for fission and capture in ^{245}Cm seem smaller than for ^{244}Cm but also appear to be systematic across the energy range. It is worth noticing the large discrepancies in amplitude for the fission cross-section resonances between all three libraries, in particular for the large resonances at 1 eV, 2 eV and 4 eV. In these cases, the amplitude for JEFF-3.0 is more than one order of magnitude larger than that for ENDF/B-VI.8.

EXFOR data related to (n, xn) reaction is almost inexistent for MAs. Only ^{237}Np presents a measurement (1997), where 630 energy points between 1– 2.5 MeV were obtained. No (n, xn) public experimental data exists for americium or curium, their cross-sections being based on theoretical models. As explained later in this chapter, these reactions are particularly relevant in fast system given that they gain importance at high neutron energies, contributing to the multiplication of the system and the production of different actinides.

4.2.4 Coolants and Structural Materials

For structural materials, the capture, (n, xn) and scattering (elastic and inelastic) cross-sections are obviously of great interest due to their effect on the multiplication of the system. Elements such as zirconium or iron are omnipresent in nuclear reactors. In addition, lead and bismuth are the cooling elements in several fast reactor designs, appearing in great quantities in these cores, thus having a great impact on the neutronics of the system, as later described in 4.3.2.

The nuclear data for the main zirconium isotope, ^{90}Zr (52% natural abundance, compared to 11% for ^{91}Zr, 17% for ^{92}Zr, 17% for ^{94}Zr and 3% for ^{96}Zr), agrees rather well for the different libraries up to roughly 10 keV, even though there are small discrepancies in the amplitudes of some resonances. As for all the isotopes studied, the high-energy resonances and the unresolved resonance region present serious discrepancies that in the case of the integral value of the capture cross-section in that energy region exceeds 100% between ENDF/B-VI.8 and the other two libraries.

The nuclear data for lead is, again, well known for low energies with increasing discrepancies as the resonances increase in energy and major differences for the unresolved region, in particular, for the capture cross-section in ^{208}Pb (most prominent isotope for lead – 53% natural abundance, 24% for ^{206}Pb, 22% for ^{207}Pb and 1% ^{204}Pb), where the differences reach three orders of magnitude at 1 MeV. The average value of the discrepancies is more than 30% from 10 keV upwards.

For ^{209}Bi, the only stable isotope of bismuth, the discrepancies in the capture cross-section presented in Figure 4.8 are noticeable at all energies, from 10% at low energies up to six orders of magnitude for some resonances. This is clearly explained by the lack of experimental data, since the points in Figure 4.8 represent the few experiments carried out to measure this cross-section.

Concerning the (n, xn) reactions in ^{209}Bi, for which there is a number of experimental measurements (54), the evaluations tend to differ in ~20% for all energies (threshold at ~7.4 MeV). The case of the inelastic scattering is similar, with an acceptable set of measurements (87), and ~30% differences above 10 MeV and large uncertainties around the threshold energy (~900 keV). The evaluated elastic scattering cross-section also presents some differences in the resonance region above 100 keV.

As elaborated in Section 4.3.2, the uncertainties in the capture, (n, ne), (n, ni) and (n, xn) reactions may have important implications for the predictions of the multiplication of a lead-bismuth cooled system.

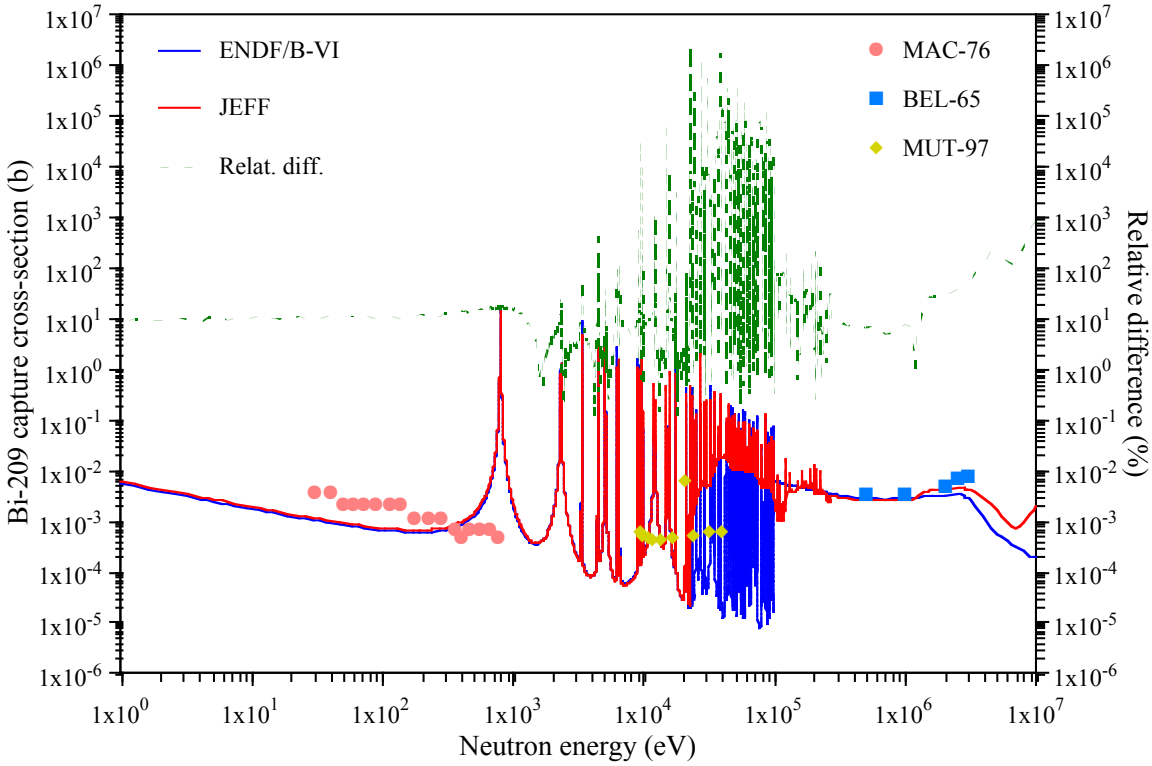

Figure 4.8. Discrepancies in capture data for ^{209}Bi between ENDF/B-VI.8, JEFF-3.0 and EXFOR.

4.2.5 Summary of the Status of the Nuclear Data for Transmutation

This introductory ND comparative analysis, although not exhaustive, evidenced some common tendencies among isotopes important to the transmutation of HLW in ADS. Fission and capture cross-sections for thermal energies are relatively well known for some isotopes, such as $^{233, 235, 238}$U, $^{239, 241}$Pu or Pb, but even this energy range presents obvious differences for non-conventional isotopes, e.g. thorium, $^{238, 242}$Pu, americium, curium or bismuth.

The resonance region generally presents large discrepancies both in the number of resonances and in the amplitude of these, due to different evaluations of the experimental data. These differences increase for the high-energy resonance region, where libraries often differ in their prediction of the energy at which those end. This energy range is of great importance for fast systems, since the neutron flux is maximum here. Therefore these differences will affect fast reactor calculations quantitatively more than differences in the thermal energy range. The unresolved resonance region shows the same tendencies with the same implications, as in the case of ^{243}Am.

Since the neutron flux in fast systems tends to peak in an energy range, i.e. 300-700 keV, where many isotopes present important differences, the high-energy reaction channels such as (n, xn) and (n, ni), which were not considered very significant in thermal systems, gain

importance in fast systems. And it is also for these reaction channels where large discrepancies are found for a vast number of isotopes.

This data seems suitable for preliminary calculations, but not for precise predictions of the behaviour of non-conventional systems, such as ADS, loaded with substantial quantities of these isotopes. Hence, an analysis of the effects of this nuclear data in several transmutation systems is required in order to assess the reliability of the calculations performed for these systems.

4.3 Analysis of Sensitivity to Nuclear Data

Accurate cross-section information is fundamental for reliable prediction of the behaviour of a nuclear reactor core. In particular, for an ADS, the level of uncertainty in $\Delta\rho$/cycle is of paramount importance (e.g. at k_{src} ~0.98 ± 2% uncertainty in $\Delta\rho$/cycle has serious consequences for safety analysis and accelerator current requirements). Thus, for a subcritical device, uncertainties in the nuclear data limit the safety margins within which such a device could operate. Hence, for $0.90 \leq k_{src} \leq 0.99$ the precision should be similar to that required for critical cores (±100 pcm for UO_2, ±40 pcm for MOX).

As previously explained, the various cross-section libraries show significant differences between their respective ND, for a wide range of energies. The use of different libraries can cause significant deviations in the results of design calculations. This analysis aimed to identify the isotopes and reaction channels responsible for the largest discrepancies in the main neutronic parameters.

A neutron cross-section sensitivity analysis [73] was previously performed also using the EA-MC code package to study EADF [46], comparing the results of calculations based on different nuclear data libraries. The results showed discrepancies in $\Delta k/k$ ranging from 500 to 2500 pcm for different types of fuels and ND libraries. Large neutron balance discrepancies for some reactions and isotopes (e.g. 25% for capture in ^{241}Pu, 16% for fission in ^{240}Pu) were discovered.

The release of new versions of the nuclear data libraries (ENDF/B-VI.8, JEFF-3.0 and JENDL-3.3) led to the present study [74], also extending the previous work to other isotopes of interest. In addition, progress in the design of TRADE [50] generated interest in studying the effects of cross-section data for thermal ADSs, thus widening the energy range examined in the study [75]. The comparison between libraries was performed using ENDF/B-VI.8 as a reference library and systematically changing the ND library of a single isotope at a time, while keeping the ND intact for the rest of the isotope inventory. In this way, the effects of the

discrepancies in the ND for every specific isotope were isolated, thus avoiding possible compensating effects.

It should be emphasised that these results show the relative discrepancies between libraries, and do not imply an assumption that one library is more accurate than another. The results simply estimate the level of uncertainty for every isotope and reaction.

4.3.1 Sensitivity Analysis on a Thermal System: TRADE

As detailed in Chapter 5, TRADE is a pilot experiment, to provide a global demonstration of the ADS concept. The experiment entails the coupling of a thermal reactor, an existing 1 MW TRIGA reactor in ENEA / Casaccia (Italy), to a 140 MeV, 1 mA proton cyclotron. For the reference configuration a multiplication coefficient k_{src} = 0.97 – 0.98, a beam power P_{beam} = 14.2 kW and an energy gain G = 15.1, with a neutron yield for 140 MeV protons in tantalum of 0.8 n/p, are predicted. The fuel elements consist of a ternary alloy uranium-zirconium-hydrogen (the H-to-Zr atom ratio is 1.7:1; the uranium is enriched to 20% in ^{235}U).

The effects of the different cross-sections for the isotopes in the fuel, ^{235}U and ^{238}U, and the main structural materials, ^{56}Fe and ^{90}Zr, were considered, together with global analysis of the different ND libraries. Table 4.1 presents the results of this analysis, where the red entries indicate large discrepancies between the reference library and the library in question. The blue entries denote small discrepancies between the results obtained when all the isotopes are chosen from the same library.

Table 4.1. Neutron cross-section data effects on k_{src} for TRADE.

Isotopes		ENDF/B-VI.8	JEFF-3.0	JENDL-3.3
U-235	k_{src}	0.97389	0.97362	0.97201
	error	±0.00029	±0.00018	±0.00017
	$\Delta k/k$ (pcm)		–28	**–193**
U-238	k_{src}	0.97389	0.97391	0.97387
	error	±0.00029	±0.00021	±0.00020
	$\Delta k/k$ (pcm)		2	–2
Zr-90	k_{src}	0.97349	0.97521	0.97572
	error	±0.00020	±0.00020	±0.00021
	$\Delta k/k$ (pcm)		**177**	**229**
Fe-56	k_{src}	0.97349	0.97425	0.97387
	error	±0.00020	±0.00021	±0.00027
	$\Delta k/k$ (pcm)		78	39
All isotopes	k_{src}	0.97389	0.97615	0.97454
	error	±0.00029	±0.00022	±0.00024
	$\Delta k/k$ (pcm)		**232**	**67**

Large discrepancies were found for ^{90}Zr between the reference library and both JENDL-3.3 and JEFF-3.0.These are significant discrepancies for an isotope, which a priori may not have seemed relevant in terms of system multiplication. Substantial discrepancies for ^{235}U between

ENDF/B-VI.8 and JENDL-3.3 can also be observed. When different libraries, are used for all the isotopes large discrepancies appear between ENDF/B-VI.8 and JEFF-3.0.

No major differences can be observed in Figure 4.9, which compares the capture and fission reaction rates in ^{235}U as a function of neutron energy for ENDF/B-VI.8 and JENDL-3.3, except for a slightly higher capture rate in the 10-300 keV energy for fission, which could cause minor differences in k_{src}.

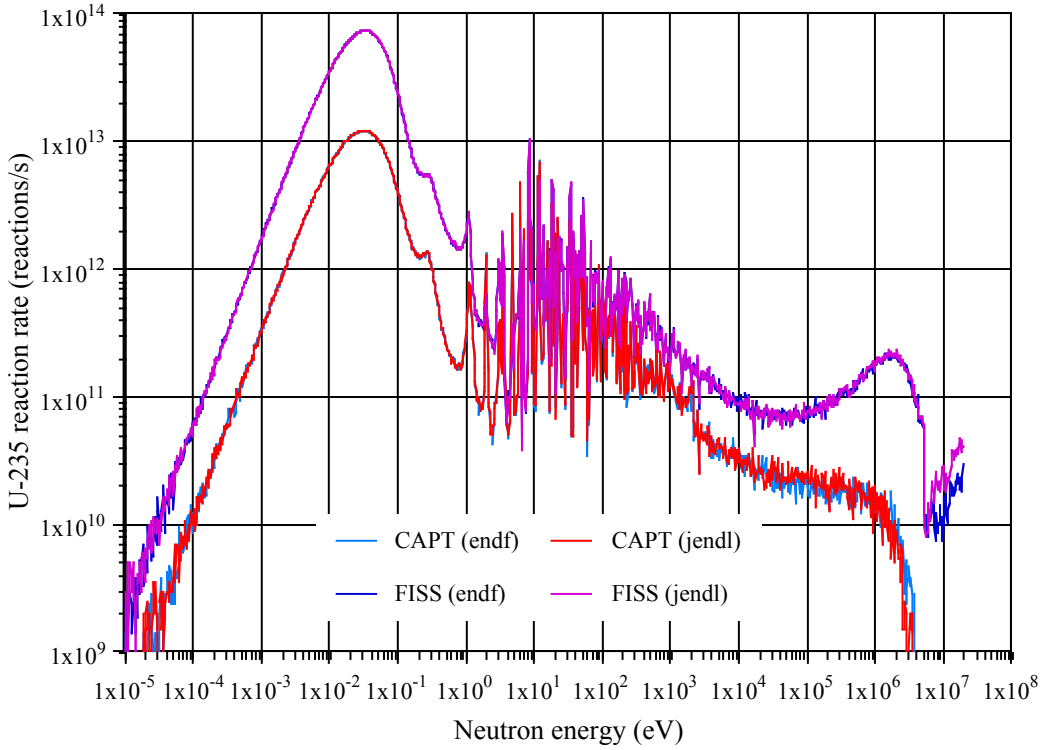

Figure 4.9. Comparison of reaction rates for capture and fission in ^{235}U using ENDF/B-VI.8 and JENDL-3.3.

On the other hand, a slight discrepancy in the MeV region can be observed in Figure 4.10 when comparing the elastic (n, ne) and the inelastic (n, ni) scattering reaction rates: JENDL-3.3 predicts more elastic and less inelastic scattering. This divergence shifts the spectrum of the neutrons, producing more moderation in the case of ENDF/B-VI.8, increasing the resonance escape probability and effectively increasing k_{src}. The lower k_{src} predicted by JENDL-3.3 when compared to ENDF/B-VI.8 is reflected in the shape of the radial neutron flux, having a higher value in centre of the core (7.96×10^{12} n/cm^2/s for ENDF/B-VI.8 versus 8.06×10^{12} n/cm^2/s for JENDL-3.3) and a slightly lower one in the periphery (3.35×10^{12} n/cm^2/s for ENDF/B-VI.8 versus 3.32×10^{12} n/cm^2/s for JENDL-3.3).

As explained in Chapter 3, the differences in the shape of the neutron flux are related to the changes in the diffusion of neutrons in a multiplying medium, evolving from an exponential distribution to a cosine distribution with increasing k_{src}.

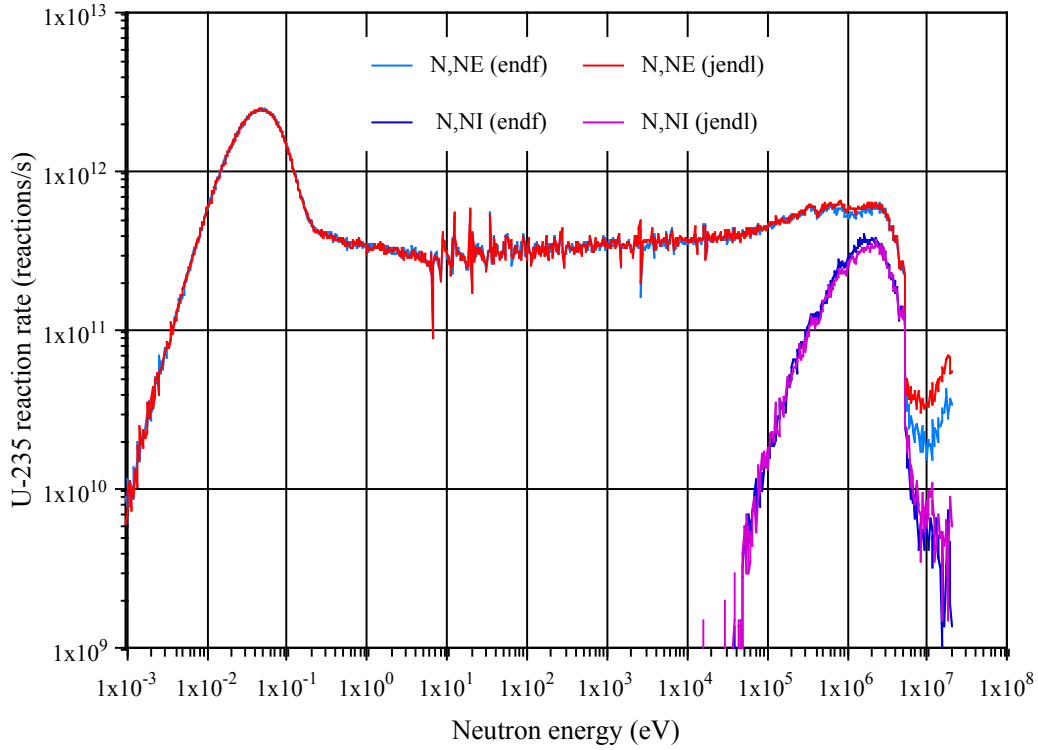

Figure 4.10. Comparison of reaction rates for (n, ne) and (n, ni) in ^{235}U using ENDF/B-VI.8 and JENDL-3.3.

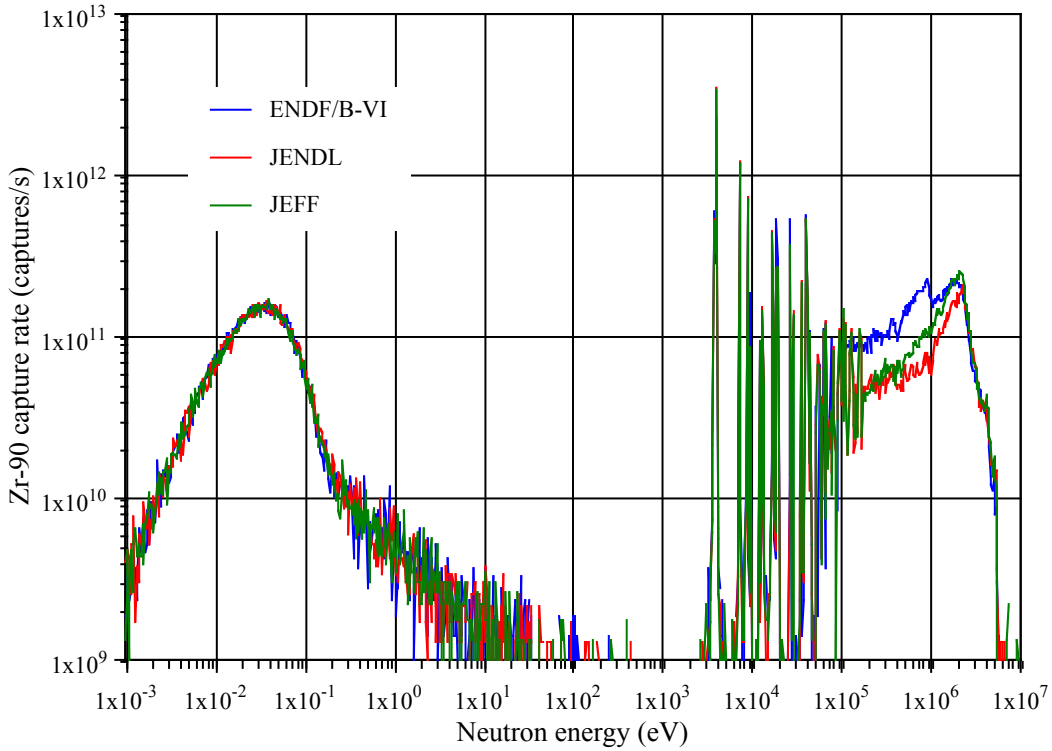

Figure 4.11. Capture rates in ^{90}Zr for ENDF/B-VI.8, JENDL-3.3 and JEFF-3.0.

The analyses using different ND libraries for all isotopes show contrasting results. JEFF-3.0 gives discrepancies with ENDF/B-VI.8 (232 pcm) well above the statistical error, whereas JENDL-3.3 is in good agreement with ENDF/B-VI.8. As Table 4.1 shows, this change is

mainly due to the lower capture rates in ^{90}Zr, presented in Figure 4.11, using JEFF-3.0 and JENDL-3.3, thus increasing the value of k_{src}. A detailed study of the energy spectrum of the capture rate in ^{90}Zr shows that the largest discrepancies are concentrated in the energy region from 50 keV to 2 MeV, identifying where the cross-section data should be particularly improved, in the context of thermal reactors.

Comparison of the neutron energy spectra for different isotopes in the fuel evidences the minimisation of possible effects in the reactor behaviour due to a shift in the neutron spectrum caused by the use of a different library. These so-called spectrum effects are reduced by repeatedly changing a single isotope in the simulations of the device, as evidenced by Figure 4.12.

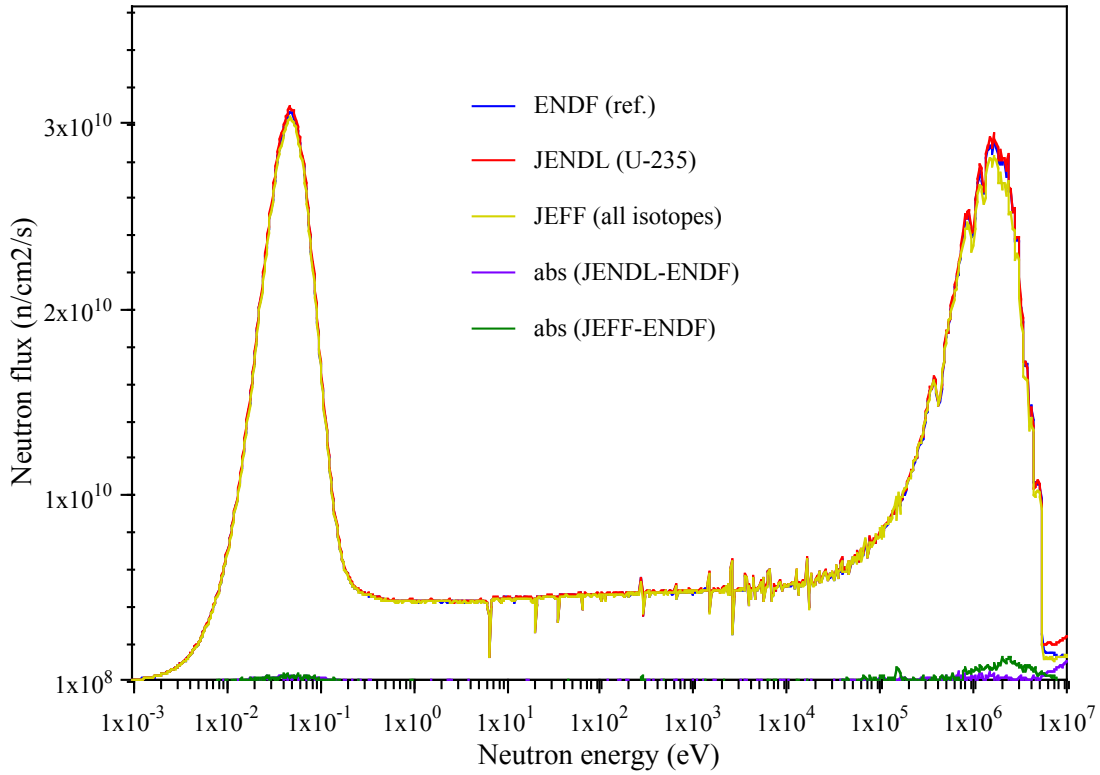

Figure 4.12. Neutron energy spectra in the fuel of TRADE for different ND libraries.

To study several isotopes of importance for transmutation, small samples were placed inside fuel pins in different positions in the core. This procedure aimed to average differences in the spectrum of every fuel region. Table 4.2 presents the neutron balance results for the isotopes and reaction channels. Reactions are classified as “capture”, “fission” and “n,xn” and their rates of occurrence are given as a relative percentage, with only reactions that contribute significantly being listed. The columns headed by ΔJEFF and ΔJENDL present relative percentage differences between the cross-section library in question and the reference (ENDF). These discrepancies are highlighted when greater than 2% and statistically

significant. The values of ΔJEFF and ΔJENDL are omitted when the occurrence of the reaction is below 1% of the total reactions.

Table 4.2. Neutron balance of the actinides analysed in TRADE (thermal spectrum).

		ENDF %	JEFF %	ΔJEFF %	JENDL %	ΔJENDL %
Th 232	Capture	97.36	97.29	–0.07	97.38	+0.02
	Fission	1.08	1.21	**+11.24**	1.14	+4.70
	n,xn	1.56	1.50	–3.8	1.49	**–4.49**
U 233	Capture	9.31	9.37	+0.67	9.33	+0.19
	Fission	90.65	90.57	–0.09	90.62	–0.03
	n,xn	0.04	0.06		0.05	
U 234	Capture	91.45	91.50	+0.05	91.50	+0.05
	Fission	8.42	8.37	–0.46	8.31	–1.25
	n,xn	0.14	0.13		0.20	
U 235	Capture	15.69	15.70	+0.06	15.69	0.00
	Fission	84.31	84.29	–0.02	84.30	–0.01
	n,xn	0.007	0.007		0.005	
U 238	Capture	96.24	96.29	+0.05	96.19	–0.05
	Fission	3.13	3.11	–0.40	3.19	+2.00
	n,xn	0.63	0.60		0.62	
Pu 238	Capture	78.73	76.29	**–3.10**	78.50	–0.30
	Fission	20.88	23.50	**+12.60**	21.47	+2.80
	n,xn	0.39	0.20		0.03	
Pu 239	Capture	28.85	28.91	+0.21	28.90	+0.17
	Fission	71.08	71.04	–0.06	71.06	–0.03
	n,xn	0.06	0.05		0.04	
Pu 240	Capture	91.02	90.94	–0.09	91.01	–0.01
	Fission	8.88	8.90	+0.20	8.89	+0.10
	n,xn	0.10	0.20		0.10	
Pu 241	Capture	22.63	23.09	**+2.00**	22.60	–0.10
	Fission	77.32	76.83	–0.60	77.31	–0.01
	n,xn	0.05	0.08		0.09	
Pu 242	Capture	90.05	89.58	–0.52	90.05	0.00
	Fission	9.68	10.04	**+3.73**	9.82	+1.50
	n,xn	0.27	0.40		0.10	
Np 237	Capture	92.98	92.96	–0.02	92.71	–0.29
	Fission	6.90	6.95	+0.78	7.15	**+3.70**
	n,xn	0.12	0.09		0.14	
Am 241	Capture	93.31	92.82	–0.52	92.73	–0.60
	Fission	6.67	7.12	+6.80	7.22	**+8.30**
	n,xn	0.02	0.06		0.05	
Am 243	Capture	94.41	94.13	–0.30	94.20	–0.22
	Fission	5.50	5.75	**+4.80**	5.71	+4.00
	n,xn	0.10	0.12		0.09	
Cm 244	Capture	77.97	77.60	–0.47	79.04	+1.37
	Fission	21.74	22.28	+2.48	20.86	**–4.05**
	n,xn	0.29	0.12		0.10	
Cm 245	Capture	13.43	13.81	**+2.83**	13.42	–0.07
	Fission	86.56	86.17	–0.45	86.57	+0.01
	n,xn	0.01	0.01		0.01	

The results for ^{235}U and ^{238}U seem to agree rather well for all the libraries. Other isotopes such as ^{233}U, ^{239}Pu and ^{240}Pu also appear to produce similar results. An unexpected discrepancy is the 2% uncertainty in capture for ^{241}Pu, since this is a fissile isotope fairly abundant in nuclear waste. Moreover, the results show large deviations in the neutron balance for several important isotopes: 11.2% in fission for ^{232}Th, 12.6% in fission for ^{238}Pu and 8.3% in fission for ^{241}Am. Isotopes such as ^{242}Pu, ^{237}Np, ^{243}Am and $^{244,\ 245}$Cm also present considerable discrepancies in the neutron balance for this particular spectrum. These significant differences could have an important effect on the neutron multiplication of the system in the case of a core heavily loaded with these isotopes.

In order to fully analyse the effects of the divergences in the nuclear data, the integral value of the reaction rates for the different isotopes were obtained, and the results for different libraries were compared. Figures 4.13 to 4.16 show the most notable differences between the reference (ENDF/B-VI.8) case and JENDL-3.3 and JEFF-3.0 results, for every isotope of interest.

Figure 4.13 shows the good agreement between calculations for the naturally occurring isotopes of uranium except for a 10% difference for inelastic scattering in ^{235}U. This divergence takes place mainly between 300 keV and 2 MeV, as can be observed in Figure 4.10. Capture in ^{232}Th and capture and fission in ^{233}U and in ^{234}U also agree well. On the other hand, discrepancies increase for the other reactions in ^{232}Th, ^{233}U and ^{234}U reaching a 33% discrepancy between ENDF/B-VI.8 and JEFF-3.0.

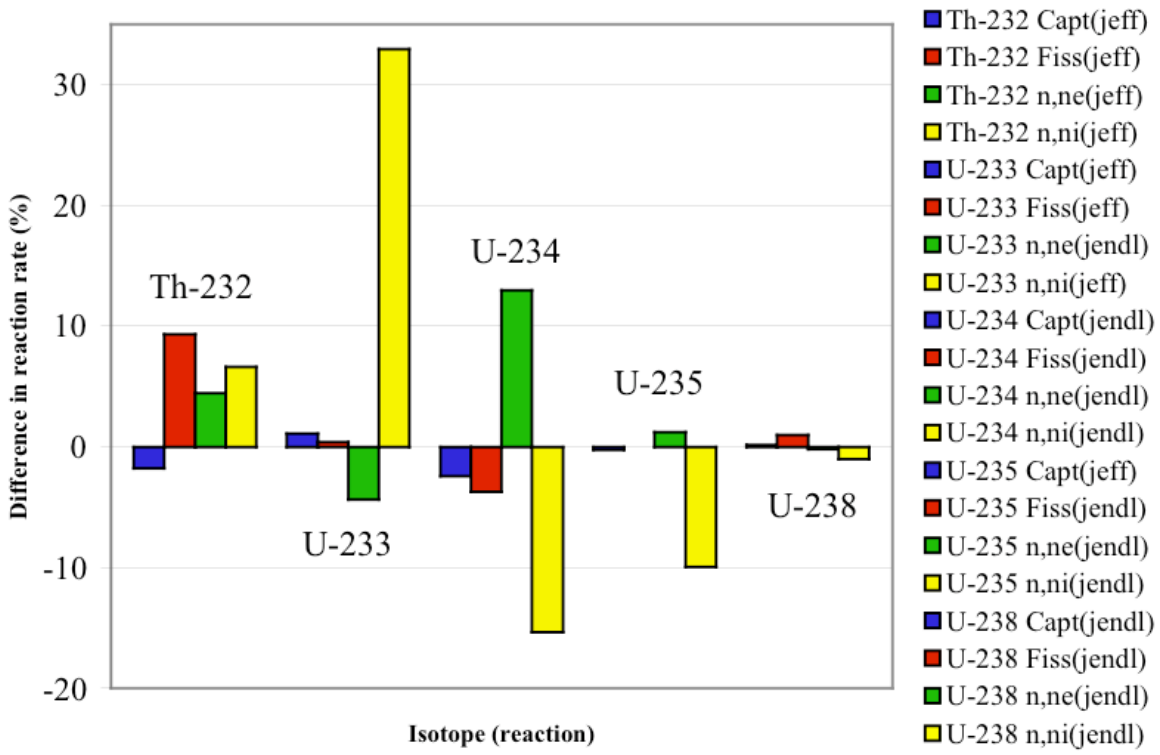

Figure 4.13. Reaction rate discrepancies in TRADE for uranium isotopes and ^{232}Th.

Figure 4.14 presents the discrepancies in the reaction rates for the main plutonium isotopes. It is immediately apparent that inelastic scattering is the reaction channel giving the largest discrepancies, above 15% for all the isotopes and reaching 56% for ^{241}Pu. Mainly because of the low yield of ^{238}Pu, the reaction channels for this isotope present noticeable discrepancies, in particular 11% in fission (ENDF-JEFF), 12% in (n, ne) (ENDF-JEFF) and 38% in (n, ni) (ENDF-JENDL).

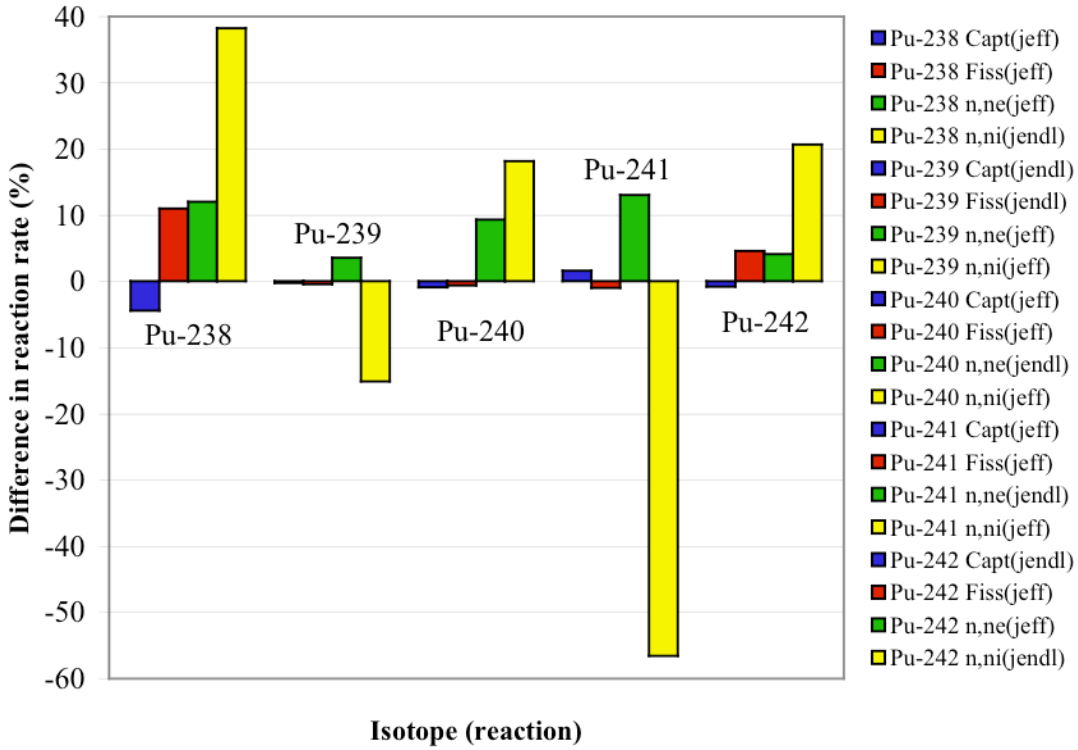

Figure 4.14. Reaction rate discrepancies in TRADE for the plutonium isotopes.

For the minor actinides involved in the study, again the inelastic scattering reaction gives the largest discrepancies. The main curium isotope, ^{244}Cm, presents the largest deviations in all the reaction channels (above 10%), as can be observed in Figure 4.15.

The analysis of the reaction rates for ^{56}Fe, ^{90}Zr (structural materials), ^{99}Tc and ^{129}I (long-lived fission fragments) provides useful information about the uncertainties concerning these elements, as shown in Figure 4.16. The (n, xn) reactions, which have a direct effect on the multiplication of the system as a source of neutrons, exhibit large discrepancies (15% for ^{56}Fe, 4% for ^{90}Zr and 50% for ^{99}Tc, for the (n, 2n) reaction); ^{129}I is a particular issue since there is no (n, xn) information in the ENDF release.

This fact together with the possibility of transmuting this isotope through this reaction (^{128}I decays after 10 minutes through β^- into ^{128}Xe, which together with $^{129, 130, 131, 132}$Xe are stable isotopes), makes this cross-section an important one [76]. In the case of capture in ^{90}Zr, differences reach 15% (ENDF-JENDL) and, as mentioned previously in this chapter, could

have an important effect on the multiplication coefficient. As for most of rest of the isotopes analysed, elastic and, especially, inelastic scattering reactions present large discrepancies, particularly for ^{99}Tc, ^{90}Zr and ^{129}I.

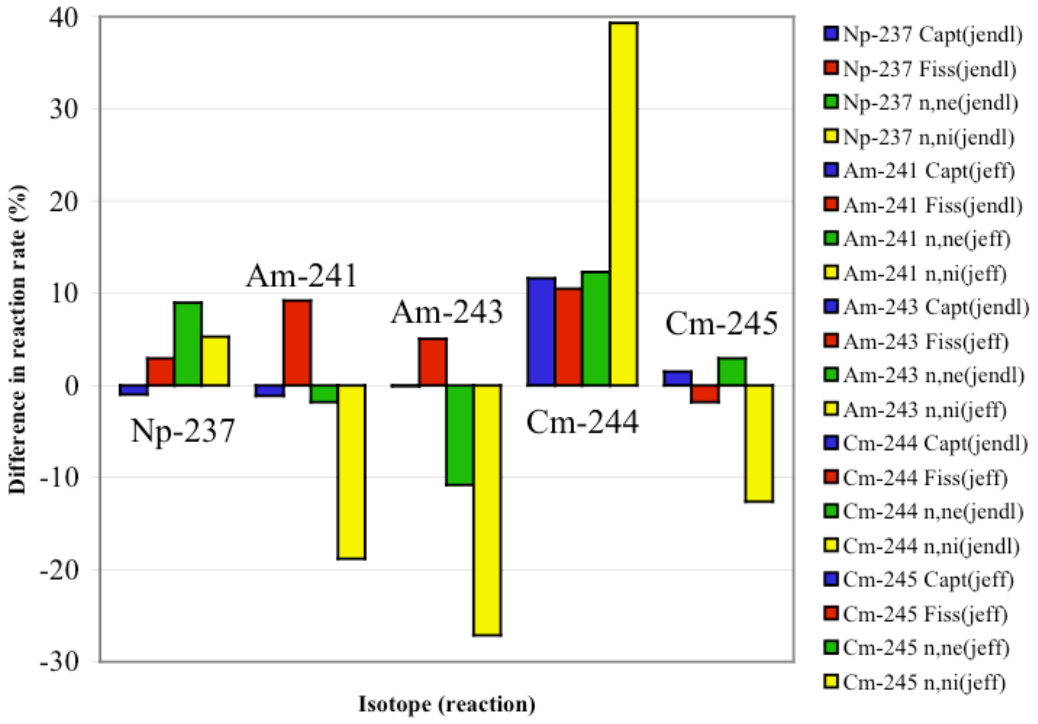

Figure 4.15. Reaction rate discrepancies in TRADE for MAs.

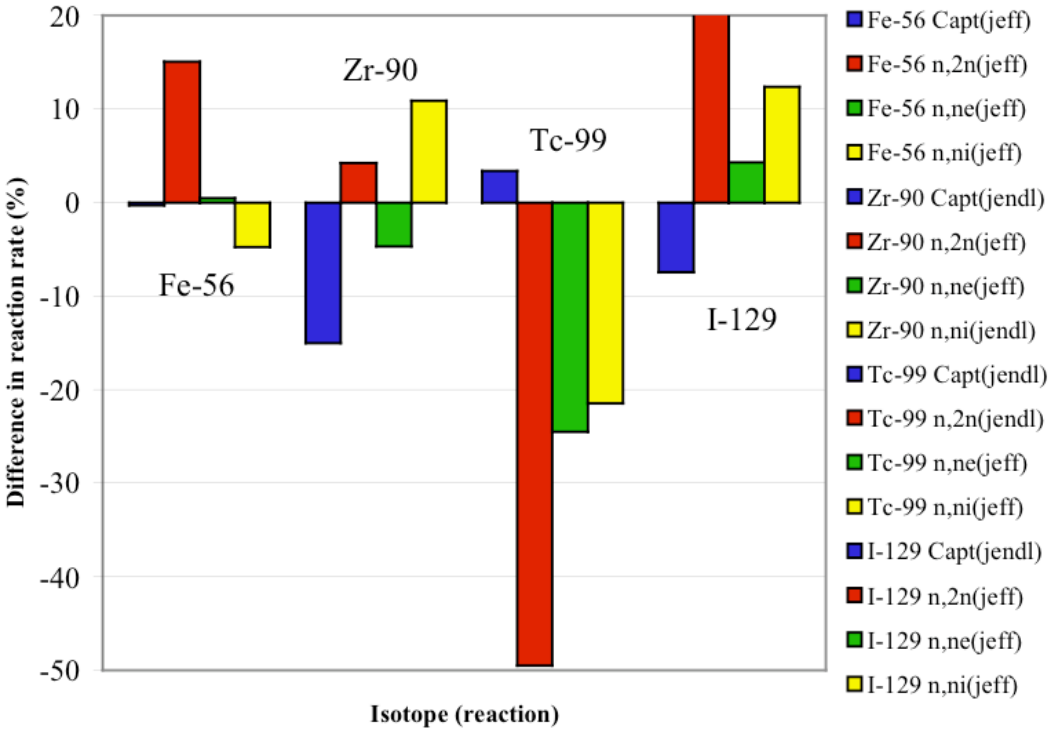

Figure 4.16. Reaction rate discrepancies in TRADE for ^{56}Fe, ^{90}Zr, ^{99}Tc and ^{129}I.

These figures show major differences in the reaction rates (especially in elastic and inelastic scattering) for many of the isotopes analysed. These have a direct effect on the neutron energy spectrum and consequently on k_{src}. The results for ^{90}Zr highlight the importance of the frequently neglected need for accurate cross-section data for structural materials.

4.3.2 Sensitivity Analysis on a Fast System: EADF

The conceptual design of EADF is based on an 80 MW_{th} annular core immersed in molten lead-bismuth eutectic, which serves both as the primary coolant and spallation target. The central cylinder contains the spallation target, coupling the proton accelerator and the subcritical core. This device should demonstrate transmutation with a large number of MAs based fuel assemblies. In this study, the fuel analysed was $ThPuO_2$-based mixed with MAs. The neutron flux in the fuel is ~10^{15} n/cm^2/s with an energy distribution peaking at ~300 keV. Chapter 6 provides an in-depth analysis of this project.

A previous study [73] analysed the effect of the discrepancies in the ND libraries for the reference fuel configuration, i.e. $UPuO_2$. This study was performed using previous library releases, i.e. ENDF/B-VI.6, JEFF-2.2 and JENDL-3.0, for the whole set of isotopes and analysing its effect for different isotopes.

Therefore, the present study [74] is based on the analysis of the effects of different cross-section data for specific isotopes (isotope per isotope) for the main isotopes involved in the design of this system (i.e. coolant and isotopes present in the fuel), together with global analysis of the different ND libraries. For this purpose, three alternative types of fuel have been analysed: a $ThPuO_2$ fuel (proposed at a second stage of device operation), a $ThUO_2$ fuel where the plutonium was substituted by ^{233}U, and a mixture of 50% Pu and 50% MAs, both with an isotopic composition typical of UO_2 spent fuel with an average thermal burn-up of 33 GWd/tHM, as described in Chapter 2. As explained earlier, this study makes use of the latest releases of the aforementioned ND libraries (i.e. ENDF/B-VI.8, JEFF-3.0 and JENDL-3.3).

4.3.2.1 $ThPuO_2$ and $ThUO_2$ fuels

The first matrix is formed by thorium-oxide containing approximately 20% of highly fissile plutonium in order to start the fission chain at the beginning of the reactor cycle. The second matrix was formed by substituting plutonium with the equivalent amount of ^{233}U to maintain the system subcritical. Table 4.3 summarises the composition of the $ThPuO_2$ fuel. In the case of ^{99}Tc and ^{129}I, small quantities were added to the external Pb-Bi blanket.

Table 4.3. Isotopic composition of the $ThPuO_2$ fuel for EADF.

$^{16, 17, 18}$O	^{232}Th	^{237}Np	^{238}Pu	^{239}Pu	^{240}Pu	^{241}Pu	^{242}Pu	^{241}Am
0.666667	0.256697	0.000018	0.000209	0.053030	0.018664	0.001985	0.000974	0.001763

Table 4.4 presents the largest discrepancies found in the multiplication coefficient. Vast differences in the predictions of this value can be observed, especially in the cases of the four major isotopes in relation to transmutation in the thorium cycle: ^{232}Th, ^{233}U, ^{239}Pu and ^{240}Pu. The importance of the differences related to these plutonium isotopes is enhanced by the small quantities of these in the fuel.

Table 4.4. Main neutron cross-section data effects on k_{src} for the $ThPuO_2$ fuel in EADF.

Reference case $ThPuO_2$: ENDF/B-VI.8, k_{src} = 0.94613 ± 0.00090		
Isotopes	JEFF-3.0 $\Delta k/k$ (pcm)	JENDL-3.3 $\Delta k/k$ (pcm)
Tc-99	+104	+146
I-129	–62	–95
Pb-206	–145	–71
Pb-207	–191	**–249**
Pb-208	+103	+130
Bi-209	–122	**+207**
Th-232	**+770**	**+703**
Pu-238	–29	–159
Pu-239	**–318**	**–625**
Pu-240	**–376**	**–627**
Pu-241	+7	–181
Pu-242	–136	**–209**
Am-241	–134	–12
All isotopes	**+317**	**–61**
Reference case $ThUO_2$: ENDF/B-VI.8, k_{src} = 0.97424 ± 0.00083		
U-233	**–1383**	**–1420**
U-234	**+205**	+61
U-235	–100	–188
U-238	–139	**–270**

It should be noticed that for both, but especially clearly in the case of JENDL-3.3, how major differences in k_{src}, due to the cross-section discrepancies for different isotopes, are hidden once a whole library is used for all the isotopes. This effect is a potential source of critical errors in the designing of the reactor. Hence, ND is key to correctly predicting the behaviour of these systems.

Table 4.5 presents the isotopes showing the largest discrepancies in the neutron balance for different reaction channels. Notice that the effects presented in Table 4.4 depend directly on the composition of the fuel and the amount of every single isotope in the core, whereas the neutron balance mainly depends on the energy distribution of the neutron flux affecting the isotope (which depends on the design of the system). Practically, this implies that discrepancies in calculations for a core highly loaded with more "exotic" isotopes, such as ^{238,242}Pu, ^{241}Am and ^{244,245}Cm, would be much greater than the ones shown above.

Capture in ^{208}Pb presents a large discrepancy between ENDF/B-VI.8 and JEFF-3.0 in the neutron balance, even though the capture cross-section is so small that this only represents a

103 pcm difference in $\Delta k/k$. ^{238}Pu shows major discrepancies in fission and capture, as does fission in ^{237}Np. On the other hand, ^{209}Bi in JENDL-3.3 shows a 12.5% discrepancy in capture, which translates into 207 pcm in $\Delta k/k$. The large effects observed for ^{232}Th, ^{233}U, ^{239}Pu and ^{240}Pu in Table 4.4 are a consequence of minor discrepancies in the neutron balance in isotopes abundant in the fuel, together with the effect of large discrepancies in the inelastic scattering cross-sections.

Table 4.5. Neutron balance of the isotopes studied in EADF (fast spectrum).

		ENDF %	JEFF %	ΔJEFF %	JENDL %	ΔJENDL %
Pb 206	Capture	89.36	85.97	–3.79	85.46	–4.36
	n,xn	10.64	14.03	–3.12	14.54	–1.96
Pb 207	Capture	92.96	91.11	–1.99	91.12	–1.98
	n,xn	7.05	8.89	–0.71	8.88	–1.50
Pb 208	Capture	27.00	20.32	**–24.74**	20.43	–24.30
	n,xn	73.00	79.68	+2.38	79.57	+1.95
Bi 209	Capture	58.95	58.92	–0.05	51.58	**–12.50**
	n,xn	41.05	41.08	–2.08	48.42	+2.57
Th 232	Capture	96.26	96.14	–0.13	96.17	–0.09
	Fission	2.46	2.64	**+7.58**	2.61	+6.31
	n,xn	1.28	1.22		1.22	
U 233	Capture	8.179	8.033	–1.79	8.04	–1.74
	Fission	91.78	91.93	+0.16	91.92	+0.15
	n,xn	0.039	0.039		0.04	
U 235	Capture	28.23	26.48	**–6.20**	28.04	–0.67
	Fission	71.77	73.52	+2.44	71.96	+0.26
	n,xn	0.00	0.00		0.00	
U 234	Capture	87.68	85.56	–2.42	84.78	–3.31
	Fission	12.32	14.44	**+17.21**	15.22	**+23.54**
	n,xn	0.00	0.00		0.00	
U 238	Capture	94.51	94.85	+0.36	94.67	+0.17
	Fission	5.15	4.86	**–5.73**	4.98	–3.36
	n,xn	0.34	0.29		0.35	
Pu 238	Capture	40.60	31.14	**–23.30**	38.54	–5.07
	Fission	59.27	68.83	**+16.13**	61.46	+3.69
	n,xn	0.13	0.04		0.35	
Pu 239	Capture	21.92	22.25	+1.51	22.49	+2.60
	Fission	78.04	77.71	–0.42	77.48	–0.72
	n,xn	0.04	0.03		0.03	
Pu 240	Capture	59.39	60.14	–0.09	60.83	–0.01
	Fission	40.52	39.74	+0.20	39.10	+0.10
	n,xn	0.08	0.12		0.08	
Pu 241	Capture	15.17	16.20	**+6.80**	16.03	+5.70
	Fission	84.80	83.76	–1.30	83.92	–1.04
	n,xn	0.03	0.04		0.06	
Pu 242	Capture	69.37	69.97	+0.86	70.46	+1.57
	Fission	30.47	29.80	–2.20	29.46	–3.32
	n,xn	0.16	0.24		0.08	

The analysis of the possible spectrum effects in the fuel evidences again a large reduction of these by the systematic evaluation of a single isotope at a time. Figure 4.17 shows the neutron spectrum in the fuel using ENDF/B-VI.8 (blue curve), using JENDL-3.0 for ^{239}Pu and ENDF/B-VI.8 for the rest (red curve), using JEFF-3.0 for all the isotopes (yellow curve) and the absolute values of the differences between the previous spectra. Differences are clearly noticeable for ENDF-JEFF in the resonance region around 100 keV and around 1 MeV, whereas there are several orders lower for ENDF-JENDL (^{239}Pu). Notice that the most probable energy in this system is around 300 keV, confirming the importance of accurate cross-section data in the resonance region.

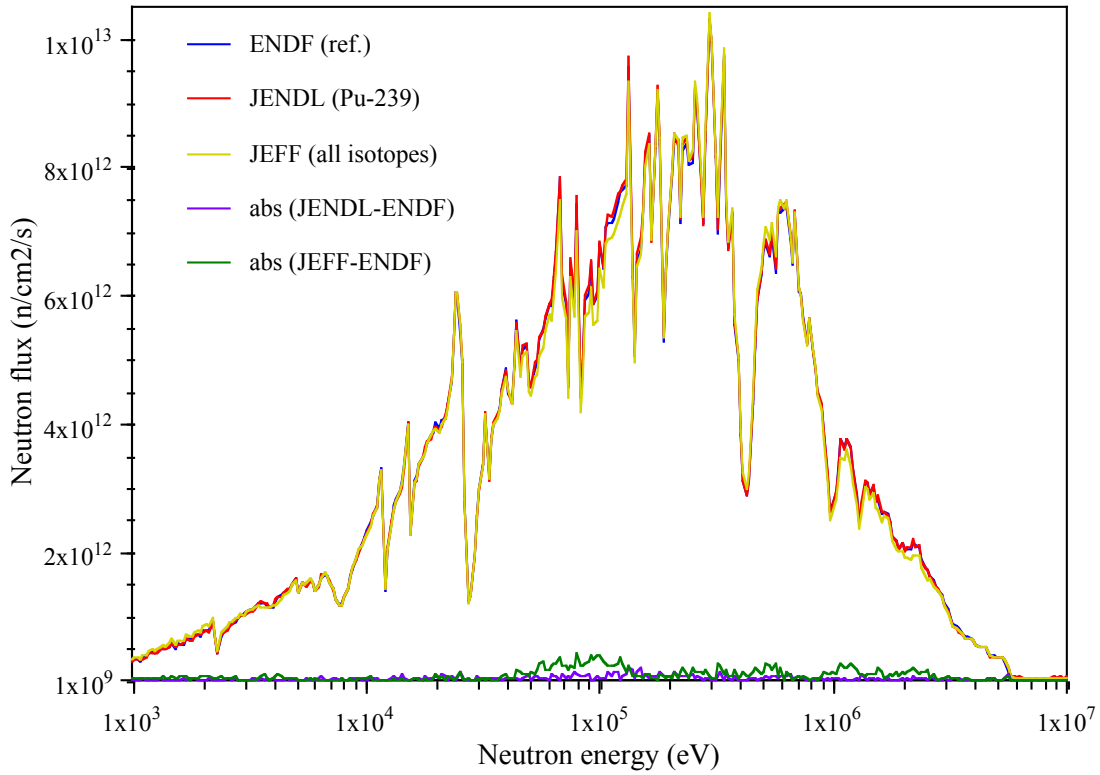

Figure 4.17. Neutron energy spectra in the fuel of EADF for different ND libraries.

Figure 4.18 shows the discrepancies in the reaction rates for thorium and uranium isotopes. Inelastic scattering seems to be the least known reaction for all the isotopes, followed surprisingly by fission in ^{232}Th, ^{235}U and ^{238}U. The uncertainty in capture for ^{235}U is also significant.

Analysis of a one-group reaction cross-section can hide the fact that discrepancies are often concentrated in a particular energy region, and that these may be compensated for across the energy range. Figure 4.19 shows the capture and (n, ni) reaction rates for ^{233}U, a good example of this situation. For this isotope ENDF/B-VI.8 presents a larger capture rate in the energy range 1-10 keV, whereas JENDL-3.3 has a higher rate from 900 keV to 3 MeV. These results compensate in the integral value but could have an important impact on the core

behaviour due to the spectrum change, consequently affecting parameters such as ν (average number of neutrons released per fission) or the resonance escape probability of the system. The same tendency can be observed in the inelastic scattering energy spectra, where major differences in the reaction rates appear from 600 keV onwards, and smaller differences from 70 to 200 keV. For the first energy range JENDL-3.3 presents a larger (n, ni) rate, whereas for the second one it is ENDF/B-VI.8 which shows a slightly larger rate.

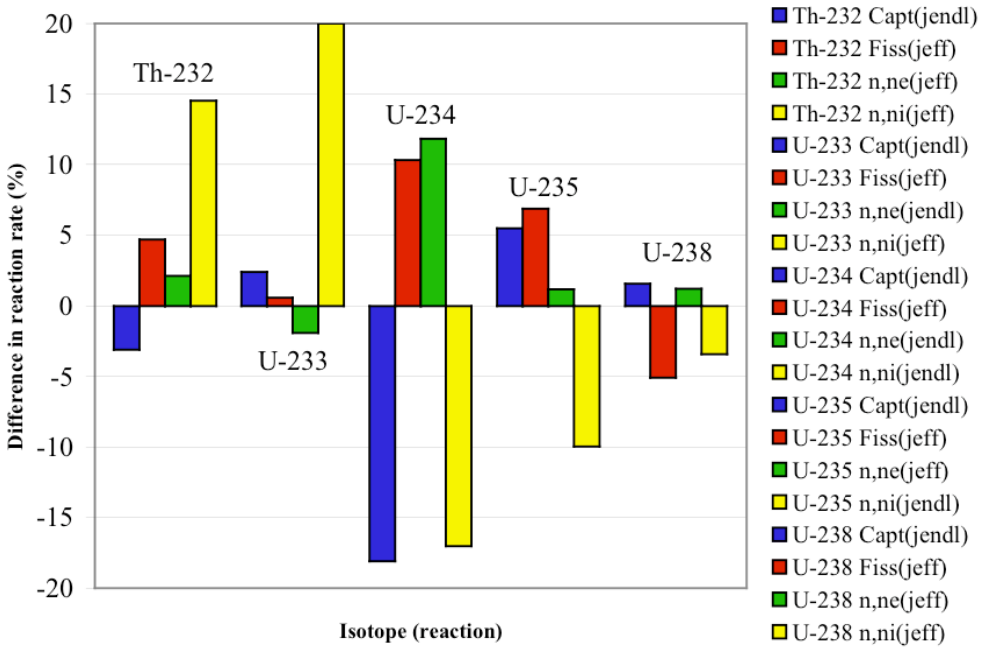

Figure 4.18. Reaction rate discrepancies in EADF for ^{232}Th and the uranium isotopes.

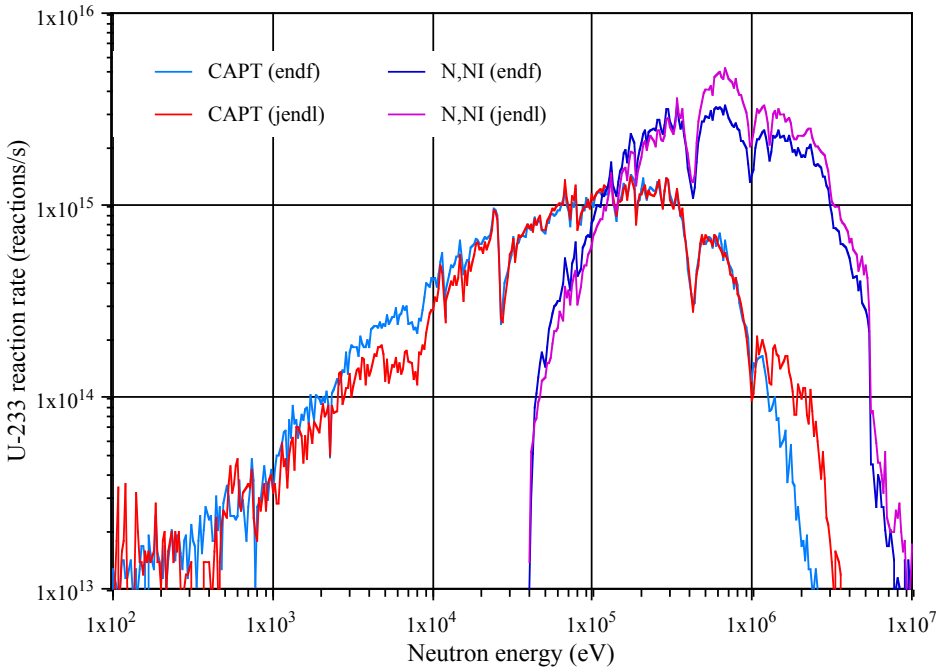

Figure 4.19. Comparison of reaction rates for capture and (n, ni) in ^{233}U using ENDF/B-VI.8 and JENDL-3.3.

For the reaction rate spectra for ^{232}Th (Figure 4.20), slight differences can be perceived for capture across the whole energy range. On the other hand, for (n, ni) differences are concentrated in the energy range starting at the threshold of the reaction (70 keV) up to 100 keV. Fission also presents slight differences across most of the energy range of this reaction.

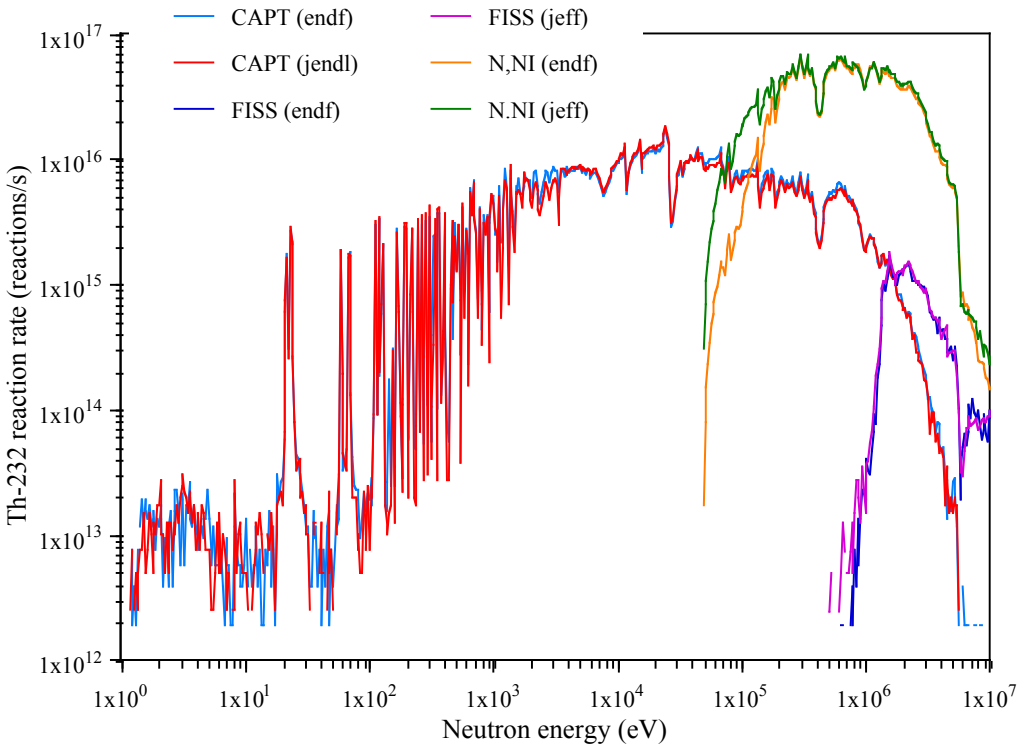

Figure 4.20. Comparison of reaction rates for capture, fission and (n, ni) in ^{232}Th for different libraries.

The reaction rates for the plutonium isotopes (Figure 4.21) exhibit larger discrepancies than the uranium isotopes. Again, the largest deviations appear in the inelastic scattering reaction, reaching 74% for ^{241}Pu. ^{238}Pu appears to be the least known isotope, with uncertainties in capture reaching 30%. Elastic scattering (12%) and capture (10%) in ^{241}Pu would also need improvement. Analysis of the reaction rate spectra for ^{239}Pu shows minor differences in the capture reaction rate spectrum, in particular for 1-2 keV, 100 keV and above 800 keV. The (n, ni) reaction rate also exhibits slight discrepancies above 100 keV.

Even though the presence of ^{240}Pu in the fuel is 2.8 times lower than that of ^{239}Pu, its influence on the variations of k_{src} is as important as that of the latter. Figure 4.22 shows the origin of this effect: the capture rate is systematically slightly higher from 1 keV onwards for JENDL, which effectively produces a lower k_{src} when this library is used. The (n, ni) rate is also larger for JENDL from 100 keV to 1 MeV. In the case of ^{241}Pu differences appear clearer both in the capture and especially in the inelastic scattering reaction rate. For this reaction, differences are evident along all the energy range for which the reaction is present (60 keV to

8 MeV). These large differences are striking because of the importance of the isotope, the magnitude of the reaction and of the error itself (almost one order of magnitude for 500 keV).

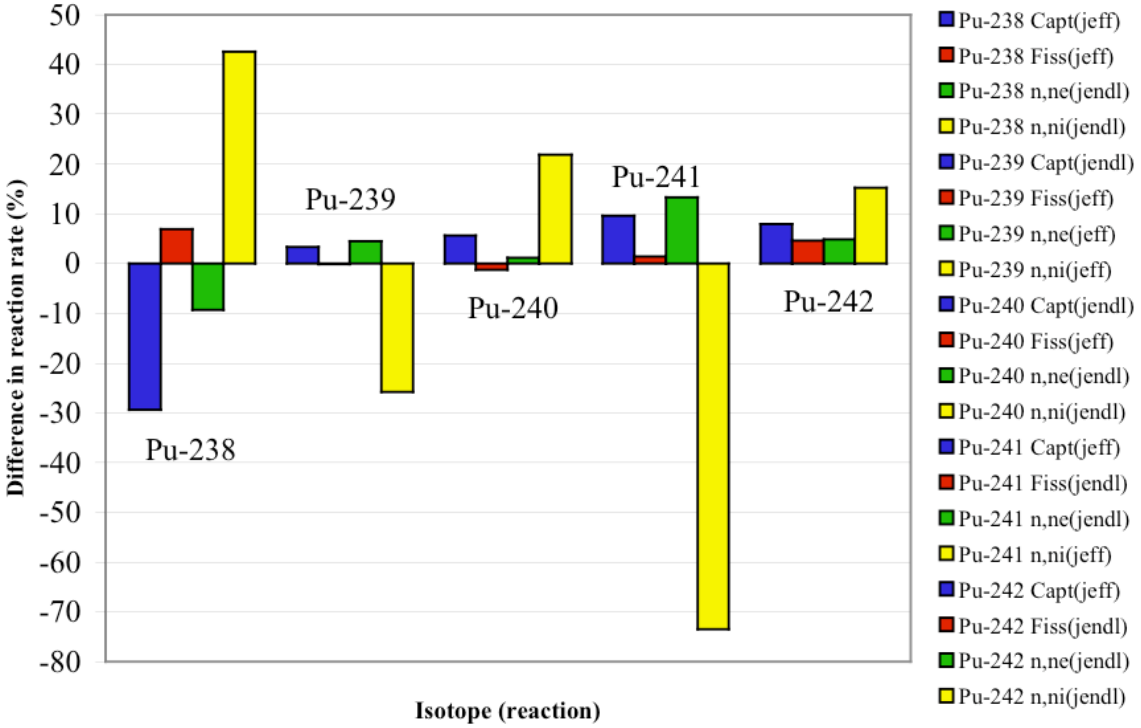

Figure 4.21. Reaction rate discrepancies in EADF for plutonium isotopes.

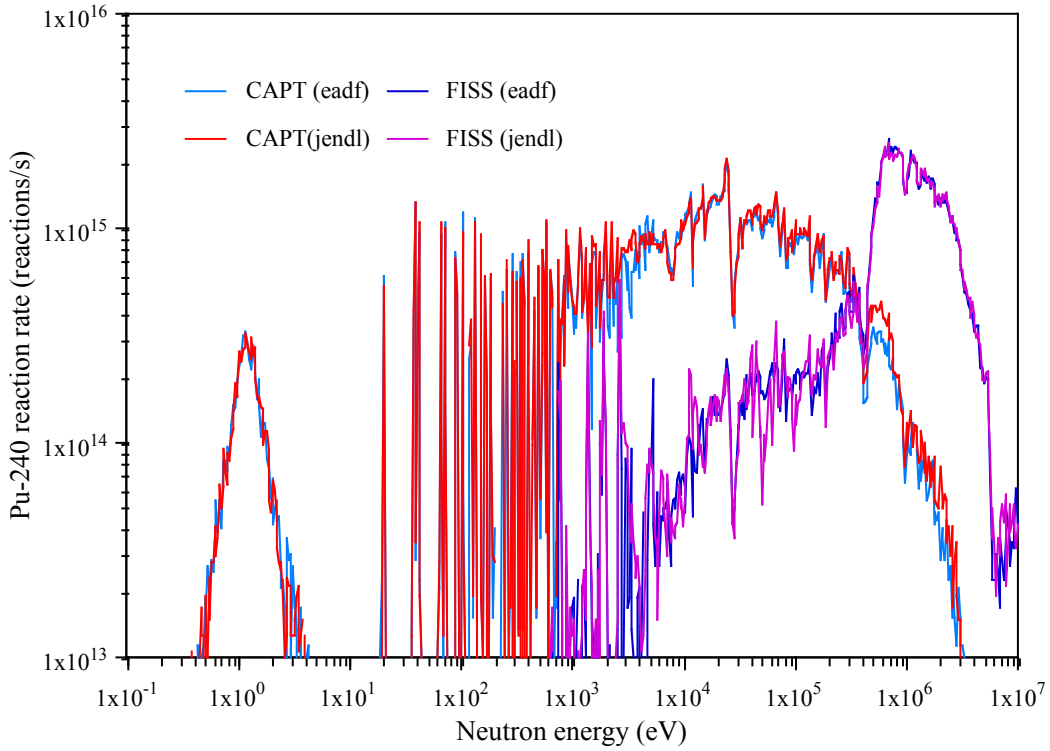

Figure 4.22. Comparison of reaction rates for capture and fission in ^{240}Pu using ENDF/B-VI.8 and JENDL-3.3.

For the coolant ($^{206, 207, 208}$Pb and ^{209}Bi) and the LLFF (^{99}Tc and ^{129}I), Figure 4.23 presents several differences worth remarking. As for the other isotopes, inelastic scattering is globally the reaction exhibiting the largest discrepancies. These differences could have an important effect on the energy spectrum of the neutron flux, therefore changing the behaviour of the system and the other reaction rates. In addition, the large uncertainties connected with the (n, 2n) reaction in all lead isotopes, ranging from 10% to 30%, could have a direct impact on the multiplication factor of the system, since this reaction accounts for rates comparable to capture (roughly 10% in $^{206, 207}$Pb but 73% in ^{208}Pb). ^{99}Tc also exhibits large inconsistencies in (n, 2n) (41%), elastic (19%) and inelastic (21%) scattering. As explained previously, ENDF/B-VI.8 lacks potentially useful (n, 2n) information for ^{129}I. The results using different libraries also disagree for capture (15%) and elastic scattering (18%) for this isotope. Finally, capture in the isotopes forming the coolant also present differences, with capture in ^{209}Bi (16%) being possibly the most relevant due to the abundance of this isotope (50% of the coolant) and the level of captures, one order of magnitude larger than in ^{208}Pb (since the latter is a double magic isotope and therefore "transparent" to the neutrons).

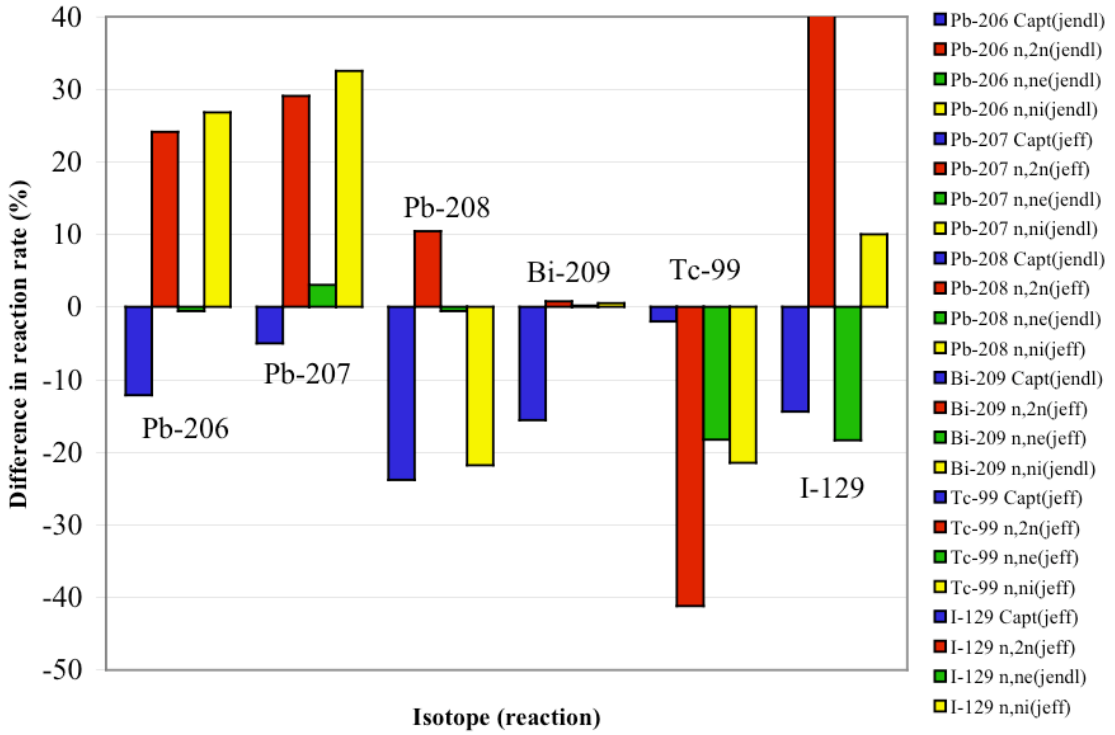

Figure 4.23. Reaction rate discrepancies in EADF for the elements in the coolant and LLFFs.

Analysis of the reaction rate spectra for ^{207}Pb shows similar trends to the other isotopes by displaying larger uncertainties at higher energies. ENDF/B-VI.8 exhibits a higher capture rate above 150 keV and lower (n, 2n) and (n, ni) rates for all their energy ranges. On the other hand, JEFF-3.0 seems to predict sharper capture resonances between 3-100 keV, and apparently this effect dominates the shift in k_{src}, for which JEFF-3.0 predicts a lower value.

For ^{209}Bi, the most abundant isotope in the coolant, JEFF-3.0 and JENDL-3.3 exhibit opposite tendencies concerning $\Delta k/k$, thus Figure 4.24 shows the comparison between the two. As expected, the capture rate is larger for JEFF-3.0 above 90 keV, whereas the rest of the reaction rates seem to agree, thus pointing out where the 329 pcm in $\Delta k/k$ are produced.

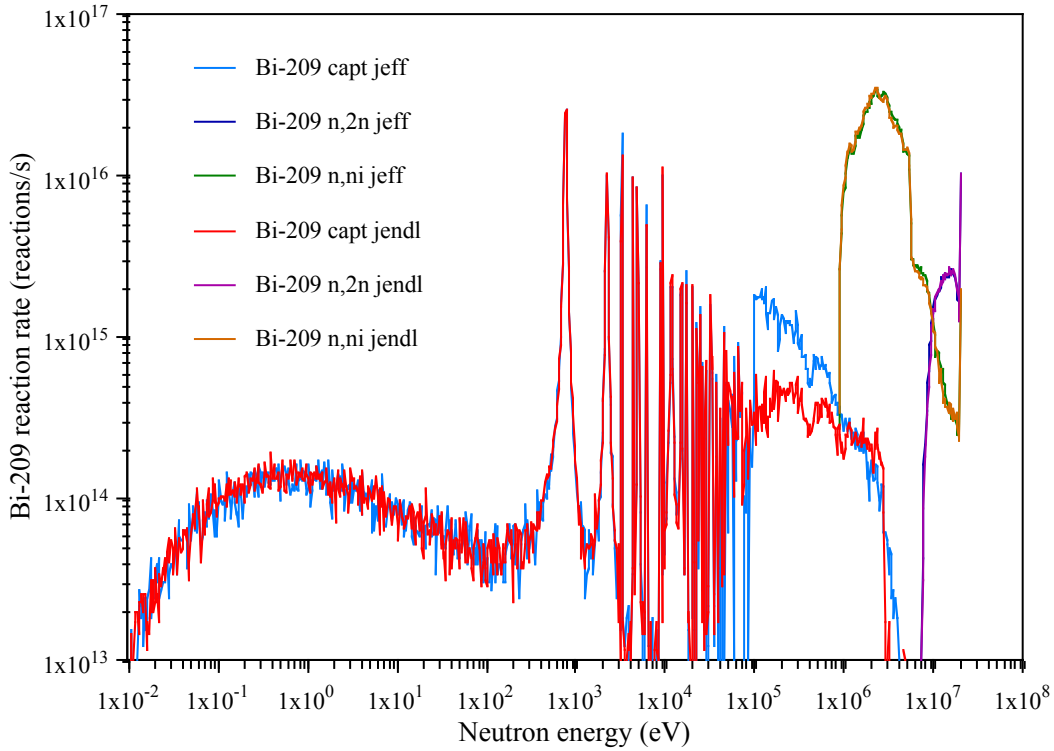

Figure 4.24. Comparison of reaction rates for capture, (n, 2n) and (n, ni) in ^{209}Bi with JENDL-3.3 and JEFF-3.0.

4.3.2.2 50% plutonium – 50% minor actinides fuel mixture

This fuel mixture was produced in order to assess the effect of large quantities of minor actinides in the core. It is formed by a mixture of 50% plutonium and 50% MAs, both with an isotopic composition typical of the UO_2 spent fuel with an average thermal burn-up of 33 GWd/tHM, as previously presented in Table 2.1.

The effect of these isotopes on the k_{src} of the system can be found in Table 4.6. Larger differences appear due to the increasing presence of less-known isotopes. Despite of the limited presence of ^{238}Pu (1.7% of the plutonium isotopes), this isotope has a remarkable effect on the k_{src}, caused by the large discrepancies in the ND, as exemplified by Figure 4.6. This effect will increase with rising ^{238}Pu concentration in the fuel during burn-up, as is the case with the use of MOX fuels. The effect of ND discrepancies in ^{240}Pu remains constant (as does its concentration in the fuel), although in this case JEFF-3.0 presents the largest deviations; this gives an idea of the complexity of the interplay between different evaluated resonances and neutron flux, since this effect is caused by a small change in the spectrum due to the different isotopic composition and the disappearance of some resonances in the neutron

flux, such as the one at 400 keV (elastic scattering in oxygen). Uncertainties related to ^{239}Pu become less important since the presence of this isotope in the fuel is reduced from 69% to 59%. On the other hand, the presence of ^{241}Pu increases from 2.6% to 11.7%, increasing the effect of the differences in ND related to it. For the MAs, the uncertainties in ^{241}Am have the strongest effect since this is the most abundant isotope in the HLW, although discrepancies in the ND for curium, and in particular for ^{244}Cm, may produce large deviations in cases with higher content of this isotope.

Table 4.6. Main neutron cross-section data effects on k_{src} for the Pu-MAs fuel in EADF.

Reference case 50%Pu-50%MAs: ENDF/B-VI.8, k_{src} = 0.86013 ± 0.00060		
Isotopes	JEFF-3.0 $\Delta k/k$ (pcm)	JENDL-3.3 $\Delta k/k$ (pcm)
Np-237	–70	–135
Pu-238	**+514**	**–318**
Pu-239	–275	–288
Pu-240	**–558**	**–499**
Pu-241	**+352**	+42
Pu-242	–142	–286
Am-241	**–499**	**+15**
Am-243	–147	+210
Cm-244	+156	+248
Cm-245	–125	–139

The discrepancies in the neutron balance for the MAs are presented in Table 4.7. These values show the above-mentioned uncertainties in ND for curium, and also large discrepancies in the results for fission in ^{241}Am and ^{237}Np. For the plutonium isotopes, the differences are similar to the values presented in Table 4.5, even though fission is slightly higher in this case due to the harder spectrum.

Table 4.7. Neutron balance of MAs in the 50% plutonium 50% MAs fuel for EADF.

		ENDF %	JEFF %	ΔJEFF %	JENDL %	ΔJENDL %
Np 237	Capture	80.38	80.05	–0.41	79.07	–1.63
	Fission	19.59	19.92	+1.69	20.90	**+6.69**
	n,xn	0.03	0.03		0.03	
Am 241	Capture	84.72	86.13	+1.66	85.07	+0.41
	Fission	15.27	13.85	**–9.30**	14.91	–2.36
	n,xn	0.01	0.3		0.02	
Am 243	Capture	87.46	88.04	+0.66	87.84	+0.43
	Fission	12.49	11.91	**–4.64**	12.13	–2.88
	n,xn	0.04	0.04		0.03	
Cm 244	Capture	62.27	52.98	**–14.92**	58.06	**–6.76**
	Fission	37.62	46.98	**+24.88**	41.92	**+11.43**
	n,xn	0.11	0.04		0.01	
Cm 245	Capture	15.10	11.45	**–24.17**	15.67	+3.78
	Fission	84.86	88.51	**+4.30**	84.33	–0.62
	n,xn	0.03	0.04		0.00	

Analysis of the reaction rates for the MAs shows discrepancies above 10% for different reaction channels in all isotopes. Inelastic scattering exhibits the largest discrepancies (above 15% in most of them) followed by capture in curium (~30% discrepancy for both isotopes). Both americium isotopes show noticeable differences for (n, ni) (~25%) and capture (~15%).

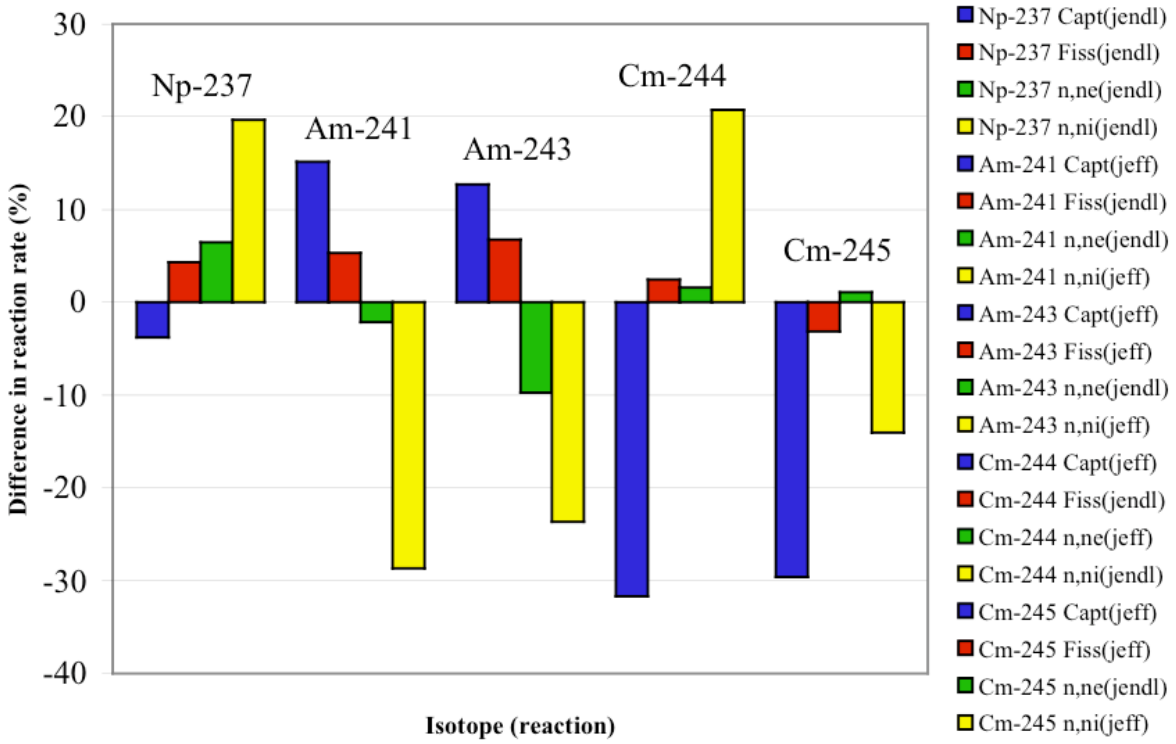

Figure 4.25. Reaction rate discrepancies in EADF for MAs for the Pu-MAs fuel.

The abundance of ^{241}Am in the spent fuel and its effect on the neutron multiplication justifies the need to improve the accuracy of the related ND. Figure 4.26 shows the discrepancies in the reaction rates for ^{241}Am between ENDF/B-VI.8 and JEFF-3.0, which seem to have an important effect in k_{src} (~500 pcm smaller k_{src} using JEFF-3.0). The capture rate calculated using JEFF-3.0 is lower for the energy range between 100 eV and 100 keV, becoming clearly larger from 200 keV (where the capture rate peaks) to 5 MeV (in fact, the capture reaction using ENDF/B-VI.8 stops at 3 MeV). There is a similar effect in the fission rate, although smaller in magnitude, showing a slightly higher value for ENDF/B-VI.8 below the fission peak at 1 MeV and a lower one above this point. The large discrepancies in capture compared to fission explain the large discrepancies in k_{src} between these two libraries. It also shows the extreme sensitivity of these systems to ND, since if the neutron energy spectrum was slightly softer, the differences in k_{src} could invert.

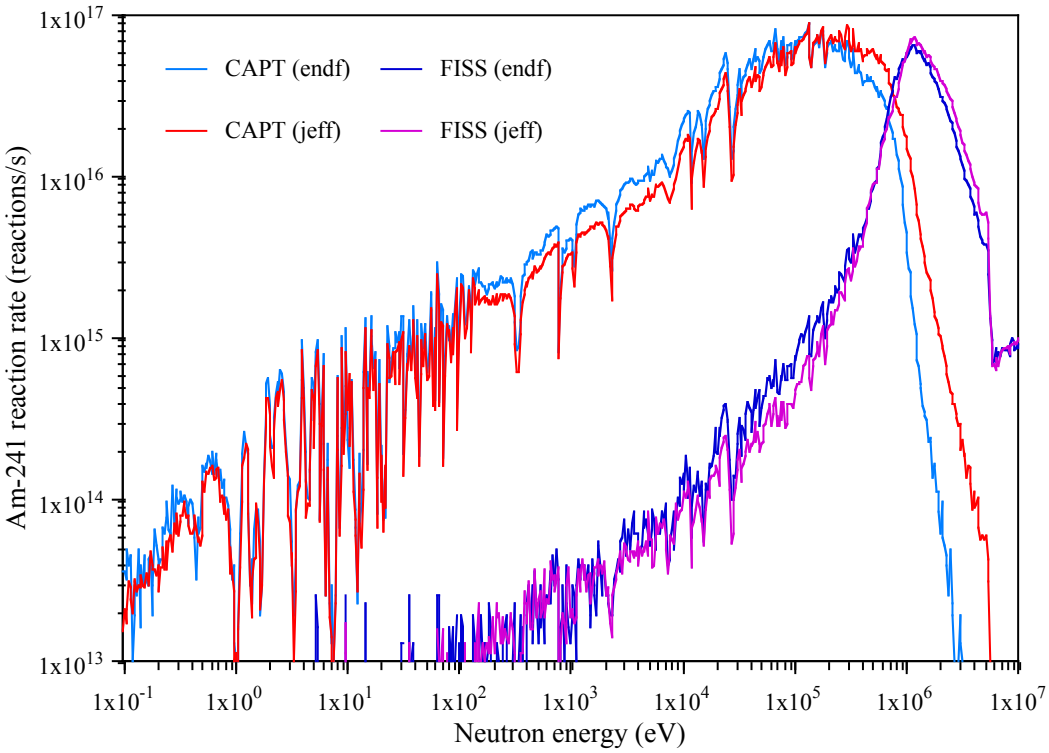

Figure 4.26. Comparison of reaction rates for capture and fission in ^{241}Am using ENDF/B-VI.8 and JENDL-3.3.

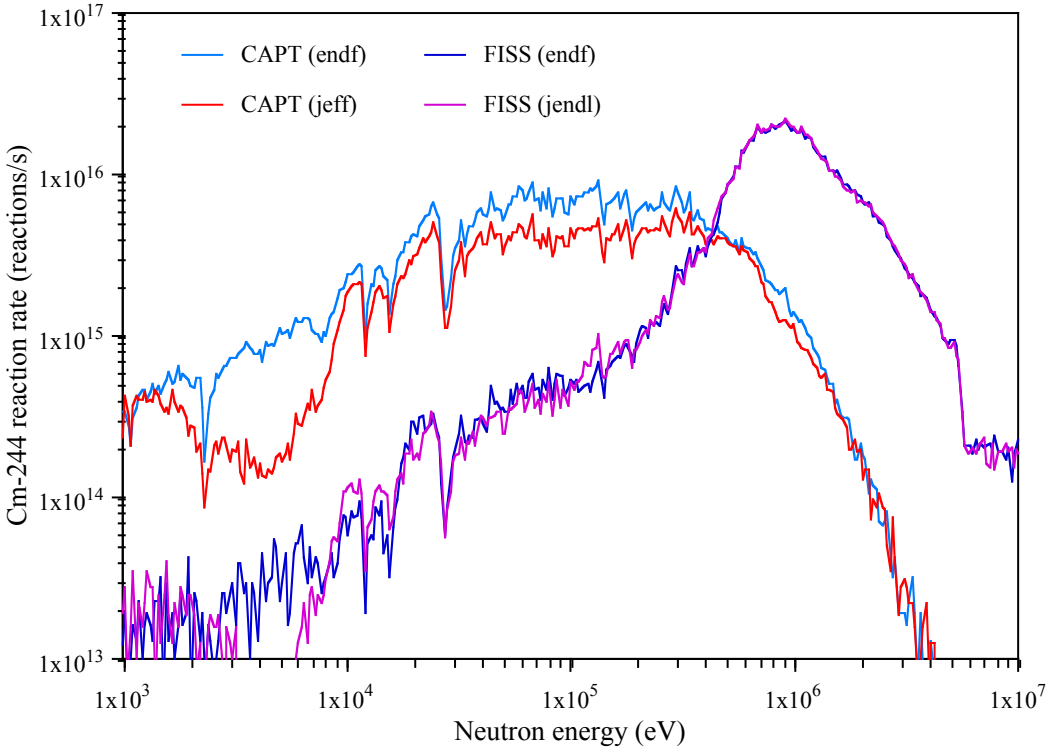

Figure 4.27. Comparison of reaction rates for capture and fission in ^{244}Cm using ENDF/B-VI.8 and JENDL-3.3.

With respect to ^{244}Cm, Figure 4.27 shows large discrepancies capture rate between 1-10 keV. ENDF/B-VI.8 exhibits almost one order of magnitude higher values for 3 keV. Beyond 10 keV, this library still evidences a capture rate up to 1 MeV, hence the higher k_{src} estimated

using JEFF-3.0 and JENDL-3.3. The fission rate also exhibits a large difference between 1-10 keV although the importance of fission at these energies is much smaller than that of capture. Beyond 20 keV, there are no major discrepancies in the fission rate for ^{244}Cm. Although the discrepancies in the capture rate appear large, the small quantity of ^{244}Cm limits the effect of these differences on k_{src}.

4.3.3 Conclusions: Cross-section priority list

The effects of the ND were found to be of major importance for reliable design of an ADS, especially in terms of safety. Also, the predictions of the spent fuel radiotoxicity may also be affected since the actinide accumulation is directly connected with the isotopes' fission and capture cross-section. The discrepancies appear larger for fast systems, even though large uncertainties were found at thermal energies for isotopes such as ^{241}Pu and ^{244}Cm.

Discrepancies in the ND for coolant and structural materials, such as ^{90}Zr in the case of TRADE, and ^{207}Pb and ^{209}Bi in the case of EADF, also have an important effect on the neutron multiplication of the system, which should not be neglected.

In the case of EADF, large uncertainties in the neutron balance for isotopes such as ^{237}Np, ^{238}Pu and ^{241}Am may have large effects on k_{src}, depending of the configuration of the fuel. Moreover, even small differences in the neutron balance for ^{233}U and ^{232}Th introduce significant changes in the neutron multiplication for the thorium-based fuel. There is also a general need to improve the scattering cross-sections, for most of the isotopes; these uncertainties perturb the spectrum, therefore affecting transmutation rates, safety parameters and reactor behaviour, for example altering the resonance escape probability.

Hence, the differences between libraries are larger for a fast system due to the poorer knowledge of ND at energies above thermal. There is a systematic inaccuracy in the inelastic scattering cross-section for all the isotopes, generally amplified in a fast neutron flux. Capture in the coolant is also a source of discrepancies, and thus differences in the neutron multiplication in the system. MAs undoubtedly present the largest discrepancies in both fission and capture, showing capture rates deviating by more than 15% for americium and curium.

Comparing sensitivity analysis results for the previous library release and the present work, there are some improvements in the fission and capture cross-sections for ^{240}Pu, from 7% and 15% to 3.4% and 8.5% respectively. The elastic scattering cross-section for ^{238}Pu also seems to have improved, from 22% to 11%, even though large differences are still present for (n, ni). For capture in ^{237}Np, JENDL-3.3 shows an improvement compared to the previous release, even though fission still shows a large discrepancy when compared to ENDF/B-VI.8. Discrepancies related to other isotopes and reactions channels seem to maintain similar

values, in particular large differences, such as capture, (n, ne) and (n, ni) in ^{241}Pu (10%, 13% and 73% respectively) or fission and capture in ^{241}Am (both 9%), remain.

Therefore, no major changes between library releases were found, with the exception of the aforementioned cases of capture in ^{237}Np and ^{240}Pu, and fission in ^{240}Pu. This demonstrates the need for new and precise ND measurements for an extended energy range and a large number of isotopes. These measurements should greatly reduce uncertainties in the calculations of the different reactor parameters.

4.4 The Neutron Time-Of-Flight Experiment (n_TOF)

The lack of reliable ND for various isotopes related to transmutation and ADS technology motivated in 1999 the proposal [77] to build an experimental facility in order to measure neutron-induced fission and capture cross-sections for several isotopes through the use of the time-of-flight technique. The facility was built at CERN and finally commissioned in April 2001 by the CERN/SL/EET group [78]. The n_TOF experiment started collecting data related to transmutation and astrophysics in 2002. Figure 4.28 presents a general view of the facility, highlighting the most relevant parameters.

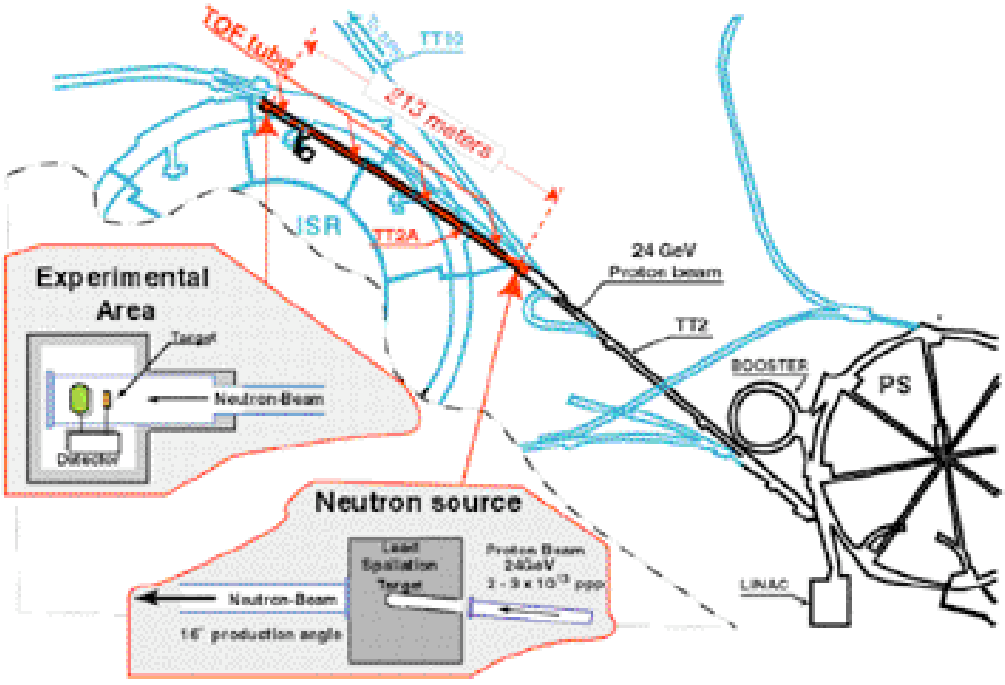

Figure 4.28. Layout of the n_TOF facility at CERN [79].

The n_TOF experiment uses the spallation mechanism as a source for neutrons by colliding high-energy protons against a lead target. The flight-path is ~200 m in order to optimise neutron flux and energy resolution. The possibility to receive narrow high-intensity pulses at low-repetition offers a high accuracy in the TOF measurements for high-energy neutrons. Hence, a high-neutron flux combined with a high energy resolution and low repetition rate make this facility an appropriate one to accurately measure over a wide energy range isotopes that could not be studied in other facilities due to their radioactivity and unavailability, such as MAs, plutonium and certain FFs. The different detectors measuring the fission and capture cross-sections are placed in the experimental area at the end of the tube.

4.4.1 Description of the n_TOF Facility

In order to measure different reaction cross-sections, the n_TOF experiment uses spallation neutrons produced by the collision of 20 GeV/c protons from the CERN PS Proton Synchrotron against an 80×80×60 cm^3 high-purity (99.999%) lead target (~30 n/proton at 1 GeV and linearly growing for higher energies) followed by 5 cm of water. The accelerator is capable of delivering up to 7×10^{12} protons (with a Gaussian bunch shape, σ_x = 7.8 mm and σ_y = 5.6 mm) per cycle concentrated in short time pulses – 6 ns r.m.s. (root mean square) – supplying up to 6 bunches per supercycle (~16.8 s). These facts result in a neutron flux at the end of the flight-path of ~6.2×10^5 n/cm^2/pulse in the energy range between 1 eV and 250 MeV (neutron fluences of 1.2×10^6 n/pulse and 8.0×10^6 n/pulse for capture and fission measurements, respectively).

The TOF tube has a 10° inclination from the proton beam direction to preserve the neutron fluence while reducing the number of unwanted charged particles. The pressure inside the vacuum tube is less than 1 mbar (neutron mean free path in air ~25 m at 1 atm) and the tube is formed by four different sectors, the first one (∅ = 80 cm), closest to the target, is made of aluminium alloy whereas the others (∅ = 80, 60 and 40 cm) are made of stainless steel. In spite of the 10° angle between the TOF tube and the proton beam, some charged particles contaminate the neutron fluence. Therefore, a 30 tonne, 140 kW, 0.195 Ω, 2 m long dipole magnet with a bending power of 1.5 T·m was placed at 145 m to sweep away these unwanted secondary charged particles. Two collimators were installed to reduce the radius of the neutron beam to 2 cm, required for the capture measurements to be performed with a 4π BaF_2 calorimeter. The first one, 2 m long (beam shaping collimator), is located at 136.7 m and is made of 1 m of iron and 1 m of concrete; its inner diameter is ∅ = 11.5 cm. The second (source screening) collimator with ∅ = 1.8 cm inner diameter, is placed at 178 m and is formed by 50 cm of 5% borated polyethylene, 125 cm of iron and 75 cm of 5% borated polyethylene. For the fission measurements, the second collimator is replaced by another one

with a larger inner diameter of ∅ = 4 cm in order to exploit the full neutron fluence of the installation. Figure 4.29 shows a schematic view of the TOF tube, presenting its main details.

Initially, two concrete shielding walls of 2 and 3.2 m thickness and a chicane were placed in the tunnel that houses the TOF tube to ensure proper background conditions. In September 2001 an iron wall of 3.2 m thickness located at ~150 m was added to reduce further the background, by diminishing the muon component, which otherwise produces a neutron background from negative muon captures [80].

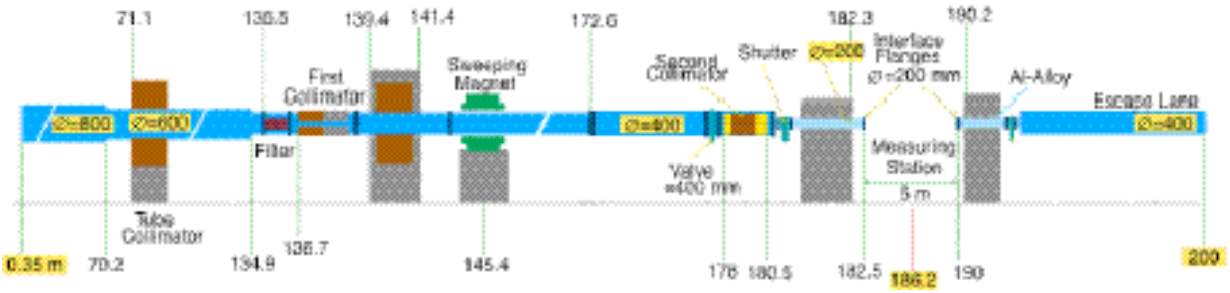

Figure 4.29. TOF tube sections from the spallation target (0 m) to the end of the TT2A tunnel (200 m) [78].

The neutron flux and its energy spectrum at the end of the flight-path is one of the most important parameters of the facility, and its simulation posed a serious difficulty due to the large length of the neutron flight-path in the n_TOF tunnel [77]. Indeed, only one neutron out of 10^7 emerging from the lead target will reach the detector station at the end of the neutron tube due its small solid angle.

The beam 2D profile was determined using Micromegas detectors [81], and the neutron flux was characterised [78] using ^{235}U and ^{238}U fission chambers and by triple gold-foil activation at 4.9 eV, where gold presents a well-known resonance. Figure 4.30 presents the results of the simulations and the aforementioned measurements of neutron energy spectrum at the measuring station. The simulations exhibit a good agreement with the experimental values, in particular for high-energies. The integrated value of the fluence is ~9.6×10^5 neutrons / 7×10^{12} protons (∅ = 1.8 cm collimator).

The energy resolution function $\Delta E/E$ of the facility was also evaluated during the commissioning of the facility, which for non-relativistic particles can be estimated using Equation 4.1:

$$\frac{\Delta E}{E} = \frac{-2\cdot\Delta t}{t} = \frac{2\cdot\Delta\lambda}{\lambda + L} \qquad \text{(Eq. 4.1)}$$

This equation shows the relation between the neutron energy $E = m_n/2\cdot(L/t)^2$ and the effective neutron path λ inside the lead target followed by the 5 cm thick water moderator, L being the

length of the flight-path. This effective neutron path can be evaluated as $\lambda = v \cdot t$, where v is the neutron speed when entering the tube and t is the time elapsed since the generation of the neutron.

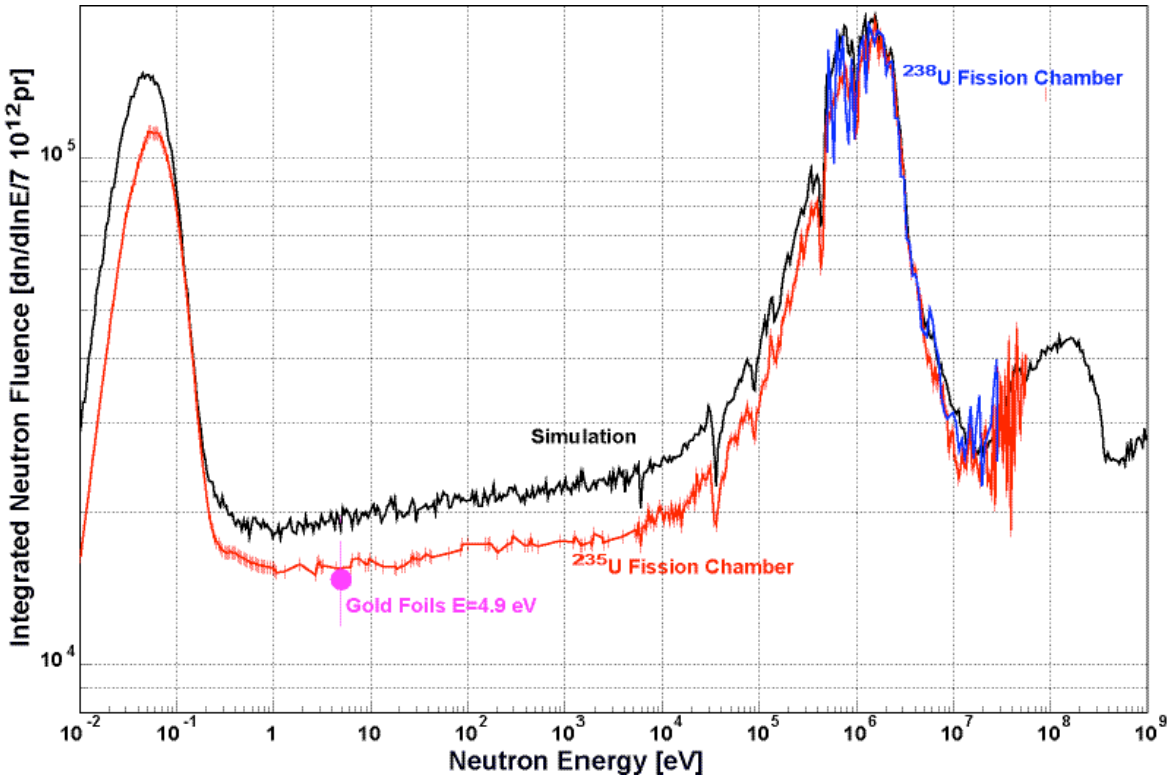

Figure 4.30. Neutron fluence energy spectra from fission chamber and gold foil activation measurements [78].

Figure 4.31 presents the distribution of λ for different neutron energies (a) and $\Delta\lambda$ as the r.m.s and variance of a Gaussian fit of λ at its peak, for the energy range of interest (b). The value of λ in the lead target is a few centimetres for the lowest energies and increases with energy up to ~50 cm and its variance $\Delta\lambda$ also varies greatly depending on the energy. At thermal energies λ presents a distribution somehow similar to a Maxwell distribution due to continuous scattering in the moderator, and above those energies $\Delta\lambda$ rapidly decreases to reach a constant value for energies between 1-100 eV. For higher energies, $\Delta\lambda$ rises due to the increasing importance of evaporation, thus time delay, in the generation of neutrons below several MeV. Beyond these energies, $\Delta\lambda$ is greatly reduced due to the direct knock-out of neutrons in the spallation reaction followed by their escape into the beam tube without interacting.

The interest in using λ to assess $\Delta E/E$, instead of, for instance, t, is that this function only depends on $\Delta\lambda$ for a given $L >> \lambda$, and that therefore there is a one-to-one relationship them. The resolution function $\Delta E/E$ was validated by comparing well-known measured cross-sections with the database at narrow resonances (e.g. 7.1 eV ^{235}U) and shown to be an

accurate upper limit for the resolution, although only indicative of $\Delta E/E$ since Figure 4.31 is only an approximation to the unknown real resolution function.

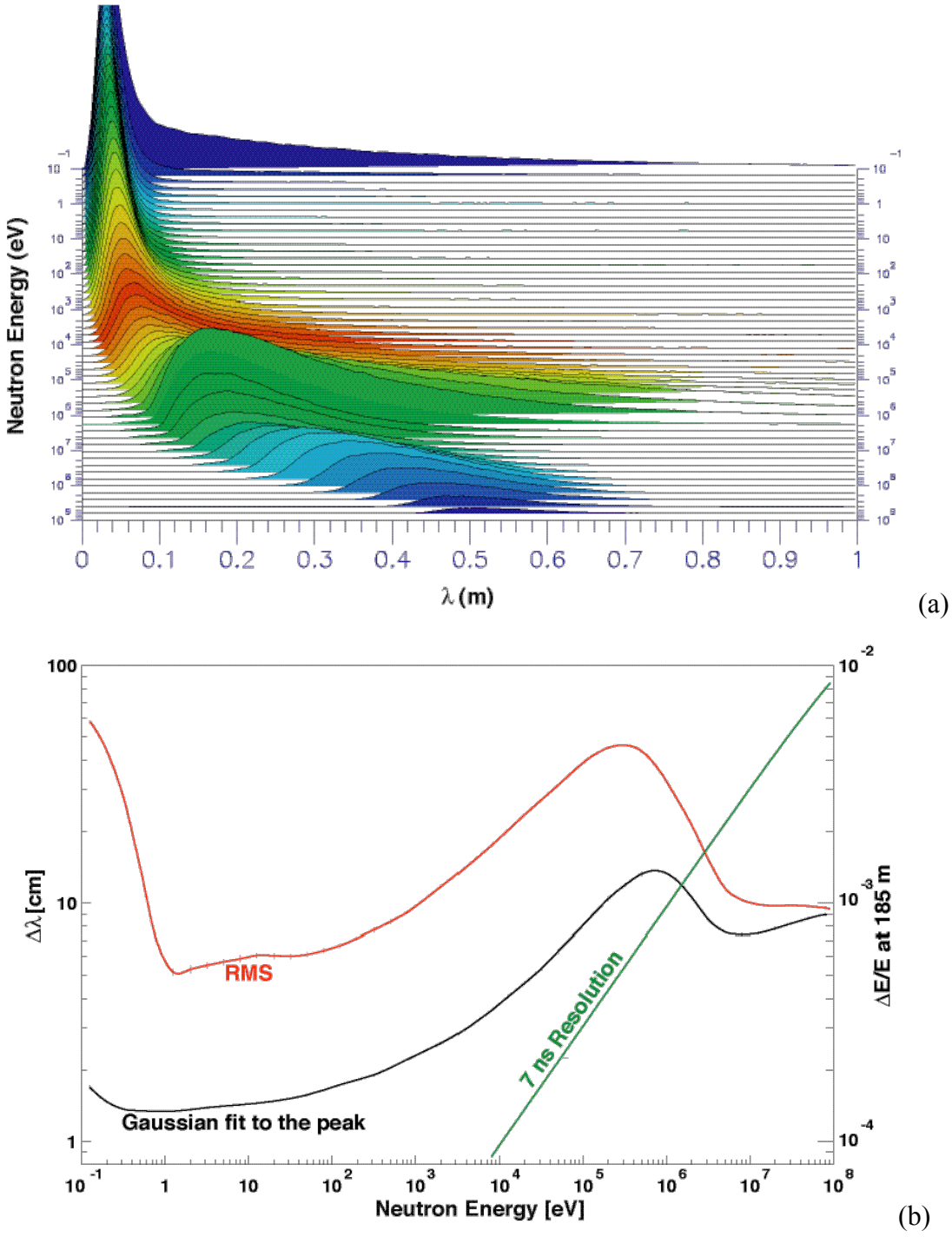

Figure 4.31. (a) MC distribution of λ evaluated at the energy of observation [78]; (b) simulation of the energy resolution at 185 m, where the 7 ns resolution due to the proton beam becomes dominant for high-energies [78].

Cross-section measurements were performed using a large range of detectors such as C_6D_6 γ-ray detectors [81] and a 4π BaF_2 calorimeter [82] for capture, and Parallel Plate Avalanche

Counters (PPACS) [83] and Fission Ionisation Chamber (FIC) [84] for fission measurements. The involvement of the CERN-SL-ECT group, of which the author is a member, in the definition and production of the latter, justifies a brief description of this detector and some preliminary measured data.

4.4.2 Fission Ionisation Chamber (FIC)

The measurement of fission reactions with a counter based on the ionisation produced by the fission fragments in a gas, at the n_TOF facility was already proposed in [60]. After the good results achieved during the second n_TOF Commissioning [78] by using a Parallel Plate Induction Fission Chamber from the Physikalisch-Technische Bundesanstalt (PTB, Braunschweig, Germany), it was decided to build a dedicated counter based on the same principle but optimised for the facility [85] since this type of detector is also simple and easy to operate.

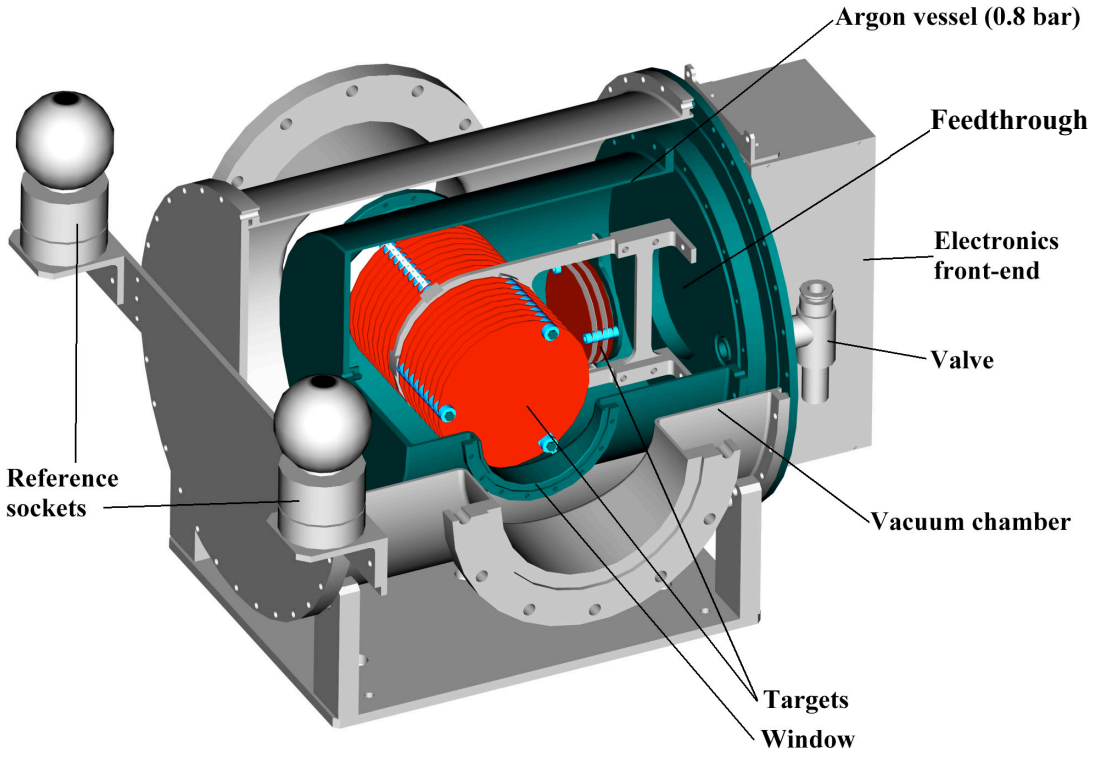

Figure 4.32. Schematic view of the FIC assembly and its main elements [79].

Figure 4.32 shows the configuration of the detector. Apart from the windows, made with kapton foils 125 μm thick, all metallic parts are made out of aluminium alloy. The detector is filled with gas (90% argon, 10% CF_4) at 0.8 bar and no gas circulation is needed since it operates in a non-proportional mode. The targets are stacked on the supports together with the other electrodes, facing the neutron beam. A total of 16 targets and 18 electrodes can be

mounted together with a 5 mm gap between layers. There is another stack of 3 targets and 4 electrodes mounted perpendicular to the previous one, in order to evaluate the background produced by scattered neutrons. In the configuration for the 2002 run [84], the counter was equipped with the following available targets:

- ^{234}U: 7 targets, total mass ~37.7 mg in the main line;
- ^{234}U: 1 target, total mass ~5.4 mg in the background line;
- ^{235}U: 1 target, total mass ~5.06 mg in the main line;
- ^{238}U: 2 targets, total mass ~20 mg in the main line;
- ^{238}U: 1 target, total mass ~10 mg in the background line.

The fissile isotopes are deposited on both sides of 100 μm thick aluminium foils with diameter ∅ = 72 mm in the form of a chemically stable compound such as, for example, U_3O_8. All electrodes are electrically connected to the feed-through located on the flange. The targets are held at ground potential by the preamplifier input while the facing electrodes are at –300 V potential. The front-end electronics and the HV distribution board are located immediately after the feed-through.

4.4.3 Measurements at n_TOF: Preliminary Cross-section Data

The ongoing measurements at n_TOF have produced a myriad of promising results. The ND acquired in the experiment is still in the process of being evaluated by several research groups in the n_TOF collaboration. This section presents some preliminary results for several isotopes and reactions which show important discrepancies with previous measurements and evaluated data. It should be remarked that these results are still preliminary and require a more thorough analysis in order to be considered final. The fission results for actinides were obtained using FIC and are the fruit of a joint effort between the EET group at CERN, the IPPE (Obninsk, Russia) and JINR (Dubna, Russia) research groups.

Figure 4.33 shows the adjusted fitting of the fission cross-section obtained using FIC with previous experimental data for the well-known fission cross-section of ^{235}U, in the resonance region between 8-25 eV. Since the cross-section measurements in FIC are relative to the fission cross-section of ^{235}U, these measurements served to accurately calibrate the energy of the measurements (determining the total flight-path) by adjusting them to some well-known resonances. They also help to experimentally determine the energy resolution, to some extent since the Doppler broadening of resonances leads to loss of information.

The preliminary results of the measurements of the fission cross-section of ^{234}U seem quite promising, in particular concerning the energy resolution in the resonances, as exemplified by Figure 4.34, where the n_TOF measured resonances appear sharper (higher and narrower)

than those of the, arguably, most relevant previous measurements (by James in Oak Ridge in 1977, when ~4700 energy points between 2 eV and 9 MeV were obtained).

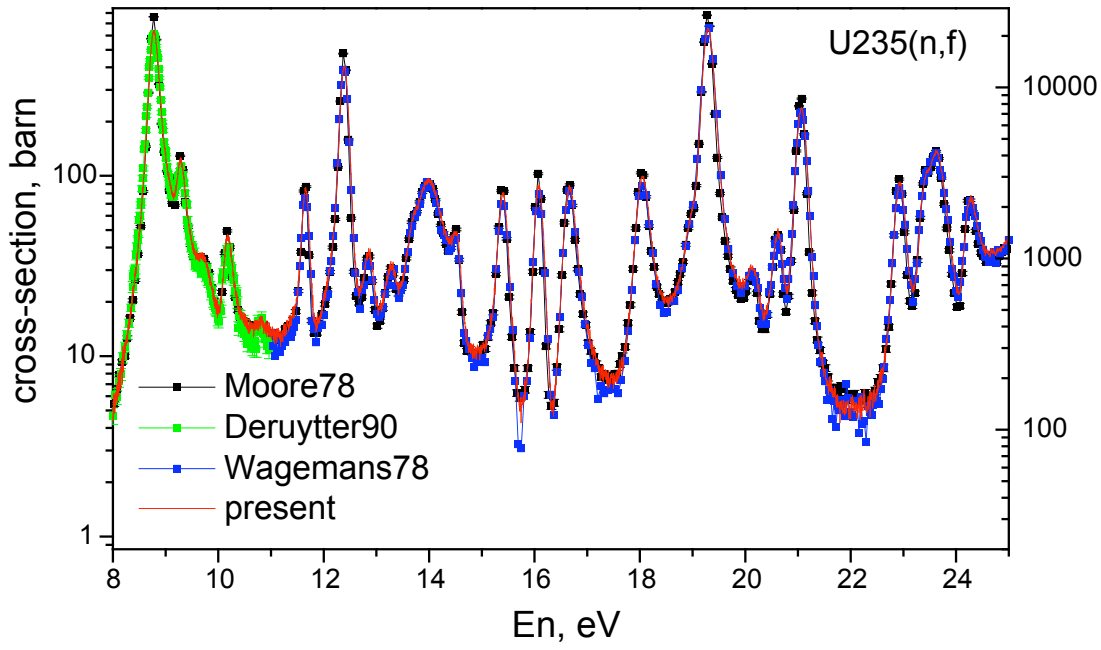

Figure 4.33. Comparison of the measured ^{235}U fission cross-section with some previous experimental data [86].

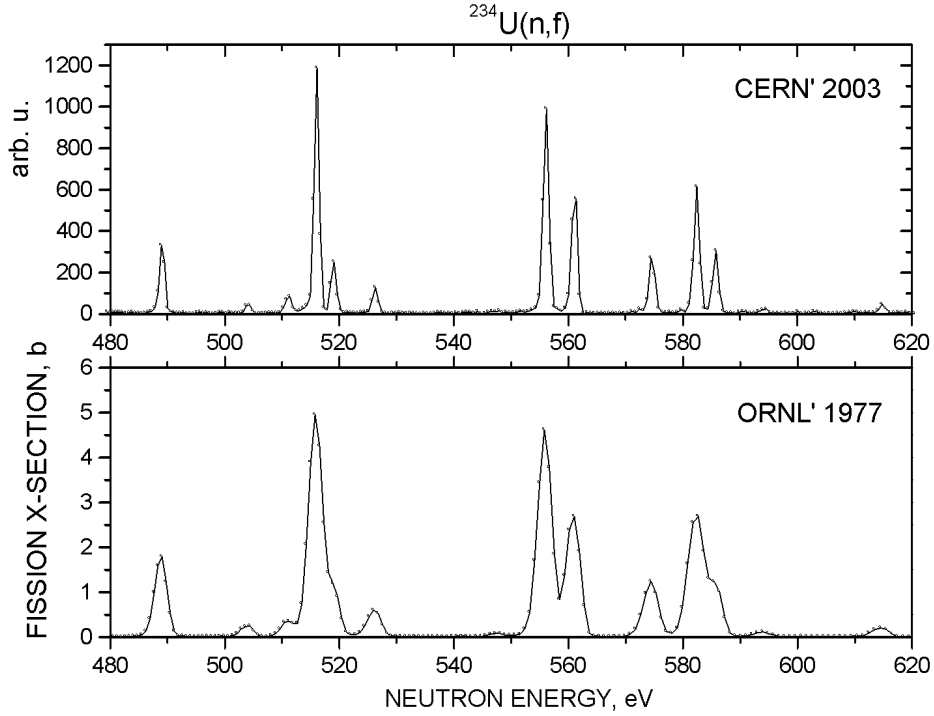

Figure 4.34. Comparison of some FIC measurement for ^{234}U and previous experimental data [86].

Figure 4.35 presents the comparison between ^{236}U fission cross-section measurements relative to that of ^{235}U. This figure gives an idea of the level of statistics obtained at different energies.

The fine details between 500-100 keV may be of relevance in the analysis of a fast system, as elaborated in Section 4.3.2, therefore further beam-time is scheduled to improve the statistics below 700 keV.

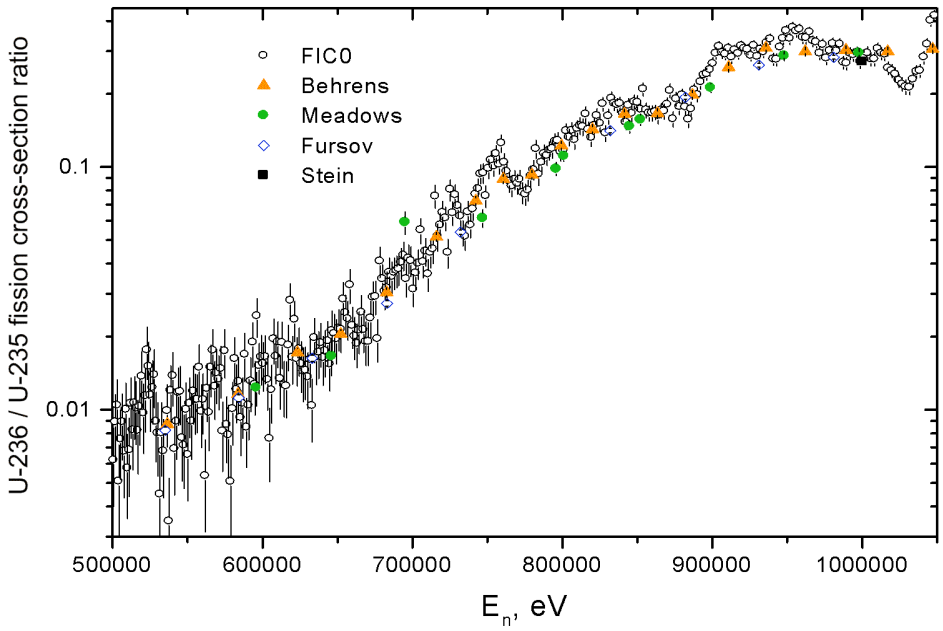

Figure 4.35. Comparison of the fission cross-section ratio for ^{236}U between different measurements [86].

The fission cross-section for ^{232}Th has an important impact on the neutronics of a thorium-based ADS, in particular since it accounts for more than 1% of the fissions produced in the system and discrepancies in this cross-section may provoke differences of hundreds of pcm in the computation of k_{src}.

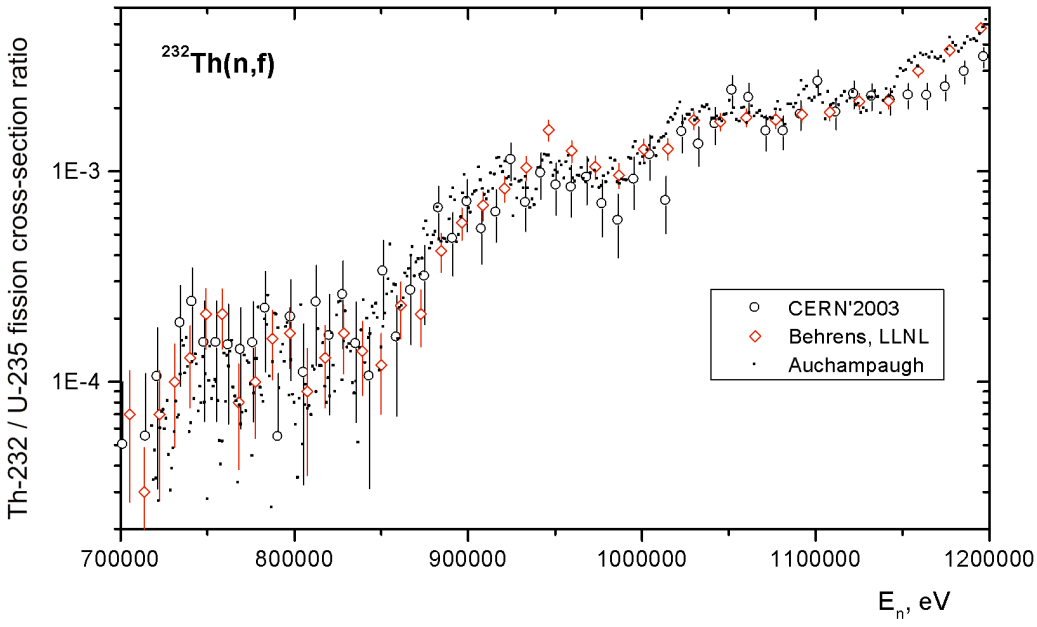

Figure 4.36. Comparison of the fission cross-section ratio for ^{232}Th between different measurements [86].

Figure 4.36 shows the preliminary results of the measurements for this isotope performed in n_TOF compared with previous measurements. The data above 1 MeV show clear discrepancies with previous measurements and indicate the need of a new evaluation. The statistical uncertainties due to the small cross-section in the sub-threshold region may require further measurements.

The measurements of the fission cross-section for ^{237}Np presently show some promising results, such as the one shown in Figure 4.37, where the n_TOF measurements of the resonances in the 28-42 eV range seem more accurate than and rather different to previous measurements and the evaluated data in ENDF/B-VI. Indeed, the resonance at 39 eV is eight times larger than the respective evaluated data, and similar behaviour can be observed in the other three resonances in this energy range. The capture measurements for ^{237}Np are currently taking place using a Total Absorption Calorimeter (TAC) and preliminary will results may be available in 2005.

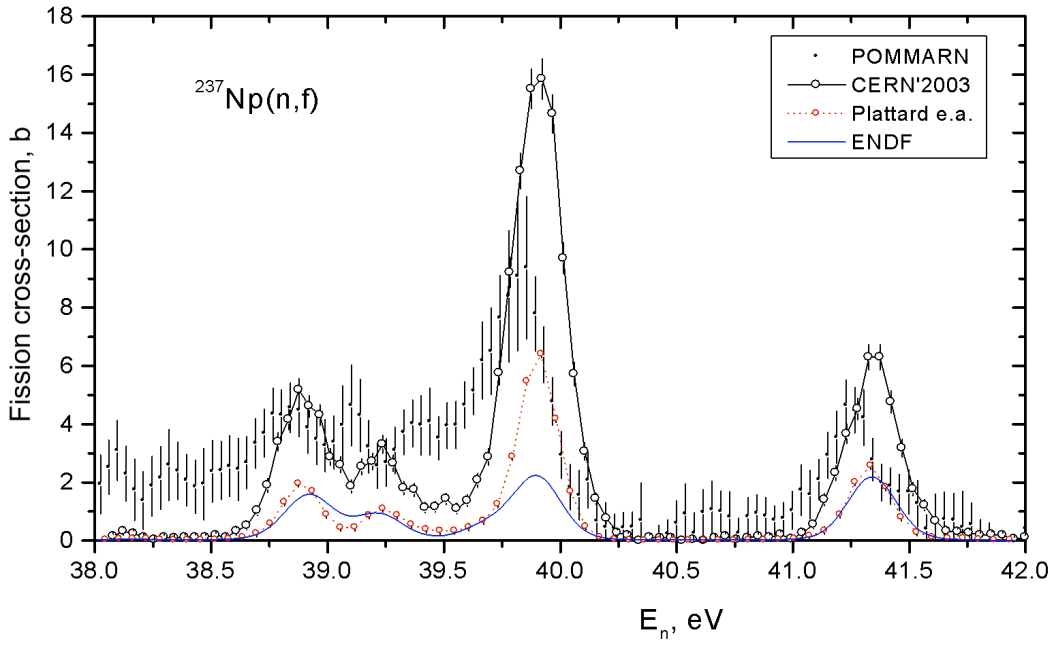

Figure 4.37. Comparison of the fission cross-section for ^{237}Np between 38 – 42 eV [86].

For ^{207}Pb and ^{209}Bi, the preliminary analyses of the n_TOF results show discrepancies, particularly in the resonance region, that justify a new evaluation of their capture cross-sections. Figures 6.38(a) and 6.38(b) show the radioactive kernel (area of the resonance, thus proportional to the cross-section using the Breit-Wigner formula) for some resonances in ^{207}Pb and ^{209}Bi, respectively. For example, the n_TOF cross-section measurement for ^{207}Pb shows resonances at 16 keV and 30 keV, which are not included in the evaluated data files, although they were detected in previous measurements. For ^{209}Bi, up to 50% smaller cross-sections were found for some resonances compared to the evaluated data. The data in the

evaluated files is based on an experiment performed in Oak Ridge (Macklin, 1976) whose experimental setup showed a higher sensitivity to neutrons. The discrepancies found between the n_TOF experimental data and the ND libraries justify a cross-section evaluation for the isotopes in question, in order to include the new data in the ND files.

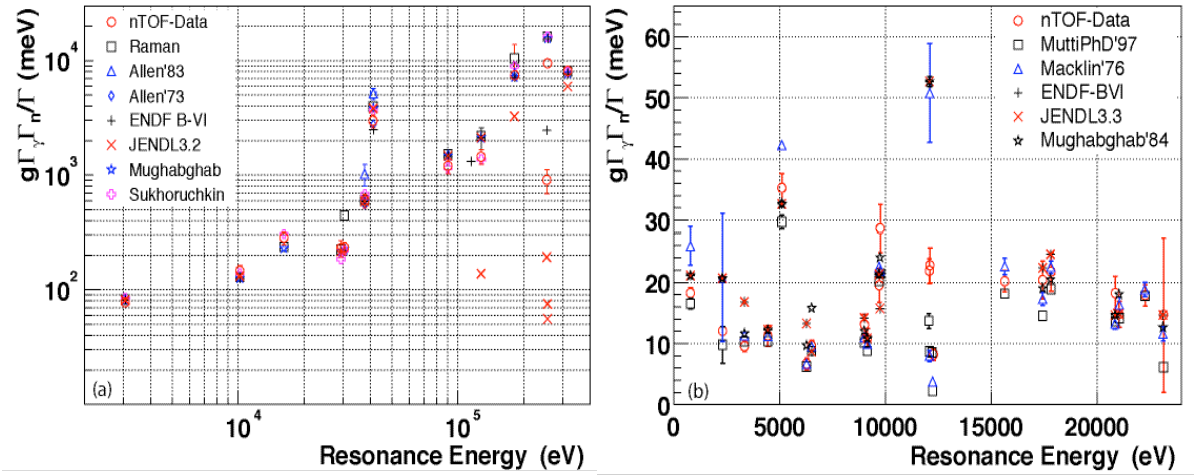

Figure 4.38. ^{207}Pb (a) and ^{209}Bi (b) capture radioactive kernel (resonance area) [87].

These preliminary results for the isotopes measured in n_TOF show very promising possibilities for reducing the uncertainties of the ND for many isotopes related to transmutation. This section was not meant to be exhaustive but to give several of the measured and evaluated data for several isotopes whose ND discrepancies showed relevance in the previous sensitivity analysis.

The high neutron flux combined with the development of detectors that are less sensitive to the neutron background have improved the accuracy of the measurements and reduced the statistical uncertainties. The very broad energy range of the measurements (from thermal energies to 250 MeV) and the good energy resolution of the facility (allowing the accurate detection of narrow cross-section resonances) are other positive characteristics, and produce results for energies which were not previously measured.

The author's participation in this experiment began during the commissioning of the facility [78] in 2001. His involvement included the analysis of the radioprotection and shielding aspects of the facility, particularly for the reduction of the muonic background [80]. The author also participated in the calibration measurements of the FIC detector performed in PTB (Germany) [86] and has actively taken part in the 2002, 2003 and 2004 measuring campaigns at CERN. Finally, the results of [74], [75] and this dissertation have helped to determine the measurement priority list and to expand it for future measurements. In fact, these measurements are a worldwide effort, involving a number of countries including Japan, Russia and the European Union, to improve the ND related to HLW transmutation in ADS, as

well as the fundamental knowledge of nuclear physics (e.g. 2nd and 3rd fission wells in ^{234}U or ^{232}Th).

The n_TOF measuring campaign will conclude at the end of 2004. The data collected is currently been analysed and some of it may be available in 2005. There are plan to evaluate this data and include it in the ND files (probably in JEFF). The organisation of future activities after the PS shutdown in 2005 (for example new cross-section measurements in 2006) is currently being considered.

Clearly, the simulations presented in this dissertation are subject to the discrepancies in ND between libraries that were previously explained. The new measurements obtained in n_TOF also show that some of the previously evaluated data may not be completely accurate. Therefore, the calculations in Chapter 5 and 6 may be precise only within a certain range, for example thousands of pcm in k_{src}, due to those uncertainties.

Chapter 5

The TRADE Experiment

The European Roadmap towards the experimental demonstration of ADS [46] indicates several experiments which would allow to validate the separated components of an ADS. The validation of the ADS concept may be summarised in three different levels, depending on the type of experiments required:

- Level 1: validation of the different components taken separately (accelerator, target, subcritical core, dedicated fuels and fuel processing methods). FEAT, TARC and MUSE European experimental programmes and the MEGAPIE project are examples of experiments at this level.
- Level 2: validation of the coupling of the different components in a realistic environment, i.e. using existing critical reactors adapted to the objectives at significant power levels.
- Level 3: validation in an installation explicitly designed for demonstration (e.g. the ADS installation described in the aforementioned European Roadmap, XADS). This third step should evolve to a demonstration of transmutation fuels, after a first phase in which the subcritical core could be loaded with standard fuel.

The case for the licensing of a system such as the one foreseen in Level 3 could present difficulties, especially in absence of a preliminary coupling experiment at power. Therefore, the completion of an experiment where an existing low power reactor, with well-known safety features, is made subcritical and coupled with an accelerator by a spallation target hosted inside the core, is a necessary step towards the demonstration of the ADS concept.

The domain of interest in such an experiment is to show reliable operation of the system, from start-up to nominal power level, up to shutdown, in the presence of thermal reactor feedback effects. The presence of control rods in the system allows the verification of different modes

of operation and the determination and monitoring of reactivity levels. The joint cooling of the spallation target and of the subcritical core could be studied, together with the solution of some practical engineering and safety problems of specific interest for an ADS, such as the configuration of the beam ingress into the core and the radioprotection and shielding aspects of the beam-line inside the containment building.

The possibility of running the experiment at different levels of subcriticality (e.g. different fuel loading patterns), allows the transition from an external source-dominated regime to a core thermal-feedback-dominated regime to be explored. This transition is relevant, in particular to the understanding of the dynamic behaviour of an ADS, since future full-scale ADS prototypes for transmutation may have both a very low delayed neutron fraction and very low temperature reactivity feedbacks (see Chapter 6 for an in-depth dynamic analysis of the Energy Amplifier Demonstration Facility, EADF).

Prof. Carlo Rubbia suggested that this pilot experiment, which will be the first example of ADS component coupling at real power, could be performed on the TRIGA (Training, Research, Isotopes, General Atomics) reactor [88] at the ENEA-Casaccia Centre (Italy), an existing pool reactor of 1 MW thermal power, cooled by natural convection of water in the reactor pool.

5.1 Description of the TRADE Facility

The TRADE experiment is based on the coupling of an upgraded commercial proton cyclotron with a solid tantalum target, surrounded by the aforementioned reactor core in a subcritical configuration. This is achieved by removing the core's innermost fuel ring (ring B) and the loading / unloading of the core's outermost fuel ring (ring G) to reach the desired subcriticality level in small reactivity steps.

The spallation target will be hosted in the central thimble, at present used for high neutron flux irradiation. The target performance levels will be limited by the geometry of the irradiation channel; in spite of this, an adequate power deposition in the target (10-40 kW) should be achieved. For this reason, natural and forced convection cooling of the target should be envisaged. Figure 5.1 shows the main elements of the coupling in the reactor area (a) and a close-up view of the core and the entering beam-line (b), where the target in the central thimble may be seen. These figures are graphical representations of the detailed FLUKA / EA-MC model used to simulate the behaviour of the reactor, the results of which are detailed in this chapter.

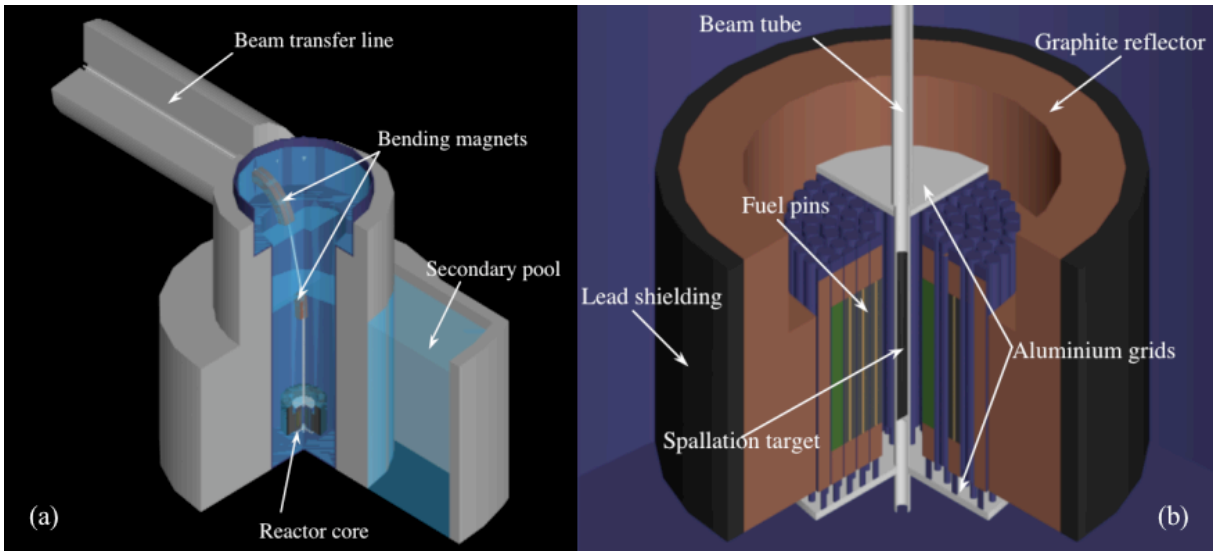

Figure 5.1. View of the main elements in the reactor area (a) and the TRIGA core (b) of TRADE.

5.1.1 Experimental Set-up

Due to the modularity of the TRIGA reactor, different fuel rod subcritical distributions and control rod arrangements are possible. The chosen reference core configuration for the analyses (Figure 5.2) is characterised by:

- The central channel (future spallation target);
- 6 fuel rods removed from ring B (water);
- 9 fuel rods in ring C (+3 control rods);
- 18 fuel rods in ring D;
- 24 fuel rods in ring E;
- 28 fuel rods in ring F (+1 source channel, +1 control rod);
- 23 fuel rods in ring G (+11 graphite pins, +1 rabbit channel, +1 loop channel).

The core consists of an annular structure, with six coaxial cylindrical rings of fuel elements plus one central element, immersed in water which serves as the coolant (Figure 5.2). A detailed description of the reactor can be found in [89]. The reactor and the experimental facilities are surrounded by a concrete shield structure and the core and reflector assemblies are located at the bottom of an aluminium tank (190.5 cm diameter). The overall height of the tank is ~7 m, thus the core is shielded by about 6 m of water. The core, surrounded by the graphite reflector, consists of a lattice of fuel elements, graphite rods and control rods. There are 127 channels divided in seven concentric rings (1-36 channels per ring). The channels are loaded with fuel rods, graphite rods and control rods depending on the power level required.

The diameter of the core is 56 cm, while the height is 72 cm. Neutron reflection is provided by graphite contained in an aluminium tank which is surrounded by 5 cm of lead acting as a

radiation and thermal shield. An empty aluminium tube (15 cm diameter and 0.6 cm thick) traverses the graphite reflector tangentially to the reactor core for thermal flux irradiations. The core components are contained within top and bottom aluminium grid plates: the top grid has 126 holes for fuel elements and control rods and a central thimble for high-flux irradiations. The reactor core is cooled by natural convention of the water in the reactor pool.

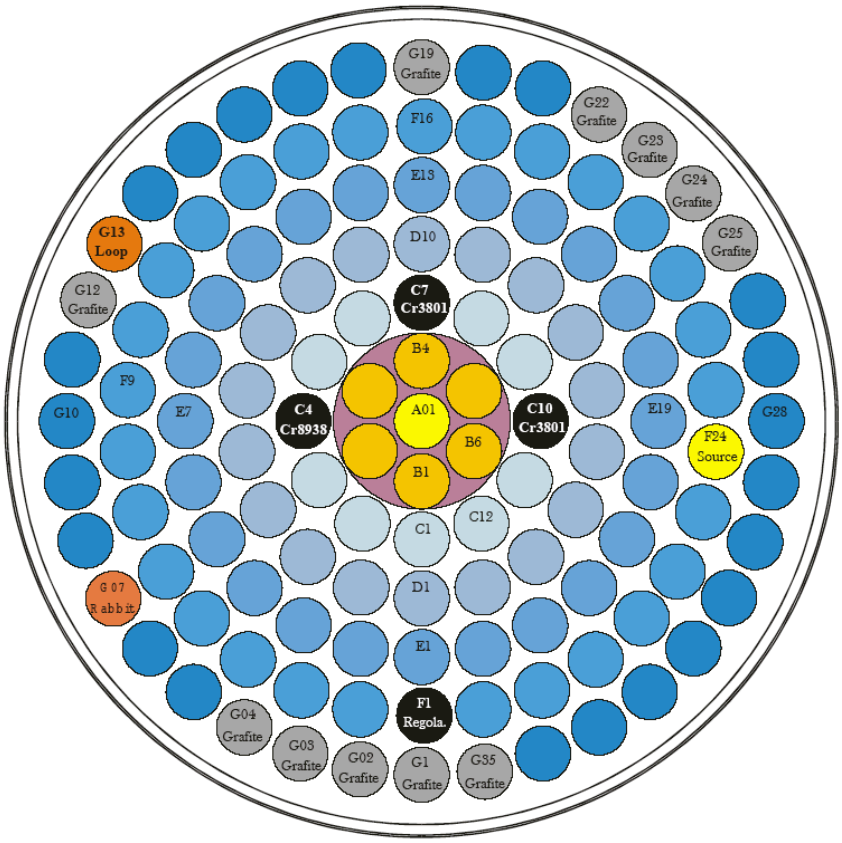

Figure 5.2. TRADE experiment fuel distribution reference configuration [50].

The fuel elements consist of a stainless steel cladding (AISI-304, 0.05 cm thick, 7.5 g/cm^3 density) characterised by an external diameter of 3.73 cm and a total height of 72 cm, end cap included. The fuel is a cylinder (38.1 cm high, 3.63 cm in diameter, 5.8 g/cm^3 density) of a ternary alloy uranium-zirconium-hydrogen (the H-to-Zr atom ratio is 1.7 to 1; the uranium, enriched to 20% in ^{235}U, accounts for 8.5% of the mixture in weight: the total uranium content of a rod is 190.4 g, of which 37.7 g is fissile) with a metallic zirconium rod inside (38.1 cm high, 0.5 cm in diameter, 6.49 g/cm^3 density) to improve the heat transfer inside the fuel. There are two graphite cylinders (8.7 cm high, 3.63 cm in diameter, 2.25 g/cm^3 density) at the top and bottom of the fuel rod. Externally two end-fittings are present in order to allow the remote movements and the correct locking to the grid. The control rods are made of graphite with powdered boron carbide, where ^{10}B is the actual neutron absorber, with a 20% natural abundance and a thermal (n, α) cross-section of ~4000 b. The graphite rods are similar to the control rods but without boron inside the central volume.

5.1.2 Spallation Target Design

The design of the spallation target is arguably the most challenging issue in TRADE. Since this is the first ADS experiment at real power, the interactions between high-energy beam and target and the coupling of the latter with the reactor core entail unprecedented problems in nuclear core design. The presence of an external decoupled neutron source (the spallation target) and the beam energy deposition in it require detailed studies to assess the performance of the experiment and guarantee safety during operation.

The design of the target has undergone several modifications since the initial proposal of a solid tungsten target, with a conical void to homogenously distribute the power deposited (and the neutrons produced) along the inner surface. The accelerator would supply ~0.13 mA (at the beginning-of-life (BOL)) of 110 MeV protons (~14 kW deposited in the target). Due to difficulties in the fabrication of the tungsten target and foreseen mechanical constraints (large stresses due to the concentrated energy deposition), it was proposed to use tantalum instead of tungsten [90]. Tantalum offers better machining and mechanical properties and similar neutronic characteristics, although it is considerably more expensive. The neutron yield for 110 MeV protons is the same for both elements (~0.45 n/p), as are the current requirements [91].

Moreover, an energy upgrade for the accelerator was considered in order to improve the spallation neutron yield, reducing the current requirements, and allowing the possibility of the later use of this machine as a booster for the large accelerator (at least 600 MeV) coupled to the fast lead-bismuth cooled ADS prototype. The energy range between 140-300 MeV was studied [92], and 140 MeV was found to be optimal for efficient proton use (large numbers of protons escape the target for higher energies), target durability (shorter core lifetime with increasing proton energies due to increasing radiation damage) and radioprotection risk assessment (increasing high-energy neutrons escapes with increasing proton energies), as explained in 5.1.3.

Several geometrical options for the target were also analysed due to the very restricting geometrical and thermo-mechanical requirements. Up to ten designs of the cylindrical target (with a conical void inner surface) have been studied. For the final configuration, the neutron yield is ~0.75 n/p and the power deposited in the target is ~11 kW (smaller than for 110 MeV due to the increase in neutron yield and source importance, φ^*).

Figure 5.3 shows the energy deposition in the TRADE core for an RZ view (a) and for an XY view (b), for a normalised beam current of 1 mA. The maximum energy deposition occurs at the target contact surface with tip of the conical void (due to the Gaussian profile of the beam and the protons scattered at small angles towards the tip), reaching ~930 W/cm^3 for the nominal beam current 0.08 mA (~12 kW/mA/cm^3, beyond the scale in Figure 5.3(a)). The

power density in the fuel pins ranges from 2 to 10 W/cm^3 depending on the position and the power required from the core. Notice the small energy deposition in the control and graphite elements (Figure 5.3(b)). In any case, it is clear that the thermo-mechanical requirements of the spallation target are much greater than those of a conventional core due to a maximum power density at least two orders of magnitude larger, thus the need for a detailed target design.

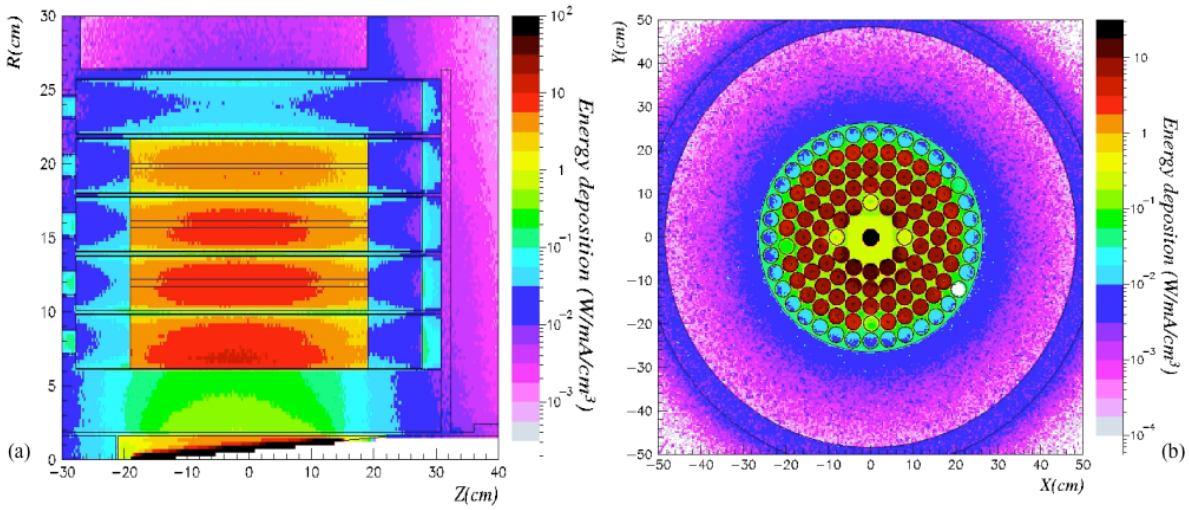

Figure 5.3. RZ (a) and XY (b) energy deposition in the TRADE core for 1 mA of 140 MeV protons.

The activation of the target is a major concern for the experiment. The activity of the target after one year of operation for the reference configuration, i.e. k_{src} ~0.977 and 200 kW of core thermal output, is ~242 TBq (Figure 5.4(a)), where the captures in tantalum (activation products) dominate the decay activity for ~10 years. Beyond 20 years, the spallation products, in particular hafnium (i.e. ^{172}Hf), lutetium (i.e. ^{173}Lu) and finally tritium dominate the medium-lived activity (< 100 years).

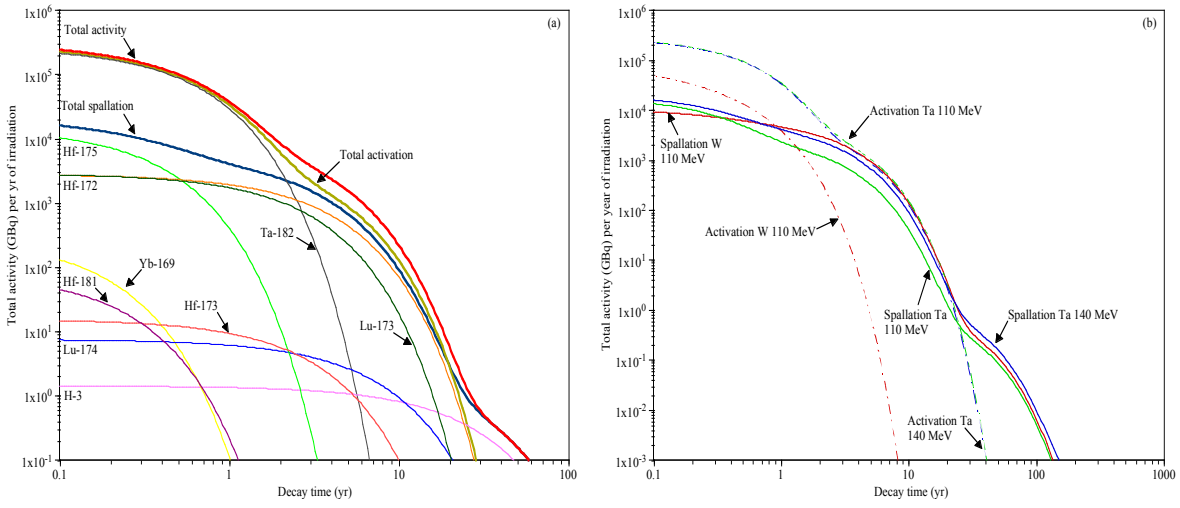

Figure 5.4. Evolution of the activity for: (a) the Ta 140 MeV target, compared to the W target (b), for TRADE.

It is worthwhile to compare the total activity for different target designs. Figure 5.4(b) shows the lower activity from activation products for the tungsten target with 110 MeV protons compared to the tantalum target with 110 MeV and 140 MeV protons. The lower capture cross-section of the former entails less neutron captures in the target, and therefore less activation products.

5.1.3 Radioprotection Aspects

Another important and unusual aspect of the design of an ADS facility is the radioprotection. The impact of particles escaping the beam transfer line (BTL), the bending and focusing magnets and the core, due to losses during normal operation as well as for accident scenarios, requires detailed study to guarantee the safety of the staff working in the facility.

An exhaustive analysis of the BTL shielding requirements to keep the dose to workers below an acceptable and legal maximum (10 μSv/h) was performed [93], considering normal losses (1 nA/m per mA of beam current in the straight section and 100 nA/m/mA in the bending magnets). Several shielding materials and thicknesses were analysed as well as the doses in several accident conditions [94].

The results obtained for different shielding and beam pipe materials are summarised in Table 5.1. The use of borated barite concrete was recommended because of its larger density (3.5 g/cm^3 compared to 2.4 g/cm^3 for conventional Portland concrete), the considerable total cross-section of barium for high and epithermal energies (particularly, the capture resonances of ^{135}Ba) and the absorption of the thermal neutrons through the (n, α) reaction in ^{10}B (20% of natural boron). The reference configuration (140 cm of barite concrete with a 2 mm stainless steel beam pipe) gives an acceptable dose rate at the surface of the BTL shielding, unlike the water shielding case analysed in [95], which reaches 70 μSv/h for 20 cm of iron followed by 120 cm of water.

The effects of the different shielding materials on the neutron energy spectrum may be observed in Figure 5.5. The effect of the large total macroscopic cross-section for iron at high-energies produces a shift of the neutron flux (due to inelastic processes such as spallation) towards the fast region (10^3-10^6 eV), where the total cross-section is smaller compared to other shielding materials. The resonance in ^{54}Fe at ~10 keV may be clearly seen for the cases where a significant amount of iron is used.

The barite concrete also to reduces significantly the high-energy neutron flux by producing spallation in barium and latter capturing those neutrons at lower energies. Since the dose is dominated by the high-energy component of the neutron flux, the use of barite is a very efficient method of reducing the neutron-induced dose.

Table 5.1. Effective dose due to 1 nA/m losses in the TRADE BTL for different shielding configurations.

Shielding Configuration	Beam pipe	Effective dose at the surface (μSv/h)	Eff. dose 5 m from the surface (μSv/h)
1 m normal concrete	8 mm Al	350	64
1 m barite concrete	8 mm Al	100	18
1.4 m barite concrete	8 mm Al	9.5	2.4
1.4 m barite concrete	8 mm AISI304	7.9	1.8
1.4 m barite concrete	2 mm Al	8.3	1.9
1.4 m barite concrete (ref. config.)	2 mm AISI304	7.5	1.7
20 cm Fe, 1.2 m barite concrete	8 mm AISI304	3.7	0.8
20 cm Cu, 1.2 m barite concrete	8 mm AISI304	3.2	0.8
20 cm Cu, 1.2 m barite concrete	2 mm Al	3.9	0.9
5 cm Cu, 15 cm ^{10}B-poly, 1.2 m barite conc.	2 mm Al	10.5	2.4
20 cm ^{10}B-poly, 1.2 m barite concrete	2 mm Al	10.8	2.5
20 cm Fe 1 m H_2O, 20 cm Fe	2 mm Al	33.2	7.7
20 cm Fe 1 m ^{10}B-H_2O (B 6.7% at.), 20 cm Fe	2 mm Al	34.6	8.1
20 cm Fe, 1 m H_2O	2 mm Al	70	16.3
1.4 m Fe	2 mm Al	1	0.2
2 m barite concrete	2 mm AISI304	0.4	0.12
20 cm Fe, 1.8 m barite concrete	8 mm AISI304	0.2	0.06
20 cm Cu, 1.8 m barite concrete	8 mm AISI304	0.2	0.06

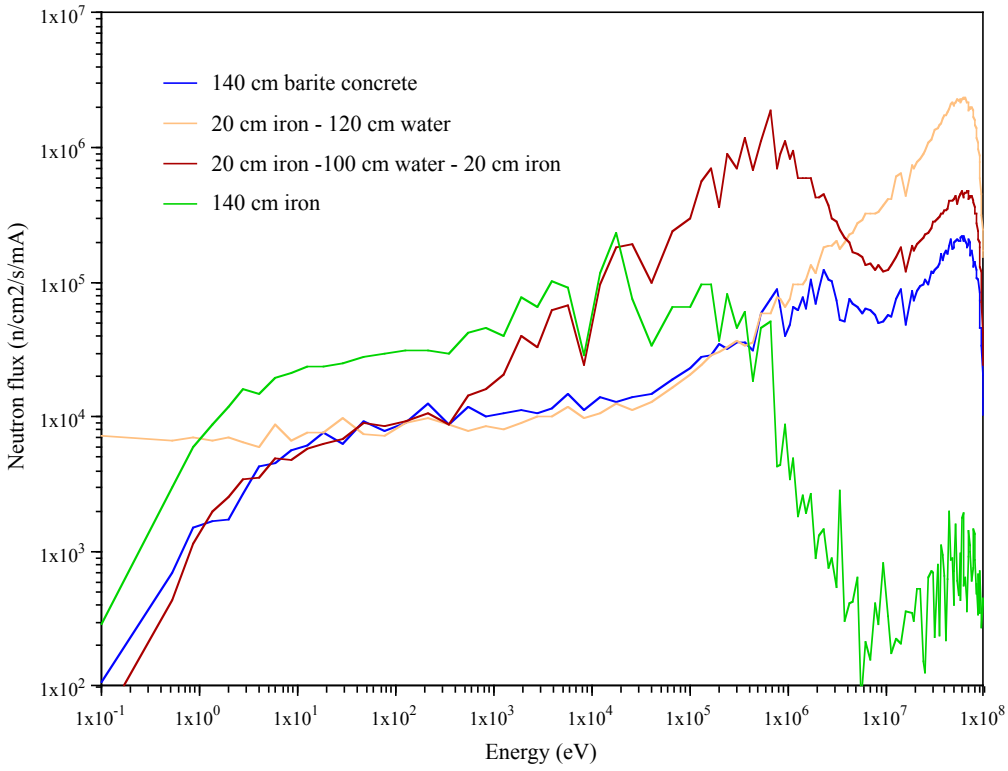

Figure 5.5. Neutron flux spectrum for different BTL shielding configurations.

A delicate issue in the design of the BTL is the design of the bending and focusing magnets, which are needed to drive the proton beam into the core. In principle, the BTL includes a set of permanent samarium-cobalt (Sm_2Co_{17}) bending magnets. The magnetic field produced by these magnets is rather sensitive to the radiation damage, thus a study of the demagnetisation due to the ~4×10^6 Gy/yr/mA expected dose was performed [96], and an acceptable magnetic field loss (below 0.1% per year) was found. On the other hand, the effective dose due to the losses in the bending magnets during normal operation and in an accident scenario (collision of the proton beam on the magnet) were found to be unacceptably high (~30 mSv/s/mA for the latter case), requiring important changes in the BTL layout in order to shield these elements.

5.1.4 Significance of TRADE towards an ADS Demonstration

In order to be a representative experiment for the validation of the ADS concept, several requirements have to be met, defining certain parameters, such as the choice of the external neutron source. A core power of several hundred kW is needed to explore the dynamics, reactivity control and power monitoring in an ADS, from a source dominated regime of $k_{rsc} \approx 0.9$ to a reactor feedback dominated regime $k_{rsc} \approx 0.99$. The use of ~140 MeV protons is suggested after considering several factors. In order to explore deeply subcritical configurations higher proton energies (e.g. 300 MeV) would be advisable, due to the lower target energy deposition for the same subcriticality and core power levels (Figure 5.6). The higher φ^* and proton range in the target material (thus, spreading the energy deposition) for higher proton energies are responsible for these enhanced characteristics. Nevertheless, the limited size of the spallation target and the high-energy proton leakage into the core [92], the accelerator cost and the size of the BTL magnets and the radioprotection problems posed by these for higher energies [93] indicated ~140 MeV as an optimum. Moreover, this proton kinetic energy allows the reactivity range planned for XADS to be explored without exceeding the maximum power level in the target (~30 kW) for a nominal power output in the core of 200 kW. It would also permit deeply subcritical configurations (i.e. $k_{rsc} \approx 0.90$) to be explored at 200 kW for short periods of time (~50 kW in the target), or during longer periods at the expense of a lower core power.

In terms of neutron spectrum, the thermal spectrum in TRADE allows some experiments representative also of a fast neutron spectrum to be performed. In fact, although the kinetic parameters of TRADE and of a fast neutron spectrum are very different, their kinetic response to perturbations are similar, except for the shifting to lower frequencies of the thermal system transfer function (due to longer neutron lifetimes), as presented in Figure 5.7. In fact, the responses to perturbations in reactivity increase in parallel (the thermal system being less sensitive to higher frequencies) until they reach their respective plateaux, where both systems

present the same response for small reactivity changes at low frequencies. For a reactivity drop of –5000 pcm (approximately the worth of a control rod) the magnitude of the transfer function is very close after the response saturates (at ~100 kHz for the fast and ~300 Hz for the thermal system).

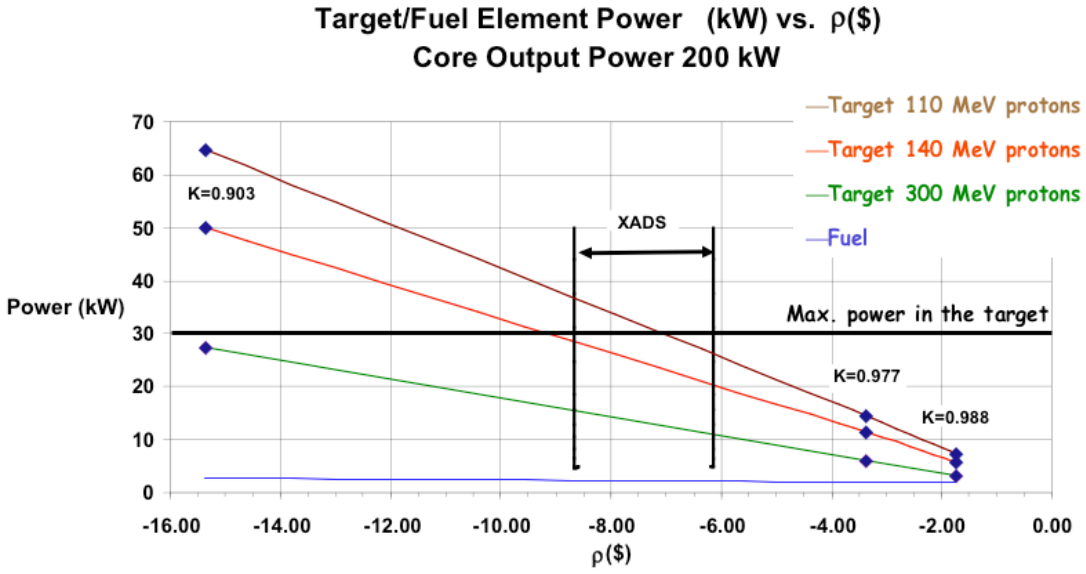

Figure 5.6. Reactivity change for different subcritical configurations and proton energies [97].

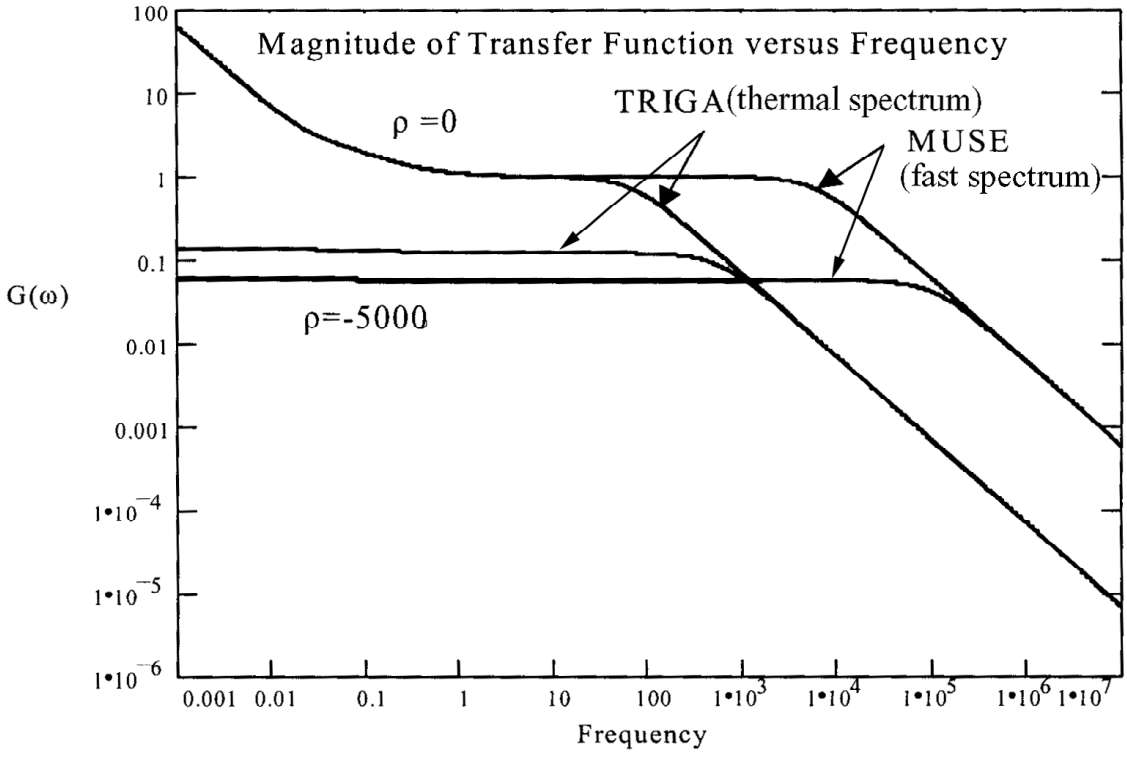

Figure 5.7. Transfer function for different perturbation frequencies in a TRIGA core and in MUSE [98].

These features allow the dynamic behaviour of an ADS to be investigated and validated independently from the neutron spectrum and make the TRADE experiment a natural successor to the FEAT, TARC and MUSE experiments and an essential precursor to a future high-power ADS experiment.

The design and handling of the spallation target, the establishment of licensing procedures for ADS, the analysis of the impact of the BTL in the reactor building and the development of specific detectors are also very relevant issues towards the experimental demonstration of a fast ADS.

Moreover, the intrinsic safety of the TRIGA reactor in terms of temperature effects may be applied to the TRADE experiment. The power and temperature coefficients for a core power rise from a cold start to 200 kW are ~–3.0 pcm/kW (–6.8 pcm/K), and from 200 kW to 500 kW are ~–2.8 pcm/kW (–14.2 pcm/K) [50]. The large negative values of these reactivity coefficients are related to the choice of the fuel. This fuel design presents a larger Doppler broadening compared to oxide fuel due to the large amount of hydrogen, producing a high epithermal flux. This fact, together with a high chemical and mechanical stability, and an efficient retention of the volatile FFs, qualify this fuel as an excellent one for high-power density facilities.

5.1.5 Experimental Objectives

The experiments relevant to ADS development to be carried out in TRADE may concern the fields presented in the following, non-exhaustive, summary:

- The dynamic regime: the possibility to operate at some hundred kW of power and at different subcriticality levels ($0.90 \leq k_{src} \leq 0.99$) will allow the dynamic behaviour of the system vs. the neutron importance of the external source to be validated experimentally.
- Subcriticality measurements at real power in order to obtain relevant information on the optimal subcriticality level of a full-scale ADS.
- Correlation between reactor power and proton current. This correlation can be studied at different subcriticality and power levels.
- Reactivity control by different means and possibly by neutron source importance variation, keeping the proton current constant. In principle, this can be achieved by changing the neutron diffusion properties of the buffer medium around the spallation source (e.g. using different materials in the empty innermost fuel ring close to the target).
- Start-up and shut down procedures, including suitable techniques and instrumentation.
- The study of the impact of beam failures in the behaviour of the core is of major importance for ADS. TRADE presents the advantage of lower response frequencies that make possible the study of slower dynamic feedbacks than in a fast ADS.

Moreover, an important feature of the TRADE set-up is the possibility to carry out, before the coupling with the accelerator, a preliminary experimental campaign by inserting into the current central thimble a known standard neutron source, and performing static and dynamic measurements for different subcriticality levels. For example, for the second type of measurements, the configuration of the TRIGA reactor allows the application of a wide variety of techniques devoted to the determination of the subcriticality level, such as source jerk, pulsed neutron source analyses, rod drop and modified source multiplication. This set of experiments will provide a link with the MUSE experiments and characterise the subcritical core from a safety point of view. In fact, the experiments in TRADE will benefit from the extensive experimental techniques development performed in the zero-power MUSE experimental program, since most of the experimental techniques are directly applicable, in particular in the domain of reactivity level measurement and monitoring.

5.2 Neutronic Characterisation

The description of the subcritical and critical configurations illustrates the core layout for the different experiments and their comparison evidences the fundamental differences with respect to the behaviour of the neutron population inside the core for different k_{src} values. The determination of the neutronic characteristics of these configurations is essential in order to predict their behaviour during operation and understand the experimental results. Furthermore, precise understanding of the behaviour of the neutron population in the system may give an insight into the transmutation potential of such systems.

Several neutronic parameters of the proposed TRADE configurations were analysed using the FLUKA / EA-MC Monte Carlo code, including realistic models of in-vessel structures, which may affect the overall neutronics. An extensive study of these aspects was published in [99].

The analysis of the spallation neutron population is also a necessary step for the design of the system, since the distribution is essentially different and independent from that for fission neutrons.

5.2.1 Subcritical Configurations

Three subcritical core configurations were chosen to analyse the behaviour of the reactor at different levels of subcriticality, as future candidates for the experimental phase. Two other working conditions were also analysed to compare with the previous ones and to assess the core behaviour in different thermal conditions:

- A reference configuration (FC1) consisting of 102 fuel rods (reference core configuration with the 3 control rods withdrawn, i.e. fuel follower inserted) resulting in a $k_{src} \approx 0.977$, operated at 200 kW_{th} and cooled by natural convection.
- A second configuration (FC2) consisting of 107 fuel rods (FC1 with 5 additional fuel rods in ring G, i.e. 28 fuel pins in that ring) resulting in a slightly subcritical core, i.e. $k_{src} \approx 0.988$, operated at 200 kW_{th} and cooled by natural convection.
- A third configuration consisting (FC3) of 79 fuel elements (FC1 without fuel rods in ring G, and the control rods partially inserted) resulting in a deeply subcritical core, i.e. $k_{src} \approx 0.901$, with the spallation target cooled by forced convection.
- A critical core configuration (FC4) consisting of 108 fuel rods (FC1 with the control rods at critical level, as in FC3) operated at different power levels (i.e., 200 kW, 500 kW and 1 MW) and cooled by natural convection has been also analysed to compare with the subcritical ones.
- Studies of the different configurations operating at higher power ratings (500 kW_{th} and 1 MW) in order to analyse the thermal-hydraulic characteristics of both the core and the spallation target were also performed. The average fuel temperature for the three power levels analysed, i.e. 200 kW, 500 kW and 1 MW, would be $T_{fuel} \approx$ 114 °C, 174 °C and 321 °C.

5.2.2 Nominal Parameters

The main neutronic parameters for the three TRADE subcritical configurations, in addition to the critical case for comparison purposes, are summarised in Table 5.2. Even though TRADE will operate with control rods, the source multiplication coefficient of 0.977 (different to the value of $k_{eff} \approx 0.974$) was chosen to avoid criticality conditions with adequate safety margins, under all normal conditions as well as for transient and accident conditions, like in a fast ADS prototype. The general operation margins for an ADS may be summarised in three different levels: due to uncertainties in reactivity measurement (~1000 pcm), due to uncertainties in ND (~1000 pcm) and due to a possible cold shutdown (absence of temperature feedbacks, ~500 pcm).

If the experiment was to produce a constant reactor power (P_{th}) of 200 kW for the different configurations, there would be a need to strongly increase the accelerator current (I_p), from 0.05 mA for $k_{src} \approx 0.99$ to 0.42 mA for $k_{src} \approx 0.90$. Similarly, for the same configuration, an increment in I_p would imply an increment in P_{th} and power deposition in the target. On the other hand, k_{src} (and thus k_{eff}) would remain constant, since these parameters only depend on the definition of the system and the nature of the fuel (k_{eff}) and also the source neutron spatial and energy distribution (k_{src}) but not on the intensity of the source or the power produced in

the core. Nevertheless, the reactor power would indeed affect the time evolution of the multiplication coefficients since it has a direct effect on the burn-up of the fuel, and therefore on the evolution of its isotopic composition. For FC2, the value of φ^* is close to 1 since the system is very close to criticality, and therefore k_{src} and k_{eff} are very similar. Even though the difference between k_{src} and k_{eff} becomes larger with decreasing multiplication, the value of φ^* is in the reference case (FC1) is higher than in FC3 due to be better confinement of the source neutrons in FC1. The higher spallation neutron flux required for FC3 (Figure 5.8(a)) and the more diffusive medium in the core (23 fuel rods in FC1 are substituted by graphite rods in FC3) enhance the leakage of the spallation neutrons.

Table 5.2. Main neutronic parameters of the TRADE k_{src} configurations.

Global parameters	Symbol	FC4	Reference case	FC2	FC3
Initial fuel mixture	LEU	UZrH	UZrH	UZrH	
Initial fuel mass	m_{fuel} (kg)	245.9	235.2	246.4	181.0
Initial U concentration	m_U/m_{fuel} (wt.%)	8.5	8.5	8.5	
Initial fissile enrichment	$^{235}U/^{238}U$ (at.%)	20	20	20	
Thermal power output	P_{th} (kW)	200	200	200	
Proton beam energy	E_p (MeV)	—	140	140	
Spallation neutron yield	N (n/p)	—	0.75	0.75	
Net neutron multiplication	M	—	38.3	71.0	9.8
Source multiplication coeff.	k_{src}	1.000	0.977	0.988	0.901
Effective multiplication coeff.	k_{eff}	1.000	0.974	0.988	0.891
Neutron source importance	φ^*	—	1.134	1.035	1.113
Energetic gain	G	—	16.7	30.4	4.4
Gain coefficient	G_0	—	0.39	0.37	0.44
Accelerator current	I_p (mA)	—	0.09	0.05	0.42
Beam power	P_{beam} (kW)	—	12.7	6.8	58.7
Core power distributions					
Av. fuel power density	P_{th}/V_{fuel} (W/cm^3)	4.8	4.9	4.7	6.5
Spec. fuel power density	P_{th}/m_U (W/gHM)	9.7	10.0	9.6	13.3
Radial peaking factor	P_{max}/P_{avg}	1.45	1.48	1.46	1.76
Axial peaking factor	P_{max}/P_{avg}	1.45	1.51	1.48	1.78

Table 5.3 summarises the neutron-induced reactions taking place in different locations in the whole reactor core and also, specifically, in the fuel elements. The fuel is clearly absorbing the majority of the neutrons (~64%), followed by the cooling water (~19%) and the cladding (~10%). Even though there is a large neutron leakage out of the core (as later described in Section 5.2.3 and illustrated by the neutron flux radial profile in Figure 5.8(a)), the small number of neutron escapes (~0.02%) shows that the neutron population is well contained inside the system (by the ~6 m of water above the core, the graphite reflectors, the lead

shielding and the concrete around the vessel). This fact implies that the system is rather sensitive to the insertion of empty channels, such as the beam tube, hence the need for several bending magnets in the core to avoid neutron streaming upwards through the beam tube, The similar values for neutron absorption in the different fuel rings show a rather flat radial neutron distribution in the core for the reference configuration. The importance of the (n, xn) reactions, unusually large for a thermal system, is related to the interaction of the spallation neutrons in inner fuel elements, where (n, xn) reactions account for ~1.6% of the total. The large number of captures in the tantalum target (~2.4%) justifies the need for a precise study of the activation of the target and its disposal scheme.

Table 5.3. Neutron-induced reactions in different parts of TRADE.

Reactor core			
Neutron Absorption Inventory		Neutron Absorption Inventory	
Reactor vessel	0.001%	Absorber rods	0.85%
Neutron shield	1.03%	Cladding	10.47%
Aluminium lining	1.22%	Fuel ring C	9.59%
Upper grid	0.04%	Fuel ring D	12.89%
Lower grid	0.06%	Fuel ring E	15.17%
Spallation target	2.42%	Fuel ring F	15.58%
Primary coolant	19.07%	Fuel total	63.74%
Core reflector	0.77%	Escapes	0.02%
Main Nuclear Reactions		Main Nuclear Reactions	
Capture	58.55%	(n, xn)	1.17%
Fission	38.83%	Others	1.41%
Fuel assemblies			
Neutron Absorption Inventory		Neutron Absorption Inventory	
LEUZrH fuel	68.85%	Central Zr bar	0.09%
AISI-304 cladding	12.01%	Coolant	19.05%
Main Nuclear Reactions		Main Nuclear Reactions	
Capture	53.48%	(n, xn)	1.20%
Fission	44.91%	Others	0.45%

5.2.3 Neutron Flux Distribution

As explained in Chapter 3, the power distribution in a subcritical system is rather sensitive to the core's intrinsic multiplication factor. As the latter increases towards unity (the criticality condition), the neutron flux higher harmonics disappear and the neutron spatial distribution in the core tends towards the fundamental harmonic. Since the spallation neutron distribution is completely decoupled from the core, only the intensity varies for the different configurations, altering the neutron flux level and energy spectra in the inner regions of the core.

5.2.3.1 Spatial Distribution

The radial (Figure 5.8(a)) and axial (Figure 5.8(b)) neutron flux distribution (200 kW reactor power) for the high k_{src} configurations, i.e. FC1 and FC2, as well as for the critical case, have moderate peaking factors ($\phi_{max}/\phi_{avg} \propto P_{max}/P_{avg}$ ~1.5), suggesting that the thermal-hydraulic properties of the core are compatible with a presence of an intense spallation neutron source in the central channel. In the case of FC3, the high fluxes in the central regions of the core produce large peaking factors (~1.8), which is particularly important in the central fuel elements close to the spallation target.

As mentioned above, there is large neutron leakage from the core indicated by the exponentially decreasing radial flux in the outer regions in Figure 5.8(a). This is the result of the presence of higher harmonics (even for the critical case) in the neutron flux. The axial flux distributions for FC1, FC2 and FC4 exhibit similar behaviour, with a parabolic distribution centred in the middle of the core and a moderate power peaking factor, due to domination by the fission neutrons of the total neutron population. On the other hand, the effect of the spallation neutrons in FC3 is evident from the displacement of the neutron flux axial distribution (the blue curve in Figure 5.8(b)), since they account for ~10% of the total neutron population. Although the production of the spallation neutrons is isotropic, the scattering (and thus the transport) is forward peaked, as further illustrated in 5.2.3.3.

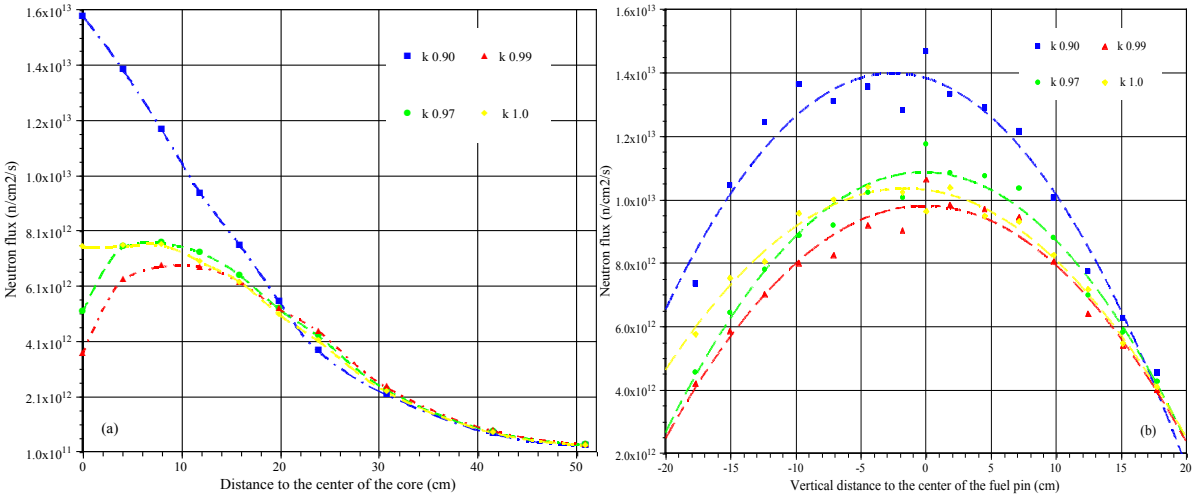

Figure 5.8. Radial (a) and axial (b) neutron flux for 200 kW and different subcriticality levels in TRADE.

Figure 5.9 shows the axial (a), and radial neutron fluxes for FC3 and a 1 mA proton beam. The parabolic neutron flux distribution in the Z direction may be seen, as well as the efficient reflection produced by the surrounding water. The effect of the inserted control rods is visible in Figure 5.5(b), followed by a prompt homogenisation of the flux.

The neutron flux distribution for higher power levels, i.e. 500 kW and 1 MW, is essentially the same, only varying proportionally in intensity. That is, for FC1 producing a core power of

500 kW the neutron flux in ring C is ~1.9×10^{13} n/cm^2/s and the power deposited in the target ~28 kW. Obviously, the thermal-hydraulic requirements may change qualitatively, in particular concerning the cooling of the spallation target, thus limiting the time the system operates at power levels beyond 200 kW.

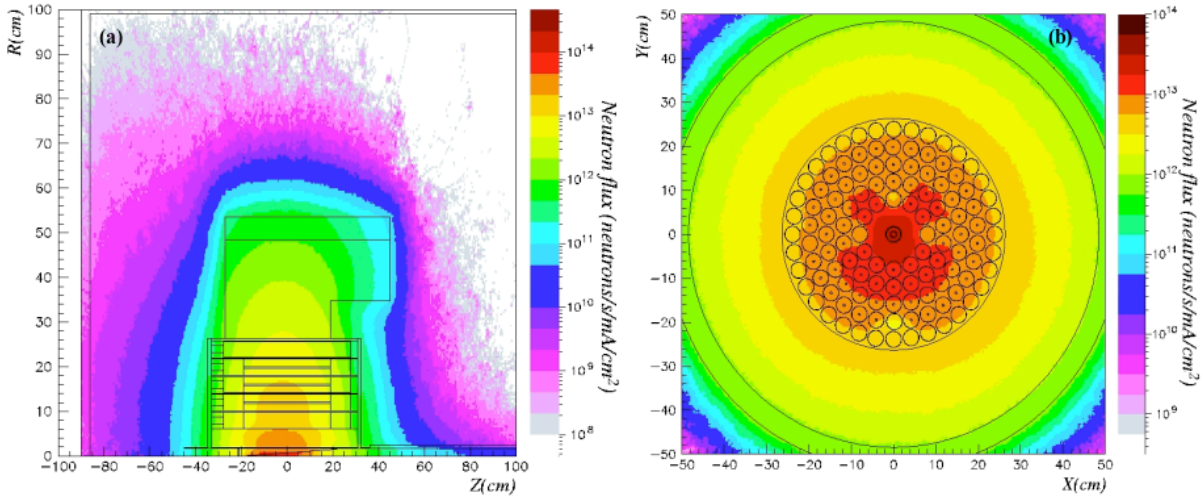

Figure 5.9. RZ (a) and XY (b) neutron flux distribution of the TRADE core for $k_{src} \approx 0.90$ (FC3).

5.2.3.2 Neutron Energy Spectra

The analysis of neutron flux spectra is a necessary step in order to characterise the system. TRADE is essentially a thermal system, cooled and moderated by water and using a fuel matrix rich in hydrogen. Despite the important fuel enrichment (20% ^{235}U) and the rather small pitch between fuel elements (~2.35 mm for ~18 mm radius fuel elements), the abundance of hydrogen guarantees the thermalisation of the fission neutrons inside the fuel, therefore defining the very characteristic two-humped spectrum (the thermal and the high-energy humps).

Moreover, the presence of a water buffer region (empty fuel channels in ring B) causes a prompt energy loss for the spallation neutrons and their diffusion, increasing the efficiency of the source neutrons (and thus φ^*), as illustrated in the next section.

Figure 5.6 shows the neutron energy spectrum for different regions of the core for FC1. The target presents a harder neutron flux and the energy spectrum shows a high-energy peak around 2-3 MeV (the spallation peak) and the resonances of tantalum (in particular, the ~15,000 b resonance at 4 eV). The thermal hump (Maxwell distribution) is due to the neutrons reflected into the centre of the core. The fuel regions present similar neutron energy spectra, with decreasing integral value with the distance from the centre of the core.

The graphite reflector and the lead shielding present well-thermalised spectra with almost no high-energy peak and a continuous epithermal region more than one order of magnitude

smaller than their thermal peak. The effect of the ^{10}B in the control rods is clear, absorbing the thermal neutrons in the region.

The presence of the spallation source produces a relative energy shift from the high-energy flux (target region) to the thermal distribution (reflector region) permitting, to a limited extent, the analysis of different elements under different spectrum conditions.

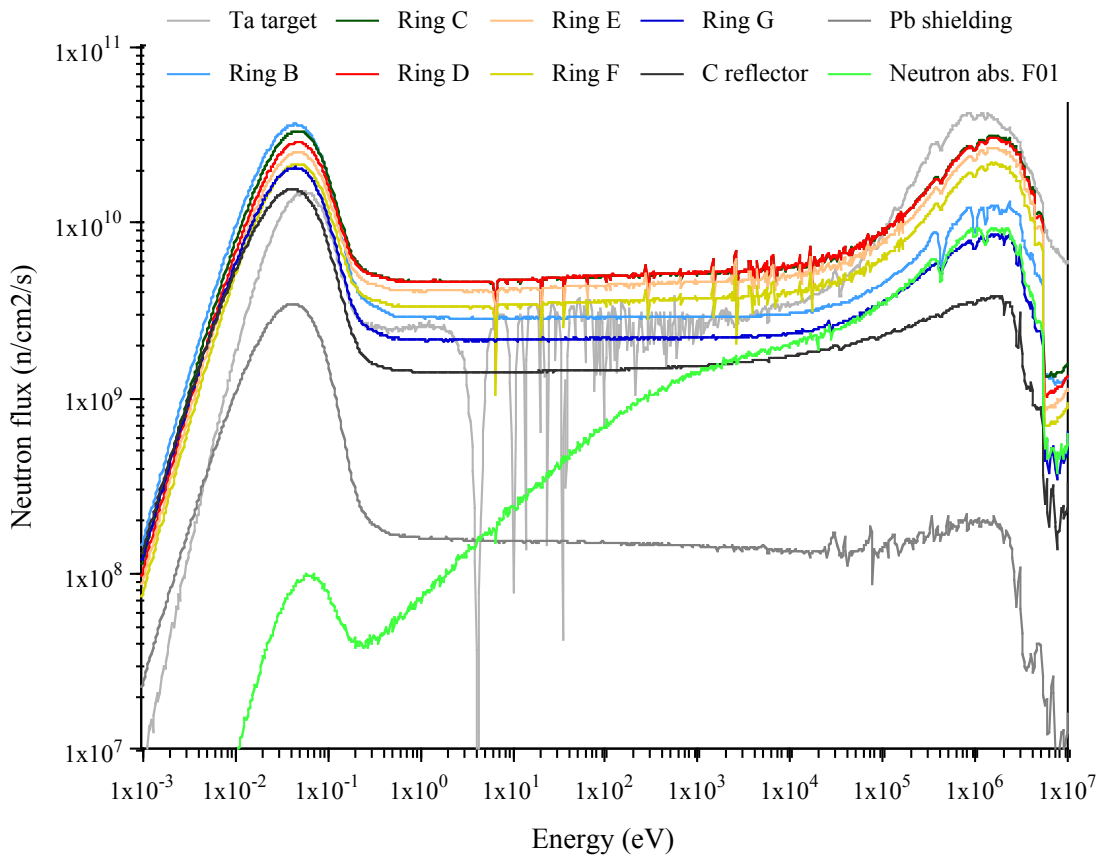

Figure 5.10. Neutron energy spectra for different parts of the core in TRADE.

5.2.3.3 Dynamic Behaviour of Fission and Spallation Neutrons

Study of the nature and behaviour of the spallation neutrons is essential in order to understand the operation of an ADS, since, as explained in Chapter 3, the origin and behaviour of these neutrons is decoupled from the multiplicative assembly. Figures 5.11(a), (b), (c) and (d) show the differences in the time evolution (up to 1 ms) of the neutron population for different TRADE configurations.

In the case of FC1, the neutron population is dominated by the fission neutrons after ~20 μs (Figure 5.11(a)). The spallation neutron population falls exponentially whereas the total neutron population is sustained by fission. At 100 μs, the spallation neutrons account only for 5% of the total neutrons and at 1 ms they account for 0.1%. Since this is a subcritical configuration ($k_{src} \approx 0.97$), the total neutron population slowly decreases, although dying out

at longer time scales. The spatial distribution and survival time of the spallation neutrons is strongly correlated to φ^*, hence the importance of properly diffusing and confining these inside the core. Of the total spallation neutrons at 1 ms, ~30% reached ring B and ~7% ring C (Figure 5.11(b)). There is a ~20 μs delay in reaching ring C before which only very high-energy neutrons, also producing spallation in the fuel, have reached this region. The neutrons reaching rings B and C after a few hundred μs are the ones which have been scattered to lower energies inside the spallation target. These neutrons have a lower probability of escaping the target (increasing the gap between the total number of spallation neutrons and those in the fuel rings), since they may be trapped in the resonance region of tantalum and eventually captured.

The time evolution of the neutron population for subcritical and critical configurations gives an excellent basis for understanding the multiplicative processes undergone in every case by the system. Figure 5.11(c) shows the neutron population survival probability normalised to one source neutron. There is a clear qualitative difference between the source-dominated regime ($k_{src} \approx 0.90$) and the fission-dominated regime ($k_{src} \approx 0.97$-0.99). In the first case, a large number of spallation neutrons is required to maintain the multiplicative reaction (10% of the total), and their weight in the total neutron population, although falling exponentially, is still remarkable after several hundred μs. The strong subcriticality of this configuration may be observed from the negative slope of the evolution of the total neutron population, dying out in a few ms. On the other hand, FC1 and FC2 exhibit similar behaviour, except for a certain difference in the neutron population lifetime. For these configurations, the spallation neutrons are quickly absorbed, producing the first fissions, which are later propagated by fission neutrons throughout the multiplicative medium. Clearly, the neutron population dies away with a longer period the closer the configuration is to the critical state. Finally, in the case of $k_{eff} = 1.0$ the initial neutron source is amplified until the neutrons are completely diffused in the core, after which the population remains approximately constant. This behaviour is similar to that of the fission neutrons in FC2.

Analysis of the neutrons' behaviour for different materials in the buffer region indicates that, although the total neutron population remains unaffected by the material used, the leakage time varies greatly, as illustrated in Figure 5.11(d). Since the neutron energy loss after a scattering reaction in lead is rather small, the neutrons escape ring B much faster (almost as quickly as in vacuum) through this buffer material. Therefore, the difference in spallation neutron migration time (correlated with the energy spectrum of these neutrons) suggests the possibility of performing different experiments for different neutron energies, without affecting the magnitude of the feedback.

This analysis is also very important to predict the response of the system to beam failures. Figure 5.11(a) shows a 35% decrease in the neutron population compared to the initial value

(not considering the spallation neutron peak) after 1 ms. In this sense, TRADE will help to understand the dynamic coupling between a spallation neutron source and a reactor core for different subcritical levels, thus response frequencies. It will be easier to perform these dynamic measurements in TRADE than in EADF since, as explained later in Chapter 6, the dynamic response of the latter is significantly faster (99.9% of the neutron population has disappeared after 1 ms).

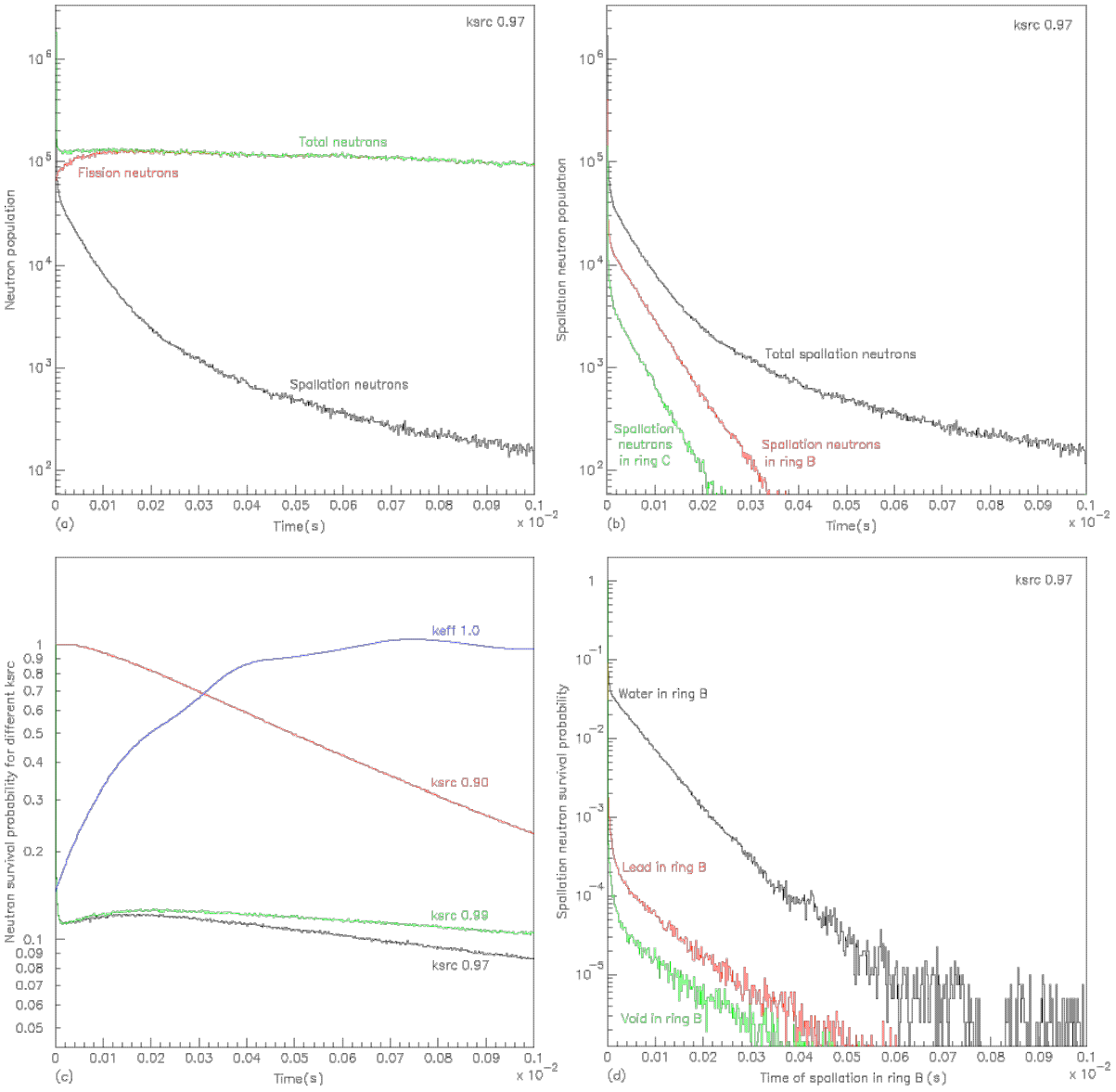

Figure 5.11. Time evolution of the neutron population up to 1 ms from the proton pulse: (a) for FC1, (b) for the spallation neutrons in different positions in the core, (c) for different k_{src} and (d) for different materials in ring B.

In all three subcritical cases (FC1, FC2 and FC3) the neutron population is dominated by the fission neutrons (roughly 97%, 99% and 90% of the total neutron population) and only in the deeply subcritical FC3 configuration is the spallation neutron population noticeable in the overall neutron distribution, causing an asymmetrical axial neutron distribution close to the

spallation target, in particular for neutrons above 20 MeV, as illustrated in Figure 5.12. The angle of asymmetry (following the forward-peaked elastic scattering for high-energies) of the source neutrons is proportional to the proton beam energy, thus preventing the use of a higher energy proton beam. Moreover, these high-energy neutrons are scarcely affected by the presence of a moderating medium, and represent a major contributor to the outside dose and atom displacements in the reactor structures [99]. This is not the case for the protons, which for 140 MeV are entirely confined inside the target region, since most of their energy is lost through ionisation (~94% of the proton energy loss).

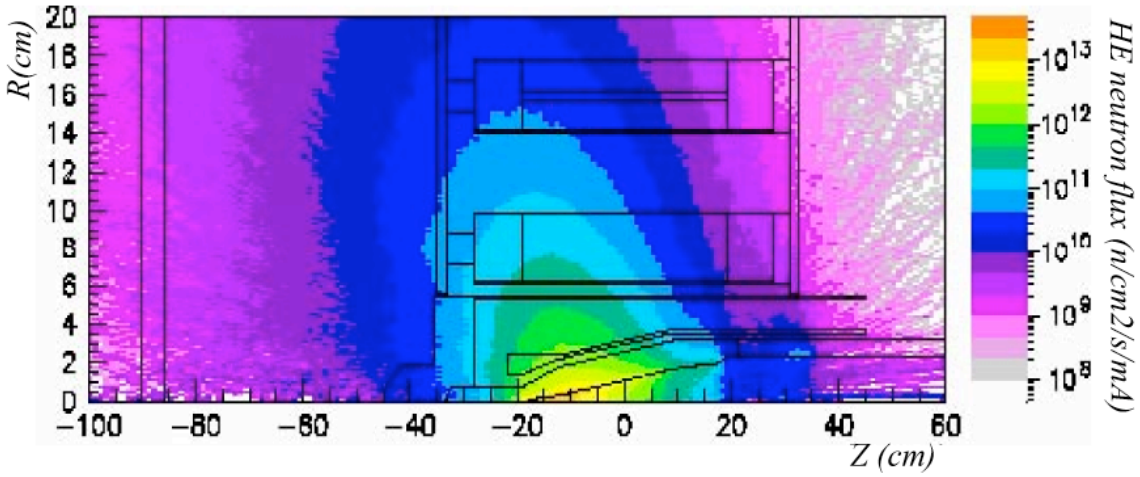

Figure 5.12. High-energy neutron distribution around the spallation target of TRADE for 140 MeV protons.

5.2.3.4 Burn-up Evolution

The simulation of the time evolution of the system, fuel core composition (fissile materials, MAs production, FFs, poisons etc.) is a characteristic feature of the EA-MC code. It may help to assess the transmutation capability of TRADE for plutonium, MAs and LLFFs since the level of burn-up is high enough to produce measurable quantities of transmuted isotopes. The evolution of the system has been calculated for one year of burn-up at different power levels, i.e. 200 kW, 500 kW and 1 MW. Over this period, the reactivity of the system dropped 2069 pcm, 4482 pcm and 8220 pcm respectively.

Therefore, a core thermal output of 200 kW requires ~0.27 mA, and ~1 mA for 500 kW. In the case of 1 MW output power, this reactivity swing would have to be compensated by a drastic change in the accelerator current, requiring over 3 mA after one year. This required current would entail unacceptable power depositions in the spallation target (Figure 5.13(a)), making this core power level impossible to reach safely for the FC1 configuration. On the other hand, an output power of 200 kW is attainable for the whole cycle, thus implying an average burn-up of ~5 GWd/tHM (Figure 5.13(b)). This average burn-up level represents ~12 GWd/tHM burn-up in the central part of the core, i.e. 6% of the initial fissile material.

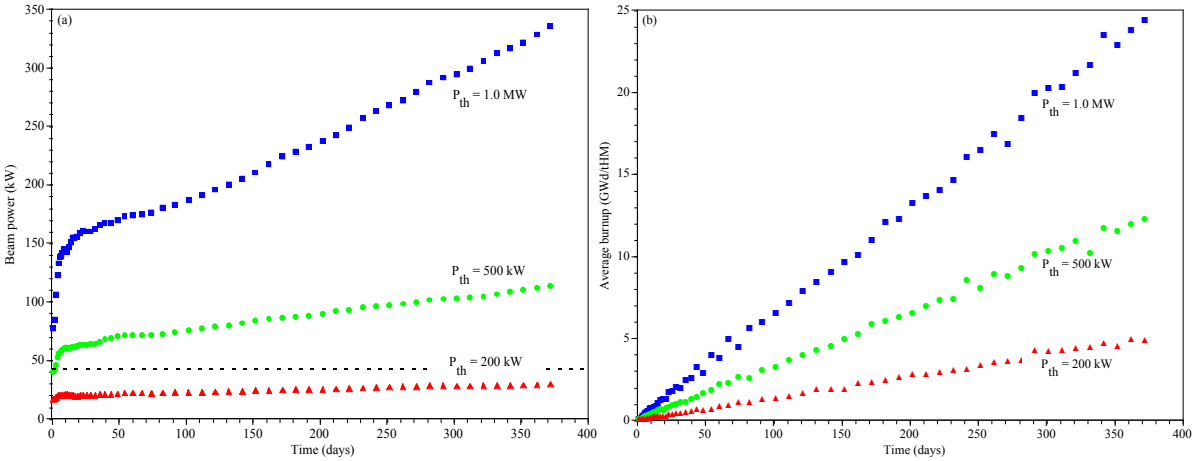

Figure 5.13. Evolution of the beam power (a) and fuel burn-up (b) for FC1 in TRADE.

These results show that the desired subcriticality levels and power distributions can be achieved. In particular, TRADE may allow a significant range of subcriticality levels to be investigated, from $k_{src} \approx 0.90$ (source dominated regime) to criticality (core feedback dominated regime) for an extended burn-up cycle. For a standard core output power of 200 kW, the corresponding accelerator current, i.e. 90 μA for FC1, produces power depositions in the target that can be removed. The final list of experiments to be performed in TRADE, which is still to be defined, includes a whole range of dynamic and reactivity measurements. However, the extended burn-up, the different neutron energy spectra in the core and the presence of an intense spallation source may allow experiments specifically related to HLW transmutation.

5.3 Transmutation Studies

As mentioned earlier, TRADE is primarily an experiment to validate the coupling of the main elements of an ADS, without dealing with the transmutation aspects. However, it could also be used to investigate the transmutation potential of a thermal ADS, by means of dedicated fuel pins loaded with different samples of LLFFs and TRUs. These experiments may be possible due to the large amount of fissile material present in the fuel (20% ^{235}U in the uranium), allowing extended burn-ups in the central part of the core of ~30% per MW_{th}·yr. Even though it may not be possible to reach such burn-up levels due to the limitations in power deposition in the target (see Section 5.1.4), the ~6% burn-up level attainable at 200 kW is sufficient to produce results which could be chemically analysed. Moreover, the stability under irradiation (e.g. helium production, swelling etc.) of matrices specific for transmutation could also be studied.

In order to analyse the viability of these experiments and to identify the key parameters in the transmutation process, the most radiotoxic non-fissile isotopes present in the HLW were placed in the simulated TRADE core. By changing the conditions to which these isotopes were subject (i.e. position in the core, transmutation matrix, neutron spectrum), the feasibility of transmutation of these isotopes and the matrices was assessed.

5.3.1 Sensitivity of Transmutation to the Position in the Core

As a first stage, several samples of the isotopes to analyse were placed in the central part of either a fuel pin or a graphite rod, in different positions in the core, in order to analyse the sensitivity of transmutation to the position in the core (and thus, to the variations in the neutron spectrum). The volume of these cylindrical samples was 65 cm^3 (r = 1.815 cm, h = 3.176 cm), a sixth of the volume of the fuel, and the number of atoms of the analysed isotope was kept constant (~2.336×10^{23} atoms/cm^3) in order to analyse the transmutation potential of the isotopes, independently of abundance. The calculations were performed simulating 5×10^6 protons in all the cases (~2×10^7 transported neutrons) in order to obtain sufficient statistical relevance and comparable results. The FC3 set-up was chosen ($k_{src} \approx 0.90$) so as also to study the effect of the spallation source on the transmutation potential.

The number of captures in several LLFFs for different positions in the core is presented in Figure 5.12(a). The value of the neutron flux is clearly vital to the transmutation rate since the number of captures decreases drastically with decreasing flux for most of the isotopes. On the other hand, ^{90}Sr, ^{126}Sn, ^{137}Cs and, to some extent, ^{93}Zr present rather low capture rates and seem unaffected by the flux change, showing the difficulties for transmuting these elements

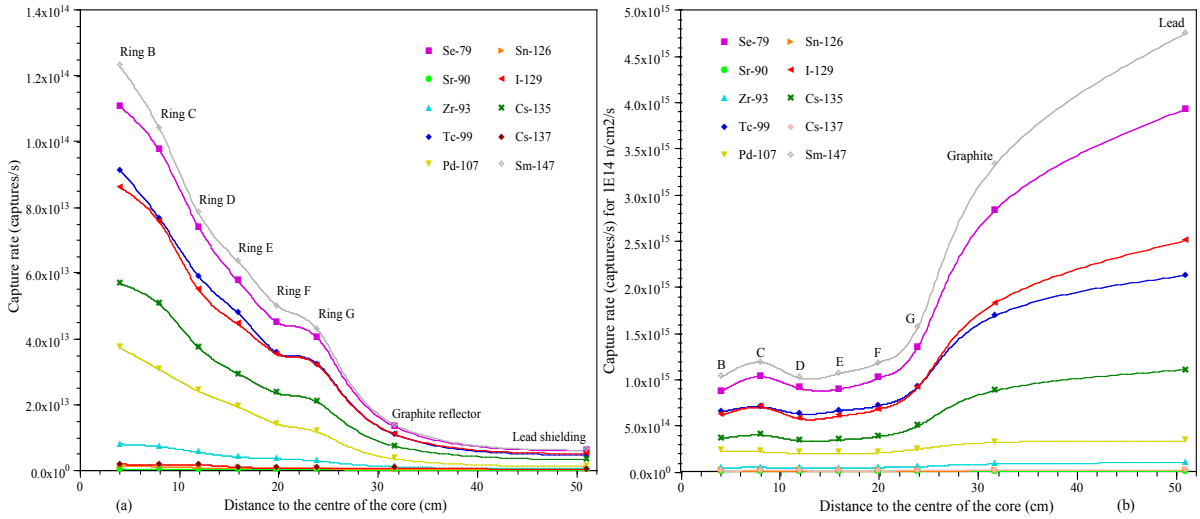

Figure 5.14. Capture rate vs. position in TRADE for several LLFFs (a) and rate normalised to 10^{14} n/cm^2/s (b).

For the isotopes that seem affected by the change in the integral value of the flux, there is a noticeable change in slope from rings F to G, clearly seen in Figure 5.12(b) by normalising to

a common neutron flux. This change in slope, ~5 larger capture rate for some isotopes between the fuel region and the lead shield, is related to the neutron energy spectra in the regions, and it is particularly important for ^{99}Tc and ^{129}I, which are the most radiotoxic isotopes of the LLFFs, and for ^{147}Sm and ^{79}Se. As mentioned before, the elimination of ^{93}Zr, ^{107}Pd and ^{135}Cs may present some difficulties due to the low transmutation rates and the presence of stable isotopes of these elements in the waste that would be activated.

Even though this system is not designed to maximise the transmutation efficiency, the half-lives of the isotopes in the reactor may give an idea of the reactor dwell time to transmute the given isotopes. These transmutation half-lives are normalised to an average flux of ~10^{14} n/cm/s (typical of the LWR) in order to compare the effects of the different spectra. As mentioned before, only ^{79}Se, ^{99}Tc, ^{129}I, ^{147}Sm and perhaps ^{135}Cs present reasonable transmutation half-lives, as shown in Table 5.4. For example, the transmutation half-life for ^{99}Tc ranges from 51 years (ring B) to 25 years (lead shielding). On the other hand, isotopes such as ^{90}Sr, ^{126}Sn and ^{137}Cs display unreasonable dwell times (thousands of years), advising against this method of transmutation unless more accurate and radically different capture cross-section data is measured.

Table 5.4. Transmutation half-lives for LLFFs in different positions in TRADE for 10^{14} n/cm^2/s.

Isotope		Ring B	Ring C	Ring E	Ring F	Ring G	Graphite	Lead
Decay half-life (yr)		Transmutation half-life (yr) for 10^{14} n/cm^2/s						
^{79}Se	1.1×10^{6} yr	38 yr	32 yr	37 yr	33 yr	25 yr	12 yr	8 yr
^{90}Sr	29 yr	31125 yr	23472 yr	23037 yr	19534 yr	21032 yr	14914 yr	17821 yr
^{93}Zr	1.5×10^{6} yr	744 yr	710 yr	859 yr	714 yr	617 yr	387 yr	340 yr
^{99}Tc	2.1×10^{5} yr	51 yr	47 yr	50 yr	46 yr	36 yr	19 yr	15 yr
^{107}Pd	6.5×10^{6} yr	147 yr	151 yr	162 yr	161 yr	135 yr	103 yr	99 yr
^{126}Sn	1×10^{5} yr	5632 yr	5188 yr	6238 yr	6025 yr	4135 yr	3104 yr	2463 yr
^{129}I	1.6×10^{7} yr	54 yr	47 yr	55 yr	49 yr	36 yr	18 yr	13 yr
^{135}Cs	2.3×10^{6} yr	91 yr	83 yr	96 yr	86 yr	67 yr	37 yr	30 yr
^{137}Cs	30 yr	3411 yr	3274 yr	3890 yr	3712 yr	3072 yr	3072 yr	1538 yr
^{147}Sm	1×10^{11} yr	32 yr	28 yr	31 yr	28 yr	21 yr	10 yr	7 yr

These results show the potential decrease in radiotoxicity achievable by inserting LLFFs targets in a 10^{14} n/cm^2/s reactor core under different neutron spectra. Notice the large half-life reduction for major isotopes in the HLW, such as ^{99}Tc ($\tau_{1/2}$ going from 2.1×10^{5} yr to 15 yr) and ^{129}I ($\tau_{1/2}$ reducing from 1.6×10^{7} yr to 13 yr). These reductions justify the efforts towards developing efficient transmutation strategies for LLFFs, since the feasibility is well-proven. Moreover, these results may be greatly improved by the definition of transmutation matrices for these isotopes which would enhance capture inside the resonances, thus making use of the ARC effect (see Chapter 3).

In order to illustrate the process undergone by the LLFFs samples in the core, Figure 5.15(a) shows the normalised neutron flux in the ^{99}Tc sample for three positions in the core (in B, G

and in the lead shielding), superimposed on the capture cross-section for this isotope. The deeper depletion of the neutron flux in the 5.6 keV (~5400 b) and 21 keV (~1600 b) resonances for the sample placed in lead can be clearly seen. This fact, together with greater importance of the thermal flux in this position, explains the higher transmutation efficiency for this element (as well as for ^{147}Sm, ^{79}Se, ^{129}I and ^{135}Cs) in the more epithermal and thermal fluxes. This hypothesis is corroborated by Figure 5.15(b), where the normalised capture rate for these core regions are shown. The largest number of captures occurs due to the thermal peak, especially for the samples in ring G and in the lead shielding followed by the resonance region, where the flux is heavily depleted (since there is no fuel to produce neutrons in this energy range). Therefore, the dilution of the LLFFs in the core or the design of transmutation matrices in order to achieve an isolethargic flux in the resonance region, and could be placed in the periphery of the core, seem of great importance in order to maximise the transmutation rates.

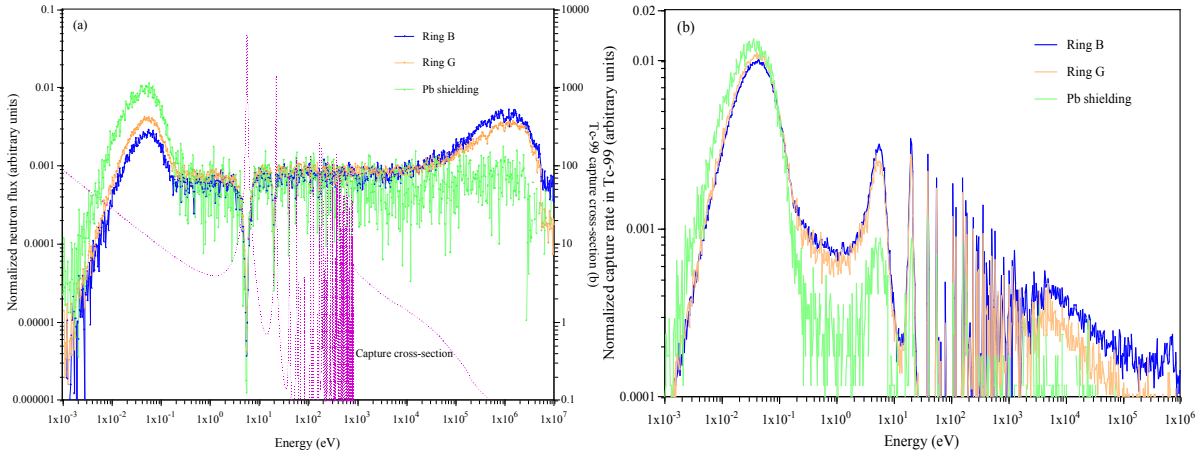

Figure 5.15. Normalised neutron flux (a) and capture rate (b) in the ^{99}Tc sample for different positions in TRADE.

For TRUs, the same procedure was used to analyse transmutation potential. Samples of the main TRUs fissionable isotopes, thus excluding the fissile isotopes, were placed in different positions and the absorption half-lives, normalised to a neutron flux of 10^{14} n/cm^2/s, were calculated (Figure 5.16(a)). Since the thermal capture cross-section is orders of magnitude larger than the threshold fission cross-section for these isotopes and the system is dominated by the thermal flux, the average reactor dwell time for these isotopes decreases with distance to the centre of the core.

Nevertheless, Figure 5.16(b) shows that almost all the absorption reactions result in the emission of a photon, rather than fission, thus continuing the production of TRUs. In fact, the fission-to-absorption ratio gives a better indication of the transmutation efficiency for these elements. Figure 5.16(b) shows these values for ^{237}Np, ^{238}Pu, ^{240}Pu, ^{242}Pu, ^{241}Am, ^{243}Am and ^{244}Cm in different positions in the core. The values are remarkably low for all the isotopes,

with a maximum ratio of 0.26 for ^{238}Pu in ring B. This isotope, together with ^{244}Cm, gives ratios twice the size of the rest, due to the smaller differences between capture and fission cross-sections at low energies.

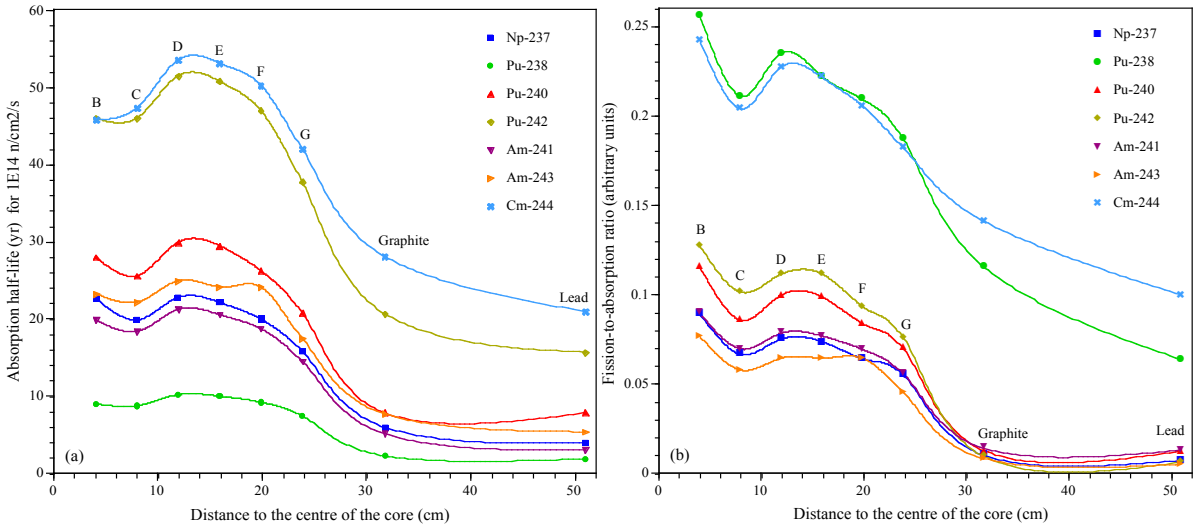

Figure 5.16. Absorption half-life (a) and fission-to-absorption ratio (b) in different positions of the core of TRADE for several TRUs.

All these isotopes follow basically the same trend, with larger fission-to-absorption ratio close to the target, due to the presence of high-energy spallation neutrons, and a negligible ratio in the periphery of the core, where the fission high-energy hump disappears and the thermal peak gains importance (Figure 5.10). The larger significance of the thermal region, in which capture is favoured over fission, produces the decrease in the ratio for ring C compared to rings D and E. In the case of $^{241, 243}$Am and ^{237}Np, the fission ratio falls below 10% of all the absorption reactions in any position of the core.

The shorter absorption times for most of these TRUs under a very thermal flux (in the graphite reflector and lead shielding, below 10 yr) combined with their very low fission-to-absorption ratio implies an increase in the toxicity of the waste, since capture is enhanced under these circumstances and so is the production of MAs, also depleting the neutron population (thus requiring a higher enrichment to maintain the reaction). On the other hand, in the regions where the fission-to-absorption ratio is slightly larger, the absorption half-lives are significant for most of these isotopes (compared to the ~1.7 yr for ^{235}U), hindering the effective elimination these isotopes.

Figure 5.17 illustrates the differences in the neutron flux and reaction rates for different positions in the core for ^{241}Am (and, in general, for the studied TRUs). The neutron flux in the sample was normalised and plotted against the ^{241}Am fission and capture cross-sections (Figure 5.17(a)), showing the decrease of the thermal flux (compared to Figure 5.10). This change in the flux is due to the large ^{241}Am thermal capture cross-section (~1000 b) and

explains the major role of capture in the reactions occurring in the ^{241}Am sample. The shift of the importance in the flux between the high-energy regions and the epithermal and thermal regions shown in Figure 5.17(a), explains the drop in the fission-to-absorption ratio for the more distant positions (Figure 5.16(b)). Since the neutron spectrum becomes softer with distance from the spallation source, this ratio decreases accordingly, as well as the energy range where the absorption reactions occur. From Figure 5.16(b) it is clear that in order to maximise the number of fissions in ^{241}Am, and thus the transmutation efficiency of the device, a harder spectrum is required. This is the case for all non-fissile actinides, and the reason why fast systems are proposed for TRUs elimination.

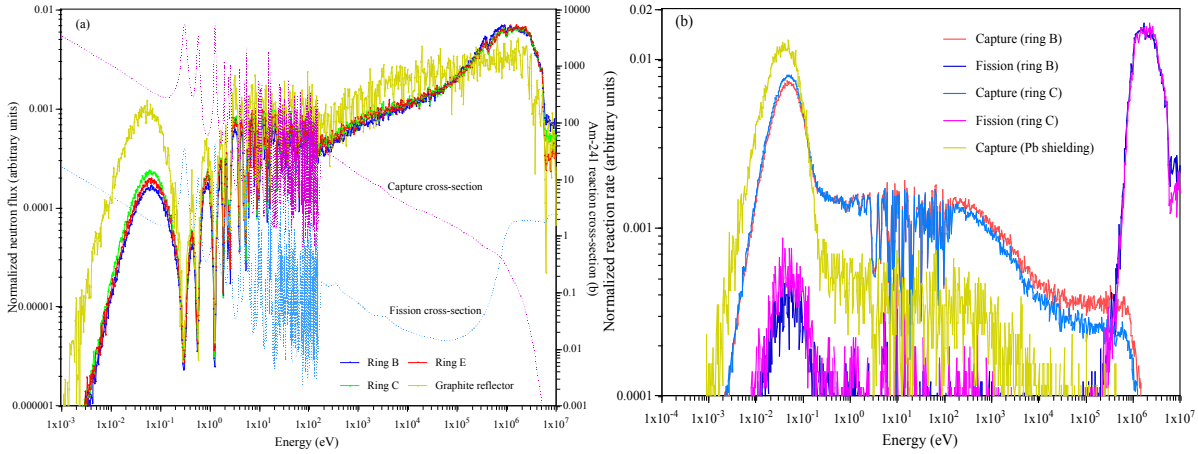

Figure 5.17. Normalised neutron flux (a) and reaction rate (b) in the ^{241}Am sample for different positions in TRADE.

5.3.2 Effect of the Moderator

The neutron spectrum is a key factor in making possible the transmutation of HLW, therefore study of the effect of the moderator in transmutation is a necessary step to assess the feasibility of nuclear waste transmutation and determine the optimal conditions for this process.

A preliminary analysis was performed changing the nature of the coolant in the core in order to evaluate its effect on the system. The effect of water was compared to the most common coolants and moderators in nuclear reactors, i.e. graphite, sodium, lead and helium. Although the whole nature of the coolant was changed in every case, the neutron energy spectra in the fuel in ring C display a striking similarity (Figure 5.18(a)).

These results are related to the large quantity of hydrogen in the fuel, which softens the neutron spectrum independently of the nature of the moderator. Even though the high energy neutron peak is present in the fuel in all cases, the presence of an equally large thermal peak, in particular when using water or graphite as moderator, dominates the reactions occurring in

this region (and, in fact, in the rest of the core, except for the spallation target) due to the greater reaction cross-sections for this energy range. This effect is enhanced by the small fuel pitch (~2.35 mm), reducing the role of the moderator in the characterisation of the neutron energy spectrum.

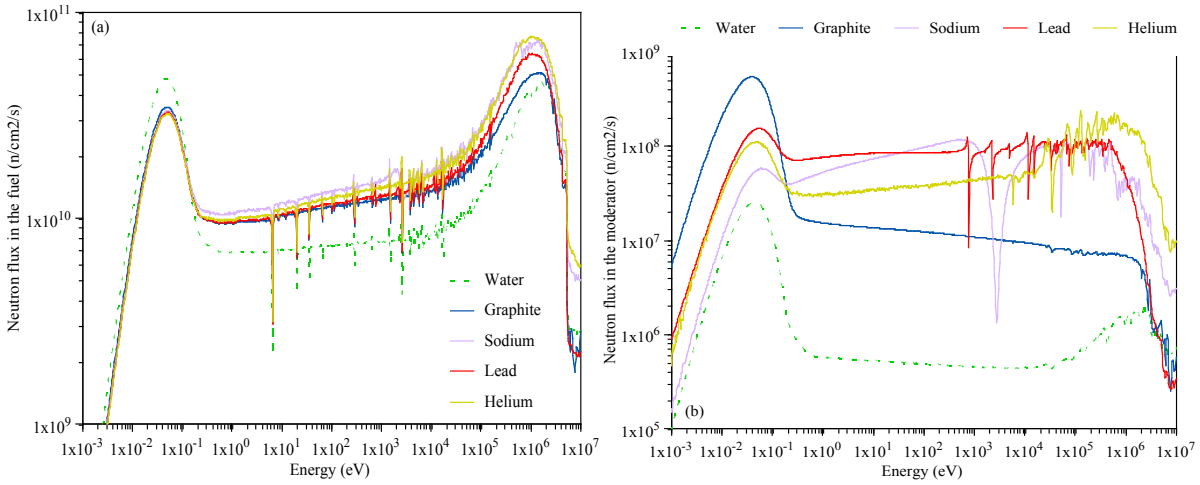

Figure 5.18. Neutron energy spectra in the fuel (a) and in the moderator (b) for different moderating materials.

The spectrum in the moderator is obviously affected by the neutron thermalisation in the fuel, presenting a highly isolethargic flux in lead or sodium, except at ~3 keV, where ^{23}Na presents an enormous resonance (the total cross-section increasing from 2 b to 400 b). The spectrum in the helium coolant is similar to that in the fuel, except for a decrease in the high-energy peak (no fissile material). For graphite and water, the thermal Maxwell distribution clearly dominates the neutron spectra. The neutron flux in graphite, and in particular the thermal one, is one order of magnitude larger than in water due to the small total cross-section of ^{12}C compared to ^{1}H and the larger neutron diffusion length in graphite.

Hence, in order to study the effect of the moderator on the transmutation of HLW (and to suggest possible experimental settings for TRADE), the moderator in rings B, C and D was replaced by the aforementioned elements, and a uranium-zirconium metallic fuel was used in rings C and D. The substitution of this inner buffer material produces a much more characteristic spectrum for every material, permitting an investigation of the HLW transmutation sensitivity to the moderator.

The comparison of the neutron spectra in the fuel and moderator between the different cases is illustrated by Figure 5.19(a) and (b), respectively. In the case of the fuel, the high-energy peak is clearly the most relevant energy region of the spectrum. The contribution of the thermal part to the energy spectrum is approximately two orders of magnitude smaller, except in the case of water, where the thermal peak can still be perceived.

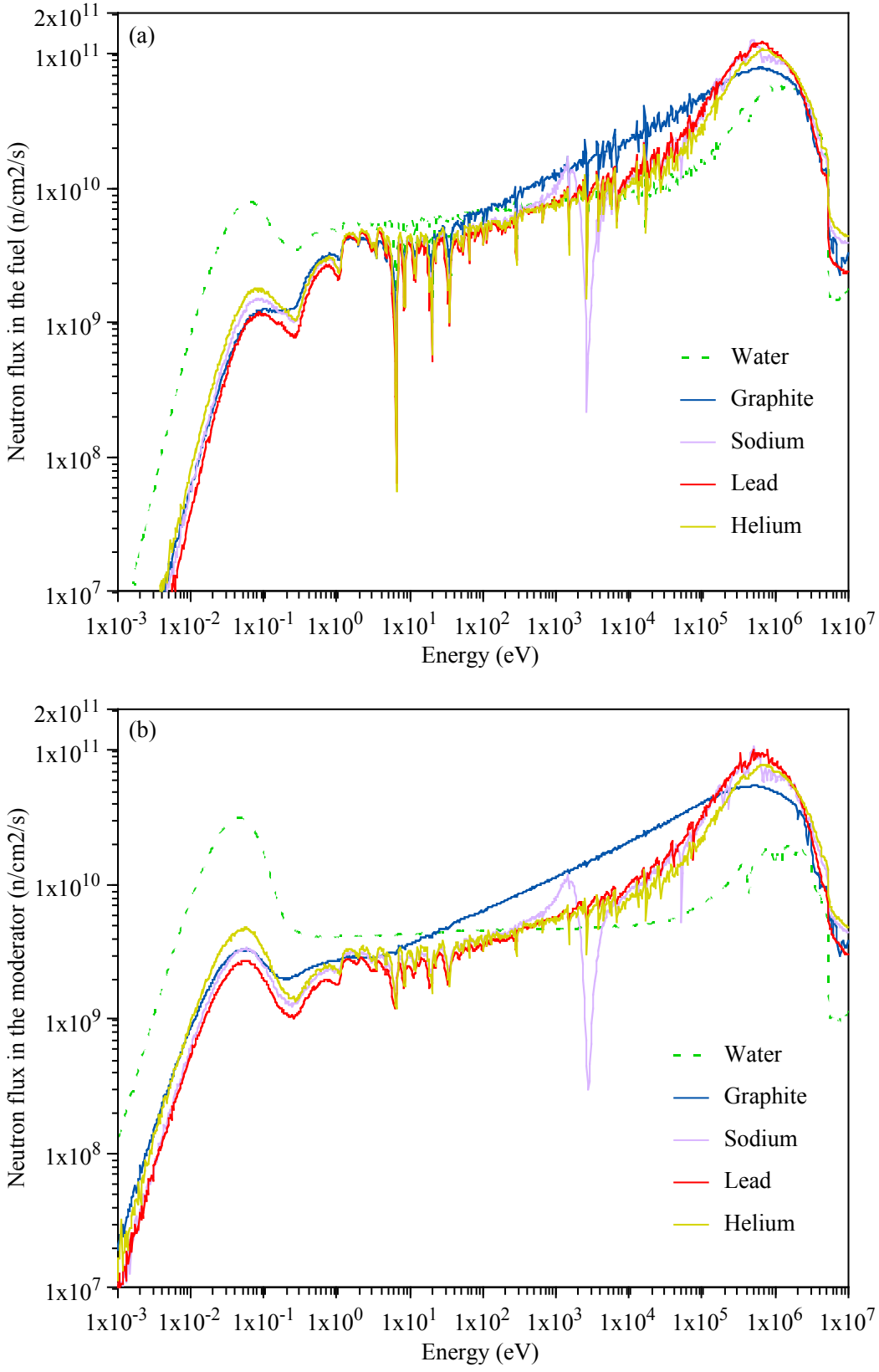

Figure 5.19. Neutron energy spectra in the fuel (a) and inner buffer (b), for the UZr fuel and different buffers.

The effect of uranium resonances on the neutron flux can be clearly observed in the fuel, e.g. at 6 eV for ^{238}U and at 0.2 and 1 eV for ^{235}U, as a reduction of the neutron flux in those

regions. In the case of sodium, the aforementioned elastic scattering resonance at ~3 keV produces a deep depletion of the flux at this energy, since the neutrons at that energy are rapidly scattered to a lower energy (hence the fill-up region right after the resonance).

The use of graphite as a moderator produces a high fast and epithermal spectrum, decreasing with energy, as can be clearly observed in Figure 5.19(b). This effect is due to the constant (~4 b) ^{12}C total cross-section between 0.01 eV and 100 keV, which produces a neutron slowing down in small lethargy steps. This shift in the spectrum from the high-energy peak to the fast and epithermal plateau is less pronounced in the case of sodium, lead and helium due to their greater diffusion lengths. In fact, since helium is completely transparent to neutrons, there is a thermal contribution to the flux coming from the water around the reactor and around the outer fuel rings (E, F and G).

5.3.2.1 LLFFs Sensitivity

The effect of these neutron energy spectra on the transmutation of ^{99}Tc and ^{129}I is presented in Figure 5.20. The capture rate for both isotopes when using water as a moderator is generally ~3 times larger than in the other cases. Consequently, the isotope absorption half-life is greatly reduced for this energy spectrum. Therefore, in order to efficiently transmute these isotopes, and LLFFs in general, the neutron energy should be greatly moderated before reaching the isotopes to transmute, by using a very efficient moderator, such as water, in compact systems or by using appropriate transmutation matrices to contain the isotopes and optimise the neutron energy spectrum.

Moreover, the positive effect of hydrogen from the UZrH fuel on the transmutation rates is obvious by comparing Figure 5.14(a) and Figure 5.20(a). The capture rates in ring C in the former are almost twice those in the latter. This fact translates into a larger half-life in the core before transmutation occurs (Figure 5.20(b)).

Hence, there is a clear need of a high thermal and epithermal (from 1-1000 eV) flux in order to transmute these isotopes. In this type of compact, small-pitched core, these conditions may be mainly achieved by using a hydrogen-rich environment. In addition, the effect of dilution of the isotopes in specific transmutation matrices should be studied in order to maximise the efficiency of the process.

Nevertheless, the possibility of transmutation of LLFFs in high-flux reactors moderated by an element showing a large diffusion length (addressed in Chapter 6) should not be neglected. In this scheme, the neutron energy flux may be tuned more precisely than in thermal systems to enhance the transmutation process.

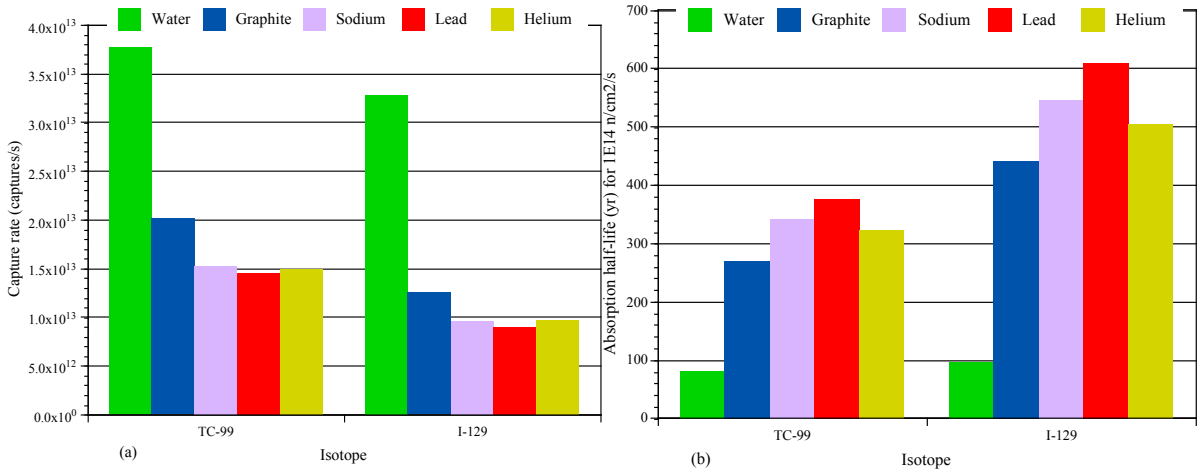

Figure 5.20. Capture rate (a) and transmutation half-life for a flux of 10^{14} n/cm^2/s (b) for ^{99}Tc and ^{129}I.

5.3.2.2 TRUs Sensitivity

In the case of TRUs, the effect of the neutron energy spectrum imprinted by the moderator is clear for all the isotopes analysed. The fission rates when lead or helium is the moderator are 50-100% higher compared to the case of water (Figure 5.21(a)). The fission-to-absorption ratios are also increased by the replacement of the water in the inner rings by a less moderating material, as illustrated by Figure 5.21(b). In fact, these ratios increase significantly for all the non-fissile isotopes, and in particular for ^{238}Pu, ^{240}Pu and ^{242}Pu, which are particularly important in transmutation schemes for different reasons.

Although ^{238}Pu one of the least abundant plutonium isotopes in HLW, extended fuel burn-ups and use of MOX fuel would imply the accumulation of this isotope after fuel reprocessing. Additionally, in MAs elimination schemes, it would also be produced through the α-decay of ^{242}Cm ($\tau_{1/2} \approx 163$ d; originated by neutron capture in ^{241}Am becoming ^{242}Am, which in turn may undergo a β^- decay, $\tau_{1/2} \approx 16$ h). Finally, the use of plutonium-rich fuels in fast systems would enhance the (n, xn) reactions in plutonium, in particular (n, 2n) in ^{239}Pu, consequently increasing the ^{238}Pu stockpile. This isotope may then be responsible for a large part of the radiotoxicity of the spent fuel, since it presents a medium half-life ($\tau_{1/2} \approx 88$ yr) and decays emitting a highly ionising 5.5 MeV α-particle, thus producing a large quantity of decay heat in the first one hundred years after discharge. The case of ^{244}Cm is somewhat similar, since it produces a large amount of decay heat and should be eliminated in an efficient way in order to reduce the risks while handling the spent fuel. ^{240}Pu and particularly ^{242}Pu are gates to the americium isotopes (^{241}Am and ^{243}Am respectively); therefore, neutron capture enhancement in the former would entail an increase in the production of the latter.

For ^{237}Np, ^{241}Am and ^{243}Am, the number of fissions per absorbed neutron is relatively small for these case studies. Nevertheless, lead produces fission-to-capture ratios 2-3 times higher than water and reduces the risk of further capture – decay chains. These rates may be

sufficient to continuously reduce the MAs stockpile in a uranium-free HLW transmutation scenario, since the equilibrium concentration of these species in the thorium cycle is very low, as discussed in Chapter 3.

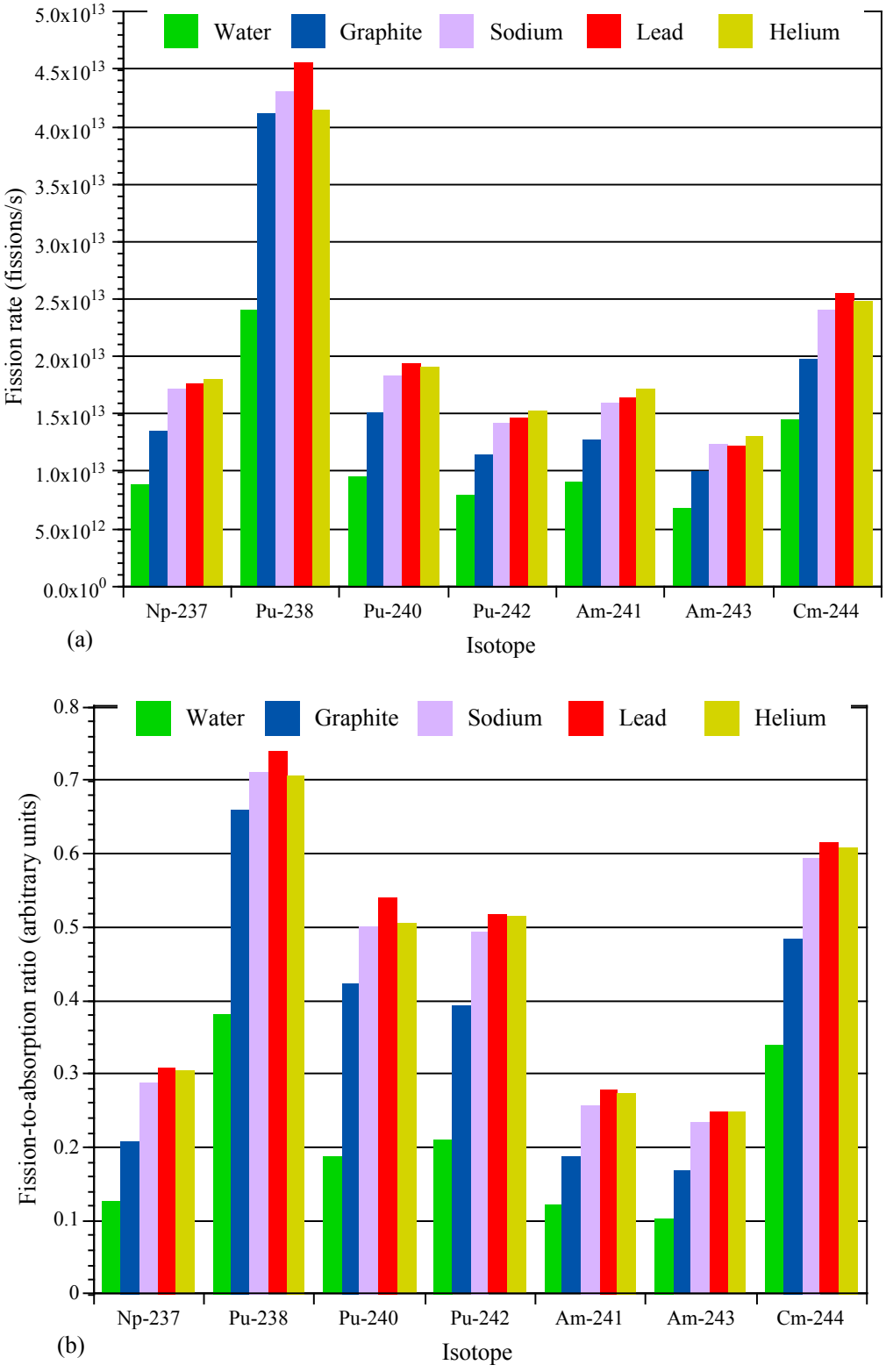

Figure 5.21. Fission rates (a) and fission-to-absorption ratios (b) for non-fissile TRUs and different moderators.

These results, combined with the large differences in the fission-to-absorption ratios between water and the other moderators, show the advantages of large-diffusion length high-A materials as coolant and moderator in order to efficiently transmute TRUs, since fission is enhanced at high neutron energies.

Nevertheless, double capture transmutation strategies for ^{237}Np and ^{241}Am have been proposed [100]. These strategies should be studied and compared against the fast-fission approach.

5.3.3 LLFFs Transmutation Sensitivity of a Dedicated Matrix

The use of dedicated matrices in order to transmute LLFFs in a thermal spectrum, such as the one produced in LWRs, has been repeatedly proposed as an economical approach to eliminate this type of waste [9 & 101]. In particular, the use of a ZrH_2 matrix loaded with different quantities of ^{99}Tc and ^{129}I was studied in [102]. Here, the transmutation targets proposed in the TARC experiment, i.e. $KTcO_4$, PbBi(Tc) and PbI_2, have been analysed and compared with the ZrH_2 mixtures, since the effect of the matrices and the isotope dilution are key factors in the development of successful LLFFs transmutation schemes.

The transmutation efficiency of these matrices is summarised in Table 5.5. The results previously presented for a sample of the pure isotope placed in ring C are also included for purposes of comparison. The mass of the isotope contained in the sample is obviously a critical factor for the absolute transmutation rates. Nevertheless, the efficiency of the capture process clearly decreases with the concentration of the LLFFs. The isotope transmutation half-life decreases strongly with dilution for ^{99}Tc and ^{129}I. For the former, it goes from 47 yr for a metallic target to 23 yr for 3% ^{99}Tc diluted in lead-bismuth. The case of ^{129}I is rather similar, showing that dilution in the matrix is necessary in order to achieve transmutation rates that may substantially reduce the stockpile of these elements.

Table 5.5. Transmutation rates for ^{99}Tc and ^{129}I in a thermal spectrum using different matrices.

	Transmutation Matrix	Isotope mass (g)	Capture rate (captures/s)	Capture rate per gram of isotope (captures/s/g)	Transmutation half-life (yr) for 10^{14} n/cm^2/s
^{99}Tc	Metallic ^{99}Tc	262.0 g	7.7×10^{13}	2.9×10^{11}	47 yr
	60% ZrH_2 – 40% ^{99}Tc	310.0 g	9.5×10^{13}	3.1×10^{11}	43 yr
	$KTcO_4$	62.7 g	3.7×10^{13}	5.9×10^{11}	31 yr
	97% PbBi – 3% Tc	20.7 g	2.0×10^{13}	9.7×10^{11}	23 yr
^{129}I	Pure ^{129}I	341.0 g	7.6×10^{13}	2.2×10^{11}	47 yr
	40% ZrH_2 – 60% CaI_2	85.9 g	4.2×10^{13}	4.9×10^{11}	27 yr
	PbI_2	35.2 g	2.2×10^{13}	6.3×10^{11}	24 yr

This dilution actually enhances the efficiency of the TARC process, avoiding the depletion of the neutron flux in the thermal region and especially in the resonance region. In this sense, the

matrices proposed in [101] as a heterogeneous transmutation scheme (dedicated rods placed in the core) are rather efficient compared to the use of the pure isotope. On the other hand, since the LLFFs transmutation efficiencies not only affect the transmutation rates by which these isotopes are eliminated, but also importantly their concentration equilibrium, an efficient transmutation method to be investigated may be the dilution of the LLFFs in the core reflector or the homogeneous dilution of these isotopes in the fuel (although this last method would produce lower transmutation rates due to the harder spectrum in the fuel).

Analysis of the isotopic evolution of the samples shows a slight reduction of the concentrations of ^{99}Tc and ^{129}I, and the production of the daughter products ^{100}Ru and ^{130}Xe (Figure 5.22(a) and (b)). Even though the system is not optimised to transmute HLW, the transmutation rates seem rather small, with large differences in the equilibrium concentrations between the LLFFs and their stable transmutation products.

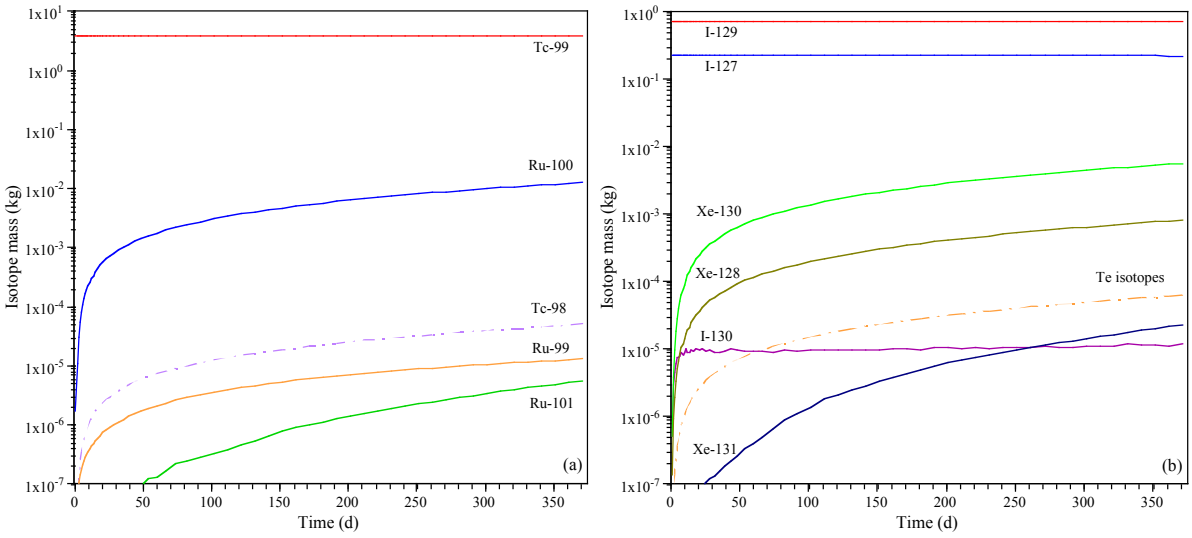

Figure 5.22. Burn-up evolution for the ^{99}Tc (a) and ^{129}I (b) – ZrH_2 transmutation matrices in TRADE.

The case of ^{99}Tc shows a better transmutation rate than ^{129}I, with a concentration of ^{100}Ru increasing faster than that of ^{130}Xe. Additionally, ^{100}Ru is a radiation-stable species, with a low capture cross-section ($\sigma_{th} \approx 8$ b, with only one known resonance), thus the concentration of daughter products ($^{101,\ 102}$Ru) from this isotope is very low, and these isotopes are also stable. In fact, the transmutation of ^{99}Tc may be economically profitable, as suggested in [103], given that ruthenium is a very rare and expensive element and its production in large quantities in nuclear reactors seems feasible. For ^{129}I, besides a lower production of its transmutation daughter product, ^{130}Xe, the presence of ^{127}I in the HLW iodine (75% ^{129}I, 25% ^{127}I) generates ^{128}Xe. The fact that these are gaseous by-products complicates the process, since dissolution of iodine in the fuel would deteriorate the mechanical performance for medium and long burn-ups.

Hence, a high concentration of stable daughter isotopes seems to be an essential prerequisite for a successful transmutation scheme. Transmutation rates of the order of tens of kilograms per year are required to reduce the stockpile of LLFFs, as presented in Chapter 2. In this sense, a combination of LLFFs dilution in a non-capturing matrix, high neutron flux with important thermal and epithermal spectra, extended burn-up cycles and positioning of the targets at the periphery of the core (to avoid poisoning the reactor and increase the neutron economy) appears to be an optimal method to transmute LLFFs. In the case of ^{129}I, the use of some type of powder matrix and the presence of an upper plenum may be necessary in order to evacuate the gas released (i.e. xenon) and avoid further neutron capture.

5.3.4 MAs Multiple Absorption Transmutation Scheme

The possibility of eliminating the most abundant MAs in HLW (i.e. ^{237}Np and ^{241}Am) by inserting a suitable sample in a thermal spectrum has been proposed in [100]. This method would take advantage of these isotopes' large capture cross-section at thermal energies ($\sigma_{th} \approx$ 200 b and 800 b, respectively) and the very high fission cross-section ($\sigma_{th} \approx$ 3000 b) of the short-lived daughter isotopes ($\tau_{1/2} \approx$ 2.1 d for ^{238}Np and $\tau_{1/2} \approx$ 16 h for ^{242}Am) and their further β^--decay.

In the case of ^{237}Np, this implies the production of ^{238}Np, rapidly decaying into ^{238}Pu, which, through a second capture in a thermal spectrum, would produce the fissile ^{239}Pu. For ^{241}Am, the aforementioned neutron capture and β^--decay into ^{242}Cm may be followed by an α-decay ($\tau_{1/2} \approx$ 162 d into ^{238}Pu) or by a neutron capture ($\sigma_{th} \approx$ 200 b) to produce the readily fissile ^{243}Cm.

These multiple absorption schemes, although quite indirect and neutron expensive methods for transmuting these species, should still be evaluated as possible alternatives to eliminate these isotopes. Figure 5.23(a) and (b) illustrate the isotope evolution applying this method, for ^{237}Np and ^{241}Am, respectively, showing a reduction of ~6% in these isotopes during a one year burn-up cycle at 1 MW. On the other hand, the concentration of ^{238}Pu, and hence ^{239}Pu, for both cases is rather different. In fact, this transmutation approach seems more feasible for ^{237}Np given that the concentration of the fissile ^{239}Pu is approximately one order of magnitude higher than in the case of ^{241}Am.

Moreover, Figure 5.23(a) shows small concentrations of 'parasitic' TRUs, such as ^{234}U, originating from the α-decay of ^{238}Pu ($\tau_{1/2} \approx$ 88 yr), and the inevitable ^{240}Pu, which, in turn, enhances the production of more MAs. Alternatively, enhancing neutron capture in americium seems to complicate the elimination of the HLW, diversifying the nature of the elements involved (Figure 5.23(b)). The production of ^{242*}Am (the first isomeric state; thermal branching ratio ~20%) is favourable, since this is a very fissile isotope ($^{fiss}\sigma_{th} \approx$ 10,000 b). In

contrast, the short-lived ^{242}Am (ground state) rapidly decays either by β^- emission or by electron-capture. In the first case ^{242}Cm is produced, which rapidly reaches its equilibrium concentration due to its short half-life, and consequently produces an equal amount of ^{238}Pu. The electron-capture process in ^{242}Am, responsible for a noticeable generation of ^{242}Pu, combined with neutron capture in ^{242*}Am ($^{capt}\sigma_{th} \approx$ 2,000 b), produces more ^{243}Am. This isotope is the gate to ^{244}Cm, whose medium half-life ($\tau_{1/2} \approx$ 18 yr) and energetic α-decay (5.8 MeV) gives it a major role in the high radiotoxicity of this fuel.

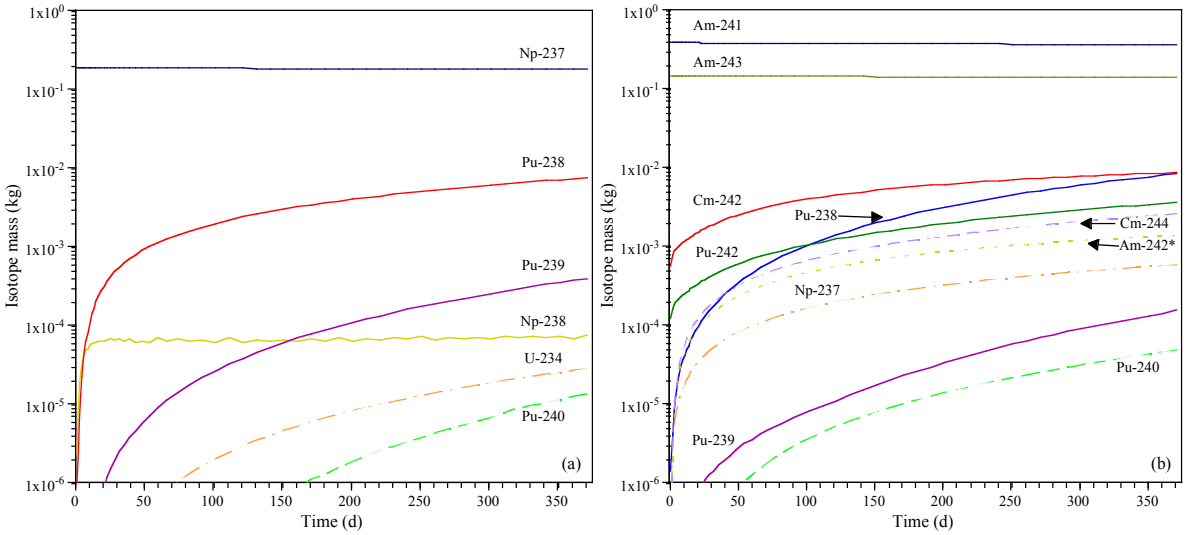

Figure 5.23. Burn-up evolution for the multiple absorption ^{237}Np (a) and ^{241}Am (b) transmutation schemes in TRADE.

On the other hand, the use these special matrices to enhance the thermal flux, producing neutron capture and then produce fission in the daughter products before their decay, namely in ^{238}Np ($\tau_{1/2} \approx$ 2.1 d) and ^{242}Am ($\tau_{1/2} \approx$ 16 h), would require very large thermal fluxes, given that for a flux of 10^{15} n/cm^2/s even their fission half-lives (3.8 d and 2.7 d, respectively) are significantly longer than their decay half-lives.

Therefore, the application of this transmutation scheme for ^{237}Np and ^{241}Am seems feasible although slow (large differences between equilibrium concentrations) and neutronically cumbersome (the need for several neutrons in order to obtain a fission). It would also increase the activity of the waste and hinder its further handling due to the production of large quantities of ^{238}Pu and, in the case of ^{241}Am, the hazardous ^{244}Cm.

5.4 Conclusions

The experimental demonstration of the ADS concept requires an intermediate step prior to the development of an industrial prototype of the device. TRADE will help the understanding of several features specific to these systems, such as the behaviour of the spallation neutrons inside a multiplicative core at real power and the transition between a source-dominated and a feedback-dominated regime. The preliminary analysis of TRADE, shows that it could well fulfil these requirements, given the compactness, versatility and intrinsic safety of the 1 MW TRIGA reactor. The accurate design of the solid tantalum spallation target and the radioprotection aspects of the facility (in particular the beam losses along the bending magnets) are major issues in the design of the experiment that are being carefully addressed.

The neutronic parameters of the experiment have been well characterised for different subcritical configuration set-ups, in order to understand the nuclear processes undergone in the core. As mentioned before, the research to be carried out in TRADE is significant to the development of a high power fast-ADS. In particular, the dynamic experiments may be extendable to this latter system except for a shift towards lower frequencies. This is explained by the slowing effect of the cooling water, particularly the buffer region around the spallation target.

Therefore, essential experiments, such as the behaviour of the system and the neutron distribution in the core after a beam failure will be studied in TRADE. The acceptable duration of these events will also be analysed at different subcritical levels, thus, with different response transfer functions. The lower response frequency will facilitate the measurements and helping to predict the dynamic behaviour of a fast ADS.

Additionally, studies have been performed in order to evaluate the transmutation potential of the system and to propose several set-ups to perform multiple experiments directly related to the transmutation of HLW.

These studies show the reduction of the half-lives for some important LLFFs, such as ^{79}Se, ^{99}Tc, ^{129}I, ^{147}Sm and perhaps ^{135}Cs, from decay half-lives of thousands of years to decades of transmutation half-lives. This is not the case for isotopes like ^{90}Sr, ^{126}Sn, ^{137}Cs and ^{93}Zr, which due to their small capture cross-section and the lack of clear resonances or poor knowledge of the ND related to these isotopes, present discouraging transmutation half-lives. Another important issue concerning the transmutation of LLFFs is the need for dilution. This is a major requirement for TARC, since it is based on the resonance capture, and the excess in concentration of the isotope to transmute would produce self-shielding effects.

For the non-fissile TRUs, it has been shown that softer neutron energy spectra decrease the fission-to-absorption ratio. The use of special matrices to enhance the thermal component in

the flux require very large fluxes (larger than 10^{15} n/cm^2/s) and if fission is not produced, the mass of actinides destroyed in the cycle is negligible (~7% of the initial mass, in TRADE). This results in an actinide mixture which is significantly more radiotoxic (mainly due to ^{238}Pu and ^{244}Cm) than the initial one.

These preliminary analyses show the need to study and design a long-burn-up, high-flux, fast neutron system in order to transmute HLW, in particular its most hazardous elements, i.e. the TRUs. This is the goal of the Chapter 6, where the safety aspects, neutronic characteristics and transmutation schemes are studied in the context of the Energy Amplifier Demonstration Facility (EADF).

Chapter 6

HLW Transmutation in Fast ADS

As presented in Chapter 3, in the early 1990s the international community began to consider the concept of ADS as a suitable alternative for the elimination of HLW. Several research programs were launched and led to the definition of several technological alternatives. Among these alternatives drawing international attention there was the Energy Amplifier (EA), a ~1.5 GW_{th} thorium-based lead-cooled ADS. This innovative inherently safe system was conceived by Prof. C. Rubbia and developed by his group (Emergency Energy Technologies) at CERN, where work is still ongoing in the context of the aforementioned European Roadmap towards the experimental demonstration of ADS [46].

The last stage of the Roadmap foresees the commissioning of a low-power (100-300 MW_{th}) experimental installation, considered a necessary step in order to demonstrate the industrial feasibility of ADS. In particular, this demonstration facility, referred to as an eXperimental ADS or XADS, would aim to successively demonstrate the following:

- The coupling of a high-power accelerator with a subcritical fast reactor.
- Qualification and operation of the innovative fuel.
- The efficiency of plutonium, MAs and LLFFs transmutation.

There are several prototypes for this demonstrator with different design characteristics. The fundamental difference between the two main candidates is the nature of the coolant. The prototype proposed by Framatome, PDS-XADS, uses helium as the primary coolant, whereas the demonstrator proposed by Ansaldo, Energy Amplifier Demonstration Facility (EADF, also known as LBE-XADS), is based on a lead-bismuth eutectic (LBE) coolant. Both present advantages and disadvantages, although in terms of safety (e.g. no separation between spallation target and coolant, and negative void coefficient) and transmutation efficiency (i.e.

possibility to benefit from a highly isolethargic flux) the lead-cooled alternative seems advisable.

Consequently, this chapter is dedicated to the neutronic characterisation of the LBE experimental facility (Energy Amplifier Demonstration Facility, EADF), and assessment of the transmutation potential of such a device for the reference fuel configuration. The burn-up evolution of the system is also analysed in detail since it plays a significant role in the assessment of this device as a future alternative for HLW elimination.

6.1 The Concept of the Energy Amplifier

The EA is the result of a 'cross-fertilisation' between the technology of modern particle accelerators and that of nuclear power, in particular the development of fast neutron breeder reactors and of fuel reprocessing. As previously explained, in an ADS the energy is produced as the result of nuclear cascades, rather than from a self-sustained chain reaction as in the conventional reactors. This is also the case for the EA, where all the nuclear processes in the core are subsidiary to the operation of the accelerator. Relativistic protons produced by a cyclotron or a LINAC initiate these nuclear cascades and the power produced is directly proportional to the intensity of the injected beam. The probability of a criticality accident is suppressed since the device operates far away from criticality at all times. The underlying physical principles of energy amplification and the transmutation possibilities of the device were demonstrated in the FEAT and TARC experiments performed at CERN, summarised in Chapter 3.

An EA module may consist of a 1500 MW_{th} unit coupled with a 1-1.5 GeV proton accelerator of 10-20 mA. A modular cyclotron was designed in order to fulfil this task, similar to the one currently operated in the Paul Scherrer Institute (PSI, Switzerland). In fact, an EA plant may consist of several ADS coupled with an extra accelerator to supply beam protons in the case of a beam failure in one of the other accelerators.

Another relevant feature of this design is the removal by natural convection of the generated heat inside the core, thus avoiding coolant pumps. As described in [1]: "The EA is a large, passive device in which a proton beam is dumped and the heat generated by nuclear cascades is extracted, without other major elements of variability".

A great asset of the EA is its potential for closing the fuel cycle, reducing the HLW stockpile due to the fuel flexibility of the device. Moreover, the fuel itself needs no access during the whole burn-up, and it may be sealed as a non-proliferation safeguard measure.

6.1.1 Description of the System

The geometry of the EA, illustrated by Figure 6.1, is rather slim (~6 m diameter) and tall (~25 m). The slenderness of the main vessel improves the uniformity of the flow of the liquid lead and of the natural circulation for heat removal, since the heat extraction is based on a natural convection-driven molten lead pool. There are four 375 MW_{th} heat exchangers to transfer the heat from the primary cooling circuit to the intermediate heat transport system (Pb-Bi eutectic). These are located above the core between the support cylinder and the walls of the vessel.

This device would operate away from criticality at all times ($0.95 \leq k \leq 0.98$), and the injected beam current would directly control the power produced. As mentioned earlier, the nominal proton current is approximately 12.5 mA; this means that 7.8×10^{16} protons would be accelerated up to a kinetic energy of ~1 GeV (at this velocity the protons become relativistic since their velocity is ~0.875 times that of the speed of light in vacuum), and then sent into a liquid lead target to generate, through the spallation process, the neutrons needed to drive the nuclear reactions in the core. The nominal external power provided by the beam $P_{ext} \approx 12.5$ MW, corresponding to an energy gain $G = P_{EA}/P_{ext} \approx 120$.

The favourable characteristics of lead in terms of neutron transparency (large diffusion length and small energy loss after scattering) and small capture cross-section (^{208}Pb is a double magic isotope), as described in Chapter 3, justifies the choice of molten lead as the coolant. The device would be operated in analogy with Fast Breeders[3], by using fast rather than thermal neutrons.

An important feature of the device is the use of natural convection alone to remove all the heat produced inside the core. Convection cooling has been widely used in pool-type reactors at small power levels. It has been shown in [1] that an extension of this very safe method to the very large power of the EA is possible, because of the unique properties of lead, namely high density, large dilatation coefficient and large heat capacity. Convection is spontaneously driven by temperature difference; therefore circulation pumps are unnecessary, providing the EA with yet another safety feature. In the convective mode, a very large mass of liquid lead (~10,000 tonnes), with a large heat capacity moves slowly ($\leq$ 2.0 m/s inside the core, about 1/3 of this speed elsewhere) transferring the heat from the top of the core to the heat exchangers located 20 metres above and returning at a lower temperature ($\Delta T \approx -200$ ºC) from the heat exchangers to the bottom of the core.

[3] Fast breeders are generally liquid sodium cooled, at a maximum temperature of 600-700 °C. The boiling temperature of lead is extremely high (1743 °C) and it is a passive element, in contrast with sodium, which is extremely reactive with any polar substance such as water.

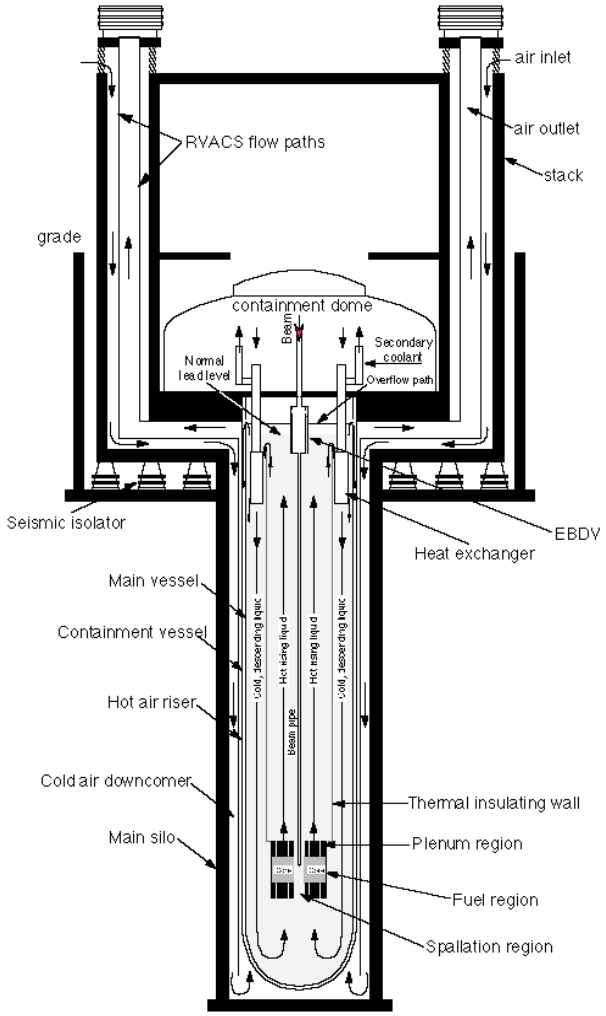

Figure 6.1. Schematic view of the 1500 MW_{th} Energy Amplifier [1].

The EA may operate with a wide range of fuels, such as thorium-plutonium-based fuels, using plutonium to drive the breeding of ^{233}U from thorium (therefore reducing the plutonium stockpile in the waste and producing fissile material). The EA may be particularly suitable for eliminating MAs given that it is a thorium-based subcritical fast system, hence, presenting very low equilibrium concentrations for higher actinides subject to a fission-favourable environment. Furthermore, the addition of LLFFs in the reactor is foreseen in order to transmute these species into short-lived isotopes, by the means of the ARC method (see Chapter 3). The EA would initially be loaded with a mixture of actinide waste and thorium, in the approximate ratio 0.16 to 0.84 by weight.

During operation, the actinides would be fissioned, while ^{233}U would be progressively produced. The bred ^{233}U would compensate for the drop of reactivity due to the decreasing actinide mixture and that due to the build-up of FFs. Therefore, a balanced operation over a long burn-up corresponding to five years of operation without external intervention would be possible without loss of reactivity in the core.

Thorium was chosen as the main fuel for the EA since the accumulated radiotoxicity related to this fuel cycle is much smaller than in the uranium cycle. The production of higher actinides during an operating cycle is greatly reduced compared with the use of ^{238}U as the matrix of the fuel. Also, in terms of availability, thorium is more abundant and more widely spread in the earth's crust than uranium. The estimations of abundance presume ~6×10^6 tonnes worldwide, which could produce 15,000 TW·yr of energy if used in EAs [1], about a factor of 100 larger than the known reserves of oil or gas and a factor 10 larger than coal. This would correspond to ~12 centuries at the present world's total energy consumption, i.e. 9405 million tonnes of oil equivalent or ~4.83 TW·yr.

The nominal power of 1500 MW_{th} would require 27.3 tonnes of mixed oxide fuel and the fuel dwelling time is expected to be 5 years at full power. The device would benefit from an extended fuel burn-up of ~120 GWd/tHM, with almost constant reactor parameters (i.e. k_{src}, thermal feedbacks and fuel composition), since the fissile material would be internally regenerated inside the thorium fuel. Reference [1] shows that the captures due to FFs may be compensated by operating initially with a breeding ratio below equilibrium. Throughout the burn-up, the growth of the fissile fuel concentration would counterbalance the poisoning due to FFs. In that case, neither refuelling nor shuffling (mainly due to the homogeneous fuel power distribution) would be necessary for the specified duration of the burn-up. At the end of the burn-up cycle the spent fuel would be fully replaced and reprocessed.

6.1.2 EA Fuel Burn-up Evolution

As explained in Chapter 3, the thorium-based fuel cycle presents many advantages compared to the uranium-based one, from the availability of the resources to the production of higher actinides. In fact, the use of ^{232}Th to breed fissile ^{233}U entails very low equilibrium concentrations of TRUs in the fuel, of the order of 10^{-8} times that of ^{232}Th, as illustrated by Figure 6.2.

The low equilibrium concentration of TRUs in the thorium fuel has important implications for transmutation. Any amount of these elements added to the fuel will be progressively transmuted until the equilibrium concentration is reached. Therefore, the plutonium and MAs transmutation rates in a thorium-based matrix are significantly larger, as elaborated later, than using uranium-based fuel, such as MOX fuel.

Figure 6.2 show the isotopic evolution with burn-up of a typical EA configuration, breeding ^{233}U from ^{232}Th. The burn-up cycle extends to 120 GWd/t of fuel (~5 years) without refuelling or shuffling. For this burn-up level, a small change in the mass of ^{232}Th may be observed due to the breeding process. The concentration of ^{233}U slowly increases and compensates for the neutron captures produced by the FFs, which are mainly responsible for

the limitations in the duration of the burn-up cycle, and the actinides presenting small fission cross-sections. A significant amount of ^{234}U (~120 kg) is produced by the end of the cycle, and from it, an increasing mass of ^{235}U (~12 kg at EOL) is produced. The production of ^{233}Pa stabilises around 30-40 kg, compensating the loss of ^{233}U. Also ^{231}Pa, ^{230}Th, ^{232}U and ^{236}U reach their equilibrium concentrations of the order of kg. Finally, TRUs, such as ^{237}Np and ^{238}Pu, appear in very small concentrations, 150 g and 30 g respectively, showing the reduced level of TRU generation for an energy production of ~66 TW·h.

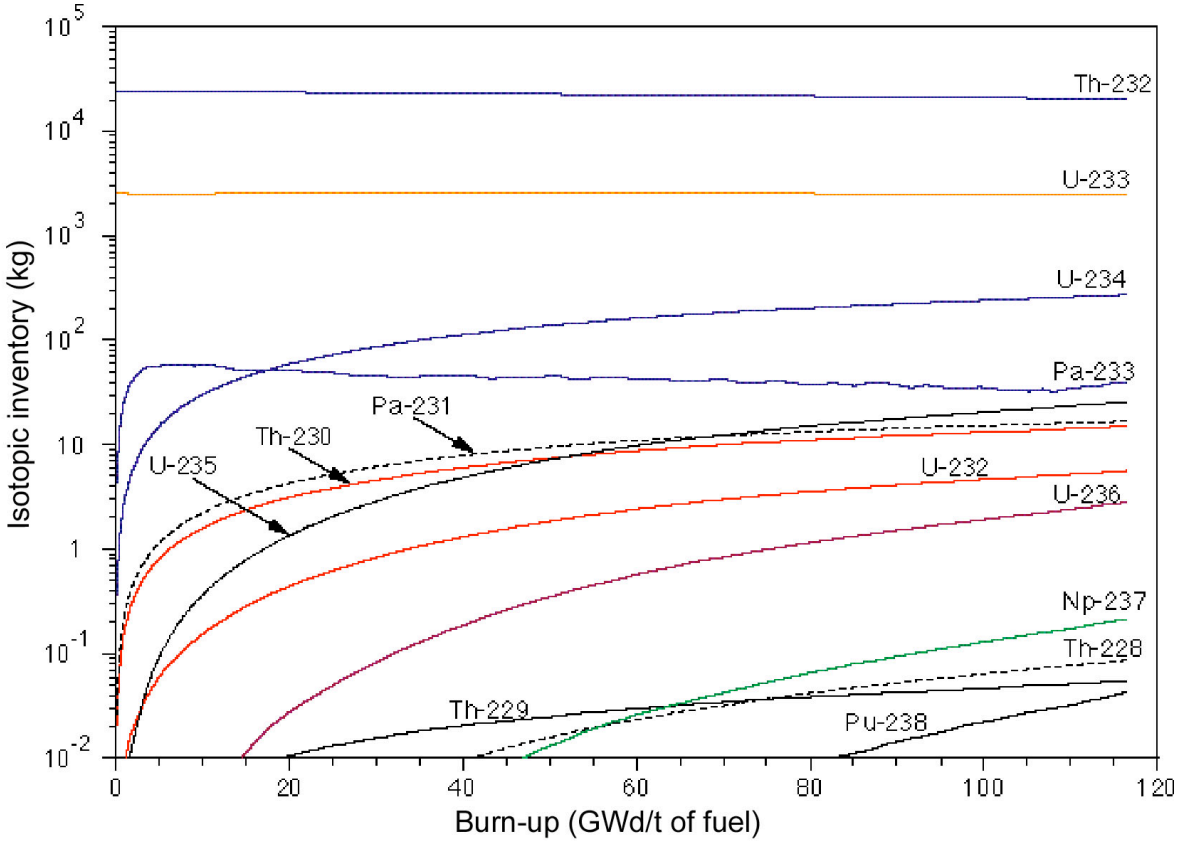

Figure 6.2. Isotopic evolution with fuel burn-up for a typical thorium-fuel EA configuration [1].

The very interesting perspectives generated by this system require the confirmation of a real size experiment, since the operation and the technical details of a large power subcritical lead-cooled device have never been tested. In this context, the EADF is a necessary step to the application of fast system technology to HLW elimination and energy production.

6.2 The Energy Amplifier Demonstration Facility

The remarkable potentialities of the ADS concept, and, in particular, of the EA, to eliminate HLW drove several European political institutions to set up a Technical Working Group (TWG) whose primary task is to define common guidelines for the development of this

technology. This TWG agreed on the need to build a demonstration facility of significant power (~100 MW_{th}) within ten years, in order to develop industrial strategies leading to the actual exploitation of the concept.

The scientific feasibility of these systems has been proven in previous experiments (see Chapter 3). Nevertheless, more experimental accuracy is needed both in nuclear physics and in ADS technology. For the former, the need for better and more comprehensive nuclear data for a large variety of nuclei has been underlined in Chapter 4. Notably, the effect of the neutron cross-section discrepancies on the prediction of the ADS parameters, for a wide range of energies, is motivating the extensive experimental programme previously described (i.e. n_TOF). For the latter, the coupling of different ADS elements and the transition between different operating regimes will be investigated in the TRADE experiment, as described in Chapter 5.

Therefore, the experimental programme to be carried out in the demonstrator can be decoupled into two concepts: XADS (eXperimental Accelerator-Driven System) and XADT (eXperimental Accelerator-Driven Transmutation). The former is meant to demonstrate the operation of the accelerator/spallation target/subcritical core layout in realistic conditions and with sufficient power. The latter seeks to prove the capability to transmute various actinides and LLFFs and to test and qualify innovative fuels for that purpose.

The basic parameter of the demonstrator is the thermal power output. This was set to ~100 MW_{th} by the TWG on the basis of transmutation rates of the order of tens of kg/yr. The Roadmap for Developing ADS for Nuclear Waste Incineration [46] establishes that a larger power output (for instance 300 MW_{th}) would considerably complicate the realisation and operation of the device and greatly increase its costs. On the other hand, a smaller system (~10 MW_{th}) would reduce the HLW fraction undergoing transmutation and the power density; likely becoming insufficient to achieve significant changes in the fuel in a realistic time.

As previously mentioned, there are several candidate designs for the demonstrator. However, the LBE-cooled system has several great advantages. First, the coolant and spallation target are the same material, so physical separation between them may be avoided. Secondly, several accidental conditions (e.g. loss-of-coolant accidents) may be handled better with this design than with helium- or sodium-cooled ones.

6.2.1 Description of the EA Demonstration Facility

As in the case of the Energy Amplifier conceptual design [1], the EADF core consists of an annular structure, immersed in molten LBE, which serves as the primary coolant and spallation target. The central annulus contains the spallation target unit, which couples the proton accelerator to the subcritical core, as may be seen in Figure 6.3. The core is arranged in

a honeycomb array forming an annulus with eight coaxial hexagonal rings of fuel and dummy subassemblies.

The choice for the accelerator between a cyclotron, a LINAC or a combination of both has not yet been taken. In any case, the EADF design includes a multi-stage (2-3) 600 MeV, ~5 mA proton accelerator, which implies a 2-4 upscaling of existing machines (i.e. the cyclotron in PSI).

The reactor assembly presents a simple primary coolant flow path with riser and downcomer channels. The core (heat source) is located below the riser channels and the heat exchangers (heat sink, at the top of the downcomer channels). This layout allows an efficient use of natural circulation of the coolant, the flow of which is enhanced by the additional injection of argon bubbles. This method, based on the principle of gas lifting, keeps the coolant circulating at a higher flow rate, the level of which may be controlled by the amount of gas injected [27].

The use of LBE as the primary coolant ($T_{melting}$ ~123 °C, $T_{boiling}$ ~1670 °C, ρ ~10.5 g/cm^3) permits the operation of the system at low temperature (compared to the use of pure molten lead, $T_{melting}$ ~327 °C), reducing erosion/corrosion problems and creep damage in the structures.

A synthetic organic diathermic fluid was chosen as the secondary coolant due to its chemical stability with the primary coolant, good thermal properties at high temperatures, low vapour pressure and stability against radiolysis under radiation.

One of the main requirements in the design of the facility is the need to accommodate different core configurations, containing MAs and LLFFs assemblies at different locations presenting the required neutron flux level and energy spectrum. As detailed later, this capability is ensured by the nature of the coolant, presenting a long diffusion length and continuous isolethargic spectrum in small energy steps.

However, EADF initially seeks to demonstrate the technical feasibility of a fast neutron ADS, cooled by molten LBE, and not that of incinerating TRUs. Consequently, the use of the well-known Super-Phénix [104] type uranium-plutonium MOX fuel (SPX), instead of a thorium-based fuel, was adopted. This SPX has already been certified and operated in the aforementioned installation, and its behaviour in this particular context is well understood.

The need for great operational flexibility may also be better achieved without any electrical energy generation constraints imposed on the system. Hence, the facility has been designed to dissipate the generated heat to the external atmosphere. A more detailed description of EADF may be found in [27].

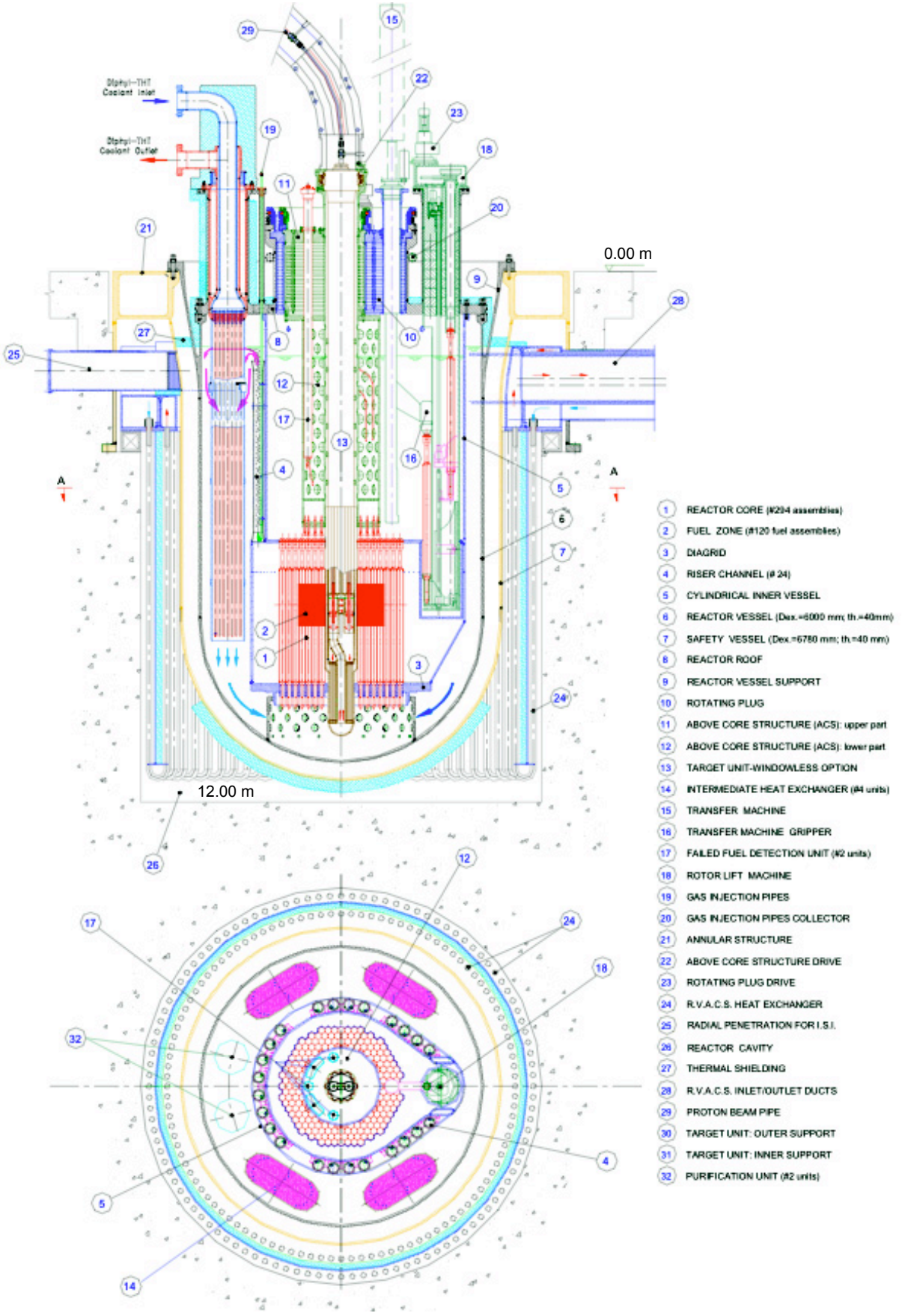

Figure 6.3. EADF front and top schematic views highlighting the main components of the device [27].

6.2.2 Reference Configuration

The EADF has been conceived to produce a nominal output thermal power of ~80 MW_{th}. As explained before, this is considered to be the minimum thermal output power in order for the experiment to be representative for transmutation, since the objective of the device is not only to operate a fast ADS at real power but also to validate the concept of transmutation at large scale (of the order of kg).

The core basic fuel subassembly is an hexagonal cluster of 90 SPX MOX fuel pins (~20% plutonium). The pin diameter and active length are ~8.5 mm and ~87 cm, respectively. These fuel pins are subdivided in 4 radial zones consisting of the steel clad, intermediate gap region, the fuel pellet and a central void region (motivated by the large amount of gaseous FFs due to extended burn-ups).

The core is arranged in a honeycomb array forming an annulus with four coaxial hexagonal rings of 120 fuel subassemblies, as illustrated by Figure 6.4. The fuel core is itself surrounded by an annular array of four rings of dummy subassemblies, which are essentially empty ducts, in order to allow the irradiation of different test fuels. The total number of fuel subassemblies is 294, allowing the irradiation of a large number of elements at once. The core inner and outer radii are correspondingly ~31.5 cm and ~85.1 cm, with an outer diameter for the region containing the dummy elements of ~1,278 cm.

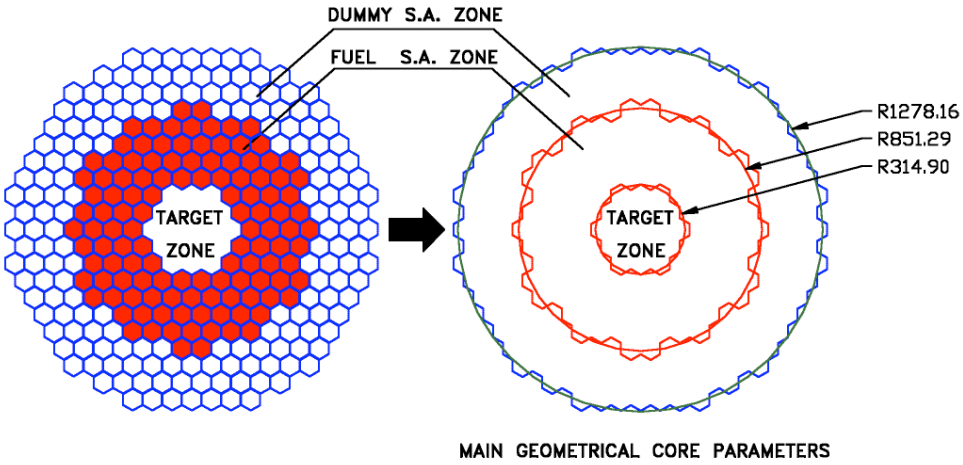

Figure 6.4. EADF core cross-section showing the subassemblies and radii of the different regions [27].

The neutron yield of protons at 600 MeV is rather reasonable (~15 n/p), and helps to limit the final size of the machine. The power deposition in the target of 5 mA 600 MeV is ~3 MW, which entails the use of a liquid spallation target (LBE) in order to dissipate such a large amount of heat without mechanical degradation. The interface between the beam line and the spallation target is one of the most complex decisions in the design. No choice has been made

between using a 'hot window' of a high melting temperature material, such as tungsten, possibly cooled by an auxiliary cooling loop, and using the 'windowless' approach, by inserting the beam line directly into the target without a mechanical barrier.

The operating temperature for the primary coolant ranges from ~300 °C core inlet temperature to ~400 °C core outlet temperature. Under these operating conditions the working temperatures remain far from the LBE freezing point (123 °C) and from the stainless steel creep temperature (~566 °C) and even from the carbon steel creep threshold (~427 °C).

The fuel pin total length is 127.2 cm, of which 87.0 cm is active. The rest is made up of the upper (16.2 cm) and lower (15.0 cm) plenum, designed to collect the volatile LLFFs during extended periods of burn-up. The outer diameter of the pin is 0.85 cm, with a stainless steel cladding thickness of ~560 μm.

The SPX fuel is a natural uranium (~82%) / plutonium (~18%) oxide ($UPuO_2$), containing some traces of both americium and neptunium isotopes. The plutonium contains ~71% fissile isotopes (mainly ^{239}Pu), and thus is a classical Fast Breeder fuel (producing ^{239}Pu from neutron capture in ^{238}U and a double β^- decay in ~2.4 days). Therefore, the fissile enrichment of the $UPuO_2$ fuel is 13.33%.

6.2.3 Nominal Neutronic Parameters

The main neutronic parameters at the Beginning-Of-Life (BOL) for the EADF reference configuration are summarised in Table 6.1. The reference fuel-loading scheme foresees ~3.8 tonnes of the SPX fuel previously described. The simulations of EADF were carried out using as a base a detailed geometrical model previously developed at CERN by the EET group.

As previously explained in Chapter 5, the value of ~0.96 for the source multiplication coefficient was chosen in order to avoid criticality conditions, with adequate safety margins. Particularly for EADF, the uncertainties in ND are larger than for a thermal system since such a device operates is a less-known energy region. As elaborated in Chapter 4, there is poor experimental information for many of the isotopes involved and even poorer for the energy regions above 1 eV (resonance and unresolved resonance regions, as well as for higher energies). The discrepancies in k_{src} found for isotopes such as ^{239}Pu and ^{240}Pu reached ~600 pcm between EADF/B-VI.8 and JENDL-3.3 (see Chapter 4); thus the total discrepancies between libraries for plutonium-rich fuels may reach 2000 pcm [73 & 74]. Moreover, the cold start-up margin is of great importance for such a system, since the breeding elements present a wide range of resonances which may produce a reactivity leap of ~1000 pcm during a cold shutdown, as explained in Section 6.2.5.1. Therefore, the safety margins under which this

device operates should be larger than for a thermal system, and specifically larger than for TRADE.

The spallation neutron yield (N) is ~15 n/p, a much more efficient yield than the 0.71 n/p of the 140 MeV target of TRADE, since the nominal proton energy for EADF (600 MeV) is much closer to the optimal value for yield (~1.2 GeV), as explained in Chapter 3. The 3.23 mA nominal proton beam current (I_p) implies an energy deposition of 1.94 MW at the beginning of cycle. The removal of such a large amount of power deposited may pose some technical problems. To solve these problems and study the physical principles occurring in this system, a 1 MW LBE spallation source experiment (MEGAPIE [49]) has been commissioned in the SINQ facility in PSI. The energy gain $G \approx 42.35$ is not the foreseen one for a full-scale EA (~120), but it is sufficient to demonstrate the concept of energy amplification in a fast ADS at power.

Table 6.1. Main BOL neutronic parameters for the EADF reference configuration.

Global Parameters	Symbol (units)	Reference case (SPX fuel)
Initial fuel mixture	MOX	$UPuO_2$
Initial fuel mass	m_{fuel} (kg)	3792.0
Initial plutonium concentration	m_{Pu}/m_{fuel} (wt.%)	18.09
Initial fissile enrichment	$m_{fissile}/m_{fuel}$ (wt.%)	13.33
Thermal power output	P_{th} (MW)	80
Proton beam energy	E_p (MeV)	600
Spallation neutron yield	N (n/p)	15.04 ± 0.14
Net neutron multiplication	M	26.69 ± 0.79
Source multiplication coeff.	k_{src}	0.96254 ± 0.001
Effective multiplication coeff.	k_{eff}	0.96124 ± 0.001
Neutron source importance	φ^*	1.036
Energetic gain	G	42.35
Gain coefficient	G_0	1.59
Accelerator current	I_p (mA)	3.23 ± 0.10
Beam power	P_{beam} (MW)	1.94 ± 0.06
Core power disributions		
Avg. fuel power density	P_{th}/V_{fuel} (W/cm^3)	259.57
Spec. fuel power density	P_{th}/m_{fuel} (W/g of fuel)	22.43
Radial peaking factor	P_{max}/P_{avg}	1.25
Axial peaking factor	P_{max}/P_{avg}	1.16

This configuration presents large fuel power densities (~260 W/cm^3) due to the high density of the fuel ($\rho \approx 11.6$ g/cm^3) and the extra need of fissions to breed the fuel in order to maintain the power output without either shuffling or adding new fuel. On the other hand, the system exhibits very low axial and radial power peaking factors (1.16-1.25) due to the large

diffusion length of the coolant, thus allowing the neutrons to reach the outer regions of fuel. This fact impacts positively on the safety characteristics of this system, imposing looser restrictions on the cooling of the fuel. These reduced power peaking factors, which may be perceived in Figure 6.5 (described in the next section), also permit a more homogeneous burn-up of the fuel, therefore allowing longer burn-up cycles.

Even though this fuel was designed for use in a sodium-cooled fast reactor (i.e. Super-Phénix), its use in EADF may help to assess the TRU elimination potential of this device. Indeed, the breeding equilibrium is given by the ratio of the absorption cross-section of the daughter product to the capture (breeding) cross-section of the parent for a specific energy spectrum. Taking into account the softer neutron energy spectrum in a sodium-cooled system (as explained later in Section 6.2.4.2), the value of the plutonium breeding equilibrium in a LBE-cooled machine is lower (~15% versus the nominal ~18% plutonium content in the SPX fuel), thus transmuting the excess concentration of plutonium.

In order to give an idea of the distribution of the neutron-induced reactions occurring in the system, Table 6.2 summarises these nuclear processes in the most relevant locations, as well as the specific reactions taken place in the fuel. As expected, the fuel is clearly absorbing most of the neutrons in the system (~60%), followed by the stainless steel reflector and the support grids (~12% and 10%, respectively). The LBE coolant only absorbs ~10%, compared to the ~20% captured by the water in TRADE. This fact is a major contributor to the higher attainable integrated flux in fast systems (typically ~10^{15} n/s/cm^2) compared to a LWR (~10^{14} n/s/cm^2). The reasonable amount of inelastic nuclear interactions occurring in the structural materials and the cladding imply only a moderate activation of these elements. Nevertheless, the radiation damage (in displacements per atom, dpa) undergone by some of these elements, and in particular by the fuel cladding (~3.2 dpa/yr), should motivate a detailed analysis of the mechanical implications. There is a small but important percentage of escapes, so the radioprotection aspects will play an important role in the construction designs of the facility.

In terms of reaction types, capture is clearly the most important nuclear process (66% of the total) due to the breeding process in the fuel and breeding blankets and the lower resonance escape probability of the system. These factors are enhanced by the high neutron flux in the resonance region, as presented in the next section. Fission accounts for 31% of the reactions and the (n, xn) reactions logically increase their importance (compared to a thermal system) to ~2% of the inelastic nuclear interactions.

For the fuel matrix, although plutonium represents ~18% of the fuel mass, it accounts for 59% of the reactions occurring in the fuel. This element produces ~89% of the fission and ~30% of the capture reactions, mostly in ^{239}Pu, mainly due to the larger absorption cross-section of the plutonium isotopes compared to ^{238}U. On the other hand, uranium contributes with ~39.5% of

the reactions, mostly captures in ^{238}U. Only ~0.3% of the reactions in the fuel are (n, xn) which implies that the majority of this type of interaction occur in the coolant and the structural materials. This fact emphasises the need to improve the related ND, as concluded in Chapter 4, since (n, xn) reactions may indeed alter the neutron multiplication of the whole system.

Table 6.2. Neutron-induced reactions in different elements of EADF for its reference configuration.

Reactor core			
Neutron Absorption Inventory		Neutron Absorption Inventory	
Reactor structures	3.82%	Reflector	12.04%
Reactor coolant	10.06%	Support grids	10.47%
Spallation target assembly	1.93%	Breeding blankets	2.95%
Fuel	59.74%	Heat exchangers	2.28%
Fuel cladding	1.54%	Escapes	0.15%
Main Nuclear Reactions		Main Nuclear Reactions	
Capture	66.01%	(n, xn)	2.14%
Fission	31.13%	Others	0.42%
Fuel matrix			
Neutron Absorption Inventory		Neutron Absorption Inventory	
Uranium	39.52%	Americium	1.42%
Plutonium	59.04%	Others (^{16}O and ^{237}Np)	0.003%
Main Nuclear Reactions		Main Nuclear Reactions	
Capture	51.10%	(n, xn)	0.33%
Fission	48.12%	Others	0.20%

6.2.4 Neutron Flux Distribution

Complementary to the description of the neutron flux distribution in TRADE, the analysis of the spatial, energy and time distribution of the neutron flux in EADF, as well as the behaviour of the spallation neutrons, helps to characterise neutronically this facility. Moreover, the comparison between both experiments allows the essential differencess between thermal and the less-known fast systems, and in particular, between a thermal ADS, such as TRADE, and a fast one, i.e. EADF, to be highlighted.

The neutron flux distribution (particularly the spatial distribution), which strongly depends on the multiplication factor, has direct impact on the performance of the facility and the achievable level of burn-up and transmutation rates. Therefore, a precise characterisation will allow, for example, the placement of the LLFFs and distribution of the fuel breeding material to be optimised.

6.2.4.1 Spatial Distribution

The radial neutron flux distribution for the reference configuration fuel is illustrated by Figure 6.5(a). The neutron flux in the spallation target region is slightly lower than in the fuel subassemblies, ~10^{15} n/cm^2/s in both locations. These considerable flux levels, as well as the high power densities produced in the core (~260 W/cm^3), are brought about by the substantial fissile enrichment (~13.3%) and the moderate fuel pitch (13.4 mm; ~1.5 times the fuel pin diameter). The flux in the incineration blanket, namely ~3.1×10^{14} n/cm^2/s (three times larger than the average flux in the fuel of a LWR), may allow significant transmutation rates for LLFFs. The low fluxes in the reactor vessel (nearly four orders of magnitude lower than in the fuel) show the good neutron confinement in the core produced by the ~6 m diameter vessel (thus, ~2.1 m of LBE coolant between the core boundary and the reactor vessel).

The axial neutron flux (Figure 6.5(b)) presents the well-known cosinusoidal shape with a peaking factor of ~1.15. As previously explained, the large neutron diffusion length in LBE and the small energy loss in every interaction produces a very moderate ratio between the average flux in the fuel and its maximum value (at the centre of the pin). In turn, this results in more homogeneous fuel breeding and fissile depletion than in a system with higher peaking factors.

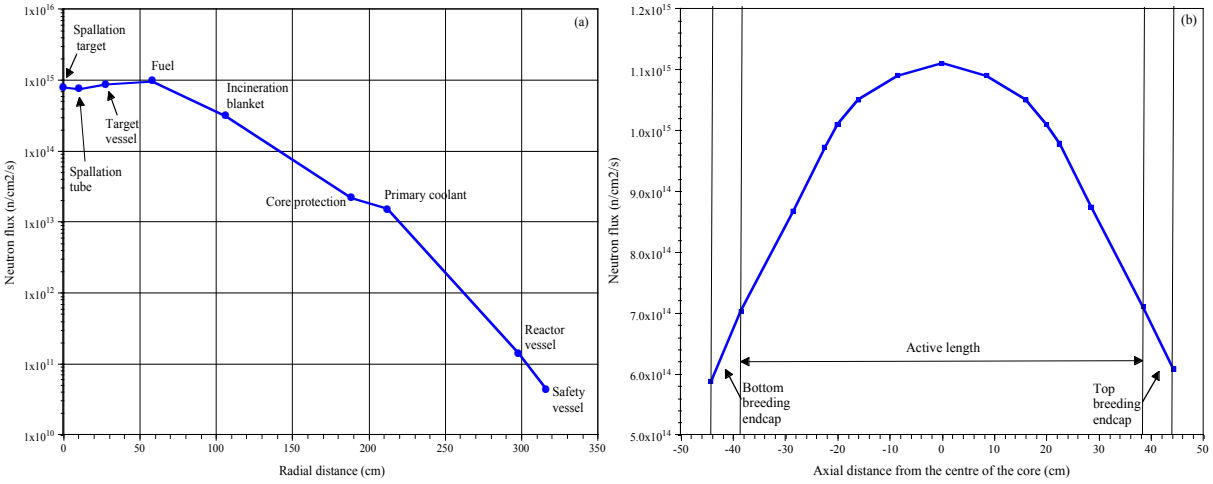

Figure 6.5. Radial (a) and axial (b) neutron flux distribution in EADF for $UPuO_2$ (reference) fuel.

The core gives good neutron containment, with a much smaller leakage than in the case of TRADE (Figure 5.8(a)), where the flux at the boundaries of the core was less than two orders of magnitude smaller.

The good containment of the neutron population has interesting implications for transmutation. The presence of absorbing elements in the periphery of the core affects the neutron population in the fuel only slightly, thus effectively decoupling the incineration

blanket from the fuel core, as shown later by the small effect on k_{src} of the LLFFs transmutation strategies.

6.2.4.2 Neutron Energy Spectra

The energy spectra in different elements of EADF, represented in Figure 6.6, show a clear domination by neutrons in the fast and high-energy regions. This is a rather representative example of the neutron energy distribution in fast systems, with a flux peak in the fuel between 100 keV and 1 MeV (the energy of the actual peak depends on the fuel pitch and strongly affects the fission-to-absorption ratio for some MAs), and very small values below 1 eV. The ^{238}U resonances in the fuel may be clearly seen (6.5 eV, 21 eV and 70 eV), as well as in the breeding blanket. Moreover, the resonance in bismuth (^{209}Bi) at 800 eV may be perceived in most of the regions represented in Figure 6.6.

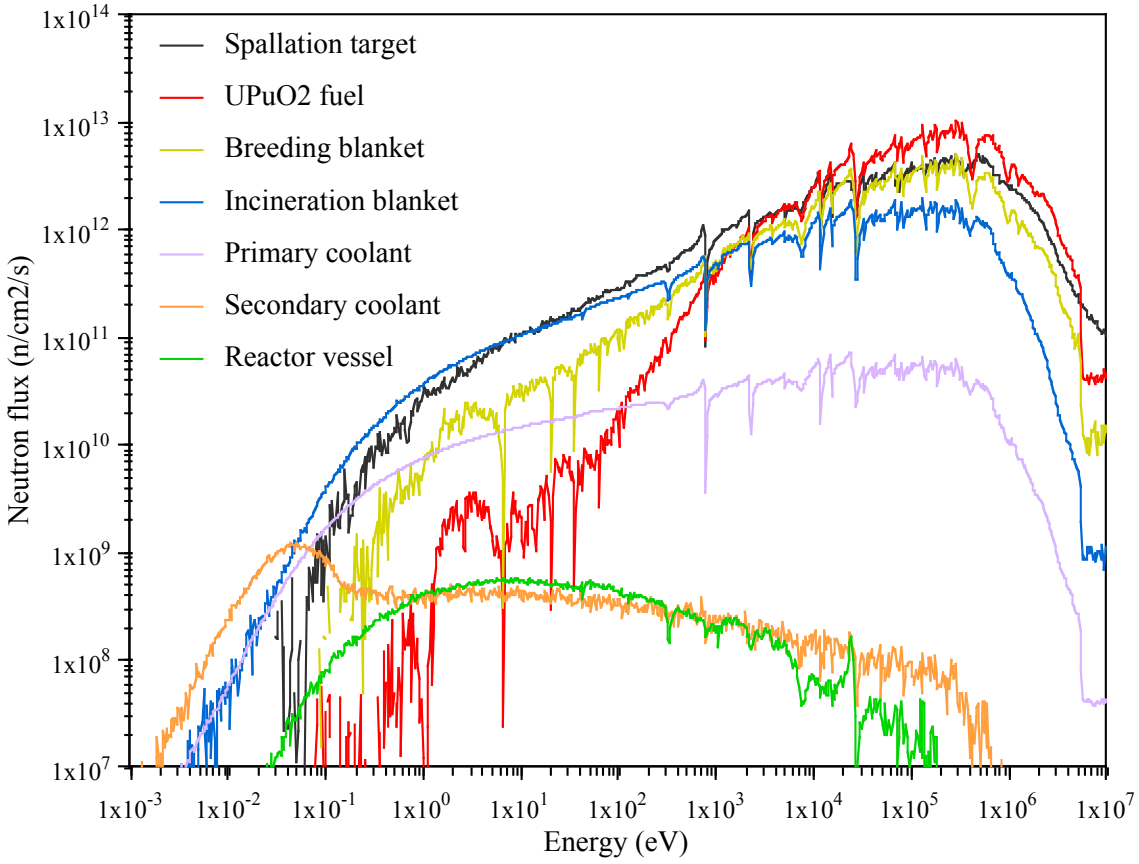

Figure 6.6. Neutron energy spectra in different regions of EADF for the reference configuration.

As mentioned before, the neutron energy spectrum in the fuel peaks at ~300 keV and falls exponentially with decreasing energy, to a value almost five orders of magnitude smaller in the tenths of eV region. As elaborated in Chapters 4 and 5, the value of the capture cross-section for actinides (in general, for all elements) decreases with energy above the unresolved resonance region, thus the ratio between fission and capture increases at higher energies.

Therefore, a harder (higher in energy) neutron spectrum will effectively enhance transmutation of otherwise fission-resilient isotopes.

On the other hand, the rather flat and smooth (except for the resonance in ^{209}Bi) flux in the coolant is produced by several elastic interactions in small isolethargic steps with an almost constant cross-section. This might help in the neutron resonance crossing of any element placed in or around the coolant region, although it also implies an enhancement in the activation of the core structures.

The high flux, and particularly in the epithermal region, in the incineration blanket permits the enhancement of the resonance captures, as understood through the TARC experiment, presented in Chapter 3. The use of different transmutation matrices for LLFFs and the dilution of these may induce high transmutation rates, and will be analysed later.

As previously indicated by Figure 6.5(a), the neutron flux beyond the core effectively decreases due to the use of such a large amount of coolant. The energy spectra in the reactor vessel and the heat exchangers illustrate this process. The effect of the hydrogen on the latter (the secondary coolant is an organic diathermic fluid – 1.6 ^{1}H per ^{12}C, $\rho \approx 0.8$ g/cm^3 – is clear from the distinctive bump in the flux at thermal energies (~0.025 eV).

The neutron energy spectrum requirements for transmutation of HLW have been extensively explained previously, drawing a clear conclusion: the need for a fast energy spectrum in order to effectively eliminate TRUs. Therefore, comparison of the neutron flux spectrum in EADF for different coolants (Figure 6.7) may be useful to understand which of the proposed systems may be better suited to transmute HLW, and in particular TRUs.

Figure 6.7(a) shows the normalised neutron energy spectra in the fuel of EADF using LBE, sodium or helium as coolants. Certain similarities in the high-energy region may be observed, although helium presents a slightly harder spectrum. Below ~30 keV the neutron flux using helium coolant becomes lower than the ones for LBE or sodium. This is, in fact, the main asset of the use of helium: the very hard spectrum due to its very large diffusion length. The main differences between LBE and sodium occur below 3 keV (resonance in sodium), where the neutron flux in the sodium-cooled fuel becomes significantly higher compared to LBE (and helium), hence enhancing the energy region where most of the captures are produced (see the sensitivity analysis for EADF in Chapter 4).

The normalised neutron fluxes in the coolant are illustrated in Figure 6.7(b). The flux in helium seems significantly harder with an epithermal region at least one order of magnitude lower that the high-energy region. On the other hand both LBE and sodium present very similar fluxes for all the energy range except for a slightly higher flux in sodium between 0.1 eV and 1 keV. Therefore LBE and sodium present isolethargic fluxes in the coolant (except

for the large resonance in sodium). This is particularly interesting for transmutation of LLFFs, since, as explained in Chapter 5, epithermal and thermal neutron spectra reduce the transmutation half-life of these species.

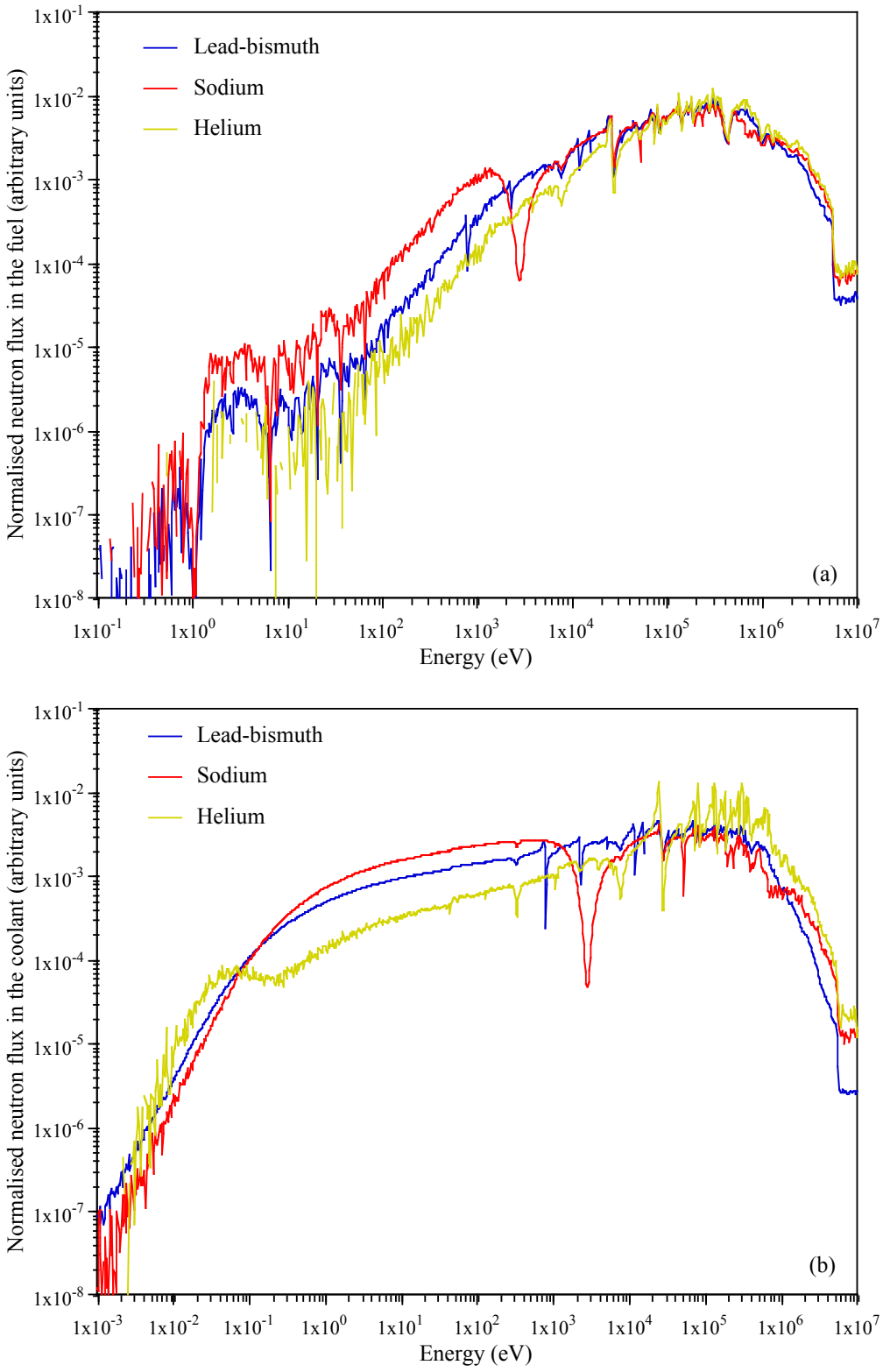

Figure 6.7. Neutron flux spectra in the fuel (a) and the coolant (b) for different coolants in EADF.

Therefore, the use of helium as coolant produces the hardest spectrum in the fuel, which enhances the elimination of TRUs, as seen in Figure 6.8, followed by LBE. Sodium presents a larger neutron flux below 2 keV, which reduces the fission-to-absorption ratio of actinides. For the coolant, helium barely perturbs the energy distribution (the moderation coming from the structures and the core itself). Such a spectrum is less compatible with the LLFFs transmutation unless special moderating matrices are produced. The neutron energy spectrum in LBE and sodium coolants show very similar characteristics, with high epithermal regions, although the flux in sodium seems slightly softer.

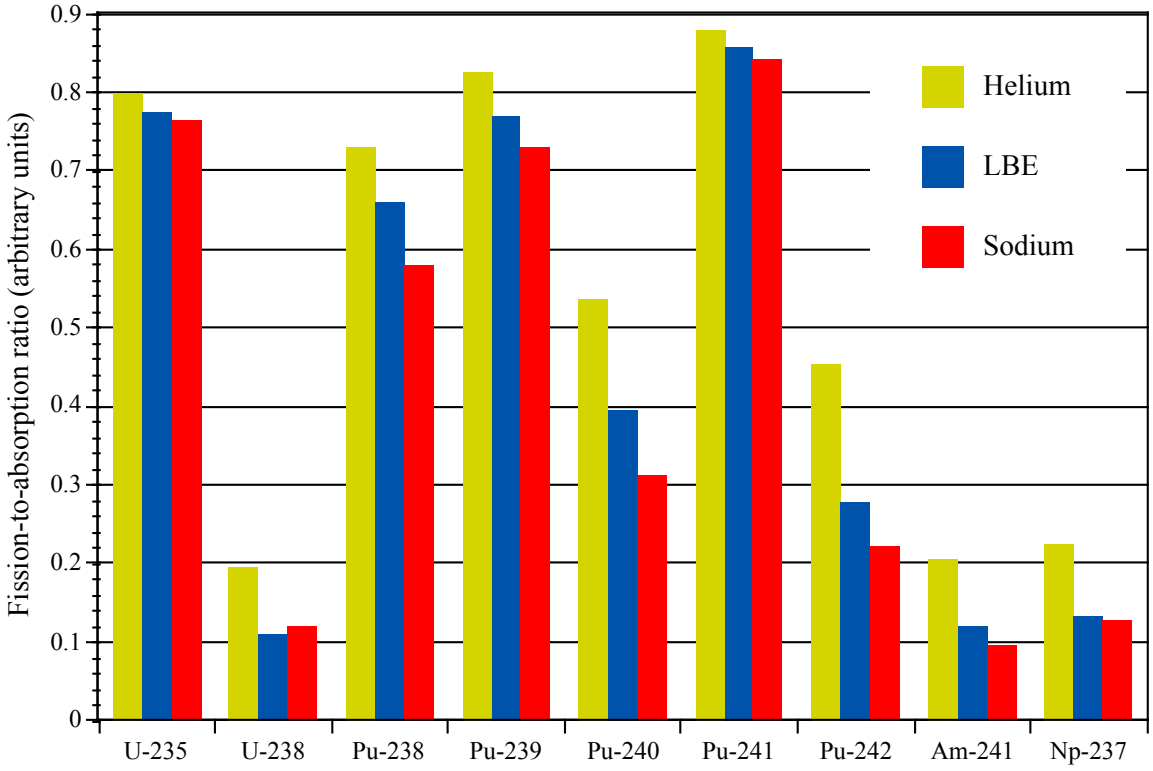

Figure 6.8. Fission-to-absorption ratios for different isotopes and coolants in EADF.

The effects of the different energy spectra on the fission-to-absorption rate for the actinides present in the fuel at BOL are presented in Figure 6.8. As mentioned above, the fission-to-absorption ratio in helium is higher than both in LBE and sodium, for all the isotopes. For the fissile isotopes, i.e. ^{235}U, ^{239}Pu and ^{241}Pu, the differences between the coolants are minor, since these isotopes have higher fission cross-sections than capture cross-sections across the energy range. For non-fissile isotopes, the ratio for helium is generally 5-17% higher than for LBE, which in turn is 2-10% higher than for sodium.

6.2.4.3 Dynamic Behaviour

The dynamic behaviour of the neutrons (both coming from fission and from spallation) in a fast ADS is rather different to that in a thermal system (hence the shift towards lower frequencies in the transfer function of TRADE). Therefore, a detailed study of this behaviour is necessary in order to completely understand the operation of EADF and the limitations of its thermal exploratory counterpart.

Figure 6.9 clearly shows the large differences in reactor period between a fast EADF and TRADE. Even though they have somewhat similar values of k_{src} (0.963 and 0.977, respectively), the time dependence of the neutron survival probability is radically different for the two systems. As elaborated in Chapter 5, the neutron population in TRADE peaks due to the spallation reaction, reaching equilibrium values after 10-20 μs. The spallation neutrons exponentially fade away, accounting for ~10% of the neutrons after 100 μs (0.1% after 1 ms, see Chapter 5). The propagation of the fission neutrons in the core can be perceived by the subtle increase in the survival probability of all the neutrons at ~150 μs, followed by a slow decrease due to the subcritical nature of the system.

On the other hand, Figure 6.9(a) shows the neutron survival probability in EADF is saturated after the initial spallation neutron production despite the rapid disappearance of these neutrons (more than 10 times faster than in TRADE and accounting for less than 0.1% of the total neutron population after 100 μs). This saturation is due to the combination of a heavy (high atomic mass) diffusing medium (with low capture cross-section; hence, giving neither important energy losses nor flux depletion) and fast fission processes. Herewith, the first important difference: the efficiency of the source. The number of fissions produced per spallation neutron is more than one order of magnitude larger for EADF (and, consequently, the proton current requirement decreases).

Between 100 and 250 μs, the neutron population diminishes steadily (note the logarithmical y-axis). Thereafter, the most relevant discrepancies between thermal and fast systems appear. The neutron survival probability in EADF presents a spiked profile, which corresponds to the capture and fission resonances of the system. This feature is only possible in a system where the moderator element is a heavy nucleus and presents a reasonable and constant elastic cross-section.

As a result of the analysis of the neutron population evolution (normalised to the initial spallation neutrons), the overall differences between the dynamic behaviour of the systems may be inferred. The fission neutron propagation in the core of EADF takes place in a few tens of μs whereas it takes ~150 μs in TRADE. Moreover, the (negative) exponential reactor period is substantially different, ranging from ~2 ms in TRADE to ~40 μs in EADF. Therefore, the prompt neutron lifetimes in these systems go from ~50 μs to ~1 μs.

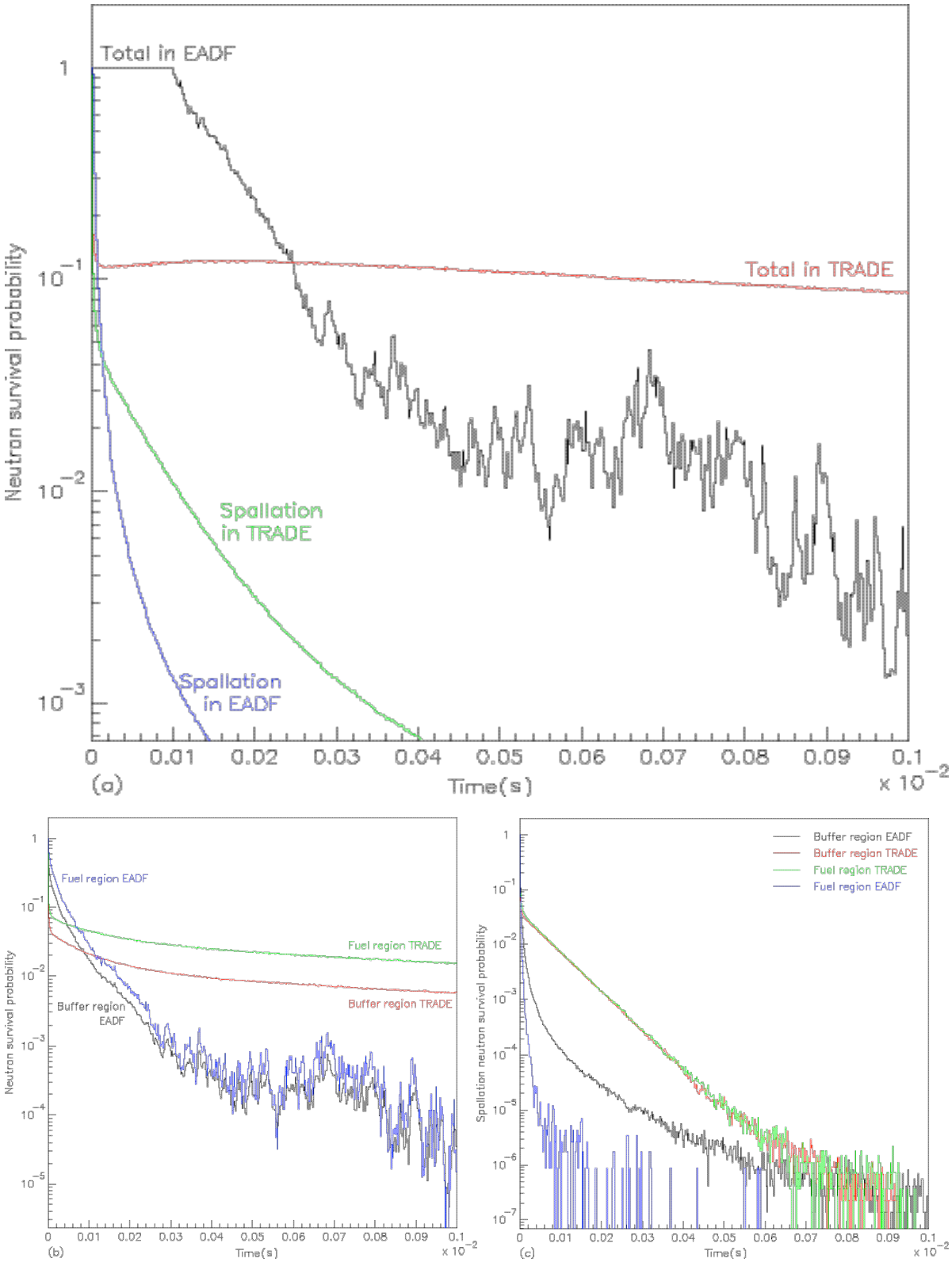

Figure 6.9. Comparison of the neutron survival probability between TRADE and EADF in the core (a) and in different regions of the system for the total neutron population (b) and the spallation neutrons (c).

These dynamic parameters have a direct impact on reactor control, and particularly on the length of the beam trips. As observed in Chapter 5, a thermal ADS may withstand a beam

failure of 1 ms (considered a normal duration for a beam trip) losing 25% of the neutrons, which can be regained if the beam is reconnected at nominal current. On the other hand, a beam trip of 1 ms on a fast system, and particularly on EADF, implies the disappearance of ~99.9% of the neutron population, therefore requiring a complete restart of the machine, since the insertion of the proton beam at nominal intensity may induce thermal shocks in the target, fuel and structures. Hence the need to study experimentally the effects of beam failures in TRADE, since the system is less sensitive to these than EADF; the knowledge gathered in this experiment will be applicable to a fast device at higher frequencies.

The evolution of the neutron population in the buffer and fuel regions of TRADE and EADF is presented in Figure 6.9(b). The neutron survival probabilities follow the characteristic trends of their respective systems. Furthermore, the transparency to neutrons of the LBE coolant may be clearly seen in the nearly overlapping population distributions, whereas in TRADE the substantially higher neutron survival probability in the fuel indicates the confinement of a large fraction of the neutrons in the fuel region due to the strong reflection effect of the water.

Concerning the behaviour of the spallation neutrons, there is no difference in the survival probability of these neutrons (which undergo an exponential attenuation) between the buffer and fuel regions in TRADE. On the other hand, the evolution of the spallation neutron population in EADF faithfully represents the different nuclear interactions occurring in different regions. These neutrons rapidly (in μs) disappear from the buffer region due to the large diffusion length of the coolant and reach the fuel (Figure 6.9(c)). In this region, they scatter and eventually produce an inelastic interaction; thus only a few of them reach resonance energies.

6.2.4.4 Spallation Target

In order to understand the behaviour of the spallation target in steady state and to determine the nuclear processes brought forth by the accelerated protons, a specific analysis was performed. Two different beam distributions were considered for the nominal beam parameters (3.23 mA of 600 MeV protons): a Gaussian beam profile (Figure 6.10(a) and 6.10(b)), with a standard deviation (σ_{xy}) half of the beam tube width (hence ~95% of the beam was confined in the tube and the remaining 5% was collimated before the collision region), and a uniform beam profile (Figure 6.10(c) and 6.10(d)).

The 600 MeV proton range in LBE (28.27 cm) may be clearly seen as a sharp drop in the energy deposition for both beam distributions (at ~–40 cm in Figure 6.10(a) and 6.10(c)). This is due to the fact that most of the energy carried by the protons is lost through ionisation (~66%) and nuclear recoils and heavy fragments (~2%). The electro-magnetic cascade is

exponentially dissipating ~30% of the beam energy and only ~2% is carried by secondary neutrons. This explains the large power densities observed close to the target, where most of the 1.94 MW beam is deposited in the first 20 cm. However, the difference in maximum power deposition between the two beam distributions is considerable. The uniform distribution gives a maximum deposition of ~450 W/cm^3, whereas for the Gaussian profile ($\sigma_{xy} \approx 4$ cm) the maximum is ~3.4 kW/cm^3, requiring an enhanced coolant flow in the target. Hence, the beam shape should be defined by a fine interplay between its optics and collimation.

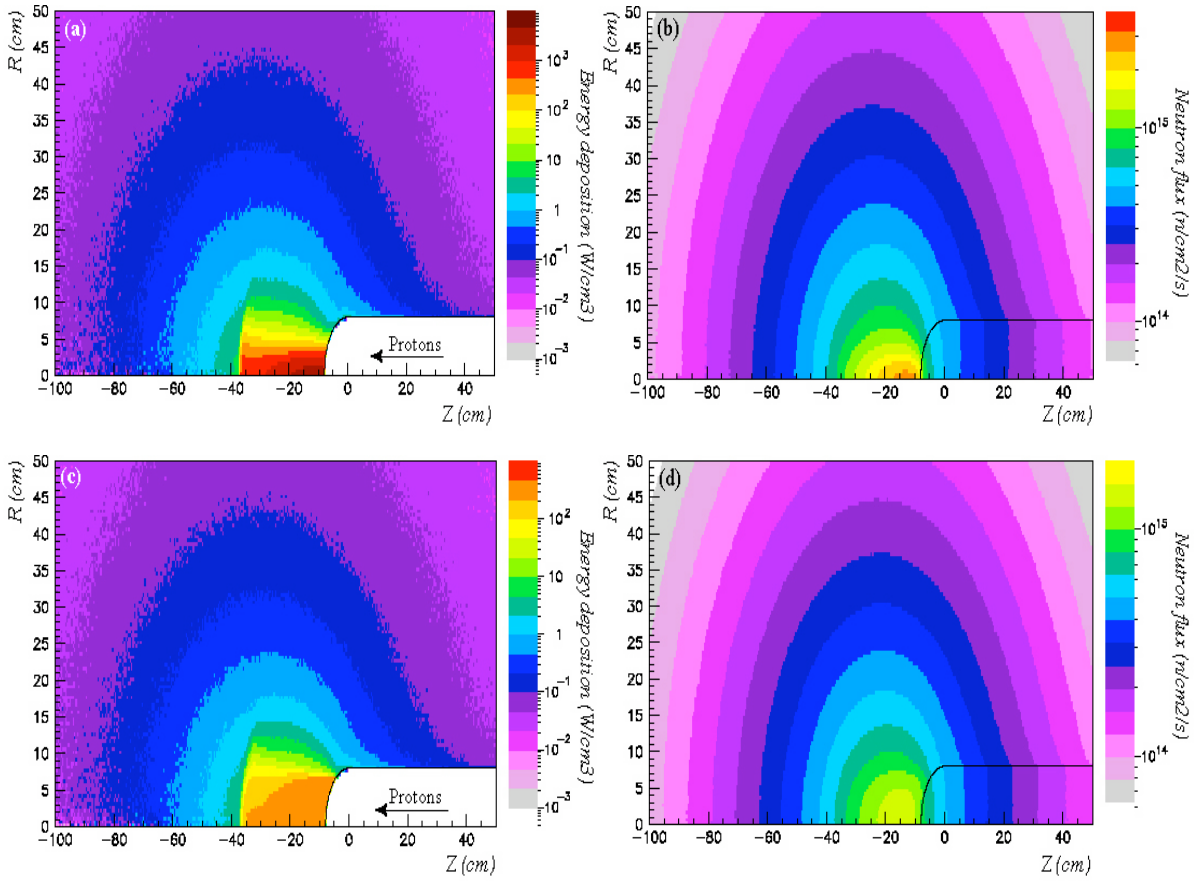

Figure 6.10. Energy deposition ((a) and (c)) and neutron flux distribution ((b) and (d)) in the spallation target of EADF for the nominal 3.23 mA, 600 MeV Gaussian ((a) and (b)) and uniform ((c) and (d)) proton distribution.

In terms of the spallation neutron flux, both beam-shapes present the same spherical distribution beyond ~10 cm from the beam axis. In the region close to the target the Gaussian beam profile obviously shows a higher flux (~3×10^{15} n/cm^2/s), which is propagated (although attenuated) along the beam axis due to the forward anisotropy of the high-energy elastic scattering.

6.2.5 Reactivity Safety Margins

Many of the parameters that determine the multiplication factor of any reactor, such as resonance capture and coolant density, depend on temperature. This is especially true for a fast neutron device operated with uranium-based fuel such as EADF, where the Doppler broadening of the capture resonances in ^{238}U (as well as in ^{232}Th) produce an effective increase in the resonance integral with temperature, therefore reducing the reactivity of the system. Additionally, the variation in the coolant density, or the loss thereof, strongly affects the behaviour of the neutron population (e.g. energy spectra, diffusion length etc.), and thus the multiplication factor.

It is well known that in order to guarantee the safety of the system the effect of these parameters on the multiplication factor (or on the reactivity) should be negative, since an overall negative feedback would tend to stabilise the system towards its equilibrium value. On the other hand, depending on the direction of the changes, positive feedback would make the system divert either towards a shutdown or, in the worst case scenario, a core meltdown. Consequently, analysis of these parameters is of great relevance for a nuclear reactor.

6.2.5.1 Temperature Coefficient

The temperature coefficient, α_T, is arguably the most important of the reactivity coefficients for a multiplicative device. Two physical effects mainly influence this parameter: the aforementioned Doppler broadening and the moderator temperature effect. The former, also called the prompt temperature coefficient due to its immediate contribution to the neutron multiplication, occurs mostly in the fuel due to the presence of well-defined capture resonances in ^{238}U and ^{232}Th, but not in other actinides. The latter, also called the delayed temperature coefficient due to the slow propagation of its effects to the reactivity of the system, is due to a complex interplay between large number of factors: for example, the energy spectrum differences between fuel and moderator, the discrepancies between fissile material and moderator absorption cross-sections, the behaviour of the reactor poisons and a myriad of other effects, such as the variation of the number of neutrons per fission reaction (which in turn depends on the neutron energy spectrum, and hence on the moderator temperature). A more exhaustive description of these effects may be found in [105].

With respect to EADF, the variation of k_{src} with fuel temperature is illustrated in Figure 6.11, together with its first derivative, representing the relative change for each temperature interval and being approximately equal to α_T (since the proportionality factor is k_{src}^2 and this is close to unity). It should be noted that the right-hand y-axis represents $-\mathrm{d}k/\mathrm{d}T$, and therefore the negative slope of the variation of k_{src} versus the temperature.

The multiplication of the system clearly decreases as the temperature increases. This produces a reduction in k_{src} of ~–960 pcm between ambient temperature (293 K, zero power) and nominal conditions (80 MW_{th} with a temperature of ~900 K).

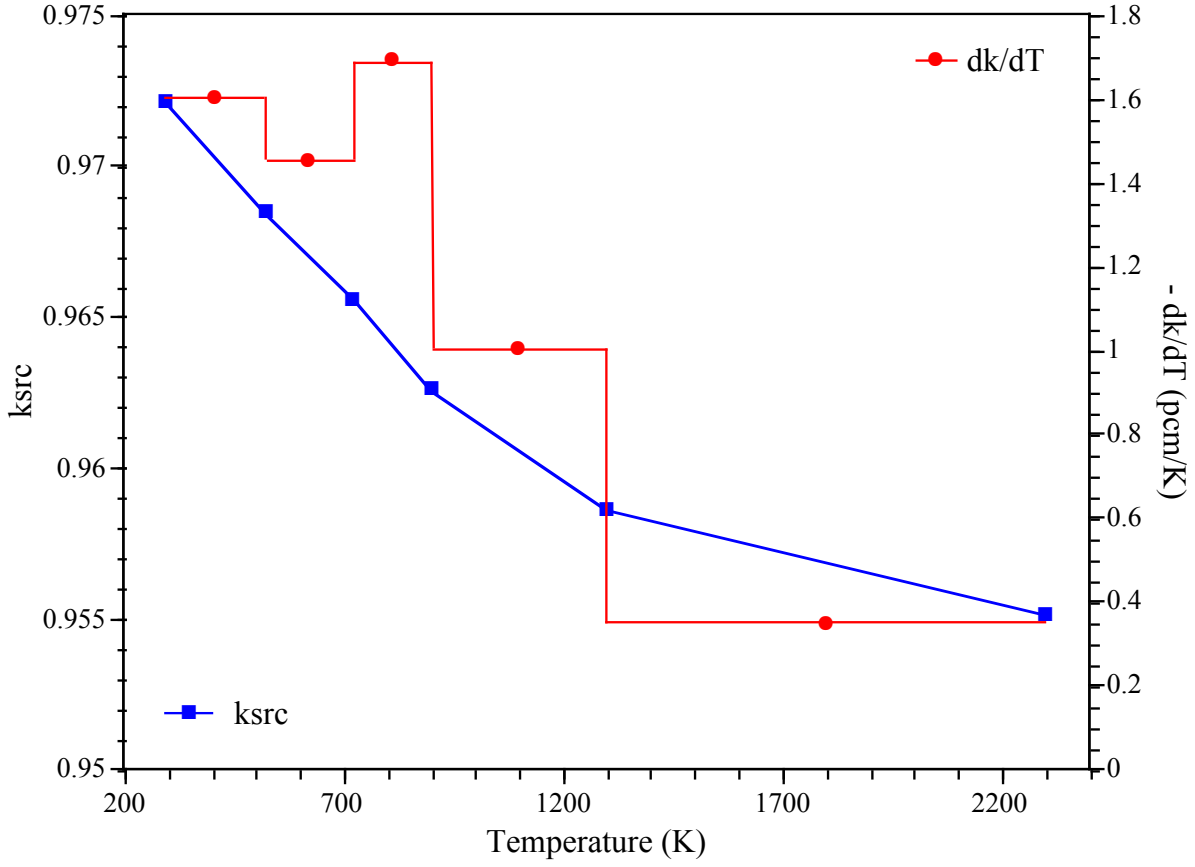

Figure 6.11. Variation of k_{src} with temperature at the BOL in EADF for the reference configuration.

For lower temperatures, the α_T presents similar values to those of a conventional PWR (–3 using UOX fuel), although smaller than for TRADE (~–10 pcm/K using LEUZrH). Nevertheless, as the temperature increases α_T seems to approach 0, although remaining negative even for high fuel temperatures (~–0.36 pcm/K between 1300 and 2300 K). In spite of this, α_T presents very reasonable values for the normal temperature range of operation (~–1 pcm/K between 900 and 1300 K), similar to those of sodium-cooled reactors (~–2 pcm/K) [105].

Similar to the start-up effects on reactivity but with the opposite sign, the result of a cold shutdown is an increase in reactivity of ~1.5 pcm/K, which in the case of a critical system would have to be dealt through precautions, given that the core gains reactivity as the temperature of the fuel is reduced and could drive to an unstable feedback situation. Therefore, the system should be designed to be subcritical enough to withstand a reactivity swing of ~1000 pcm for a temperature change from 900 K to 293 K.

6.2.5.2 Void Coefficient

Another important reactivity coefficient, partially related to the coolant temperature, is the coolant void coefficient, α_V. This coefficient represents the reactivity (or k_{src}) change with the coolant fraction present in the system. A reduction in the amount of coolant could occur due to several factors, which may or may not be temperature related. The increase of the vapour fraction in the system due to a temperature rise is a common way of controlling the reactivity in Boiling Water Reactors (BWRs). Water boiling may also occur in a Pressurized Water Reactor (PWR) accidentally due to a depressurisation of the reactor vessel. And, of course, the impact on reactivity of a Loss-Of-Coolant Accident (LOCA) must be assessed for any type of reactor, since it is behind some of the most important accidents in the history of commercial nuclear reactors, for instance Chernobyl, where excessive coolant voiding in this water-cooled graphite-moderated reactor increased the reactivity of the system due to a reduction in the neutron absorption.

The variation of k_{src} versus decreasing coolant fraction (or increasing void fraction) is presented in Figure 6.12, at the same time as its first derivative (dk/dx) in order to give an estimation of the variation of the multiplication factor for every voiding interval. The multiplication of the system is, at first, moderately reduced due to an increase in the coolant void fraction, going from the reference 0.962 to 0.926 for 40% void. As the coolant fraction decreases, α_V drops exponentially towards k_{src} ~0.66, the source multiplication of the system once all the coolant is removed from the reactor.

The moderate decrease of k_{src} for small void fractions, as in the case of the expansion of the coolant or for the injection of some argon bubbles to enhance the coolant flow, augments the safety parameters without hindering the control of the system. For example, $\alpha_V \approx -70$ pcm/% between 0 and 10% void, which will imply no burden to the accelerator since the increase in the current would be ~56 μA, 1.7% of the nominal beam current.

In case of a larger loss of coolant fraction, the negative value of α_V increases significantly, to ~–1480 pcm/% for a 90% coolant void (–940 pcm/% in dk/dx shown in the plot). Below this coolant fraction, α_V decreases (becoming more negative) rapidly, to reach a value of ~–2700 pcm/% (–1207 pcm/% in dk/dx shown in the plot) for complete coolant void. This enormous reactivity drop in the case of major coolant losses, if not an absolute guarantee, strongly indicates the stability of the system in the case of a serious LOCA accident.

These values are quite favourable if compared to the ~–190 pcm/% in a PWR [106] and especially compared to sodium-cooled systems, where reactivity changes due to voids are rather small and their sign depends on the circumstances (such as the neutron leakage) [105], and to helium-cooled systems, where the void reactivity feedback is not present.

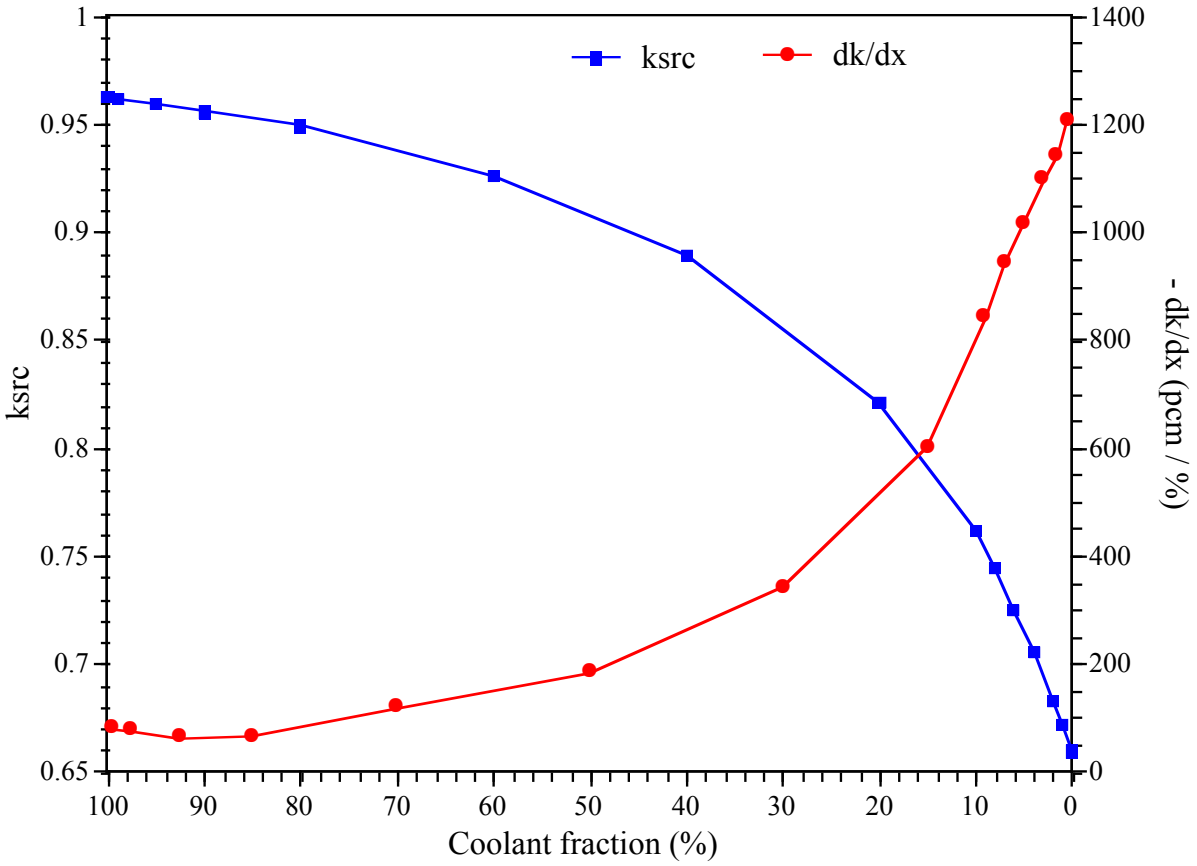

Figure 6.12. Variation of k_{src} with the void fraction in the coolant at the BOL in EADF.

In fact, these are major assets of a LBE (or lead) cooled system compared to a sodium-cooled or a helium-cooled fast system. For the same type of fuel, the prompt temperature coefficient is quite similar in all three fast systems. Conversely, the void coefficient using LBE is clearly negative and very significant for any amount of void in the system, whereas for helium-cooled systems it is nonexistent (neutrons barely interact with the helium gas), and thus total reliance on the prompt temperature feedback to compensate reactivity changes. For sodium-cooled systems, the void reactivity feedback is, at best, close to 0, as mentioned before, becoming positive for some configurations.

6.2.6 Fuel Burn-up Evolution

An essential attribute of ADS is their capability to adapt to the subcriticality level given by the fuel composition at any burn-up step. Nevertheless, this feature requires accurate design in order to maintain sensitive parameters, such as k_{src} or target power densities, below crucial safety margins. Therefore, precise analysis of the evolution of the system with time (or fuel burn-up) is necessary to accurately design such a facility.

Moreover, the evolution of the actinide inventory is of utmost importance to prove the concept of transmutation in large quantities (kg) of radionuclides and to assess the

transmutation potential of EADF. The evolution of the neutronic parameters with burn-up should indicate the feasibility of extended period of operation, without refuelling, and the composition and toxicity of the spent fuel.

The values of the main neutronic parameters at the Beginning-Of-Life (BOL) and at the End-Of-Life (EOL) are presented in Table 6.3, Their time evolution (in a 900 days cycle) shows a fuel burn-up of 20 GWd/t of fuel (or equivalently 23 GWd/tHM), which corresponds to a consumption of ~20 kg of fuel. During this cycle, the fissile enrichment drops from 13.33% of the fuel to 12.25%. The amount of plutonium in the fuel also decreases, from 18.09% of the fuel mass to 16.69%. The reduction in the fissile enrichment implies a Δk_{src} of ~2800 pcm (k_{src} at the EOL is ~0.935). Despite this drop, the energy gain at EOL, ~23.55, is still considerable and confirms the system as a formidable source of energy.

Table 6.3. Evolution of the main neutronic parameters of EADF after one burn-up cycle.

Global Parameters	Symbol (units)	BOL	EOL
Fuel mixture	MOX	$UPuO_2$	$UPuO_2$
Fuel mass	m_{fuel} (kg)	3792.0	3721.0
Plutonium concentration	m_{Pu}/m_{fuel} (wt.%)	18.09	16.69
Fissile enrichment	$m_{fissile}/m_{fuel}$ (wt.%)	13.33	12.25
Thermal power output	P_{th} (MW)	80	80
Proton beam energy	E_p (MeV)	600	600
Cycle length	T_{refuel} (d)	–	900
Fuel burn-up	(GWd/t of fuel)	–	20
Spallation neutron yield	N (n/p)	15.04 ± 0.14	15.04 ± 0.14
Source multiplication coeff.	k_{src}	0.96254 ± 0.001	0.93460 ± 0.001
Net neutron multiplication	M	26.69 ± 0.79	15.29 ± 1.00
Energetic gain	G	42.35	23.22
Gain coefficient	G_0	1.59	1.52
Accelerator current	I_p (mA)	3.23 ± 0.10	6.00 ± 0.09
Beam power	P_{beam} (MW)	1.94 ± 0.06	3.60 ± 0.06

The decline in neutron multiplication brings about an ~86% increase in the accelerator current, up to 6 mA. These parameters will determine the final engineering design of different parts of the facility, such as the cooling system and the layout of the spallation target. In this case, the current increase entails the evacuation of 3.6 MW of beam power, with a maximum energy deposition of ~6.3 kW/cm^3 (with a heat capacity of ~130 J/kg·K, the temperature increase $\Delta T \approx 5$ K/s; thus the flow of the liquid target should be carefully studied in order to avoid regions without flow, where the LBE may vaporise).

The time evolution of the source multiplication coefficient and the proton beam intensity is illustrated by Figure 6.13. The linear evolution in time (or fuel burn-up) of these two parameters is evidenced by the graph. The initial fluctuation of k_{src} is due to the effect of the

short-lived isotopes (mainly FFs) during the small time intervals (initially, three days). The slope of the linear fit shows a source multiplication loss of ~–139 pcm/GWd/t of fuel (or equivalently, such a reduction every 40 days, since burn-up is also linear with time). For I_p, the loss of reactivity brings about an increase of ~0.14 mA/GWd/t of fuel. Since most of the elements present in the fuel have already reached equilibrium concentrations by the end of the cycle, as may be observed in Figure 6.14(a), the proton current and k_{src} variations may be used to extrapolate the beam requirements for more extended burn-ups.

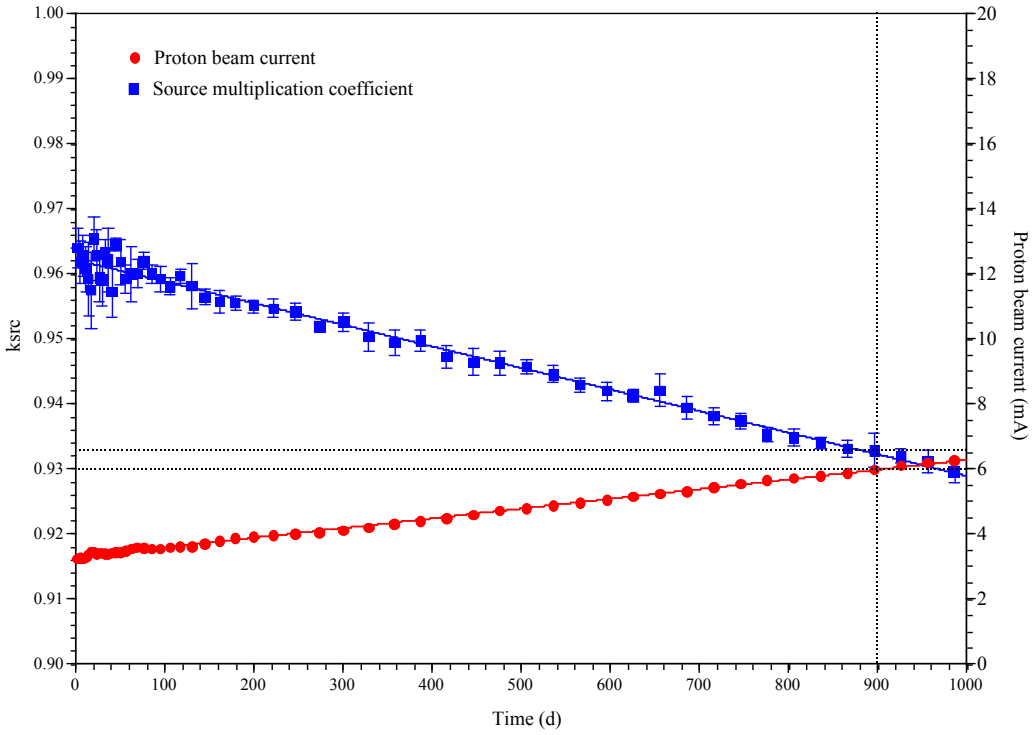

Figure 6.13. Time evolution of the proton beam current and the source multiplication for one burn-up cycle.

The evolution with burn-up of the isotopic inventory for the SPX fuel represented by Figure 6.14(a) shows how the concentration of the major isotopes in the SPX fuel (i.e. $^{235,\ 238}$U, $^{239,\ 240,\ 241,\ 242}$Pu and ^{241}Am) remain almost constant, obviously except for the small amount of used fuel. The concentration of ^{238}Pu increases by ~56%, which will contribute to the radiotoxicity of the spent fuel for more than 100 years after discharge, as elaborated in the next section. There is an increase in the inventory of higher actinides, specifically ^{243}Am and ^{242}Cm, of below 1 kg. The generation of ^{244}Cm is quite small (~20 g) but may cause some problems in the case of multiple reprocessing schemes.

By the end of the burn-up cycle (20 GWd/t of fuel, 23 GWd/tHM), the total actinides balance is ~–71 kg, of which ~–57 kg is transmuted uranium. This reduction in the mass of uranium is mainly caused by the fuel breeding process, since ^{238}U accounts for 99.5% of the uranium mass and its fission-to-absorption ratio is 11.4%. The rest of the fuel mass loss (~–14 kg) is due to the burning of plutonium. On the other hand, a small amount of MAs has been

produced, namely +401 g of neptunium, +281 g of americium and +406 g of curium produced, as illustrated by Figure 6.14(b).

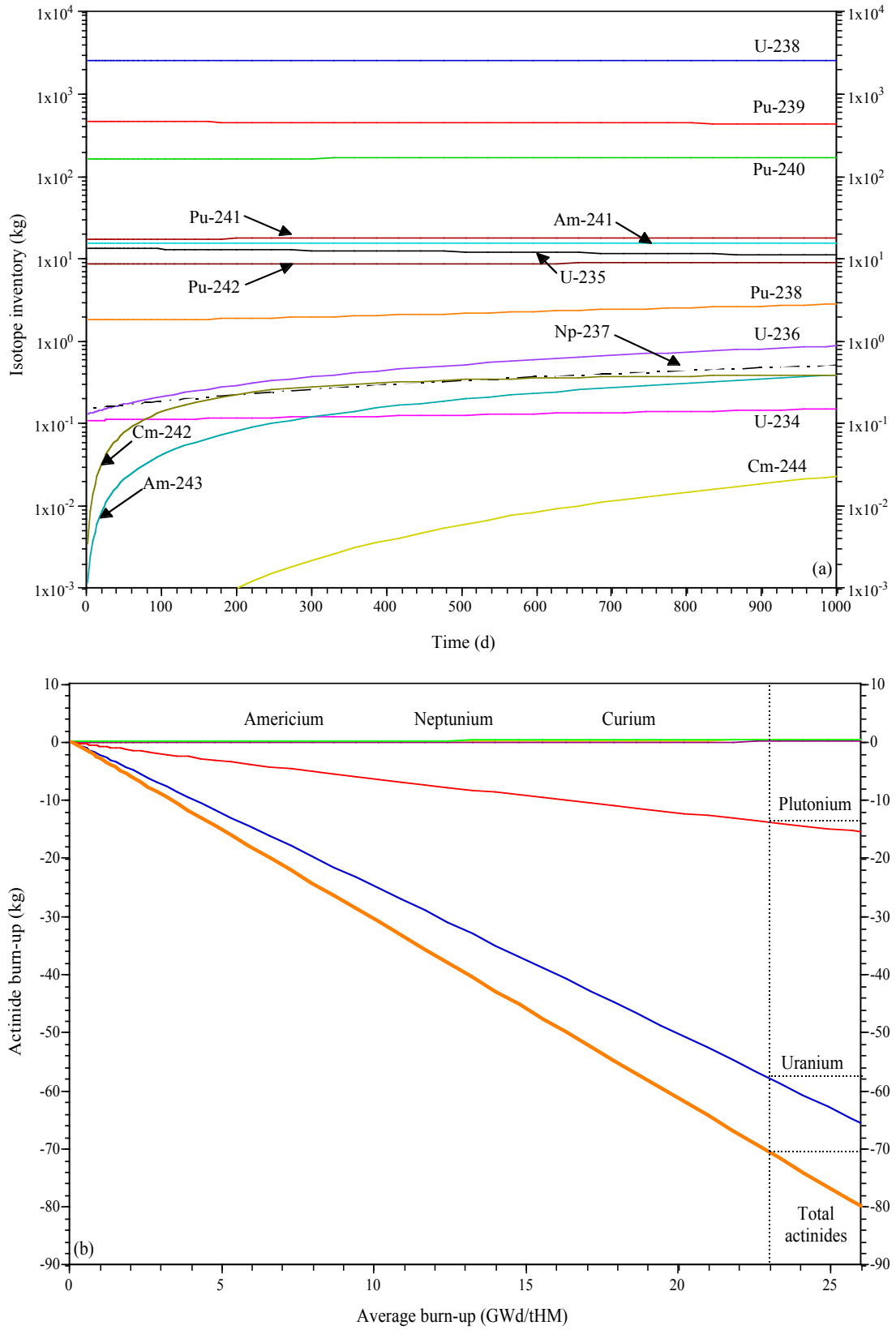

Figure 6.14. Actinide isotopic evolution (a) and mass balance (b) for the SPX fuel in EADF.

The linear relation between burn-up and elimination rates may be observed in Figure 6.14(b), where the actinide balance in EADF as a function of the fuel burn-up for the 3.35 tonnes of HM in the fuel is shown.

As the isotopic evolution of this fuel has shown, even though the plutonium concentration is reduced, there is a generation of higher actinides. Some of these isotopes contribute strongly to the radiotoxicity of the spent fuel and, although less important than plutonium due to their smaller production rates, these may pose serious radiological problems if not treated. As previously explained, the accumulation of these elements, even in deep storage repositories, entails the risk of a leak into the biosphere, as well as the menace of proliferation.

Table 6.4 compares the production of TRUs at the EOL in a PWR (using UOX and MOX) fuels and their elimination in EADF. The use of MOX fuel in thermal systems reduces the generation of plutonium but increases the production of higher actinides, in particular of americium and curium. On the other hand, EADF offers a significant amount of plutonium transmutation (–3.7 kg/tHM) and a low production of MAs, at EOL. These results clearly show the advantages of using fast systems to reduce the TRU stockpile.

Table 6.4. TRUs and LLFFs production at end of cycle in PWRs and EADF per tonne of spent fuel.

Element (kg per tonne of fuel)	PWR (UOX) 33 GWd/tHM [9]	PWR (MOX) 43.5 GWd/tHM [9]	EADF (SPX) 23 GWd/tHM
Plutonium	+9.73	+5.50	–3.70
Neptunium	+0.42	+0.16	+0.11
Americium	+0.37	+4.83	+0.07
Curium	+0.02	+0.92	+0.01
Technecium-99	+0.82	+1.00	–1.19
Iodine-129	+0.17	+0.21	–1.17

A study of LLFF transmutation potential was also carried out introducing, in one case 297 kg of ^{99}Tc in the form of $KTcO_4$, and in a second case 297 kg of ^{129}I as PbI_2, into the incineration blanket, without greatly perturbing the reactivity of the system (~1000 pcm at BOL). Table 6.4 shows the significant transmutation rates achieved (~2 kg/yr) proving the feasibility at large scale of this process.

Another way of comparing the actinide production (or elimination) rates, normalising per TW·h of thermal energy output, is illustrated by Figure 6.15. A conventional PWR (using UOX fuel) produces on average ~13 kg/TW·h of TRUs, whereas the using of MOX generates ~11 kg/TW·h. For EADF, the use of SPX entails an actinide destruction of 41 kg/TW·h, of which 34 kg/TW·h is natural uranium. These values stabilise after ~3 GWd/tHM. The plutonium transmutation rate stabilises quickly to 8.1 kg/TW·h.

For MAs, the neptunium levels rise at first due to the breeding process reaching stable levels (230 g/TW·h) at ~4 GWd/tHM. The quantities of americium and curium produced (160

g/TW·h and 16 g/TW·h respectively) are lower than those produced in PWRs using UOX (~800 g/TW·h and ~33 g/TW·h respectively) and much smaller than those produced with MOX (~4.8 kg/TW·h of americium and 910 g/TW·h of curium).

For LLFFs, at equal energy output such a strategy may eliminate the production of at least 2.5 LWRs; the transmutation rate for the previous loading is ~–2.6 kg/TW·h of ^{99}Tc or ^{129}I, whereas the production of a conventional LWR is ~1.01 kg/TW·h of ^{99}Tc and 221 g/TW·h of ^{129}I. The transmutation half-life of such a process is ~100 yr for both isotopes, worse than the ~30 yr calculated in Chapter 5 for a 10^{14} n/cm^2/s thermal flux. This transmutation efficiency may be improved, as shown by [21] and explained later, by diluting these isotopes in the periphery of the core in a large system.

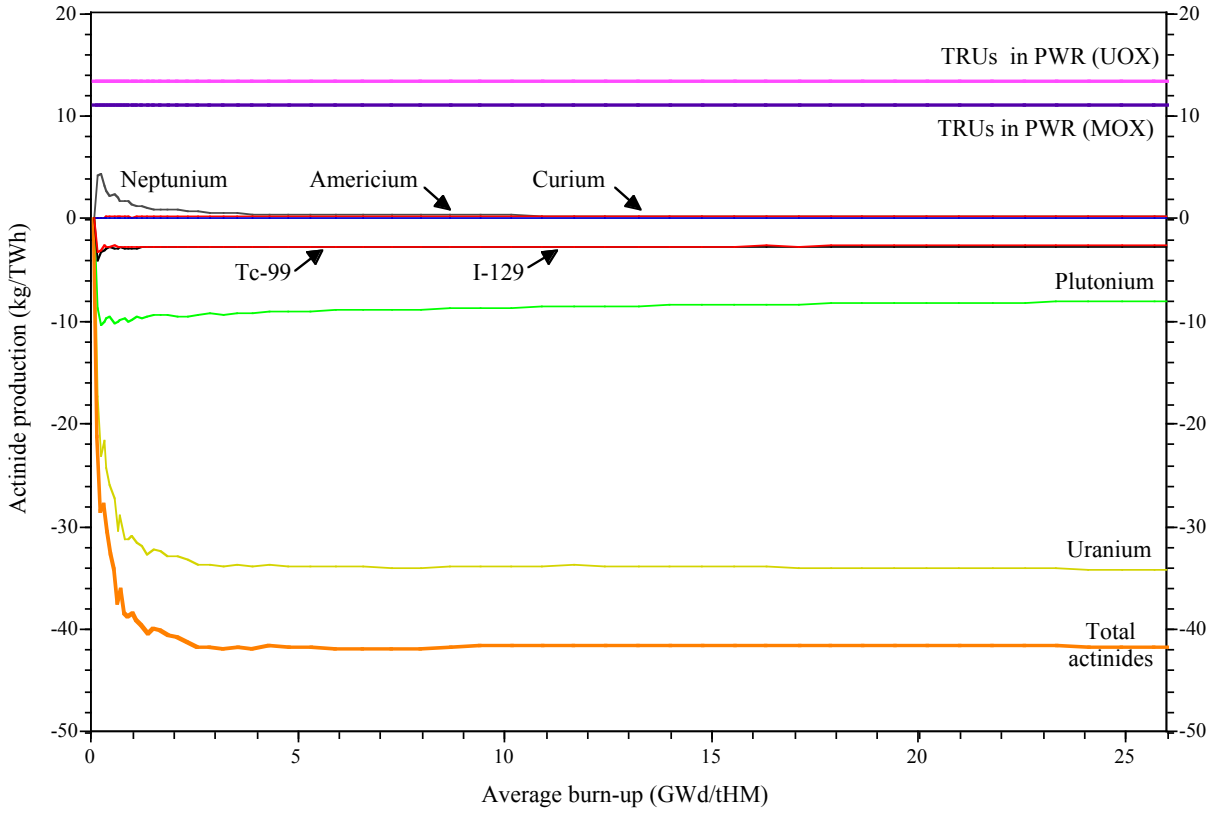

Figure 6.15. Comparison of actinide production per TW·h between EADF and a PWR (using UOX and MOX), as a function of fuel burn-up.

The comparison between the actinide balances clearly indicates that the use of $UPuO_2$ fuel in a lead-cooled system is an efficient way of reducing the stockpile of plutonium (rather than merely maintaining its present levels), with little MAs generation. Moreover, the only limitation on plutonium content in an ADS is the critical mass of the fuel, in order to maintain subcriticality.

On the other hand, the use of MOX in a critical system (either thermal or fast) is limited by the worsening of the dynamic values of the system (e.g. the delayed neutron fraction) and the

lack of negative feedback related to Doppler broadening. Moreover, any system based on the breeding of ^{239}Pu as fuel may pose proliferation problems. Even though in this particular case the concentration of this isotope of plutonium is slowly reduced, as illustrated in Figure 6.14(a) and the decreasing fissile enrichment, the use of a fuel with a plutonium concentration below equilibrium would entail the production of plutonium. As mentioned before, in the case of a sodium-cooled reactor initially fuelled with enriched uranium, this would entail the production of ~18% highly fissile plutonium mass, once ^{239}Pu reaches equilibrium.

6.2.7 SPX Toxicity at Discharge

Comparison of the radiotoxicity of the SPX fuel at BOL and at EOL shows an increase of ~20% after the burn-up cycle for ~100 years after discharge. This fact is related to the increase in the concentration of several specific isotopes, as may be discerned by comparing Figures 6.14(c) and 6.16. The dose is dominated by ^{238}Pu and ^{241}Am in the first decades, and led by ^{241}Pu after that until ~100 years after discharge. The increase in the concentration of these isotopes is the cause of higher toxicity of the SPX spent fuel compared to its initial value.

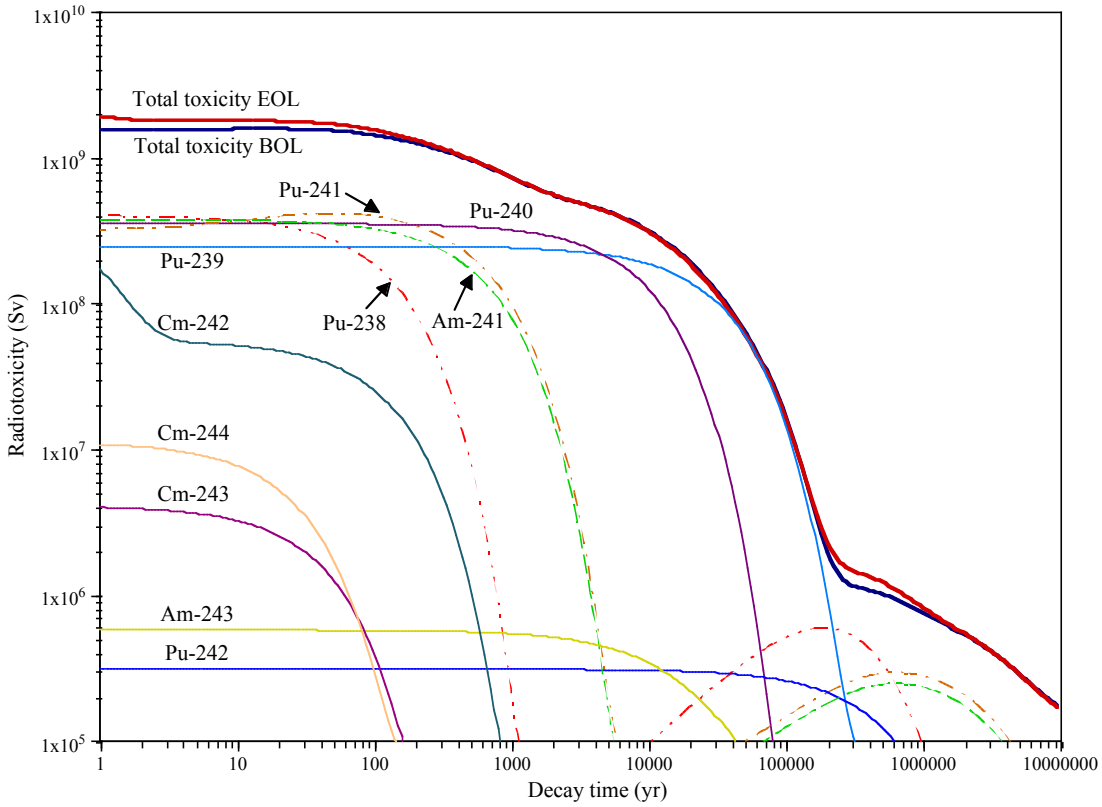

Figure 6.16. Evolution of the radiotoxic inventory for the SPX spent fuel in EADF.

After the first 100 years, ^{240}Pu becomes the most hazardous waste component, to be replaced by ^{239}Pu between 5,000 and 200,000 years after discharge. In this range of time, the

radiotoxicity drops more than two orders of magnitude and both fresh and spent SPX fuel present the same values due to the clear domination of ^{239}Pu. Beyond 200,000 years, ^{238}Pu, ^{241}Pu and ^{241}Am consecutively take the lead again, appearing from the α-decay chain of ^{242}Cm and ^{245}Cm and the β^--decay of ^{241}Pu, respectively.

The consequences of nuclear reactions other than fission in ^{239}Pu, particularly capture and (n, 2n), seem to be the origin of the increase in radiotoxicity of the SPX spent fuel. The production of ^{238}Pu (a minor isotope in PWR spent fuel) entails an increment in the dose received through waste handling during the first century after discharge. The accumulation of ^{241}Am, ^{241}Pu and, later, ^{240}Pu has the same origin and similar implications at a longer time scale.

The production of curium isotopes, although rather scarce (~406 g after discharge), may have a larger impact on the toxicity of the spent fuel if double-strata transmutation schemes are applied; thus curium production should be limited to avoid further production of ^{238}Pu, ^{241}Pu and ^{244}Cm.

6.2.8 Conclusions: The Use of MOX Fuel in Fast ADS

In the roadmap to the demonstration of a fast ADS for energy production and HLW transmutation there is a clear need to construct and operate a real power fast ADS which, taking advantage of the experience and knowledge attained through TRADE concerning the physics behaviour during operation in a large number of situations, will prove those concepts and help to foresee technological problems in the path towards an industrial prototype.

The preceding analysis confirms that the 80 MW_{th} lead-bismuth cooled EADF fulfils these requirements. The feasibility of such a device has been established with only a few technological problems yet to be solved, such as the cooling of the spallation target and the feasibility of the windowless option. The neutronic parameters show high neutron fluxes requiring acceptable proton intensities (3-6 mA at 600 MeV), moderate fuel temperatures and very small power peaking (~1.16), hence confirming some of the safe features of the device. The large negative void ($\alpha_V \approx -70$ pcm/% for small void fractions and up to $\alpha_V \approx -1200$ pcm/% for complete void) and temperature (i.e. ~–1.5 pcm/K around the 900 K nominal fuel temperature) coefficients evidence the passive safety of EADF.

The use of LBE as a coolant for EADF has been compared with other alternatives, in particular with the use of helium or sodium. The use of helium as coolant offers the advantage of a harder neutron spectrum, enhancing fission in TRU, whereas sodium presents a noticeably softer neutron spectrum. On the other hand, the aforementioned reactivity feedbacks of a LBE-cooled device are more favourable than those of the other options,

especially if they are compared with the non-existence of void reactivity feedback in helium and with the, at best, very small coefficient in sodium-cooled systems.

A value of $k_{src} \approx 0.96$ was chosen due to the need to operate far from criticality at all times, taking into account the limitations in ND presented in Chapter 4. The dynamic behaviour of the neutrons (spallation and fission) has also been investigated, showing some of the basic differences in terms of diffusion between thermal and fast systems.

The short prompt neutron lifetime of the system (~1 μs compared to 50 μs in TRADE) gives a much faster neutron population decrease than in a thermal system, for the same neutron multiplication. This fact shows the great sensitivity of a fast system to beam interruptions, since after a 1 ms beam trip the neutron population in EADF would drop to 0.1% of its initial value. Hence the need to investigate these types of events in a system such as TRADE, whose safety features are well known and give a slower response to beam interruptions and reactivity insertions.

Study of the effect of burn-up on the fuel composition is another goal of EADF. A fuel burn-up of 23 GWd/tHM eliminates a significant amount of plutonium with a small MAs production, particularly compared to the use of MOX in LWRs. In fact, comparing TRU production in terms of energy output, EADF may eliminate ~60% of the plutonium produced in a PWR using UOX. The transmutation of large quantities of ^{99}Tc and ^{129}I is also possible without disturbing the multiplication of the system, posing fewer problems in terms of safety and neutron economy.

These results show that the use of MOX fuel in fast systems is an option in order to reduce the plutonium stockpile at a considerable rate, obtaining thermal power at the same time. However, this method may not be the optimal approach to plutonium elimination since it is based on the breeding of fissile plutonium itself, thus limiting the transmutation rate. Moreover, the presence of plutonium in the core entails an increase in the MAs stockpile, even in fast systems, eventually shifting the problem towards the elimination of MAs, reduced in mass but comparable in radiotoxicity.

Furthermore, these uranium-plutonium fuels could also be used to enrich plutonium if its initial concentration was lower than its equilibrium concentration in the system, therefore posing serious proliferation threats. In fact, this is one of the reasons (together with concerns about the use of sodium in proximity to water) why Super-Phénix was shut down in 1998 by the French government after strong pressure from public opinion.

6.3 HLW Transmutation Strategies and Assessment

From the previous section, it seems clear that the use of uranium-plutonium fuel is not effectively closing the fuel cycle since the production of MAs is enhanced by these types of fuel, even when used in fast systems.

Therefore, two main approaches to HLW transmutation have been conceived: (i) the use of a thorium-based fuel, using plutonium as a seed to start the fission chain, thus eliminating a significant amount of TRUs while producing energy based on the thorium cycle. The use of devices operating in this way would represent ~30% of the installed nuclear power capacity. (ii) The use of a few ADS at the end of a multiple strata fuel cycle, where these systems would be heavily loaded with MAs in order to eliminate them through the use of different fuel matrices, effectively closing the fuel cycle. These systems would represent ~9% of the energy produced by nuclear power.

The first is the approach proposed by C. Rubbia at CERN, in which part of the energy load is generated by thorium-based EA, while the second is the approach taken in the multi-tiers strategies proposed by the Japan Atomic Energy Research Institute (JAERI) in the scope of the OMEGA (Options Making Extra Gains for Actinides & FFs / One Method Expecting General Acceptance of Nuclear Energy) programme or alternatively by the French Commissariat à l'Énergie Atomique (CEA).

6.3.1 The Use of Thorium-TRU Fuel in ADS

As previously explained, the thorium-cycle offers a realistic alternative to the use of MOX and other uranium-plutonium fuels to reduce the TRUs stockpile and obtain energy from this process. This may be a strategy for the use of the EA, eliminating large quantities of TRUs coming directly from spent fuel in a single integrated cycle (single stratum), using thorium-based fuel, since this fuel offers reduced production of those elements. This scheme was thoroughly studied in [21] as an alternative to geological storage to eliminate the HLW for the case of Spain.

The basic model of a lead-cooled 1 GW_{th} EA was taken as a base in order to assess the potential of such a strategy. The thorium oxide fuel was 'enriched' with ~24% TRUs, i.e. 2.95 tonnes, from PWR spent fuel, of which 20% was plutonium (~2540 kg), 1.3% neptunium (~158 kg), 2% americium (~250 kg) and 0.04% curium (~6 kg). The isotopic composition was that of PWR spent fuel with a level of burn-up of ~33GWd/tHM, after a cool-down period of ~15 years.

This TRU concentration is optimal to maximise the transmutation rate avoiding large reactivity swings between Beginning-Of-Cycle (BOC) and End-Of-Cycle (EOC), thus keeping the proton current below 15 mA for the burn-up cycle. Figure 6.17 shows the evolution of k_{src} with burn-up for that particular fuel load in the EA. The initial k_{src} of ~0.974 reaches a maximum value of ~0.986 at 50 GWd/t of fuel. This maximum is reached due to the increasing concentration of ^{233}U, which has reached ~330 kg, i.e. approximately half of its equilibrium concentration, and even though the mass of plutonium has been reduced by 364 kg (~14% of the initial mass), as illustrated by Figure 6.18. A higher initial concentration of plutonium would entail of the reduction the fuel mass in order to keep the core safely subcritical. Hence, the breeding of ^{233}U would be reduced and the initial fissile elements would be burned faster, producing a larger reactivity swing. In fact, $\Delta k/k$ is 0 between BOC (0 GWd/t) and EOC (120 GWd/t) for this particular TRU loading, as may be observed in Figure 6.17.

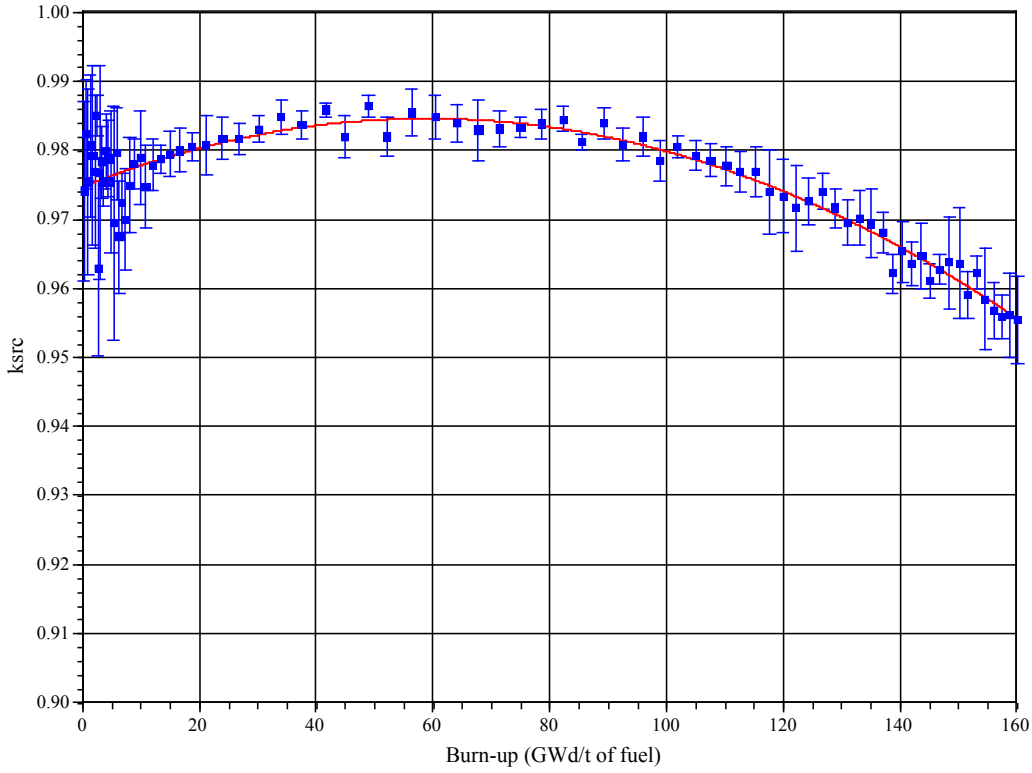

Figure 6.17. Evolution of k_{src} with burn-up for an EA using (76% thorium / 24% plutonium) oxide fuel.

Figure 6.18 shows the evolution of the actinide inventory in the system for a burn-up cycle of 120 GWd/t of fuel (~3 years). The transmutation of plutonium with this configuration during this period is –770 kg (–30% of the initial plutonium mass). The transmutation of americium is also important, accounting for –71 kg (–30% of its initial mass), although some of it is transformed into curium (+23 kg, four times the initial mass). The balance of ^{237}Np is also rather favourable since –68 kg (–45%) is eliminated.

As previously explained, since the thorium fuel is basically plutonium-free, any quantity of TRUs added will decrease to their equilibrium concentrations. Since the equilibrium concentrations of TRUs are at least 10^{-5} that of ^{232}Th (see Figure 6.2), the TRU masses will be reduced to tens of grams at equilibrium. Figure 6.18 shows that none of the hazardous elements used as 'enrichment' has reached its equilibrium concentration, thus all their masses will continue to decrease in a second cycle. The curium concentration is the only one that rose, but this has already started decreasing towards equilibrium. Therefore, if the equivalent mass of the transmuted elements was added to the fuel at the end of the cycle, a similar transmutation rate would be obtained.

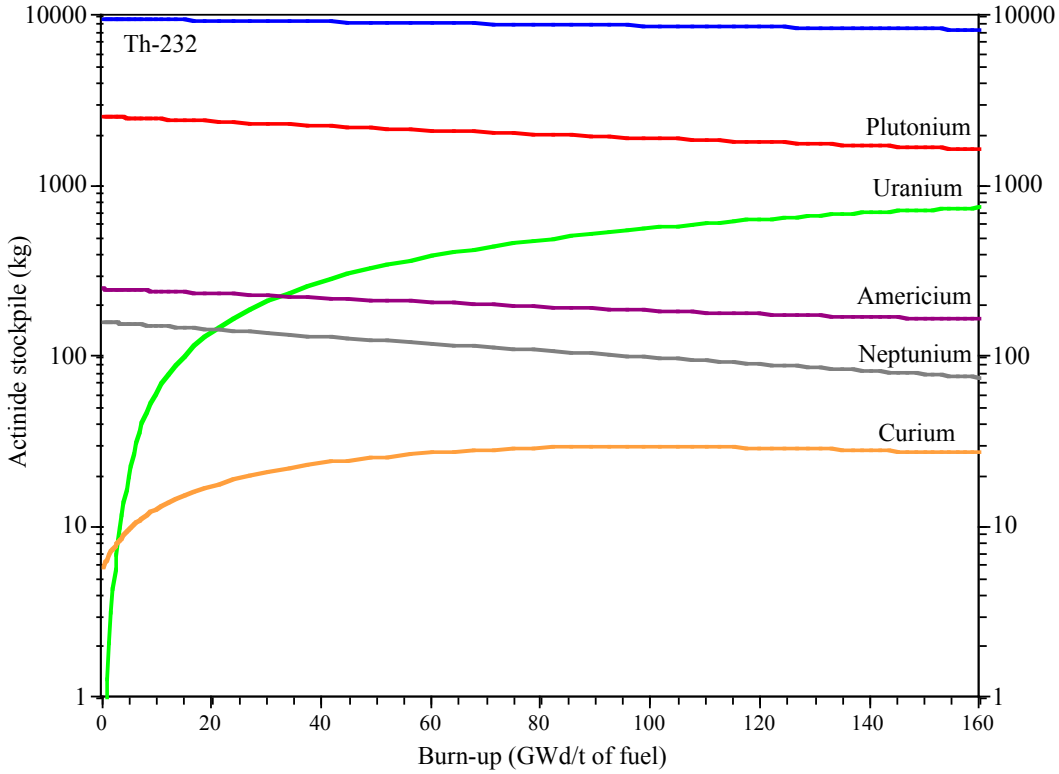

Figure 6.18. Stockpile evolution for different elements present in a 1 GW_{th} $ThPuO_2$ EA.

The isotopic evolution of the system is summarised in Figure 6.19. Obviously, there is a large production of ^{233}U (~610 kg), since the cycle is based on the breeding of this fissile element. On the other hand, the fuel presents three orders of magnitude smaller quantities of ^{236}U than of ^{233}U. This shows again the very small equilibrium concentrations of higher actinides in the thorium cycle, since any TRU produced in this cycle would have to be produced by neutron capture in ^{236}U.

As previously mentioned, the concentration of plutonium is significantly reduced (–770 kg, –30% of the initial concentration), in particular that of ^{239}Pu (–752 kg, –50%) and ^{241}Pu (–61 kg, –31%). A similar situation occurs with ^{237}Np (–68 kg, –43%) and ^{241}Am (–83 kg, –38%), although part of their mass is transformed into ^{238}Pu (+80 kg, +165%) or , in the case of

^{241}Am, into ^{242*}Am (+4.3 kg, +1365%), ^{243}Am (+7.3 kg, +25%) and curium (+13.6 kg, +246%), as shown in Figures 6.19(a) and 6.19(b).

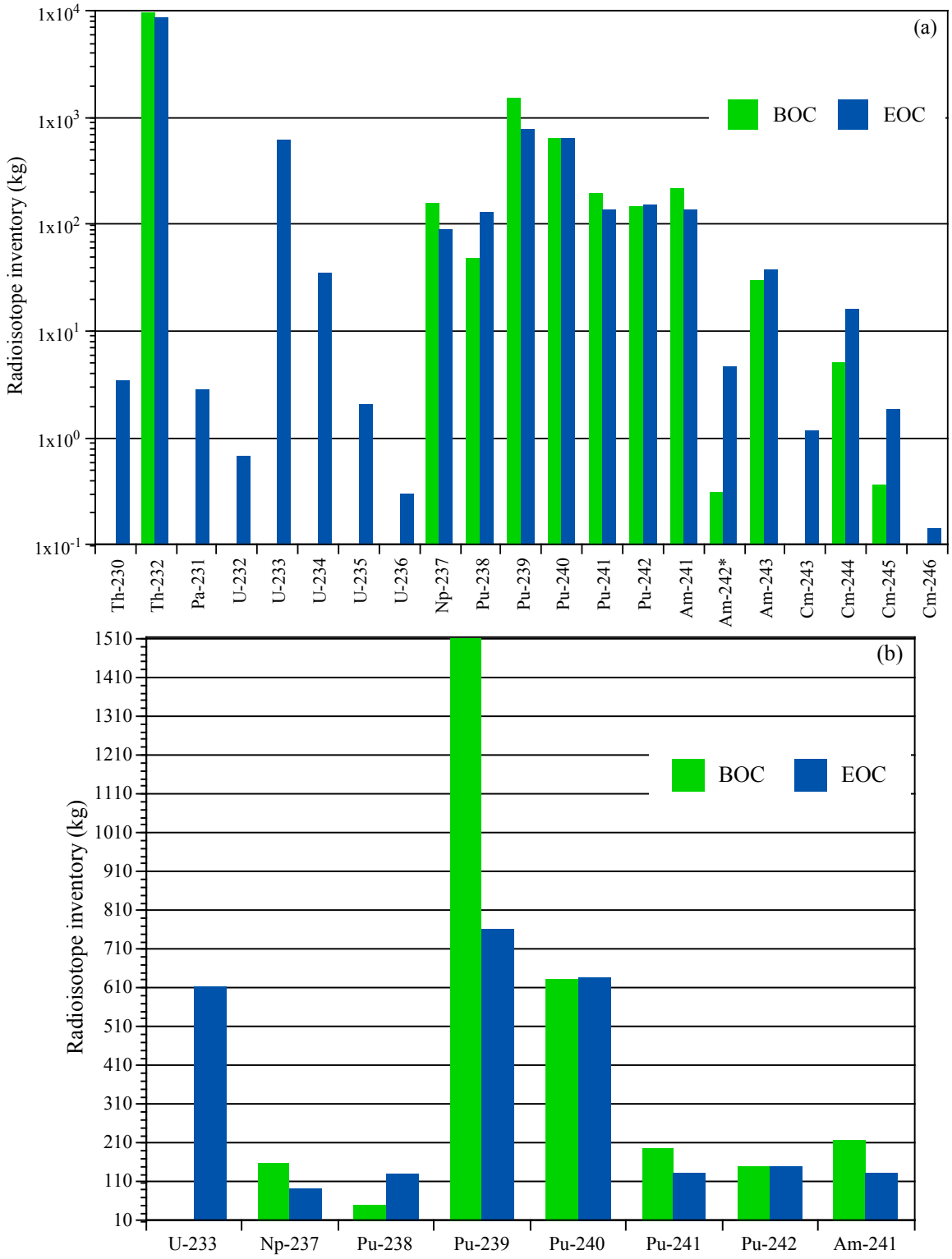

Figure 6.19. Isotopic inventory in a 1 GW_{th} EA using $ThPuO_2$ fuel for 120 GWd/t fuel burn-up.

In order to compare the HLW transmutation capability of different systems the actinide balances per TW·h in a PWR, EADF and EA have been summarised in Table 6.5. The advantages of an EA in terms of TRU elimination are clearly visible. For the same energy output, one EA could eliminate the waste of ~2.5 conventional PWRs. This applies not only to plutonium but also to neptunium and americium, whose mass balances are clearly negative, unlike in the case of a MOX-based fast system, such as EADF. The mass of curium increases slightly mainly being ^{244}Cm (α-decay, $\tau_{1/2} \approx 18$ yr), which could be reinserted in the reactor in a second cycle or extracted and placed in a secular repository for ~50 years to become ^{240}Pu, which may be reinserted into the fresh fuel.

Table 6.5. Comparison of the actinide balance per TW·h for different systems, including the EA.

Actinide balance (kg/TW·h)	PWR (UOX) 41 GWd/tHM [9]	EADF ($UPuO_2$) 23 GWd/tHM	EA ($ThPuO_2$) 120 GWd/t of fuel
Plutonium	+11.3	–8.1	–27.6
Neptunium	+1.18	+0.23	–2.55
Americium	+1.04	+0.16	–2.65
Curium	+0.03	+0.016	+0.86
Technecium-99	+1.01	–2.62	–3.8 [21]

For ^{99}Tc, [21] shows that with a dilution in lead of 260 ppm, that is a fractional density of 2.686 mg/cm^3, 50 kg/yr of ^{99}Tc could be transmuted in 25 m^3 in an EA, thus resulting in a transmutation half-life of 1.4 years, much shorter than in a well thermalised spectrum (~15 years for ^{99}Tc calculated in Chapter 5).

Effectively, these numbers imply that the reference 1.5 GW_{th} EA [1] is able to eliminate continuously the TRUs and LLFFs waste of 1.5-2 LWRs (3 GW_{th}), thus potentially allowing a progressive shift from the uranium-plutonium fuel cycle to the less polluting thorium fuel cycle operated in fast ADS.

The application of this strategy to the elimination of nuclear waste in the UK would entail the construction of ~8 EA in order to eliminated the HLW of the 23 operating reactors (11.85 GW_e). These EAs would also add 4.74 GW_e (40% thermal efficiency) to the grid (~30% of the nuclear energy once the units were connected to the grid and ~5% of the total electrical energy production) allowing a reduction in the use of greenhouse gas-emitting energy sources and the replacement of the oldest nuclear power plants after their decommissioning. The case of Spain (9 operating reactors) would be similar, requiring the construction of 5 EA units, which would produce ~3 GW_e. On the other hand, France would require the construction of ~42 EA units (~25 GW_e) to deal with the waste of its 59 reactors (63.47 GW_e).

This transmutation scheme was designed to eliminate 99.9% of the radiotoxicity of the HLW, reducing its toxicity to that of the original fuel uranium ore in ~500 years, as presented in

Chapter 2 by Figures 2.1 and 2.3. This scheme would eliminate the need for a geological repository, only requiring secular disposal for the remaining waste.

Another great advantage of this transmutation strategy is its inability to enrich plutonium to build nuclear weapons, since the HLW from spent fuel is used directly to produce the EA, avoiding plutonium separation. A small fraction of ^{238}U may be added to the fuel to avoid production of uranium with high ^{233}U (fissile) concentrations.

6.3.2 Double Strata Strategy for Transmutation of MA

The use of ADS as a back-end of the fuel cycle has been lately proposed as an alternative method to geological disposal after HLW separation. In fact, several strategies have been suggested, some including the use of MOX in LWR, others the use of Fast Burner Reactors (FBR) or both, to eliminate the plutonium present in the HLW. They may be summarised in the double strata scheme presented in Figure 6.19, where the first stratum includes the options just mentioned. As explained previously, these processes produce an increasing amount of MAs, which cannot be effectively eliminated in those systems without an unacceptable degradation of their safety parameters. Therefore, a second stratum has been proposed in order to deal with these elements.

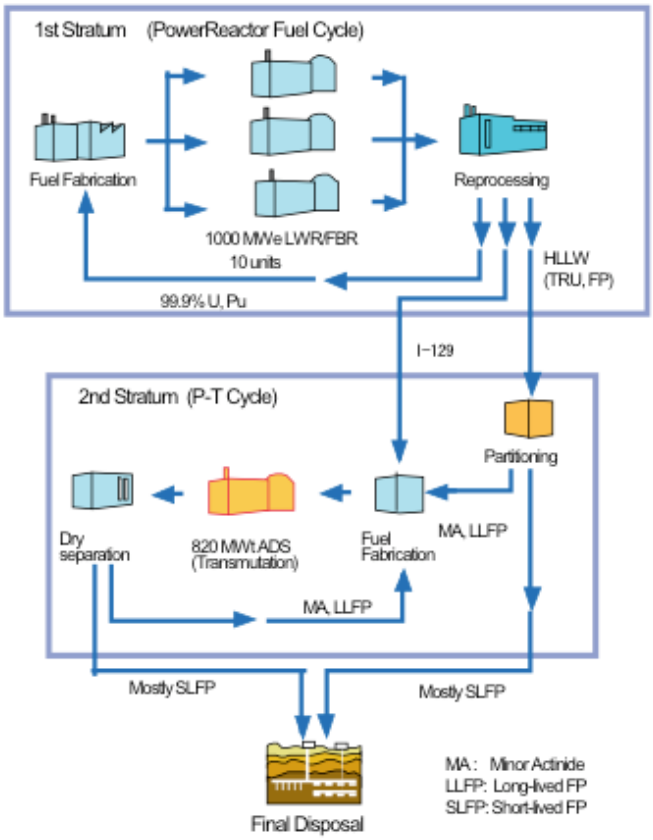

Figure 6.20. HLW management strategies: Advance Fuel Cycle and Double Strata Fuel Cycle [19].

The so-called Partitioning & Transmutation (P&T) stratum is supposed to take the spent fuel effluents after reprocessing and, once the appropriate fuel is fabricated, eliminate them in an ADS dedicated to this purpose. This strategy foresees a mass flow from the first stratum to the second one of ~3.5% of the mass of the spent fuel, 3.4% corresponding to FFs and 0.1% corresponding to MAs.

Once the partitioning is achieved, the mass inserted in the ADS depends on which LLFFs transmutation scheme is chosen. In the case of only MAs being used in the fuel, the aforementioned 0.1% (i.e. ~30 kg/GW_e/yr from a LWR) would finally make it into the ADS. If ^{99}Tc and ^{129}I were also included, 0.25% of the initial spent fuel would be treated in the transmutation stage. In any event, the mass of the elements finally configuring the ADS fuel would be minimal compared to the initial mass of spent fuel.

Another important asset for this transmutation strategy is the independent development of each stratum. Although the P&T cycle still requires some research and development (R&D), which is, in fact, the core of this dissertation, this R&D only refers to the second stratum. Therefore, the commercial cycle remains unaffected except for the HLW accumulation due to the delay in applying transmutation.

It should be noted that, although the size of the waste stream finally going to the repositories would be greatly reduced, these would still be required, although with much less restrictions on safety and secular confinement, particularly to hold the short-lived FFs.

6.3.2.1 Specific Fuel Matrices for MAs Transmutation

The high power densities and the deep levels of burn-up foreseen for these MA burners entail the development of new types of fuel matrices capable of containing large amounts of MAs (some of them being volatile) and withstanding extreme irradiation without failing. The MA fuel distribution should be homogeneous, with no separation among MAs, in order to facilitate fuel fabrication and reduce handling doses. For these purposes, several fuel types have been considered, and the most promising ones may be summarised in three groups: metallic, oxide and nitride fuels. Table 6.6 shows some general information on these types of fuels.

Table 6.6. Main characteristics of some of the dedicated fuels for MAs transmutation [107].

Fuel characteristics	Metallic fuels [TRU – Zr]	Oxide fuels [TRU – O_X]	Nitride fuels [TRU – ^{15}N]
Heavy metal density (g/cm^3)	~12.5	~10	~13.5
Melting point (K)	~1500	~3000	~3000
Thermal conductivity (W/m·K)	~20	~3	~20
Reprocessing knowledge and irradiation database	Limited	Good	Poor

All of them present advantages and disadvantages, starting from the high density (required to produce a harder neutron spectrum), high conductivity but low melting point of the metallic fuels, to the high melting point and good knowledge of but low conductivity of the oxide fuels. The properties of the nitride fuels seem remarkable: high density, high conductivity, high melting point and low irradiation damage. On the other hand, these are poorly known fuels and they require the enrichment of the nitrogen with ^{15}N (0.366% of natural nitrogen), since (n, p) reactions in ^{14}N may be significant, producing ^{14}C ($\tau_{1/2} \approx 5730$ yr).

Therefore, all these fuel types require further investigation in order to determine the best one to be used in the MA burner. This is a key issue to the development of this transmutation scheme, and why several research institutes, such as ANL (US), CEA – Cadarache (France) and JAERI (Japan), among others, are currently putting great emphasis on the study of one or more of these fuel types under irradiation.

6.3.2.2 ADS Dedicated to Transmutation of MAs

In this transmutation strategy, ADSs have been proposed to eliminate large amounts of MAs in a safe and efficient way. Their intrinsic safety due to their operation below criticality makes them ideal for handling fuels presenting negative safety characteristics, such as small delayed neutron fractions and low or even no negative reactivity feedbacks.

The thermal power output of such a device is still undecided, with systems ranging from a couple hundred MW to 1 GW under consideration. A possible candidate may be a 250 MW_{th} compact reactor, which, due to its high specific power and compactness, would be a perfect industrial prototype to explore a large number of transmutation schemes. Therefore, preliminary calculations were performed in order to study the viability of such a strategy and assess the achievable transmutation rates.

The reactor is a stainless steel cylindrical tank of ~9 m height and 4.4 m diameter containing the fuel core and the LBE coolant, similar to EADF. The cylindrical fuel core is 1.9 m in height and 1.7 m in diameter. The core is formed by 7.5 mm × 7.5 mm fuel cells containing ~6 mm diameter cylindrical fuel pins. The central part of the core was voided in order to insert the proton beam line and create a ~30 cm buffer region in order to effectively diffuse the spallation neutrons.

Several types of fuels were initially tested to evaluate the maximum mass of fuel that could be inserted in the core without reaching criticality, illustrated by Figure 6.21. A comparison of coolants for some of these fuels was also performed in order to assess the specific power capabilities of these systems. The mass, for a given fuel volume, was varied increasing the smear density of the fuel, since, in the final design, some void may be required to accommodate the large quantities of volatile FFs produced by the very long burn-ups.

Of the different fuels analysed, the use of pure metallic MAs offers the largest actinide masses below criticality, with the LBE case being closest to criticality, followed by helium and sodium. For TRUs, using the LWR standard spent fuel composition with a 10% smear density (~870 kg of oxide fuel), the LBE-cooled reactor becomes supercritical ($k_{eff} \approx 1.13$), whereas the same mass in sodium and helium are quite subcritical. This behaviour is similar to the EADF case, where the sodium coolant and especially the helium coolant (due to the neutron escapes) made the system noticeably more subcritical.

The addition of 10% waste plutonium to the metallic MA mixture reduces significantly the critical mass of fuel, going from 3.4 tonnes to 2.5 tonnes of fuel, which is important for the assessment of possible combined Pu-MAs burning strategies. The use of fuel matrices such as ^{15}N and zirconium softens the neutron energy spectrum via scattering reactions, hence slightly reducing k_{eff} for a given MA mass.

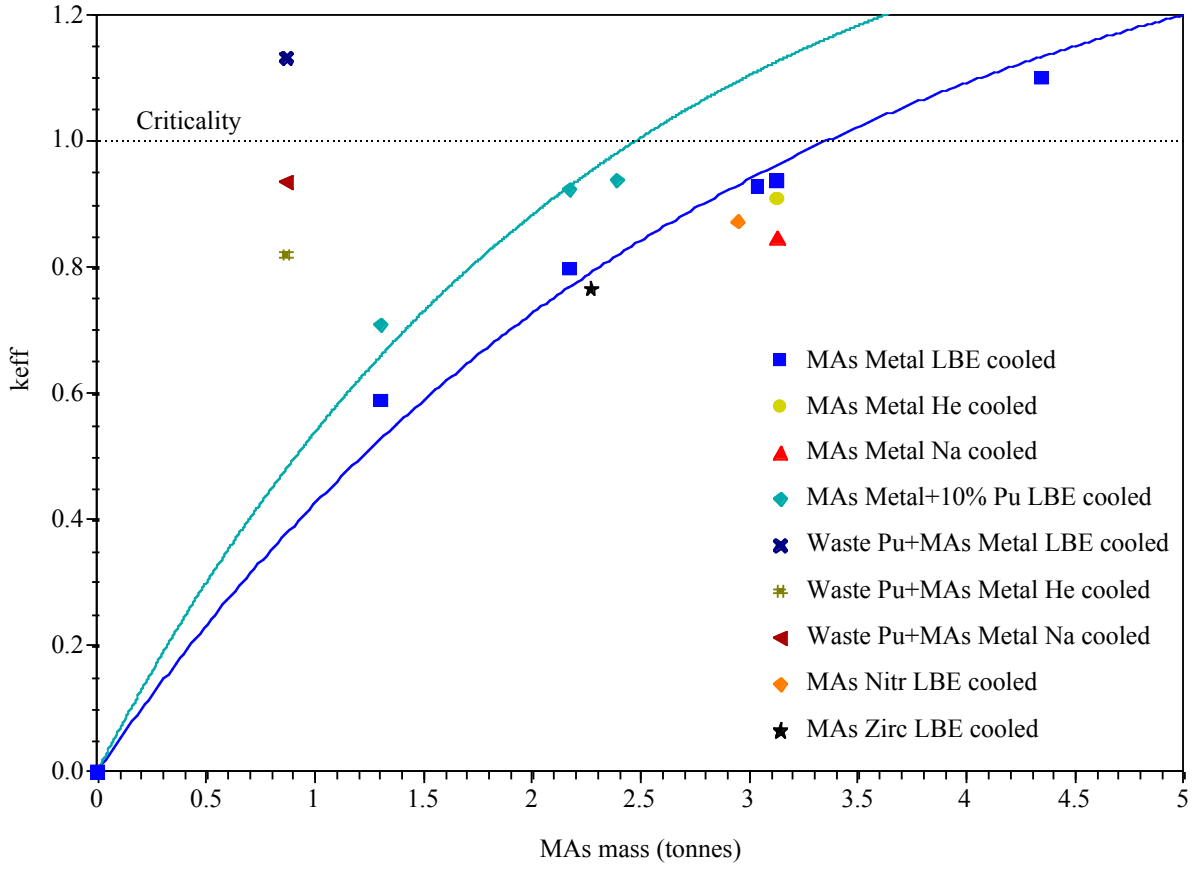

Figure 6.21. Effective neutron multiplication for different fuel types and quantities in the 250 MW_{th} MA burner.

Therefore, a pure MA metallic fuel was chosen as a case study in order to evaluate the transmutation potential of the device. The MA composition is similar to that coming from a first stratum combining LWR UOX and MOX use, i.e. 12.5% ^{237}Np, 50% ^{241}Am, 25% ^{243}Am and 12.5% ^{244}Cm. The initial fuel mass inserted in the core is ~2.16 tonnes, in order to avoid criticality conditions during the burn-up cycle, as illustrated by Figure 6.22(a).

During the extended burn-up cycle k_{src} changes significantly, from the initial k_{src} of ~0.786 (producing an energy gain of $G \approx 4.3$) to a maximum k_{src} of ~0.969 after 4.5 years (1650 days) of operation, equivalent to a fuel burn-up of 225 GWd/tHM. This very low initial k_{src} entails an excessive proton current (~64 mA), proving the need to increase the initial fuel mass. However, the large reactivity increase after 225 GWd/tHM, i.e. $\Delta k \approx 1830$ pcm, makes that impossible, since the system would become supercritical during burn-up if the fuel mass was significantly increased. Therefore, it will be necessary to add plutonium (~10%) to the MA fuel in order to increase the initial reactivity of the system and reduce the reactivity swing during burn-up.

In the maximum multiplication state, the system has an energy gain of $G \approx 49$, requiring a beam current of ~10 mA. The rise in k_{src} is due to a combination of the decrease in the neutron captures in the MAs, the increase in the fissile isotopes previously bred and the relatively small FF capture fraction (6% of the neutron absorbing reactions), as observed in Figure 6.22(b). The fissile isotopes responsible for the increase in k_{src} are: ^{238}Pu (240 kg, for which 60% of the absorbed neutrons produce fissions, as explained in Chapter 4), ^{245}Cm (45 kg, 85% fission fraction) and, to some extent, ^{239}Pu (15 kg, 80% fission fraction).

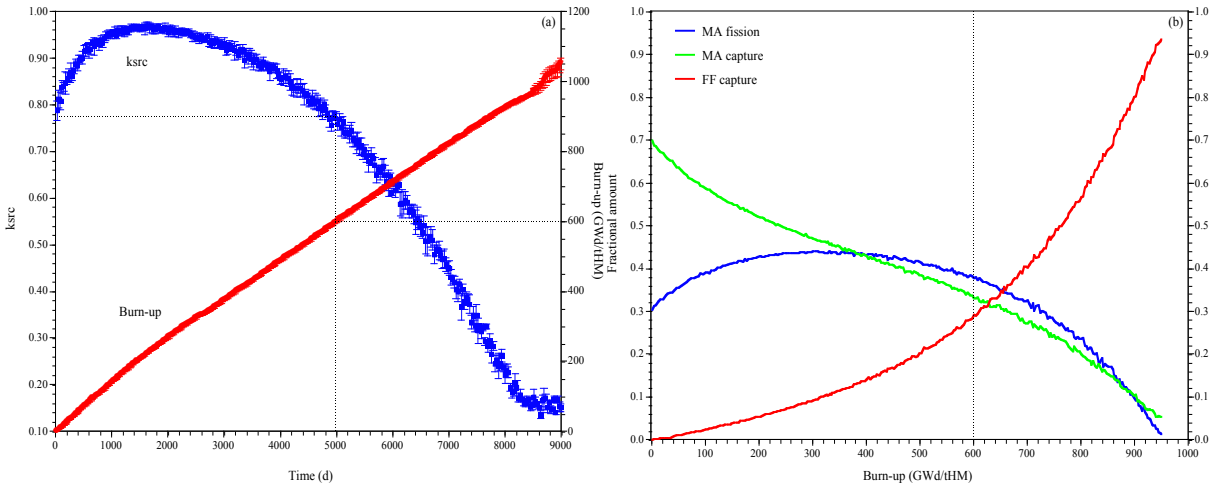

Figure 6.22. Time evolution of k_{src} and fuel burn-up (a), and the fractional amounts of captures and fissions in MAs and captures in FFs during burn-up.

From this maximum, k_{src} slowly decreases until about 13.6 years (~5000 days, 600 GWd/tHM burn-up) when the slope becomes steeper and G drops below 5. It is perhaps at this point that a long cool-down period (30-60 years, enough for 70%-90% of the ^{244}Cm to have decayed) followed by reprocessing could be foreseen, although, as explained later, the radiotoxicity of the spent fuel is smaller than that of fresh fuel. Thus, if the technology to produce this fuel is developed, reprocessing it may not be a difficult task. When the fuel burn-up has reached 600 GWd/tHM (hence the line marking the status of the reactor parameters at that level of burn-up), the number of captures in the FFs is of the same order of magnitude as the number of

captures or fissions in MAs. The cool-down period would allow the decay of the short-lived FFs poisoning the reactor and reprocessing would allow the insertion of 'fresh' MAs.

Figure 6.23 explains the system's behaviour previously shown in Figure 6.20. The mass balance in this 250 MW_{th} device at the EOL (600 GWd/tHM) is ~–1,400 kg of actinides, 65% of the initial actinide mass (Figure 6.23(a)). While the total amount of actinides is reduced at a constant rate of ~–100 kg/yr, equivalent to the yearly production of 3-4 conventional 1 GW_e LWRs, the composition of the actinide mixture changes significantly. The concentration of the americium isotopes (Figure 6.23(c)) and ^{237}Np (the only neptunium isotope shown in Figure 6.23(a)) fall exponentially, transmuted either by fission or by neutron capture and subsequent decay. The concentration of plutonium isotopes (Figure 6.23(b)) increases due to captures mainly in the abundant americium isotopes up to +410 kg at 400 GWd/tHM and then decreases (+340 kg at 600 GWd/tHM). For curium (Figure 6.23(d)), there is a small concentration increase (+27%) until 100 GWd/tHM due to the captures in americium (^{242}Cm from ^{241}Am and ^{244}Cm from ^{243}Am). Beyond that level of burn-up, the curium mass is steadily reduced down to 210 kg at EOL (–25% of curium eliminated).

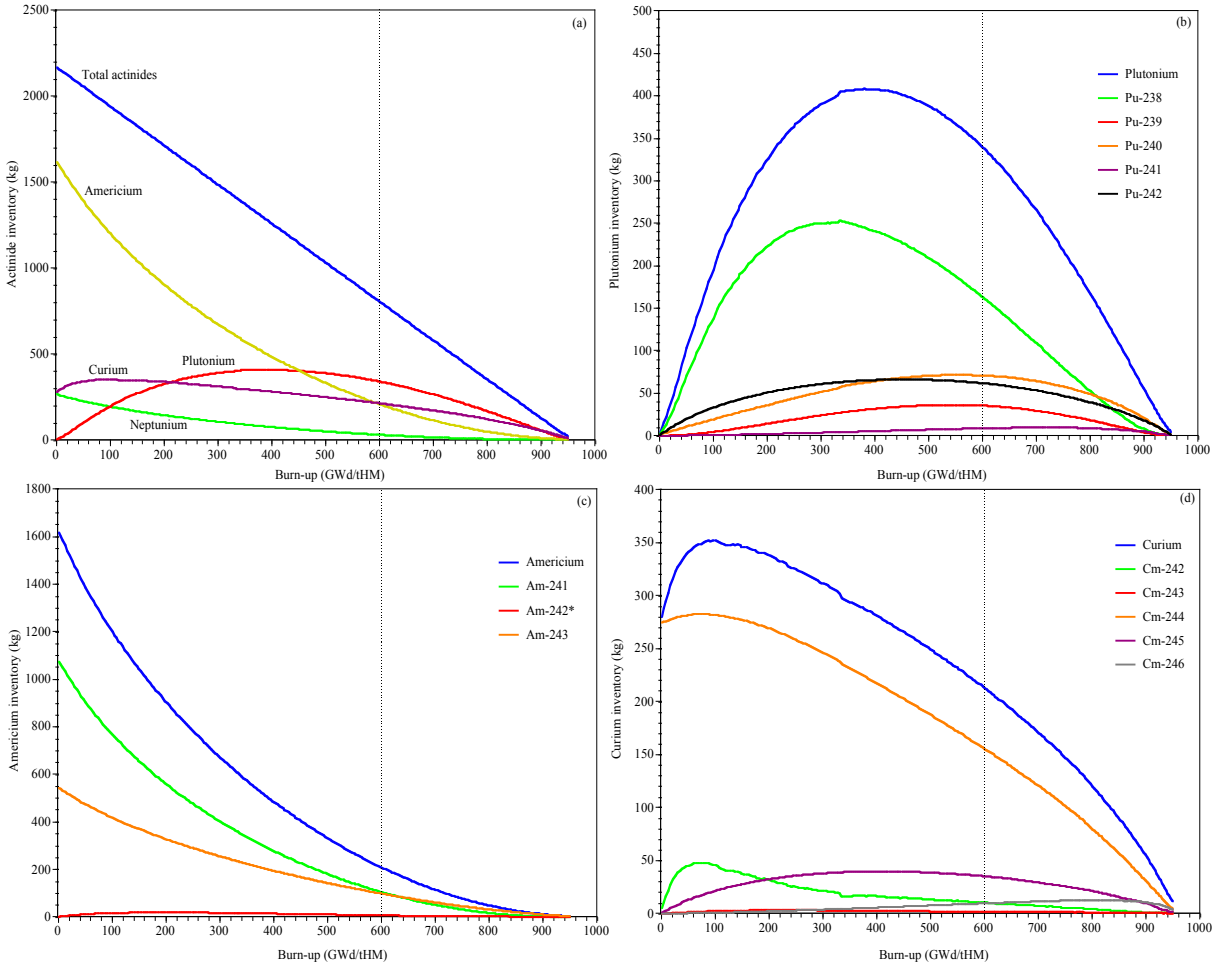

Figure 6.23. Detailed evolution of the actinide mass in the MA burner with burn-up.

Of all the isotopes produced by neutron capture in MAs, ^{238}Pu is the most abundantly produced, as several decay reactions result in its production. First, neutron capture in ^{241}Am followed by the β^--decay of ^{242}Am ($\tau_{1/2} \approx 16$ h) into ^{242}Cm ($\tau_{1/2} \approx 163$ d), which yields ^{238}Pu after an α-decay. Neutron capture in ^{237}Np produces the same result after the β^--decay of ^{238}Np ($\tau_{1/2} \approx 2$ d). As mentioned before, the production of ^{238}Pu (together with ^{245}Cm and, to a lesser extent, ^{239}Pu) causes the k_{src} increase previously shown.

Another isotope of great importance during burn-up is ^{244}Cm, since this isotope presents strong α activity for approximately half a century. The mass of ^{244}Cm increases slightly up to 100 GWd/tHM (+10 kg, +3.6%), thereafter gradually decreasing down to 160 kg (–44%).

These results show that such a device may be quite efficient in reducing the MAs stockpile coming from the conventional waste stream. A transmutation rate of 100 kg/yr would imply ~1.4 tonnes of MAs eliminated during a cycle period of 14 years and an average net electricity production of ~60 MW (taking into consideration the accelerator requirements). Therefore, such a device (250 MW_{th}) could effectively eliminate the MA waste produced by 3 conventional 3 GW_{th} LWRs (at a rate of ~30 kg/GW_e/yr, as explained in Chapter 2), while the plutonium would be dealt with by either LWRs using MOX (although this would increase significantly the production of MA, as explained before) or by FBRs.

The application of this transmutation strategy to the case of France would involve the construction of ~5 MA burners (1 GW_{th}) serving 59 LWRs (63.47 GW_e). For the UK a single 1 GW_{th} device would be sufficient to deal with the MA waste of the 23 reactors (11.85 GW_e). Spain would only need a 600 GW_{th} MA burner to deal with its MA waste. In all these cases, the MA burners would produce ~3% of the installed nuclear power.

It also seems clear that the ND related to the previously considered unimportant ^{238}Pu and ^{244}Cm is of extreme importance to these systems, since the large discrepancies in ND for these isotopes, presented in Chapter 4, will have a significant effect on the uncertainties in the design and operation of these devices. Indeed, the ND analysis in Chapter 4 shows a discrepancy in k_{src} of ~500 pcm for a ^{238}Pu concentration of 0.31% weight in the 50% plutonium / 50% MA fuel. A similar situation occurs for ^{244}Cm, which produces a ~250 pcm discrepancy in k_{src} for a concentration of 2.2% in the same type of fuel. These effects would be magnified in the MA burner as the concentration of these isotopes increases with burn-up, affecting the prediction not only of k_{src} but also of safety parameters, such as the Doppler reactivity coefficient. Therefore, the presence of significant quantities of these isotopes in critical reactors will entail serious design problems, since ND for them is poor and critical systems are far more sensitive to reactivity changes than subcritical ones. This may have dire implications for multiple recycling MOX schemes, both in thermal systems and FBRs.

The radiotoxicity of the spent fuel from the MA burner should also be studied in order to assess the feasibility of the fuel fabrication and reprocessing. Figure 6.24 shows the evolution of the radiotoxicity of 1 tonne of spent fuel of the MAs after a fuel burn-up of 600 GWd/tHM and the main isotopes contributing to this radiotoxicity. The toxicity of 1 tonne of fresh MA burner fuel as well as 1 tonne of PWR fuel (both fresh and spent) is also presented. As may be expected, the initial radiotoxicity of 1 tonne of 'fresh' fuel formed by pure MAs is orders of magnitude larger (~1,000 times greater) than that of PWR spent fuel due to the high concentration of ^{244}Cm. This may cause problems during the fuel fabrication stage, since the doses to workers and structures involved may exceed safety limits with present technology.

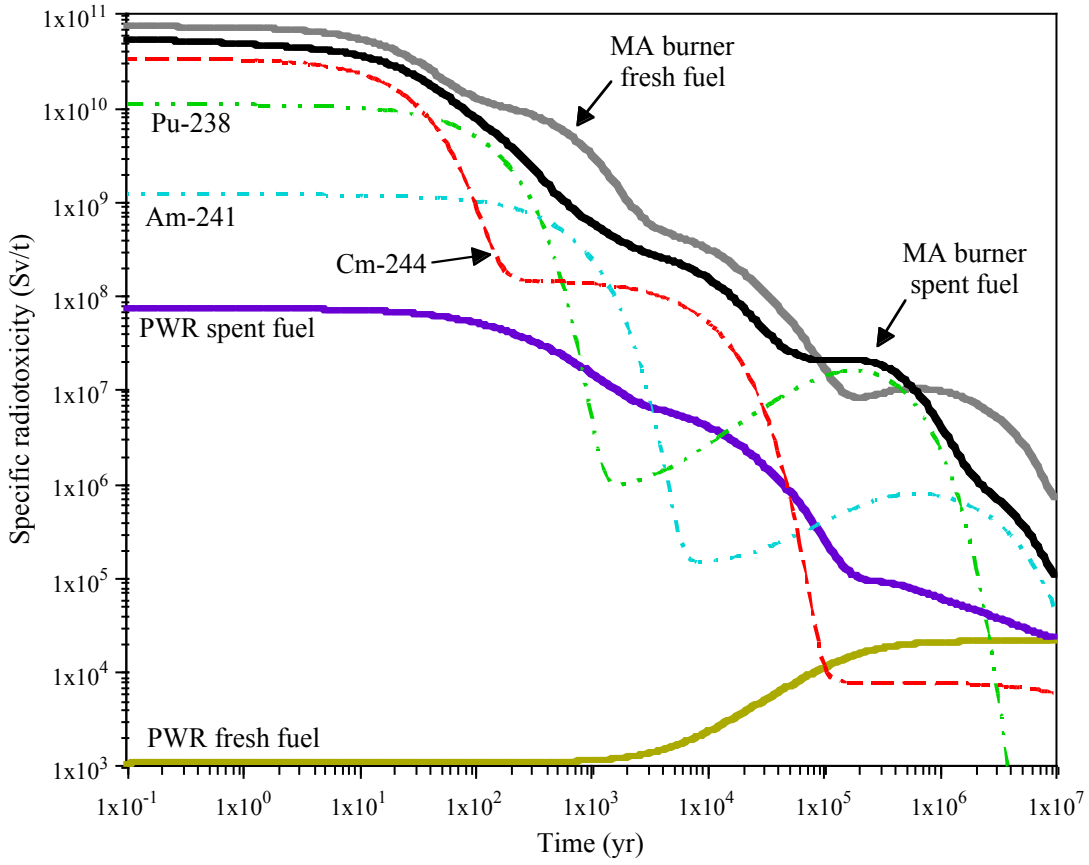

Figure 6.24. Evolution of the radiotoxicity of 1 tonne of spent fuel from the MA burner compared to 1 tonne of fresh fuel and the fuel coming from a conventional PWR.

Therefore, although there may still be some technological barriers to fully develop a MA burner (in particular concerning the accelerator and fuel fabrication), such a device has great potential for transmutation of TRUs, and, in particular, for efficiently eliminating the MA waste stream coming from the commercial cycle in a double strata transmutation scheme. On the other hand, the partitioning phase may entail some proliferation and radiological risks, since the plutonium separated could be diverted towards weapons production and the pure MAs present a very high specific radiotoxicity.

In this HLW transmutation strategy, the options to eliminate LLFFs, in particular ^{99}Tc and ^{129}I, are numerous. Strategies ranging from creating specific targets to insert in LWRs (taking advantage of the large number of units available) to the dilution of these isotopes in fresh UOX fuel (somewhat inefficient due to the hard neutron spectrum in the fuel) have been considered in [9]. It seems that the insertion of these isotopes in moderated sub-assemblies in FBRs or in thermal high flux reactors (HFR) yields good transmutation rates (~100 kg/yr) and process efficiency (~15 yr transmutation half-lives), although still far from the short transmutation half-life (~1.4 yr) predicted in [21] using the TARC method [23].

6.4 Transmutation Strategies Assessment

Two rather different conceptual approaches to transmutation have been studied. The analyses of both schemes show the clear applicability of the concept of transmutation to the commercial nuclear fuel cycle. In fact, none of these transmutation strategies present major technological challenges, although both still require some development in specific areas, such as an increase in proton beam current delivered (the cyclotron in PSI currently delivers ~1.6 mA at 590 MeV) or the precise design of a tens of MW spallation target.

As explained in Chapter 3, the thorium cycle offers clear advantages in terms of MA production since the quantities of isotopes produced beyond ^{235}U are orders of magnitude smaller than the fuel mass (e.g. for a mass of 600 kg of ^{233}U there are 300 g of ^{236}U at the end of a 120 GWd/t cycle). This approach offers the advantage of effectively treating the HLW in the spent fuel without the need for TRU separation. In fact fresh fuel may be fabricated separating the FFs from the actinides, and then uranium from the rest, and finally using these in the thorium-based systems (~76% fuel in an EA). The feasibility of transmutation of LLFFs, in particular ^{99}Tc and ^{129}I, in these systems has also been studied. Great dilution is required in order to achieve a larger efficiency (transmutation rates of 50 kg/yr are predicted in the EA with a dilution of 260 ppm in lead).

These systems would be designed to produce a significant amount of power, i.e. 1.5 GW_{th} in the case of the EA, and could therefore supply part of the energy demand which would otherwise be produced by conventional power plants. This fact could allow a progressive change from conventional uranium-based nuclear power plants to reactors based on the thorium cycle, once this is properly established.

The need to develop a completely new fuel cycle might, in fact, be the main drawback of this approach, as it may, for some, be a significant economic burden. The uranium cycle is well established in the nuclear industry, and, even if transmutation is accepted, the impact on the

commercial cycle should be minimised. In this context, the concept of the double strata and the MA burner is developed: a compact flexible system, with reduced power output dedicated to the elimination of MAs.

Unlike in the thorium-TRU strategy, the plutonium would be managed by using MOX, either in LWRs or in FBRs (still to be fully developed industrially), at the expense of a higher production of MAs. Moreover, the partitioning phase gains importance in this strategy, since the plutonium has to be separated from the MAs at EOC. This plutonium separation creates proliferation risks, which cannot be neglected, since the threats of diversion have regained importance.

Table 6.7 shows the actinide inventory balance per TW·h for a PWR, the EA and the MA burner. The MA burner shows a large efficiency in eliminating MAs, in particular americium, while producing plutonium. These results show that a 1 GW_{th} MA burner could eliminate the MAs of ~10 LWRs (1 GW_e, ~3 GW_{th}) combining the use of UOX and MOX, whereas the 1.5 GW_{th} EA would reduce the stockpile of MA at a lower rate (1 EA to 1.5 LWRs). Conversely, the EA would eliminate both the MA inventory (at a slower rate) and waste plutonium, which in the case of transmutation in double strata is left for the commercial cycle. However, the MA burner fuel will have to be doped with plutonium (~10%) in order to control the reactivity swing during burn-up and raise the initial neutron multiplication, relieving some strain on the accelerator requirements.

Table 6.7. Comparison of the actinide balance per TW·h for different systems, including the MA burner.

Actinide balance (kg/TW·h)	PWR (UOX) 41 GWd/tHM [9]	PWR (MOX) 43.5 GWd/tHM [9]	EA ($ThPuO_2$) 120 GWd/t of fuel	MA burner (pure MAs) 600 GWd/tHM
Plutonium	+11.3	+5.5	–27.6	+10.7
Neptunium	+1.18	+0.16	–2.55	–7.7
Americium	+1.04	+4.83	–2.65	–46.3
Curium	+0.03	+0.92	+0.86	–2.3

Fewer units of the MA burner (1 GW_{th}) would be required, 1 per ~10 LWRs (1 GW_e), ~3% of the installed nuclear capacity (e.g. ~10 MA units in the US or ~5 in Japan), compared to the 1 EA (1.5 GW_{th}) per 1.5 LWRs (~30% of the installed power, ~65 EA units in the US or ~30 in Japan). Scaling to the 363 GW_e/yr produced globally, the elimination of the MA waste being produced would require the construction of ~37 MA burners, producing ~13 GW_e plus the extensive use of MOX in LWRs, whereas the elimination of the HLW in EAs would involve the construction of ~242 EA units. The added value in the latter scenario is the addition of ~145 GW_e to the grid, which would help meet increasing world energy demands and relieve dependence on fossil fuels. In fact, this energy equates to ~5% of the primary energy consumption (~223×10^{18} J/yr, see Chapter 1), reducing greenhouse gas emission by ~160 million tonnes of carbon equivalent.

Hence, MA burners would entail a smaller impact on the present nuclear industry, although it is not clear which scheme would require more technological development in order to be industrially operational. The fuel fabrication process in the double strata approach seems more complicated than that of the EA (which uses TRUs directly from the spent fuel), due to the added difficulties of the partitioning phase. The design of MA burner fuel itself requires further investigation, since such large concentrations of MAs (some of them, like ^{244}Cm, very radioactive) hinder the production these high actinide density fuels, and the very high power densities foreseen for these types of devices require the development and analysis of specific fuels, such as the nitride fuels.

Therefore, further experimental studies should be carried out in order to determine the final strategy to transmute HLW. In this context, EADF appears as a milestone since the device would not only validate the concept of safely transmuting HLW in fast ADS and help in the development of the technology required to produce an industrial prototype, but also allow the irradiation and study of new types of fuels, such as $ThPuO_2$ or TRU-^{15}N, experimentally validating the benefits and handicaps of both systems.

Chapter 7

Final Conclusions

In previous Chapters of this dissertation, the need for alternatives to traditional energy sources has been discussed. Global warming, produced by the emission of CO_2 and other greenhouse gases, the limited availability of fossil fuels and the world's growing energy demands justify thorough research into non-conventional sources of energy with the potential to substitute traditional ones within a reasonable timescale.

In this context, the future role of nuclear power seems clear. Producing no greenhouse gas emissions with extensive fuel resources, nuclear power represents an established technology, ready for the challenge.

However, the dangers posed by the high-level nuclear waste (HLW) produced by nuclear reactors cannot be neglected. From the threats of nuclear weapon proliferation to the latent risk of leakage into the biosphere, these dangers require a permanent solution if nuclear energy is to achieve public acceptance. The negative view that public opinion has about nuclear power is often wrongly disregarded by the nuclear industry. Indeed, public opinion has driven several political decisions, adverse to nuclear energy, such as the progressive abandonment of nuclear power in Germany or the shut-down and decommissioning of Super-Phénix. This attitude could change if the HLW hazard was removed and danger of supercritical excursions was avoided.

Numerous studies have proposed different alternatives for disposing of or destroying HLW. Arguably, none of these alternatives presents the intrinsic safety and elimination potential that transmutation in Accelerator-Driven Systems (ADS) offers. While other systems merely store HLW without any long-term safety guarantees, transmutation in ADS promises to be a safe,

economically and technically viable, efficient method of transforming HLW into low activity waste requiring only secular storage for a few hundreds years.

The physical principles of HLW transmutation in ADS are now well understood, including the spallation reaction, acting as an external neutron source, which poses no major problems in terms of radiotoxicity, particularly when compared to that of the spent fuel. For the accelerator, the optimal proton energy in terms of neutron yield was found to be ~1.5 GeV, which is slightly beyond present cyclotron technology but easily achieved by other modern accelerators. The thorium fuel cycle has also been studied, illustrating its advantages in terms of low actinide production and fuel availability. Also the application of Monte Carlo (MC) techniques to solve design problems in advanced nuclear systems has been described, with specific reference to the validity and operation of the FLUKA / EA-MC code package and its compilation of Nuclear Data (ND).

7.1 Main Contributions

The roadmap towards the validation of the ADS concept and its application on a large scale foresees several experiments in order to study and develop several ADS components. The research detailed in this doctoral thesis covers the three specified levels towards the experimental demonstration of transmutation in ADS:

- Level 1: the validation of separate components – in the present case, the assessment of the lack of experimental ND and the effects of the discrepancies between evaluated ND libraries on the key reactor parameters. This work set a priority list for the isotopes and reaction channels to be measured, for example, in the neutron Time-of-Flight (n_TOF) experiment.
- Level 2: The neutronic design of the first real power ADS in the form of the coupling of a 1 MW_{th} TRIGA reactor with a 110-140 MeV, 1 mA proton accelerator, i.e. the TRIGA Accelerator-Driven Experiment (TRADE). The limitations of such a device were analysed and some possible experiments proposed.
- Level 3: The neutronic analysis of the Lead-Bismuth Eutectic (LBE) 80 MW_{th} Energy Amplifier Demonstration Facility (EADF) together with a comparison with other fast system options, in particular sodium- and helium-cooled systems. The limitations for transmutation of using MOX in a fast system were also highlighted.
- Finally: A comparative assessment of two major transmutation strategies – the use of thorium-plutonium fuel in fast ADS and the double strata approach, where the plutonium is eliminated by the use of MOX and the minor actinides (MAs) are burnt in a dedicated ADS (MA burner).

In this context, the improvement of ND is a necessary step to accurately design these systems. Therefore, the identification of the most relevant isotopes for transmutation and the aforementioned assessment of the impact of the discrepancies between ND libraries on ADS nuclear parameters were essential for configuring a measurement priority list.

Capture and/or fission reactions in some of these isotopes, such as ^{90}Zr, $^{206, 207, 208}$Pb, ^{209}Bi, ^{90}Zr, ^{234}U, ^{237}Np or ^{243}Am, have already been measured in the n_TOF facility at CERN, offering promising results. Nonetheless, the analysis of the sensitivity for the latest ND library releases presented in Chapter 4 showed that other important isotopes and reaction channels were overlooked in previous measurements, and that their related discrepancies have a major impact on ADS design. Some of these isotopes and reaction channels are:

- ^{238}Pu, present in small quantities in conventional HLW (~2%). Its related ND shows large discrepancies above 1 eV and has a strong impact on plutonium and especially on MA transmutation schemes, being the daughter product of a neutron capture followed by β^--decays in ^{237}Np and ^{241}Am. The effect of these discrepancies is perceived in the variation of the multiplication coefficient, which may be as large as thousands of pcm in the case of high concentrations of this isotope, as well as in the reaction rates, showing up to 30% discrepancies between libraries, and introducing a large uncertainty in the isotope's inventory.
- ^{241}Am, the most abundant MA isotope in commercial spent fuel after long burn-ups or multiple recycling schemes. Large discrepancies in reaction rates (e.g. 15% neutron capture) with an important effect on the multiplication of MA burners.
- ^{244}Cm, responsible for most of the MA mid-term radiotoxicity, appears in significant quantities in plutonium elimination schemes. Its related ND presents large differences for the entire energy range in all reactions. Reaction rates differ by more than 10% in TRADE, and it also presents a capture rate discrepancy of 32% in a MA fuel for fast systems. Its accumulation may have important effects on the reprocessing of the fuel.
- ^{99}Tc and ^{129}I, the cross-sections of which are poorly known, give discrepancies of up to 15% in capture rates and above 40% for (n, xn) reactions, and constitute the most significant long-lived fission fragments (LLFFs) in terms of radiological hazard.
- Inelastic scattering cross-sections show large discrepancies for all isotopes due to the complexity of their measurement. This is an important reaction channel in the definition of the neutron energy spectrum in fast systems, for example, showing discrepancies of up to 71% for ^{241}Pu.
- Contributing to the neutron multiplication of the system and damage to the structures, experimental data for (n, xn) reactions is almost nonexistent. It seems particularly relevant for coolant and structural materials in fast systems, such as $^{206, 207, 208}$Pb and ^{209}Bi.

These discrepancies clearly affect the reliability of the design calculations for ADS experiments, including those in this dissertation, and in particular for MA burners. Hence, any ADS containing a significant quantity of these isotopes would be obliged to operate at a lower subcritical level due to uncertainties in the burn-up reactivity swing. For example, an ADS fully loaded with MA may have to operate at least 3000 pcm below criticality (i.e. $k_{src} \approx 0.97$) at all times, particularly in the middle of the cycle when ~50% of the mass in the system can be ^{238}Pu and ^{244}Cm.

Secondly, the validation of the ADS concept requires a preliminary step in order to integrate its different components into a single well-known system. The feasibility of this experiment (TRADE) has been demonstrated and neutronic design calculations performed. These showed that for the innovative, solid ~30 kW spallation target design a maximum power deposition of ~1 kW/cm^3 should be expected under reference operating conditions. This means that no additional cooling system is needed for the target. However, this implies that the experiment will not be able to operate for long periods of time at nominal core power (200 kW) for deeply subcritical configurations (e.g. $k_{src} \approx 0.90$). For the target activation, a total activity of ~37 TBq is to be expected after a one year cool-down period and one year of irradiation at nominal power (~11 kW). The activity rapidly decays and 60 years after irradiation the activity falls below 0.1 TBq and is dominated by tritium.

A detailed study of the radiological impact of the beam line transfer showed that, for the reference beam losses of 1 nA/m/s, 140 cm thick barite shielding would reduce the dose at the shielding surface to 7.5 μSv/h, below the legal maximum of 10 μSv/h for unlimited access working areas.

The neutronic characterisation of the TRADE experiment confirmed that it is safe to perform such an experiment in the TRIGA core. The power peaking factors are moderate (~1.5 for $k_{src} \approx 0.977$), avoiding large thermal stresses in the fuel elements. The availability of control rods, low energy output and very large reactivity feedbacks (for example, ~10 pcm/K) guarantees safety for the large number of experiments that are to be performed in this system.

An important feature of TRADE is the longer neutron lifetime compared to EADF (50 μs versus 1 μs). This fact allows reactivity insertions and events such as beam failures to be investigated at a lower response frequency (the reactor period in TRADE for $k_{src} \approx 0.977$ is ~2 ms), and thus with a larger operational safety margin. This is an important issue considering that the exponential period of EADF is of the order of 40 μs, which would imply a total power drop for a 1 ms beam trip.

Moreover, the feasibility of LLFF and transuranic (TRU) transmutation in TRADE was assessed. For the former, isotopes such as ^{79}Se, ^{99}Tc, ^{129}I, ^{147}Sm and perhaps ^{135}Cs present

transmutation half-lives between 7 and 30 yr for very thermal fluxes of ~10^{14} n/cm^2/s. These values are quite promising, but still far from the 1.4 yr obtained in the TARC experiment. On the other hand, it seems clear that in order to achieve this transmutation efficiency, large neutron fluxes and a very large isotopic dilution is required.

For the non-fissile TRUs, the fission-to-absorption ratio was shown to decrease with softer neutron fluxes. The use of special matrices to enhance the thermal flux, producing neutron capture and fission in the daughter products before their decay, particularly ^{238}Np ($\tau_{1/2} \approx 2.1$ d) and ^{242}Am ($\tau_{1/2} \approx 16$ h), would require very large thermal fluxes (thus, higher enrichment), given that for a flux of 10^{15} n/cm^2/s even their fission half-lives (3.8 d and 2.7 d, respectively) are longer than their decay half-lives. If those flux levels are not reached, the mass of actinides destroyed in the cycle is negligible (~7% of the initial mass in TRADE), resulting in an actinide mixture that is significantly more radiotoxic (mainly due to ^{238}Pu and ^{244}Cm) than the initial one.

It seems clear that a thermal ADS would be easier to operate and control, and could produce reasonable LLFFs transmutation rates, but so could a thermal critical reactor. Conversely, the use of water as the coolant limits the neutron fluxes due to the small but relevant thermal neutron capture in the abundant ^{1}H ($^{th}\sigma_{capt} \approx 0.3$ b) compared, for example, to the 0.5 mb of ^{208}Pb. The extension of the burn-up periods is also affected by the higher $^{th}\sigma_{capt}$ of the fission fragments (FFs). Finally, such a device would be very inefficient in terms of TRU transmutation due to the low fission-to-absorption ratio for most of the non-fissile actinides, ~20% for ^{238}Pu and ^{244}Cm, ~10% for $^{240, 242}$Pu and ~5% for ^{237}Np and $^{241, 243}$Am.

Therefore, the need for a fast system to efficiently transmute TRUs and reduce the accumulated stockpile seems evident. Unfortunately, TRUs present much lower delayed neutron emission, compared to the 0.65% delayed fraction (β) in ^{235}U or the 1.91% of ^{238}U. In particular, the high concentrations of ^{238}Pu ($\beta \approx 0.16\%$), ^{239}Pu ($\beta \approx 0.21\%$) and ^{241}Am ($\beta \approx 0.14\%$) would degrade the control of a critical fast reactor, in which the prompt neutron lifetimes are orders of magnitude lower (~0.1 μs for a fast breeder reactor). Moreover, the negative effect on reactivity produced by the broadening of the capture resonances with increasing temperature (Doppler broadening) is rather small in fast systems, since the epithermal flux in these systems is ~4 orders of magnitude smaller than the fast flux and only ^{238}U and ^{232}Th present distinctive capture resonances. Taking these facts into account, the importance of developing a fast ADS is clear.

In this context, the experimental validation of the fast ADS concept producing significant transmutation rates should take place in EADF. The neutronic analysis of this device shows important safety features. The low initial subcriticality level, i.e. $k_{src} \approx 0.96$, and the 18% plutonium concentration in the uranium-plutonium fuel, higher than the plutonium

equilibrium concentration for this system, guarantee a neutron multiplication level well below 1 throughout the burn-up. The very small peaking factors minimise the thermal stress in the fuel and assure a homogeneous burn-up.

The negative reactivity feedbacks of EADF ($\alpha_T \approx -1$ pcm/K, $\alpha_V \approx -100$ pcm/% for small coolant voids and $\alpha_V \approx -1500$ pcm/% for a major coolant void) show the high passive safety of the system. These numbers have special relevance when compared to helium-cooled systems, which present a harder neutron energy spectrum slightly enhancing the transmutation rates but giving no void coefficient, and sodium-cooled reactors, where the transmutation rates are worse due to a softer spectrum and the void coefficient is, at best, close to 0.

Nevertheless, the use of uranium-plutonium fuel offers limited capabilities for eliminating plutonium and increases the stockpile of MAs. The decrease in the initial fissile enrichment has to be compensated by fissile breeding to maintain reactivity levels for extended burn-ups. Producing plutonium and higher actinides in order to maintain the reaction to eliminate plutonium does not seem an efficient way of proceeding.

Therefore, two HLW elimination strategies in fast ADS were assessed: (a) the use of thorium fuel 'enriched' with waste TRUs to reduce the HLW stockpile and produce significant quantities of energy, thus opening a gate to the progressive shift of the present uranium-based commercial fuel cycle towards thorium-based fuels; and (b) the partial decoupling of the commercial stratum, which would deal with plutonium by using MOX and perhaps fast reactors, from the Partitioning and Transmutation stratum, which would deal with the elimination of the MAs produced in the commercial cycle.

Both strategies obviously offer advantages and disadvantages. The MA transmutation rate achieved in the MA burner is ~–46 kg/TW·h, whereas an Energy Amplifier (EA) using thorium-uranium fuel eliminates ~–28 kg/TW·h of plutonium and ~–5 kg/TW·h of MAs (EADF using uranium-plutonium fuel only achieves ~–8 kg/TW·h elimination of plutonium and produces ~+40 g/TW·h of MAs).

This has certain implications for the commercial cycle. The EA thorium-uranium transmutation strategy entails ~30% of installed power being produced by EA, compared to the ~3% of installed power from MA burners required by the double strata scheme. Scaled to the 363 GW_e/yr produced globally, the elimination of the MA waste being produced would require the construction of ~37 MA burners, producing ~13 GW_e plus the extensive use of MOX in LWRs, whereas the elimination of the HLW in EAs would involve the construction of ~242 EA units. The added value of the latter scenario is the addition of ~145 GW_e to the grid, which would help meet increasing world energy demands and reduce dependence on fossil fuels.

On the other hand, the partitioning process in the double strata strategy entails proliferation risks due to the separation of plutonium from the HLW. This problem cannot be neglected since it would involve the separation of several hundreds of kilograms of highly fissile plutonium per reactor per year, increasing the risk of diversion.

Therefore, if the ADS experimental program continues successfully and assuming that the security requirements in the partitioning phase are fulfilled, the double strata strategy could be commercially applicable at medium term (~30 yr) since it does not require the development of a new fuel cycle. But the advantages in terms of availability and waste reduction of the thorium cycle are clear. Therefore, effort should be put into developing a commercial thorium cycle. In this context, the double strata strategy could be an intermediate step towards the production of clean, virtually inexhaustible energy in completely different systems, such as the EA.

7.2 Future Work

There is still a very large amount of research to be performed for the industrial validation of the transmutation of HLW in fast ADS. Hence, the following list is not exhaustive, but identifies further research that could be performed based on this dissertation:

- An analysis of the sensitivity to ND of fast ADS during burn-up is quite important. This is especially true for MA burners, since the concentration of isotopes showing large differences in ND between current libraries, in particular ^{238}Pu and ^{244}Cm, increases greatly with burn-up. This could produce very large discrepancies in the reactor parameters when calculated with different libraries.
- The correlation between uncertainties in reaction cross-sections and reactivity feedbacks should be analysed. Reactivity feedbacks are partially based on the broadening of the resonance cross-sections with temperature, and these are poorly known for many isotopes, particularly for higher actinides.
- As mentioned before, the measurement of cross-sections for isotopes, such as ^{238}Pu, ^{241}Am, ^{244}Cm, and reactions, such as (n, xn) and inelastic scattering for any isotopes involved in HLW transmutation in fast systems, is a necessary step to improve accuracy in the design of these systems.
- The study of the discrepancies in β between ND libraries and its consequent measurement for isotopes presenting large uncertainties. The delayed neutron fraction may have important consequences in the control of fast systems loaded with large amounts of MAs, which generally show very little delayed neutron emission.

- Analysis of a thorium-plutonium fuel load in EADF to study the behaviour of the system and the transmutation rates to be expected. In fact, this is a possible set-up for a second stage in EADF (XADT).
- A deeper assessment of LLFFs transmutation in different systems. The application of the TARC method is fast reactors seems quite promising, although the transmutation of ^{99}Tc and ^{129}I in LWRs should be assessed and, if possible, applied in the near future to reduce the stockpile of these elements.
- The precise design and optimisation of the fuel load of the MA burner concept seems necessary to develop the double strata scheme. More detailed definition of MA burner operation and the length of the burn-up (trying to minimise the reprocessing step) are also required. The different fuel options should be carefully studied, precisely defining its composition since some plutonium doping will be necessary to avoid large reactivity swings during the burn-up cycle.
- Finally, the study of these transmutation strategies for HLW stockpile elimination in specific countries is essential to prove the economic viability of the process and to inform the decisions that will be taken in the near future in countries like France about the fate of the HLW.

7.3 Concluding Summary

The elimination of HLW is a crucial issue if nuclear power is to be seen as a publicly acceptable energy source, particularly in the context of the growing world energy demands. HLW transmutation in ADS appears as an efficient and safe way of solving this problem permanently. There is a clear research roadmap towards the validation of this concept. The design calculations for several of the experiments involved in this validation prove their feasibility. However, there are several technological issues to be resolved, requiring the intensification of the present research efforts in the field of HLW transmutation in ADS. The involvement of the nuclear industry is also essential to successfully develop this technology and introduce new fuel cycles in innovative systems.

Bibliography

* *Papers to which the author contributed.*

[1] C. Rubbia, J.A. Rubio, S. Buono, F. Carminati, N. Fiétier, J. Gálvez, C. Gelès, Y. Kadi, R. Klapisch, P. Mandrillon, J.-P. Revol, Ch. Roche, *"Conceptual Design of a fast Neutron Operated High Power Energy Amplifier"*, CERN/AT/95-44 (ET), 1995. See also C. Rubbia, *"A High Gain Energy Amplifier Operated with fast Neutrons"*, AIP Conference Proceedings 346, International Conference on Accelerator-Driven Transmutation Technologies and Applications, Las Vegas (NV), US, 1994.

[2] Intergovernmental Panel on Climate Change, *"Climate Change 2001: Synthesis Report"*, Cambridge University Press, Cambridge, UK, 2001.

[3] Nuclear Energy Agency (NEA), *"Nuclear Power and Climate Change"*, Organisation for Economic Co-Operation and Development (OECD), 2000.

[4] Energy Information Administration (EIA), *"International Energy Outlook 2003: World Energy Consumption"*, DOE/EIA-0484, 2003.
Also: http://www.eia.doe.gov/oiaf/ieo/world.html

[5] United Nations (UN), *"Kyoto Protocol to the United Nations Framework Convention on Climate Change"*, FCCC/CP/1997/L.7/Add.1, Kyoto, Japan, 1997.

[6] BP Group, *"Statistical Review of World Energy 2003*", BP Statistical Review of World Energy, 2003. Also: http://www.bp.com.

[7] Commissariat à l'Énergie Atomique (CEA), *"Memento sur l'Énergie – Energy Data Book 2001"*, Service des Etudes Économiques, CEA Saclay, France, 2001.

[8] H.J. Cruickshank, *"Module F14 Notes – Engineering for Sustainable Development"*, Department of Engineering, University of Cambridge, UK, 2001.

[9] Nuclear Energy Agency (NEA), *"Actinide and Fission Product Partitioning and*

Transmutation: Status and Assessment Report", Organisation for Economic Co-Operation and Development (OECD), 1999.

[10] J. Ahn, E. Greenspan, D.A. Roberts, P.L. Chambré, *"Possibility of Underground Autocatalytic Criticality by Actinides in vitrified HLW"*, International Conference on Future Nuclear Systems, Global '97, Yokohama, Japan, 1997.

[11] International Atomic Energy Agency (IAEA), *"Underground Disposal of Radioactive Waste, Basic Guidance"*, IAEA Safety Series No. 54, Vienna, Austria, 1981.

[12] C. Rubbia, S. Buono, E. González, Y. Kadi, J.A. Rubio, *"A Realistic Plutonium Elimination Scheme with Fast Energy Amplifiers and Thorium-Plutonium Fuel"*, CERN/AT/95-53 (ET), 1995.

[13] I.S. Roxburg, *"Geology of High-Level Nuclear Waste Disposal: An Introduction"*, Chapman and Hall, 1987.

[14] F.J. Rahn, A.G. Adamantiades, J.E. Kenton, C. Braum, *"A Guide to Nuclear Power Technology: A Resource for Decision Making"*, John Wiley & Sons, 1984.

[15] S.Y.F. Chu, L.P. Ekström, R.B. Firest, *"The Lund/LBNL Nuclear Data Search Version 2.0, February 1999"*, http://nucleardata.nuclear.lu.se/nucleardata/toi/.

[16] World Nuclear Association, http://www.world-nuclear.org/info/reactors.htm.

[17] L.H. Baetslé, *"Role and Influence of Partitioning and Transmutation on the Management of Nuclear Waste Streams"* OECD/NEA Report on P&T, N° 3, 1992.

[18] ICRP Publication 68, *"Dose Coefficients for Intake of Radionuclides by Workers"*, Vol. 20, N° 4, 1994.

[19] T. Mukaiyama, *"Motivation and Programs for Transmutation of Nuclear Waste"*, Frédéric Joliot – Otto Hahn Summer School 2002 Lectures, CEA – Cadarache, France, 2002.

[20] *"The cost of high-level waste disposal in geological repositories"*, OECD/NEA, 1993.

[21] C. Rubbia, S. Buono, Y. Kadi, J.A. Rubio, *"Fast Neutron Incineration in the Energy Amplifier as Alternative to Geologic Storage: the Case of Spain"*, CERN/LHC/97-01 (EET), 1997.

[22] M. Salvatores, *"The Physics of Transmutation in Critical or Subcritical Reactors"*, Comptes Rendus – Physique, Tome 3 (2002) – N° 7-8, Éditions Elsevier, 2002.

[23] The TARC Collaboration, *"The TARC Experiment (PS211): Neutron-Driven Nuclear*

Transmutation by Adiabatic Resonance Crossing", CERN 99-11. Also: European Commission, *"Neutron-driven Nuclear Transmutation by Adiabatic Resonance Crossing"*, European Commission Project Report, EUR 19117, 1999.

[24] G.T. Parks, *"Module C1 Notes – Nuclear Power Engineering"*, Department of Engineering, University of Cambridge, UK, 2001.

[25] M. Eriksson, J.E. Cahalan, *"Applicability of Passive Safety to Accelerator-Driven Systems"*, Nuclear Application for the New Millennium, AccApp/ADTTA '01, ANS Winter meeting, Reno (NV), US, 2001.

[26] Y. Kadi, J.P. Revol, *"Design of an Accelerator-Driven System for the Destruction of Nuclear Waste"*, Accelerator-Driven Systems for Energy Production and Waste Incineration: Physics, Design and Related Nuclear Data, Abdus Salam ICTP, 2002.

[27] *"Energy Amplifier Demonstration Facility Reference Configuration: Summary Report"*, ANSALDO Nucleare, EA-B0.00-1-200 – Rev. 0, 1999.

[28] S. Andriamonje *et al.* Physics Letters B, 348, 697–709, 1995, and J. Calero *et al.* Nuclear Instruments and Methods A, 376, 89–103, 1996.

[29] *"Status of the MTA Process"*, Livermore Research Laboratory Report LRL-102, 1954.

[30] W.B. Lewis, *"The Significance of the Yield of Neutrons from Heavy Nuclei Excited to High Energies"*, Atomic Energy of Canada Limited Report AECL 968, 1952.

[31] E.O. Lawrence, E.M. McMillan, L.W. Álvarez, *"Electro-nuclear Reactor"*, United States Patent No. 2,933,442 Apr. 19, 1960.

[32] J.S. Gilmore, G.J. Russell, H. Robinson, R.E. Prael, *"Fertile-to-Fissile and Fission Measurements for Depleted Uranium and Thorium Bombarded by 800-MeV Protons"*, Nuclear Science and Engineering, 99, 4152, 1988.

[33] T. Mukaiyama, *"Omega Programme in Japan and ADS Development at JAERI",* Proceedings of an Advisory Group meeting, Taejon, Republic of Korea, IAEA – TECDOC – 1365, 1999.

[34] C.D. Bowman *et al.*, *"Nuclear Energy Generation and Waste Transmutation Using an Accelerator-Driven Intense Thermal Neutron Source"*, Nuclear Instrumentation and Methods in Physics Research (Sec. A), A320, 336, 1992. Also as LA-UR-91-2601, Los Alamos National Laboratory (LANL) (NM), US, 1991.

[35] F. Venneri, C.D. Bowman, R. Jameson, *"Accelerator-Driven Transmutation of Waste (ATW) A New Method for Reducing the Long-Term Radioactivity of Commercial*

Nuclear Waste", LA-UR93-752, LANL (NM), US, 1993.

[36] A. Fassò, A. Ferrari, P.R. Sala, *"Electron-photon transport in FLUKA: Status"*, invited talk in the Proceedings of the Monte Carlo 2000 Conference, Lisbon, October 2000, A. Kling, F. Barao, M. Nakagawa, L. Tavora, P. Vaz (eds.), Springer-Verlag Berlin, p. 159-164, 2001.

[37] A. Fassò, A. Ferrari, J. Ranft, P.R. Sala, *"FLUKA: Status and Prospective for Hadronic Applications"*, invited talk in the Proceedings of the Monte Carlo 2000 Conference, Lisbon, October 2000, A. Kling, F. Barao, M. Nakagawa, L. Tavora, P. Vaz eds., Springer-Verlag Berlin, p. 955-960, 2001.

[38] Y. Kadi, *"The EA-MC Monte Carlo Code Package"*, in Proceedings of the Fifth International Meeting on Simulating Accelerator Radiation Environment – SARE-5: Models and Codes for Spallation Neutron Sources, OECD Headquarters; Paris, France, 2000.

[39] M. Salvatores, M. Martini, I. Slessarev, R. Soule, J.C. Cabrillat, J.P. Chauvin, P. Finck, R. Jacqmin, A. Tchistiakov, *"MUSE-1: A first experiment at MASURCA to validate the physics of subcritical multiplying systems relevant to ADS"*, in Proceedings of the Second International Conference on Accelerator Driven Transmutation Technologies and Applications (ADTTA'96), Kalmar, Sweden, 1996.

[40] R. Soule, M. Salvatores, R. Jacqmin, M. Martini, J.F. Lebrat, P. Bertrand, U. Broccoli, V. Peluso, *"Validation of neutronic methods applied to the analysis of fast subcritical systems: the MUSE-2 experiments"* in Proceedings of the International Conference on Future Nuclear Systems (Global'97), Yokohama, Japan, Vol. 1, pp. 639-645, 1997.

[41] J.F. Lebrat *et al.*, *"Experimental investigation of multiplying subcritical media in presence of an external source operating in pulsed or continuous mode: the MUSE-3 experiment"* in Proceedings of the Third International Conference on Accelerator Driven Transmutation Technologies and Applications (ADTTA'99), Prague, Czech Republic, 1999.

[42] G. Aliberti, G. Imel, G. Palmiotti, *"MUSE-4 Experiment Measurements and Analysis"*, ANL-AFCI-092, Argonne National Laboratory (ANL), US, 2003.

[43] Technical Working Group on ADSs, *"Interim Report of the Technical Working Group on Accelerator Driven Subcritical Systems"*, Ente per le Nuove tecnologie, l'Energia e l'Ambiente (ENEA), Italy, October 1998. Also: http://www.enea.it/com/ADS/

[44] Technical Working Group on ADSs, *"Overview of the Ongoing Activities in Eaurope*

snd Recommendations of the Technical Working Group on Accelerator-Driven Subcritical Systems", ENEA, September 1999. Also: http://www.enea.it/com/ADS/

[45] European Technical Working Group on ADS, *"Nuclear Waste Transmutation using Accelerator-Driven Systems"*, ENEA, Italy, February 2000. Also: http://www.enea.it/com/ADS/

[46] European Technical Working Group on ADS, *"A European Roadmap for Developing Accelerator-Driven Systems (ADS) for Nuclear Waste Incineration"*, ENEA, ISBN 88-8286-008-6, April 2001. Also: http://www.enea.it/com/ADS/

[47] J.M. Lagniel, S. Joy, J.L. Lemarie, A.C. Mueller, *"IPHI, The Saclay High-Intensity Proton Injector Project"*, Proceedings of the Particle Accelerator Conference PAC'97, Vancouver, Canada, May 1997.

[48] A. Pisent *et al.*, *"TRASCO 100 MeV High Intensity Proton Linac"*, Proceedings of EPAC 2000, Vienna, Austria, June 2000.

[49] G.S. Bauer, M. Salvatores, and G. Heusener, *"MEGAPIE, a 1 MW Pilot Experiment for a Liquid Metal Spallation Target"*, to be published in Proceedings of IWSMT-4 (J. Nucl. Mat.) and Proc. ICANS XV (JAERI-KEK report).

[50]* The TRADE Collaboration, *"Triga Accelerator Driven Experiment (TRADE): Final Feasibility Report"*, ENEA Report, April, 2002.

[51] K.H. Beckurts, K. Wirtz, *"Neutron Physics"*, Springer-Verlag, 1964.

[52] *"CLEFS CEA – N°46 – Printemps 2002"*, Commissariat à l'Énergie Atomique (CEA), France, 2002.

[53] W. Gudowski, *"Reactor Physics: Program of the lectures"*, Royal Institute of Technology (KTH), Sweden, 1997.

[54] J.R. Lamarsh, A. Baratta, *"Introduction to Nuclear Engineering"*, 3rd Edition, Prentice Hall, 2001.

[55] J.R. Lamarsh, *"Introduction to Nuclear Reactor Theory"*, Addison-Wesley, 1966.

[56] J.L. Muñoz-Cobo, A. Escrivà, *"Física Nuclear"*, Universitat Politècnica de València – 99.4078, Spain, 1999.

[57] C. Rubbia, *"The Energy Amplifier: A Description for the Non-Specialists"*, CERN/ET/96-01, 1996.

[58] M. Winter, http://www.webelements.com/webelements/elements/text/Th/geol.html,

The University of Sheffield and Webelements Ltd, UK, 2003.

[59] W.M. Stacey, *"Nuclear Reactor Physics"*, John Wiley & Sons, 2001.

[60] C. Rubbia *et al.*, *"A high Resolution Spallation driven Facility at the CERN-PS to measure Neutron Cross Sections in the Interval from 1 eV to 250 MeV"*, CERN/LHC/98-02 (EET), 1998.

[61] S. Atzeni, Y. Kadi and C. Rubbia, *"Statistical Fluctuations in Monte Carlo Simulations of the Energy Amplifier"*, CERN/LHC/97-12 (EET), 1997.

[62] K.S. Krane, *"Introductory Nuclear Physics"*, John Wiley & Sons, 1987.

[63] F. Carminati, I. Goulas, J.P. Revol, *"A Nuclear Data Base for the EA Monte Carlo"*, CERN/AT/EET 95-008, 1995.

[64] C. Rubbia, *"Resonance enhanced neutron captures for element activation and waste transmutation"*, CERN-LHC-97-004-EET, Geneva, 1997. See also: P. Froment, M Cogneau, T. Delbar, G. Ryckewaert, I Tilquin, J. Vervier, *"The production of radioisotopes for medical applications by the adiabatic resonance crossing (ARC) technique"*, Nuclear Instruments Methods Phys. Res., A 493 (2002) 165-175.

[65]* C. Rubbia, A Herrera-Martínez, Y. Kadi, *"Humanitarian Demining: 10.8 MeV Characteristic Gamma Detection from ^{14}N"*, paper in preparation.

[66] C. Rubbia, *"Report of the Working Group on a Preliminary Assessment of a New Fission Fragment Heated Propulsion Concept and its Applicability to Manned Missions to the Planet Mars"* Italian Space Agency, Rome, Italy, April 1999.

[67] ENDF-102, *"Data Formats and Procedures for Evaluated Nuclear Data File ENDF-6"*, Cross-section Evaluation Working Group, BNL-NCS-44945, Rev.2/97, Brookhaven National Laboratory (BNL) (NY), US, 1997.

[68] *"EXFOR, database of experimental nuclear reaction cross-section"*, IAEA Nuclear Data Section, 2004. Also: http://www-nds.iaea.or.at/zvd/ and http://www.nndc.bnl.gov/exfor/

[69] P.F. Rose (Ed.): *"ENDF-201, ENDF/B-VI Summary Documentation",* BNL-NCS-17541, 4th Edition (1991). "*Revision 8"*, BNL (NY), US, 2001.

[70] K. Shibata *et al., "Japanese Evaluated Nuclear Data Library Version 3 Revision-3: JENDL-3.3",* J. Nucl. Sci. Technol., 39, 1125, 2002.

[71] R. Jacqmin, R. Forrest, J. Rowlands, A. Nouri and M. Kellett: *"Status of the JEFF-3 Project",* Proceedings of the International Conference on Nuclear Data for Science and Technology, Vol. 1, p.54, 2002.

[72] S. Ganesan, *"A review of the current status of nuclear data for major and minor isotopes of the thorium cycle"*, Proceedings of the International Topical Meeting on Advances in Reactor Physics and Mathematics and Computation into the Next Millennium, Pittsburgh (PA), US, 2000.

[73] M. Dahlfors, Y. Kadi, *"Sensitivity Analysis of Neutron Cross Sections Relevant for Accelerator-Driven Systems"*, Journal of Nuclear Science and Technology, Supplement 2, p. 1198-1201, 2002. Also: C. Rubbia, M. Dahlfors, Y. Kadi, *"Sensitivity Analysis of Neutron Cross Sections Relevant for Accelerator-Driven Systems"*, in the Management Report of the n_TOF-ND-ADS EC programme under contract no. FIKW-CT-2000-00107.

[74]* A. Herrera-Martínez, M. Dahlfors, Y. Kadi, G.T. Parks, *"Importance of Neutron Cross-sections for Transmutation"*, Proceedings of the International Workshop on Nuclear Data for the Transmutation of Nuclear Waste (TRAMU), ISBN 3-00-012276-1, GSI-Darmstadt, Germany, September 2003.

[75]* Y. Kadi, A. Herrera-Martínez, M. Dahlfors, *"The TRADE Experiment: Importance of Neutron Cross-Sections"*, Proceedings of the International Conference on the Physics of Fuel Cycles and Advanced Nuclear Systems: Global Developments, PHYSOR 2004, Chicago (IL), US, April 2004.

[76] V. Henzl *et al.*, *"Study of ^{129}I Transmutation by High Energy Neutrons Produced in Lead Spallation Target"*, Proceedings of the International Workshop on Nuclear Data for the Transmutation of Nuclear Waste (TRAMU), ISBN 3-00-012276-1, GSI-Darmstadt, Germany, September 2003.

[77] The n_TOF Collaboration, *"Proposal for a Neutron Time of Flight Facility"*, CERN/SPSC 99-8, CERN, 1999.

[78]* C. Borcea, P. Cennini, M. Dahlfors, A. Ferrari, G. García-Muñoz, P. Haefner, A. Herrera-Martínez, Y. Kadi, V. Lacoste, E. Radermacher, F. Saldaña, V. Vlachoudis, L. Zanini, C. Rubbia, S. Buono, V. Dangendorf, R. Nolte, M. Weierganz, *"Results from the Commissioning of the n_TOF Spallation Neutron Source at CERN"*, Nuclear Instruments and Methods in Physics Research A 513 (2003) 524–537, 2003.

[79]* The n_TOF Collaboration, *"CERN n_TOF Facility: Performance Report"*, CERN/INTC-O-011; INTC-2002-037; CERN-SL-053-ECT, 2003.

[80]* V. Vlachoudis, C. Borcea, S. Buono, P. Cennini, M. Dahlfors, A. Ferrari, A. Herrera-Martínez, Y. Kadi, V. Lacoste, E. Radermacher, C. Rubbia, L. Zanini, *"Radioprotection and Shielding Aspects of the n_TOF Spallation Source"*, CERN-SL-2002-010-ECT and Proceedings of the 6th Meeting on Shielding Aspects of Accelerators, Targets and Irradiation Facilities, SATIF-6 SLAC (CA), US, April, 2002.

[81] R. Plag, M. Heil, F. Kaeppeler, P. Pavlopoulos, R. Reifarth, and K. Wisshak, *"An optimized C6D6 detector for studies of resonance-dominated (n, g) cross sections"*, Nuclear Instruments and Methods A, 2002.

[82] M. Heil, *et al.*, Nuclear Instruments and Methods A, 459, 229, 2001.

[83] C. Stéphan, L. Ferrant, B. Berthier, S. David, L. Tassan-Got, C.O. Bacri, F. Rejmund, C. Moreau and the n-TOF Collaboration, "*Neutron induced fission cross-section measurements"*, Journal of Nuclear science and Technology, Supplement 2, 276, 2002.

[84]* The n_TOF Collaboration, *"A Detailed Study of Hyperdeformed States of Uranium in the $^{234}U(n,f)$ Reaction"*, CERN/INTC 2002-022, P145-Add.1, 2002.

[85] P. Cennini, V. Lacoste, *"Proposal for a Fission Detector based on the measurement of the ionization produced by the absorption in gas of the Fission Fragments"*, SL-Note-2000-006-EET, 2000.

[86]* P. Cennini *et al.*, *"High Resolution Measurements of Neutron Induced Fission Cross-sections of $^{236, 238}U$, ^{232}Th and ^{237}Np from 1 eV to 1 MeV"*, to be published in the Proceedings of the 12th International Seminar of Interaction of Neutrons with Nuclei (ISINN-12), Dubna, Russia, 2004.

[87] C. Domingo-Pardo, PhD Thesis, University of Valencia (Spain), 2005.

[88] Training, Research, Isotopes, General Atomics (TRIGA): General Atomics official website http://triga.ga.com/

[89] L. Di Palo, G. Focaccia, E. Lo Prato, F. Marsili, M. Perni, A. Verri, *"RC-1 REATTORE 1 MW – Progetto Definitivo e Rapporto di Sicurezza"*, CNEN Centro Studi Nucleari Casaccia, 1966.

[90]* The International TRADE Collaboration, *"2nd TRADE Progress Report"*, ENEA Report, March 2003.

[91]* F. Pisacane, G. Bianchini, N. Burgio, M. Carta, A. D'Angelo, A. Santagata, S. Monti,

Y. Kadi, A. Herrera-Martínez, L. Zanini, M. Salvatores, *"Evaluation of the Spallation Target Design Characteristics for the Triga Accelerator-Driven Experiment (TRADE)"*, Proceedings of the Accelerator Applications in a Nuclear Renaissance Conference, AccApp 03, San Diego (CA), US, June 2003.

[92]* Y. Kadi, C. Rubbia, P. Agostini, M. Carta, A. Herrera-Martínez, C. Krakowiak, L. Maciocco, S. Monti, M. Palomba, F. Piscane, M. Salvatores, *"The TRADE Experiment: Status of the Project and Physics of the Spallation Target"*, Proceedings of the International Conference on the Physics of Fuel Cycles and Advanced Nuclear Systems: Global Developments, PHYSOR 2004, Chicago (IL), US, April, 2004.

[93]* A. Herrera-Martínez A. Ferrari, Y. Kadi, L. Zanini, G.T. Parks, C. Rubbia, N. Burgio, M. Carta, A. Santagata, L. Cinotti, *"Radiological Impact of the TRiga Accelerator-Driven Experiment (TRADE)"*, CERN-SL-2002-007-ECT and Proceedings of the 12th Biennial RPSD Topical Meeting, Santa Fe (NM), US, April, 2002.

[94]* L. Zanini, A. Ferrari, A. Herrera-Martínez, Y. Kadi, C. Rubbia, N. Burgio, M. Carta, A. Santagata, L. Cinotti, *"Radioprotection calculations for the TRADE experiment"*, CERN-SL-2002-043-ECT and Proceedings of the 3rd International Workshop of Utilization and Reliability of High Power Proton Accelerators, Santa Fe (NM), US, May 2002.

[95]* L. Picardi, C. Ronsivalle, M. Salvatores, S. Monti, L. Cinotti, N. Burgio, M. Carta, Y. Kadi, N. Meda, G. Locatelli, A. Santagata, L. Zanini, A. Herrera-Martínez, *"Design of the Proton Beam Line for the TRADE Experiment"*, Proceedings of the Accelerator Applications in a Nuclear Renaissance Conference, AccApp 03, San Diego (CA), US, June 2003.

[96]* L. Zanini, A. Herrera-Martínez, Y. Kadi, *"Preliminary calculations of the radiation damage of the permanent magnets for TRADE"*, SL-2002-037-ECT, 2002.

[97] M. Carta, *"TRADE – Progress in Neutronics"*, talk in TRADE status meeting, ENEA – Rome, September 2003.

[98] D. G. Naberejnev, G. Imel, G. Palmiotti, M. Salvatores, *"Physics study of the TRADE: TRIGA Accelerator Driven Experiment"*, ANL-AFCI-091, ANL, US, September 2003.

[99]* C. Rubbia, M. Carta N. Burgio, C. Ciavola A. D'Angelo, A. Dorado, A. Festini, S. Monti, A. Santagata, F. Troiani, M. Salvatores, M. Delpech, Y. Kadi, A. Ferrari, A. Herrera-Martínez, L. Zanini, G. Imel, *"Preliminary Neutronic Analyses of the TRIGA-ADS Demonstration Facility"*, in Nuclear Science and Engineering (NSE): Vol 148,

pag 103-123 (Sept 2004); also in Proceedings of the International Conference on the New Frontiers of Nuclear Technology: Reactor Physics, Safety and High-Performance Computing, PHYSOR 2002, Seoul, Korea, October, 2002.

[100] *"CLEFS CEA – N°46 – Printemps 2002"*, Commissariat à l'Énergie Atomique (CEA), France, 2002.

[101] Nuclear Energy Agency, *"Actinide and Fission Product Partitioning and Transmutation"*, Seventh Information Exchange Meeting, Jeju, Republic of Korea, October 2002.

[102] Y. Kim, R.N. Hill, W.S. Yang, H. Kahlil, *"Transmutation of Long-Lived Fission Products in the ATW System"*, Proceedings of the Actinide and Fission Product Partitioning and Transmutation: Seventh Information Exchange Meeting, Jeju, Republic of Korea, Nuclear Energy Agency, October 2002.

[103] A.A. Kozar et al., *"The Achievement of high ^{99}Tc Transmutation Rates in the SM Research Reactor"*, Proceedings of the Actinide and Fission Product Partitioning and Transmutation: Seventh Information Exchange Meeting, Jeju, Republic of Korea, Nuclear Energy Agency, October 2002.

[104] G. De Antoni, ANSALDO Nucleare (private communication).

[105] S. Glasstone, A. Sesonske, *"Nuclear Reactor Engineering"*, 4th Edition, Chapman & Hall, 1994.

[106] M. Kauchi, Y. Shimazu, *"Optimal Burnable Poison-Loading in a PWR with Carbon Coated Particle Fuel"*, Journal of Nuclear Science and Technology, Vol. 40. No. 1, p. 22-29, January, 2003.

[107] T. Ogawa, *"Dedicated Fuels for Transmutation: Nitrides and Alloys"*, Frédéric Joliot – Otto Hahn Summer School 2002 Lectures, CEA – Cadarache, France, 2002.